Operation and Performance of a Sidestream Aerobic Granular Sludge Pilot Reactor for Mainstream Bioaugmentation

Maxwell Armenta

A thesis

submitted in partial fulfillment of the

requirements for the degree of

Master of Science

University of Washington

2019

Committee:

H David Stensel, Chair

Mari-Karoliina H. Winkler

David A. Stahl

Program Authorized to Offer Degree

Civil and Environmental Engineering

University of Washington

Abstract

Operation and Performance of a Sidestream Aerobic Granular Sludge Pilot Reactor for Mainstream Bioaugmentation

Maxwell Armenta

Chair of the Supervisory Committee:

H David Stensel

Department of Civil and Environmental Engineering

A pilot sidestream sequencing batch reactor (SBR) was fed centrate diluted with secondary effluent to grow aerobic granular sludge enriched with phosphorus accumulating organisms (PAO) and ammonia oxidizing bacteria (AOB) for bioaugmentation of a BOD-only continuous-flow mainstream treatment system at low solids retention time (SRT) to achieve nitrogen and phosphorus removal. The SBR cycle consisted of anaerobic, aerobic, settling, decant, and idle phases. The settling time was 7 minutes and 50% of the volume was removed during effluent decanting. Acetate was fed in the anaerobic phase for uptake and conversion to storage products by PAOs. Under aeration, denitrifying PAOs (dPAOs) utilized stored carbon for NO_3^-/NO_2^- reduction within the anoxic granule core simultaneously with nitrification on outer granule layers. Alkalinity production during denitrification was sufficient to maintain reactor pH above

7.0 for uninhibited nitrification rates. The reactor was operated for about 10.5 months after a 95-day startup and 31-day stabilization period. Over the 10.5-month period the removal efficiencies for ammonia (NH_3) and total inorganic nitrogen (TIN) averaged 90% and 85%, respectively, at NH_3-N loading rates of 0.38 ± 0.07 g/L-d. Simultaneous nitrification and denitrification (SND) efficiency averaged 94% and was over 80% for each sampling day, with the exception of 3% of measurements. Periodic PAO and nitrifying inhibition occurred by unknown changes in the centrate or secondary effluent; however, granular integrity was maintained, and microbial activity rapidly recovered.

Five stable performance periods totaling 107 days were identified during the 10.5-month period. The SND performance and required COD:NH_3-N feed ratio (COD:N) was affected by aeration DO concentration, anaerobic acetate feed rate, and effluent NH_3-N concentrations. The NH_3-N removal and SND efficiencies of 96 ± 5% and 93 ± 4%, respectively were achieved at an NH_3-N loading rate of 0.44 ± 0.02 g/L-d and COD:N feed ratio of 2.94 ± 0.19 g/g.

The SRT, controlled by effluent solids and manual wasting, was 23 to 40 days during stable performance periods. MLSS concentration ranged from 11.3 to 15.0 g/L with over 90% granules based on 212 µm sieve size. The sludge settling velocity was over 9 m/hr. The weighted average granular size diameter, assuming spherical geometry, ranged from 1.0 to 1.5 mm during stable performance periods and the size distribution ranged from 0.212 to 3.0 mm. The average granular size and distribution provided more than sufficient surface area without limitation to nitrifier growth or nitrification rates. Specific nitrification rates ranged from 1.8 to 2.6 g NH_3-N/g VSS-hr and were influenced by NH_3-N loading rate, COD:N feed ratio, and bulk liquid DO

and NH_3-N concentrations. Shortcut nitrogen removal was achieved when there were low ratios of DO to NH_3-N concentration in the bulk liquid. Maximum suppression was found at a DO:NH_3-N ratio of 0.2 or less.

For my parents,

Lynda Jo & Mathew Armenta

Acknowledgements

This paper is dedicated first and foremost to my loving mother and father. Their unconditional love and support allowed me to attend and thrive at both the University of California, Los Angeles and the University of Washington. I literally would not be where I am today without them. I also would like to acknowledge financial support from scholarships, especially the CHP 11-99 Foundation and Sullivan Advanced Studies Scholarship, which were monumental in my ability to repay student loans and achieve academic success. Thank you to all persons and organizations providing financial support to all students.

I am thankful for my entire family, especially to my grandparents: Martha Armenta, Manuel Jr. Armenta, Marva Packey, and John Packey; to my godparents: Manuel III Armenta and Laura Rinard; and to my sister, Mara Armenta. I am thankful always for my patient and loving girlfriend, Katherine Anne Hee. I am thankful to my dear friends, whose support during graduate school provided sanity and relief, especially to: William White, Dan Kota Nishiguchi, Ryan Rasanen, Robert Kramer, Alexander Nathan, Magaret Honig, and Winston Donniko Boyce.

I am thankful to have been a part of the Stahl/Winkler lab group. It was an enjoyable and productive working environment. Thank you especially to Stephany Wei, Bao Nguyen Quoc, and Kris Hunt for kindness, instruction, and encouragement. Thank you also to Madelyn Shapiro for answering my many, many questions regarding Gallery orders. Thank you to Bryce Figdore and John Carter for your work preceding and following this study. Thank you to my undergraduate assistant, Annie Dubner, for high-quality analytical measurements.

I am thankful to King County for providing me the support and opportunity to be a part of this project under the King County Graduate Student Research Fellowship Program. I am especially thankful to Bob Bucher and Pardi Sukapanpotharam for their hard work on this project and for being enjoyable, amazing people to work with. I am thankful for the West Point Treatment Plant Laboratory for measuring alkalinity and total suspended solids in composite effluent samples, and for measuring mixed liquor concentrations.

I am thankful for my committee and advisor. Thank you to Professors Stahl, Stensel, and Winkler for their patience, guidance, and brilliance. Thank you especially to Professor Stensel for providing the opportunity for me to study at the University of Washington. Thank you for developing my abilities as an engineer and scientist (and writer).

Lastly, thank you to God. Thank you for everything.

I would like to acknowledge that the opportunities afforded to me are in part due to socioeconomic advantages I am afforded due to my actual and perceived gender and racial identity. My ability to identify as a white male has been advantageous in the engineering field.

This study was done as part of the joint National Science Foundation Award (CBET 1603707), Water Research Foundation Contract (TIRR3C15) and King County Participation and Partnership for the University of Washington GOALI project: Bioaugmentation of Activated Sludge with High Activity Nitrifying Granules/Flocs: Population Selection, Survival, Biokinetics.

Table of Contents

List of Figures

List of Tables

List of Abbreviations

AN	anaerobic
AO	anoxic
AOA	ammonia oxidizing archaea
AOB	ammonia oxidizing bacteria
BOD	biological oxygen demand
COD	chemical oxygen demand
COD:N	acetate-COD to ammonia-nitrogen feed ratio
COD:Nr	acetate-COD feed to total inorganic nitrogen removed ratio
COD:NOr	acetate-COD feed to nitrite-N plus nitrate-N removed ratio
CR	consumption ratio
DO	dissolved oxygen
DNA	deoxyribonucleic acid
dPAO	denitrifying PAO
dGAO	denitrifying GAO
EBPR	enhanced biological phosphorus removal
EUB	total bacteria
FA	free ammonia
FISH	fluorescence in situ hybridization
floc	flocculent activated sludge
FNA	free nitrous acid
GAO	glycogen accumulating organism
GOALI	Grant Opportunities for Academic Liaison with Industry
HRT	hydraulic residence time
KC	King County
MLVSS	mixed liquor volatile suspended solids
MLSS	mixed liquor suspended solids
NDN	nitrifying and denitrifying
NO_X	nitrite plus nitrate as N
NOB	nitrite oxidizing bacteria
OHO	ordinary heterotrophic organism
OUR	oxygen utilization rate
OX	aerobic
PAO	phosphorus accumulating organism
PI	proportional integral
PCR	polymerase chain reaction
PHA	poly-beta-hydroxyalkanoate
PVC	polyvinyl chloride
qPCR	quantitative polymerase chain reaction
RNA	ribonucleic acid
SA/VOL	surface area to volume ratio
SAUR	specific acetate uptake rate
SBR	sequencing batch reactor
SD	secure digital
SND	simultaneous nitrification and denitrification

SNR	specific nitrification rate
SRT	solids retention time
SSDM	sum of squared deviations from mean
STP	South Treatment Plant
SVI	sludge volume index
TIN	total inorganic nitrogen
TSS	total suspended solids
UW	University of Washington
VER	volume exchange ratio
VFA	volatile fatty acid
VSS	volatile suspended solids
WAS	waste activated sludge
WPTP	West Point Treatment Plant

List of Units and Symbols

%	percent
°C	degrees Celsius
d	day(s)
ft	foot/feet
hr	hour
in	inch(es)
L	liter(s)
m	meter(s)
min	minute(s)

1 Introduction and Objectives

Conventional biological nitrogen removal involves a nitrification process with autotrophic bacteria (nitrifiers; nitrifying bacteria) to produce nitrite (NO_2^-) and nitrate (NO_3^-) and a denitrification process of reduction of the oxidized nitrogen to dinitrogen (N_2) gas by heterotrophic bacteria consuming organic carbon. Nitrifiers are slow growers and require longer solids retention times (SRTs) and hence more tank volume than for biological oxygen demand (BOD) removal. Sidestream treatment of anaerobic digester sludge dewatering centrate has been done in aerobic nitrifying reactors with flocculent sludge at full-scale wastewater treatment plants for nitrification bioaugmentation of low-SRT mainstream treatment systems (Bowden et al., 2016). However, the improvement in nitrification efficiency or the ability to achieve nitrification at lower SRT has been limited because the bioaugmented biomass has the same SRT as the mainstream flocculent sludge.

Nitrifying bacteria have been grown in biofilms and aerobic granular activated sludge, and the use of granular sludge for activated sludge treatment has become of high interest. Granular activated sludge settles faster and thickens more rapidly to allow much higher reactor mixed liquor suspended solids (MLSS) concentration than conventional flocculent activated sludge process to allow a smaller reactor volume and treatment footprint. In addition, granular sludge has a decided advantage for nutrient removal due to the fact that enhanced biological phosphorus removal (EBPR) and nitrogen removal via nitrification and denitrification can be done within a granule.

So far wastewater treatment with granular activated sludge has only been done in full-scale using a sequencing batch reactor (SBR) process with a short settling time to favor washout of flocculent sludge, but most existing municipal activated sludge treatment plants have continuous flow designs. Changing an existing continuous flow system to an SBR system has unique challenges and thus there is much interest on how to have a granular sludge process in continuous flow treatment. A review of physical separation methods to favor retention of granular sludge in continuous flow treatment by Kent et al. (2018) included hydraulic designs for gravity separation, hydrocyclones and sieves. However, they did not address applications for sidestream bioaugmentation for nitrification and nutrient removal in low-SRT activated sludge processes.

The different characteristics of granular sludge compared to flocculent sludge provides a better approach for sidestream bioaugmentation. Differences in their physical and biological characteristics provide an opportunity for separate SRT control of the flocculent and granular sludge in bioaugmented mainstream treatment system. Figdore et al. (2018a) first showed sidestream treatment with growth of granular sludge containing phosphorus accumulating organisms (PAOs) and nitrifying bacteria using a SBR anaerobic/aerobic process. These granules were also capable of simultaneous nitrification and denitrification (SND) and nitrogen removal during aeration and are referred to herein as PAO-NDN granules. Successful bioaugmentation of nitrification and nitrogen removal was demonstrated at bench scale by adding the sidestream PAO-NDN granules to an SBR containing both flocculent and granular sludge fed a synthetic wastewater. However, this work did not address a continuous flow activated sludge process

configuration with granular sludge. This study was supported under the King County (KC) Graduate Research Fellowship Program.

The work reported in this thesis is on the sidestream process component of a pilot plant at the KC West Point Treatment Plant (WPTP) to study a continuous-flow bioaugmentation process, which is the subject of the University of Washington (UW) GOALI project supported by KC, the National Science Foundation, and Water Research Foundation. The GOALI project title is "Bioaugmentation of activated sludge with high activity nitrifying granules/flocs: Population selection, survival, biokinetics." The overall project objective is to demonstrate and evaluate the use of sidestream bioaugmentation of PAO-NDN granules to an innovative mainstream process treating municipal wastewater to provide nutrient removal and/or increase the treatment capacity. The mainstream process provides a selective pressure to sustain the granules and control separate SRTs of floc and granular sludge as shown in Figure 1-1. It consists of an anaerobic zone, aeration tank, hydraulic granular/flocculent (floc) sludge separator, and secondary clarifier. The separator takes advantage of the fact that granules settle over ten times faster than flocculent sludge and can be physically separated by differential settling velocities (Nor Anuar et al., 2007). The separator underflow with granular sludge is recycled to the anaerobic zone which is also fed influent wastewater. The separator overflow with flocculent sludge is directed to the secondary clarifier. The secondary clarifier underflow recycle with flocculent sludge is directed to the aeration tank. Achieving separate granule and floc return lines provides the ability to operate at higher SRT for the granular sludge to provide a more effective sidestream bioaugmentation than previous systems with only flocculent sludge. The anaerobic zone in the mainstream treatment

process sustains PAO-NDN granules that accomplish EBPR and SND under DO concentration control in the aeration tank.

The pilot plant sidestream SBR is operated with anaerobic and aerobic phases. During the anaerobic phase it is fed acetate to grow PAO-NDN granules. Centrate and secondary effluent dilution water are fed during the aerobic phase. Addition of secondary effluent is providing nitrifying bacteria growth at temperatures similar to the mainstream. The sidestream reactor operation began February 24, 2018 after about a 4-week shake down period.

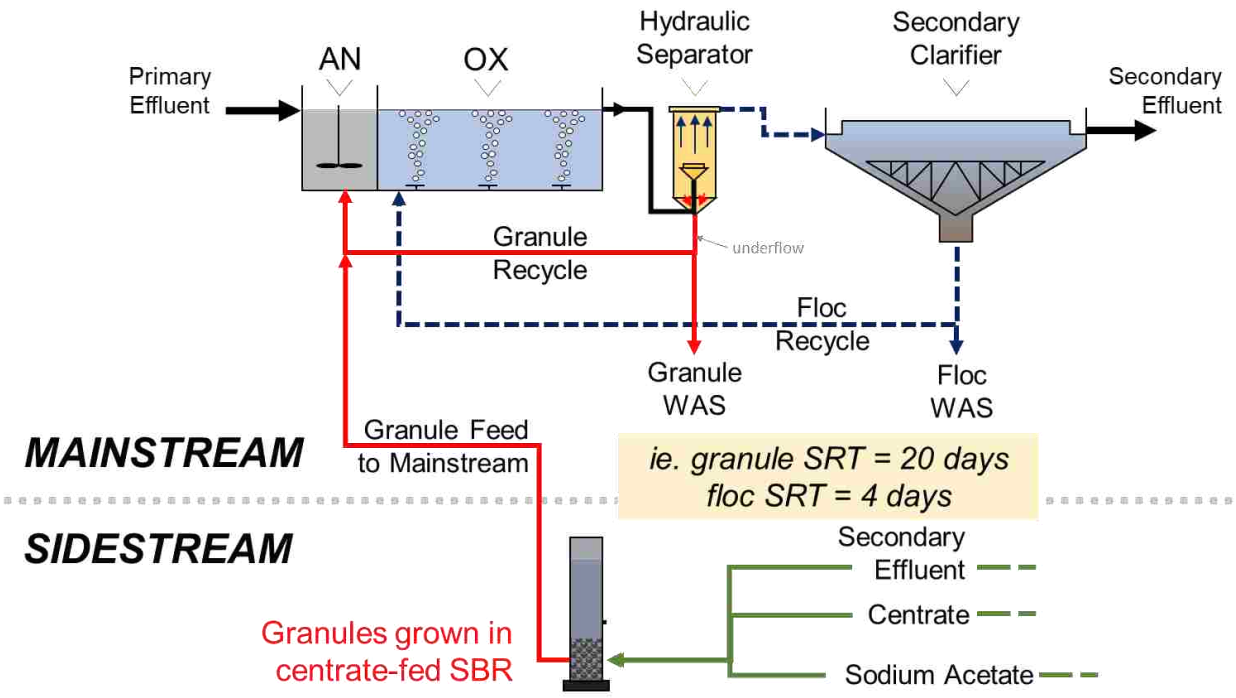

Figure 1-1. Flow scheme for sidestream aerobic nitrifying granular sludge bioaugmentation of a continuous-flow treatment system, adapted from original University of Washington design. Anaerobic (AN) and aerobic (OX) zones precede a hydraulic separator and secondary clarifier. Separate return lines allow uncoupled solids retention time (SRT) and waste activated sludge (WAS) control. Granules are grown in a sequencing batch reactor (SBR).

The main goals of the sidestream pilot plant investigation were as follows:

1. Demonstrate long-term operation of the sidestream treatment reactor with operating conditions suitable for nitrification, nitrogen removal, and granular sludge production. Evaluate treatment performance efficiency.

2. Investigate the physical and microbial characteristics of the sidestream granules.

3. Assess nitrification kinetics of sidestream granules.

4. Determine factors that affect shortcut nitrogen removal and minimize amount of supplemental acetate COD required for nitrogen removal.

Key process factors considered for the sidestream reactor operation to meet the project goals are described along with specific operating objectives as follows:

1. High sidestream NH_3-N removal efficiency is needed to minimize the amount of NH_3-N added to the mainstream system from the sidestream and to maximize nitrifying bacteria with the sidestream granules fed to the mainstream. **Objective 1 is to achieve greater than 80% NH_3-N oxidation in the sidestream process.**

2. During nitrification two moles of acid are produced per mole of NH_3-N oxidized but centrate typically has only one mole of alkalinity per mole of NH_3-N produced in the

anaerobic digester. NO_2^- or NO_3^- reduction produces one mole of alkalinity per mole of NO_X-N reduced. **Objective 2 is to achieve denitrification of more than 85% of the NO_X-N produced in the sidestream reactor to provide sufficient alkalinity for a stable pH for uninhibited nitrification and to minimize oxidized nitrogen (NO_X) in the sidestream effluent.**

3. A higher NH_3-N volumetric loading (g NH_3-N/L-d) to the sidestream reactor results in less reactor volume and cost, but treatment performance and loading must consider volumetric oxygen transfer capacity for the fine bubble aeration equipment and biomass nitrification rates. **Objective 3 is to achieve treatment objectives 1 and 2 at an NH_3-N loading in the range of 0.40 to 0.50 g NH_3-N/L-d.**

4. Nitrogen removal occurs during aeration. NO_X reduction is mainly due to denitrification by PAOs and GAOs located in the anoxic granule interior and nitrification simultaneously occurs on the granule outer layers. Enough acetate must be consumed and stored by the PAOs and GAOs during the anaerobic phase to reduce the amount of NO_2^- and NO_3^- produced during aeration. Denitrification via NO_2^-, referred to as shortcut nitrogen removal, requires less stored COD. The amount of stored carbon used for denitrification also depends on the bulk liquid DO concentration, which must be high enough for good nitrification performance but low enough to minimize DO penetration to have sufficient anoxic volume in the granule. A high bulk liquid concentration and higher NO_3^- production will require more COD addition per unit of NOx-N to be removed and thus greater cost. **Objective 4 is to minimize the sidestream COD:N feed ratio by DO**

control during aeration and identify operating methods that maximize shortcut nitrogen removal.

5. The size of the granules produced is important. Larger granules result in higher settling velocities and faster thickening rates which can result in higher reactor MLSS concentrations. Achieving settling rates greater than 10 m/hr is desired to allow for differential settling rates between granules and floc in the hydraulic separator. Granules must also be large enough to provide SND during aeration. However, if the granules are too large there is less surface area available for nitrifying bacteria to meet nitrification rates needed in the reactor. **Objective 5 is to find a reactor operating condition and granule size that satisfies the three needs for high settling velocity, good SND, and sufficient nitrification surface area.**

6. Successful biological process performance at wastewater treatment facilities requires useful monitoring and operational tools that help provide an understanding of the process health, stability and control specific operating conditions to best achieve the treatment goals. **Objective 6 is to assess the pilot plant operation stability and control system to understand important operational procedures and controls for process monitoring.**

2 Background

Granular sludge can perform SND in a single aeration phase. The combination of substrate utilization and diffusion limits oxygen penetration into granules such that aerobic and anoxic zones exist simultaneously within the biofilm (De Kreuk et al., 2007). NH_3 and NO_2^- oxidizing bacteria (AOB and NOB) are active in the aerobic, outer layers of the biofilm and convert NH_3 to NO_2^- and NO_2^- to NO_3^-, respectively. PAOs and GAOs may reside throughout the granule. PAOs and GAOs within the inner, anoxic core of the biofilm reduce NO_2^- and NO_3^- to nitrogen gases by utilizing intracellular poly-beta-hydroxyalkanoate (PHA) as an electron donor. PHA is formed during a preceding anaerobic phase where volatile fatty acids (VFAs; e.g. acetate or propionate) are converted by PAOs and GAOs into internal storage products. Although both PAOs and GAOs are capable of denitrification, enriching granular sludge with PAOs provides EBPR treatment performance and higher granule density (Winkler et al., 2011). Granular sludge for SND and phosphorus removal can be grown in a SBR by cycling anaerobic and aerobic phases to leverage synergies between nitrifying and denitrifying organisms, as illustrated in Figure 2-1.

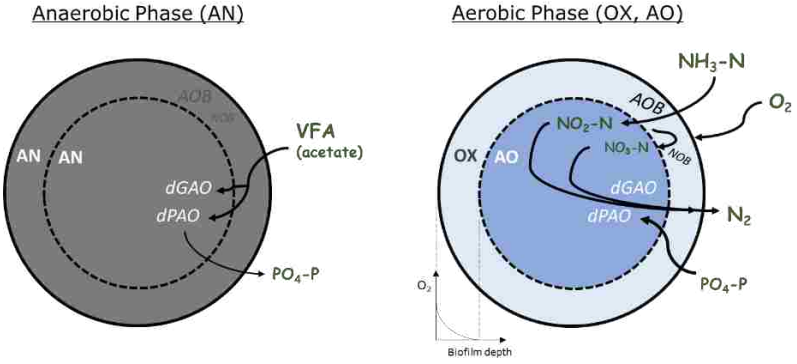

Figure 2-1. Anaerobic (AN) and aerobic (OX) phases for anaerobic COD removal, SND, and orthophosphate (PO_4^{3-}) removal by aerobic granular sludge. Diffusion resistance, DO concentration, and oxygen uptake on outer granule layers creates conditions for an anoxic (AO) zone within granules for denitrification to occur in an aerated reactor. Chemical pathways are simplified, and spatial representation of microbial populations is ideal.

2.1 *Nitrification*

NH_3 removal is most commonly accomplished in municipal wastewater treatment plants with a biological treatment process. NH_3 is removed biologically by assimilation into new biomass or through nitrification. Nitrification occurs in the presence of oxygen and is typically facilitated by two groups of microorganisms: ammonia oxidizing organisms and nitrite oxidizing organisms. Oxidation of NH_3 to NO_2^- by AOB and ammonia-oxidizing archaea (AOA) is termed nitritation. Hydroxylamine (NH_2OH) and nitric oxide (NO) are intermediate products created during nitritation. N_2O production can result by incomplete nitritation or AOB-induced denitrification of NO (Lancaster et al., 2018). NO_2^- is oxidized to NO_3^- by NOB and is termed nitratation. Recently *Nitrospira* with the ability to oxidize NH_3 to NO_3^- have been identified and are called complete ammonia oxidizers (comammox) (Daims et al., 2015).

Nitrifying organisms grow relatively slow compared to heterotrophic organisms within wastewater treatment plants and require a longer SRT to be kept in the system. Temperature affects that minimum SRT required because nitrifier growth rate, and thus nitrification rates, are lower at lower temperatures (Tchobanoglous et al., 2014a). Therefore, winter operations are a limiting factor when sizing a wastewater treatment plant for year-round nitrification.

2.1.1 Ammonia and Nitrite Oxidizing Organisms

The predominate AOB reported in municipal wastewater treatment are from the *Nitrosomonas* and *Nitrosospira* genus, and of these the *Nitrosomonas* strain was reported as the more dominant genus. AOA were discovered after the known existence of AOB and were originally isolated from marine cultures. AOA play a major role in the global nitrogen cycle and have been used in

emerging energy-efficient wastewater technology. However, AOA do not compete well at higher NH_3 and DO concentrations and are thus are typically less dominant in activated or aerobic granular sludge, excepting low-DO or low-NH_3-N environments.

The NOB populations in wastewater treatment are reported at a greater genus diversity than for AOB. *Nitrobacter and Nitrospira* are commonly reported in wastewater treatment processes, although *Nitrotoga* has also been identified as a dominant nitrifier in aerobic granular sludge for nitrification (Figdore et al., 2018b). NOB require NO_2^- accumulation for energy and growth. Therefore, NOB almost always coexist with AOB in activated or aerobic granular sludge processes.

Various equations have been used to describe nitrification kinetics for AOB and NOB. When the abundance of NOB is great enough, NO_3^- production is essentially governed by NH_3 oxidation. However, decoupling nitrification kinetics is useful for understanding the effect of temperature, DO concentration, substrate concentration, and inhibitory compounds on the growth rates and activity of AOB and NOB. A common relationship between nitrification kinetics and temperature is shown in Equation 2-1.

$$R = R_{max} \times \Theta^{20°C-T} \quad (2\text{-}1)$$

Where:

R = rate of nitritation or nitratation, mg/L-min

R_{max} = maximum rate of nitritation or nitratation, mg/L-min

Θ = temperature dependency coefficient, 1.072

T = temperature of bulk liquid, °C

A temperature dependency coefficient of 1.072 has been recommended when correcting nitrification rates to 20°C in activated sludge modelling (Melcer et al., 2003). However, this coefficient is less accurate if drastic changes in temperature occur. For example, Hwang and Oleszkiewicz (2007) found that a 10°C drop in temperature led to a 10% greater decrease in nitrification rate than predicted with a temperature dependency coefficient of 1.072.

Nitrification bacteria specific growth rates have often been described by a double Monod equation in which the bacteria growth rate is a function of the bulk liquid DO and NH_3-N or NO_2^--N concentration. The maximum specific nitrification rate (SNR) can be equated to the maximum specific growth rate divided by the synthesis yield coefficient and modeled using the Michaelis-Menten equation, shown below. For nitritation NO_2^--N replaces NH_3-N in Equation 2-2 below.

$$SNR = SNR_{max}\left(\frac{DO}{DO + K_{DO}}\right)\left(\frac{NH_3\text{-}N}{NH_3\text{-}N + K_N}\right) \quad (2\text{-}2)$$

Where:

SNR = Specific nitrification rate, mg N/g VSS-d

SNR_{max} = Maximum specific nitrification rate, mg N/g VSS-d

DO = Bulk liquid DO concentration, mg/L

K_{DO} = Half-saturation constant for DO, mg/L

NH_3-N = Bulk liquid NH_3-N concentration, mg/L; for NOB this is NO_2^--N

K_N = Half-saturation constant for NH_3-N, mg/L; for NOB this is for NO_2^--N

The nitrification rate is based on biomass concentration, as shown in the equation below.

$$\text{Nitrification Rate} = (\text{SNR})(\text{MLVSS}) \quad (2\text{-}3)$$

Where:

Nitrification rate = Rate of ammonia oxidation in reactor, mg NH_3-N/L-d

MLVSS = Mixed liquor volatile suspended solids, g/L

2.1.2 Shortcut Nitrogen Removal by Suppression of NOB

Shortcut nitrogen removal is denitrification with NO_2^- instead of NO_3^- and is advantageous by requiring 40% less carbon and 25% less aeration energy than oxidation of NH_3 to NO_3^- (Bowden et al., 2016). Suppression of NOB while maintaining AOB activity is necessary to avoid NO_3^- production. Strategies reported in literature for NOB suppression with flocculent sludge are: 1) selective wash out of NOB based on temperature and SRT control, 2) low DO concentration, 3) alternating aerobic and anoxic conditions, and 4) presence of high free ammonia concentration during nitrification (Bowden et al., 2016). The low SRT for selective washout of NOB at 3 to 5 days at 20°C is not practical for and aerobic granular sludge reactors, which are normally operated at SRTs from 10 to 50 days.

Free ammonia (FA) and free nitrous acid (FNA) inhibit nitrification and are toxic to both AOB and NOB (Tchobanoglous et al., 2014a). NOB are more sensitive to elevated FA and FNA concentrations than AOB, but acclimation of NOB may occur when exposed to FA for an extended period, after which NOB can tolerate higher concentrations (Kouba et al., 2014; Zhang

et al., 2018); however, these results were not demonstrated in aerobic granular sludge. FA and FNA concentrations depend on temperature and pH. Higher pH and temperature favors a greater percentage of FA formation at a given NH_3-N concentration, and lower pH and temperature values favor the formation of FNA at a given NO_2-N concentration (Anthonisen et al., 1976).

Reported FA concentrations necessary to inhibit NOB growth for flocculent activated sludge vary widely. Inhibitory concentrations from 0.1 to 1.0 mg N/L were reported in the first work on NOB inhibition by FA (Anthonisen et al., 1976), but it is not known if the NOB were *Nitrobacter* or *Nitrospira*. Simm et al. (2006) found no inhibition at 10 mg/L FA concentration with a *Nitrospira species* and Ushiki et al. (2017) reported threshold FA inhibition concentrations of 0.85 and 4.3 mg/L in work with pure cultures with different species of *Nitrospira*. Such differences suggest that the FA concentration to inhibit *Nitrospira* NO_2^- oxidation is species dependent. *Nitrosomonas* inhibition was reported at FA concentrations starting at 16 mg N/L (Vadivelu et al., 2006), which is higher than that reported for NOB inhibition. However, the effect of the specific AOB and species on the threshold FA concentration for AOB inhibition is not known.

2.1.3 Suppression of Nitrite Oxidation in Aerobic Granular Sludge

Investigations on NOB inhibition in granular sludge has revealed the importance of the spatial distribution of AOB and NOB in the granule and the DO and NH_3-N oxygen gradient from the bulk liquid. For elevated bulk liquid NH_3-N concentration AOB is dominant on the outer layer because it can grow faster than NOB. The consumption of DO by AOB in the outer granule aerobic layers results in lower DO concentration and thus lower NOB activity to favors AOB

over NOB activity for the granule. Stratification of AOB to the outer granule layers was also suggested from modeling studies by Picioreanu et al. (2016) as the explanation for apparent oxygen affinities between AOB and NOB in granules that is often observed. They came to this conclusion based on three-dimensional computer simulations where the stratification of AOB and NOB in granules was adjusted to observe the effect on apparent half-saturation constant compared to a homogenous distribution of AOB and NOB within the biofilm.

The effect of the reactor DO:NH_3-N concentration ratio on NOB suppression for granular sludge has been observed by a number of investigators for laboratory air lift reactor. For operation at 30°C and reactor DO and NH_3-N concentrations of 5-7 mg/L and 20-40 mg/L, respectively, Bartrolí et al. (2010) reported 98% conversion of NO_2^--N to NO_3^--N at a DO:NH_3-N ratio or 0.35, but at ratios of 0.25 or less the effluent NO_X-N consisted of 98% NO_2^--N. At lower temperatures the NOB kinetics may be greater than the AOB kinetics to thus require lower bulk liquid DO:NH_3-N ratios to suppress NOB activity. NOB activity was fully suppressed in the operation of granular sludge air lift reactors at 12.5°C by Isanta et al. (2015) and 10°C by Reino et al. (2016) with effluent NH_3-N concentrations of 40 mg/L and DO concentrations of near 1.0 mg/L and 1-2 mg/L, respectively. Their DO:NH_3-N ratios were approximately 0.05 and 0.04, respectively, but it is not known if a higher DO:NH_3-N ratio could have been used without NOB suppression for their reactors. Soler-Jofra et al. (2019) also operated an airlift granular sludge reactor with high NH_3-N concentration at 40-50 mg/L and used batch test with varying initial NH_3-N concentrations to assess DO:NH_3-N ratios for NOB suppression at 20°C. At an NH_3-N concentration of 7.0 mg/L, 97% suppression of NOB occurred at a DO:NH_3-N ratio of 0.41. At 15°C and initial NH_3-N concentration of 19.0 mg/L, 90% suppression of NOB occurred at a

DO:NH_3-N ratio of 0.13. Poot et al. (2016) operated an airlift granular sludge reactor at 20°C with effluent NH_3-N concentrations from 0.8-27.0 mg/L and DO concentrations from 0.7-2.7 mg/L and found that the degree of NOB suppression was a function of the DO:NH_3-N ratio. As the reactor NH3-N concentration increased the DO:NH_3-N ratio decreased and there was more NOB activity suppression. Based on effluent NO_3^--N and NO_2^--N concentrations from their airlift granular sludge reactor 80% suppression of NOB occurred at DO:NH_3 ratios of 0.10 or less. At DO:NH_3-N ratio ratios of 2.0-2.5 about 60% suppression was reported..

The effects of DO concentration, FA concentration, diffusion limitations, and AOB and NOB stratification were considered by Kent et al. (2019) for continuous flow aerobic granules, and they suggested that both FA and reactor DO concentration and nitrifier stratification contributed to NOB suppression. However, the effect of FA on NOB suppression appears to be stronger for smaller sized granules and their granules were less than 1.0 mm in diameter.

2.2 *Exogenous Carbon Used for Denitrification*

Supplemental carbon dosing is often used for biological nitrogen removal processes with wastewaters that have low biodegradable organic carbon to nitrogen ratios. The amount of supplemental COD required per NO_3^--N removal in an anoxic zone is depended on both carbon source and electron acceptor (Tchobanoglous et al., 2014b). The carbon consumptive ratio is dependent on the synthesis yield (g VSS/g COD) achieved with the carbon source (Equation 2-4) if used in short HRT zones before or after aeration zones. The COD consumption ratio (CR) can be modeled as shown in the equation below.

$$CR = \frac{2.86}{1 - 1.42\ Y_H} \quad (2\text{-}4)$$

Where:

CR = COD consumption ratio, g COD-used/g NO_X-N-removed

Y_H = synthesis yield, g VSS/ g COD

2.86 = oxygen equivalent of NO_3^--N, g O2/g NO_3^--N

Substrates that have a lower synthesis yields result in less COD conversion to biomass and more COD oxidized by denitrification for energy production. Expected ratios for denitrification of nitrate range between 3.3 to 8.0 g supplemental COD per g NO_3^--N removed. The supplemental carbon dose with acetate is almost double that for methanol because of their different synthesis yield coefficients.

When NO_2^- instead of NO_3^- is the electron acceptor is used a value of 1.71 g O_2/gNO_2^--N is used in Equation 2-4 instead of 2.86 and the CR is 40% lower as indicated by Bowden et al. (2016). In a general example of supplemental carbon use for nitrogen removal they show a CR of 4.8 to 6.0 for nitrogen removal via NO_3^- and 2.9 to 3.7 for nitrogen removal via NO_2^- for shortcut nitrogen removal.

In practice the COD:NO_X-N ratios with supplemental carbon addition to anoxic reactors are higher than theoretical values because of the need for a COD concentration in the reactor to drive the reaction and thus unused COD in the effluent and the COD demand for reduction of DO

entering the anoxic reactor from upstream aeration or recycle streams. For reactors with longer detention time there is COD released from endogenous decay that helps lower the COD:NO_X-N ratio.

The above fundamental considerations on supplemental COD use are difficult to directly apply for the granular sludge operation in this study. First, the acetate COD is not used directly for cell synthesis and oxidation, rather it is first transferred to carbon storage products in the PAOs and GAOs. In addition, the long SND aeration time suggest that COD products from endogenous decay may also contribute the electron donor for denitrification. Thus, at this time it is difficult to develop a theoretical consumptive ratio for the granular sludge system as a function of SRT and acetate utilization and storage by PAOs. Hu et al. (2002) concluded PAOs have a biomass growth yield coefficient that when grown with anaerobic-anoxic cycles, using NO_3^--N as the electron acceptor, is 30% lower than the anaerobic-aerobic yield of PAOs. They stated respective yields at 0.25 and 0.35 g VSS/g COD but the reactor SRT and endogenous decay coefficient was not provided to allow an estimate of the synthesis yield.

2.3 *Enhanced Biological Phosphorus Removal*

The discovery of EBPR is widely attributed to Barnard (1975). In an EBPR system, anaerobic and aerobic zones are phased to select for organisms capable of accumulating orthophosphate (PO_4^{3-}) as intracellular inclusions called polyphosphate. The net result is orthophosphate removal at rates greater than achieved by cell synthesis alone. The key to successful EBPR is enriching sludge with PAOs while minimizing GAOs. To quantify success of operation strategies the abundance of PAO and GAO can be compared directly using qPCR or sequencing techniques.

Additionally, proxy parameters can be used to characterize EBPR health. One parameter is the ratio of anaerobic phosphorus release to VFA uptake by sludge during an anerobic phase. This ratio is known as the P/C ratio and maintaining higher P/C ratios has been linked to a greater enrichment of PAOs over GAOs and a more stable EBPR process. To maximize PAO enrichment and optimize EBPR it is important to understand the metabolisms, kinetics, and overall competition between PAOs and GAOs.

2.3.1 Phosphorus and Glycogen Accumulating Organisms

To select for PAOs or GAOs in wastewater systems, a cycling anaerobic-aerobic or anaerobic-anoxic environment is necessary, where a carbon source is available during anaerobic conditions for uptake and intracellular storage by PAOs or GAOs. The most common forms of organic carbon used by PAO and GAO are acetate and propionate, both of which are VFAs. A majority of PAO and GAO studies use acetate, propionate, or a combination of both when studying PAO and GAO competition or kinetics. Newly discovered PAO species are proposed to use more complex forms of carbon as well (Nguyen et al., 2015). Both PAOs and GAOs rely on energy generation from stored intracellular products for VFA-uptake during anaerobic conditions. These storage products are enriched during preceding and subsequent aeration phases. PAOs utilize stored polyphosphate to generate energy, while GAOs utilize stored glycogen. Polyphosphate composition has been proposed at molar ratios including Ca^{2+}, Mg^{2+}, K^{+}, and PO_4^{3-}, indicating cations in the bulk solution are required for phosphorus uptake. Glycogen is branched polymer of glucose ($C_6H_{10}O_5$), or polysaccharide, commonly used as an energy storage source in organisms. Glycogen is present in PAOs but enriched in GAOs, and GAOs use this storage for energy production analogous to polyphosphate use by PAOs. The energy generated by PAOs and GAOs

in the anaerobic phase allows for the storage of VFA as PHA. PHA is a polymer that can be later used by microorganisms in aeration when electron acceptors are present.

In an aerobic or anoxic environment, PAOs and GAOs use the intracellular PHA with either oxygen, NO_2^-, or NO_3^-. The stored PHA is used in part for cell synthesis and energy. Glycogen storage is replenished during this phase as well, and PAOs accumulate PO_4^{3-}-P as polyphosphate. Both PAOs and GAOs have demonstrated the ability to use PHA with NO_2^- and NO_3^-; however, ability and kinetics vary depending on the clade. A variety of PAOs and GAOs have been reported in wastewater treatment systems. The objective of this project is to enrich PAOs and minimize the presence of GAOs within granules.

2.3.2 Effect of Environmental and Operating Conditions on Kinetics and Competition of Phosphorus and Glycogen Accumulating Organisms

A minimum pH of 7.25 was said to be required to stabilize and achieve high quality effluent in flocculent sludge EBPR systems with acetate as the anaerobically-fed carbon source (Filipe et al., 2001d). GAOs were modeled to have faster anaerobic acetate uptake rates at lower pH values (Filipe et al., 2001a), and PAOs anaerobic acetate uptake rates were independent of pH value (Filipe et al., 2001b). Both the anaerobic acetate uptake rates of PAOs and GAOs are thought to be independent of acetate concentration, though PAOs may become rate-limited by available intracellular polyphosphate (Filipe et al., 2001b, 2001a). The aerobic pH value also impacts competition in an EBPR system by affecting the phosphorus uptake rate, where lower pH values are detrimental to phosphorus uptake by PAO (Filipe et al., 2001c); however, later experimental

results showed phosphorus uptake to be constant from pH values ranging from 7.40 to 8.25 (Serralta et al., 2006).

The type of carbon source affects competition between PAOs and GAOs. Oehmen et al. (2006) operated two parallel reactors at a pH value of 7.0 with either acetate or propionate as the anaerobic VFA feed. They found that using propionate instead of acetate favored PAOs. PAOs also compete better during conditions where the VFA source is switched (for example, intermittent feeding of propionate in an acetate-fed reactor); however, switching to a longer carbon chain VFA was observed to decrease PHA oxidation rates and phosphorus removal performance (Oehmen et al., 2005). Feeding acetate over a longer duration to have a lower bulk liquid concentration was another feed source strategy to select for PAOs instead of GAOs (Tu and Schuler, 2013).

PAOs have demonstrated competitive growth advantage over GAOs at lower temperature and shorter SRT (Whang and Park, 2006). Long term operation at very low temperature of 5°C experimentally demonstrated enhancement of phosphorus removal by PAOs (Erdal et al., 2003). The effect of both temperature and pH were assessed in a PAO-GAO granule study and it was found pH greater than 7.3 was a main selection factor for PAO whereas temperature greater than 23°C mainly selected for GAO (Weissbrodt et al., 2013).

2.3.3 Denitrifying Phosphorus and Glycogen Accumulating Organisms

Originally, PAOs and GAOs were studied in cycling anaerobic-aerobic systems; however, both organisms can use either NO_2^- and/or NO_3^- as an electron acceptor. Meinhold et al. (1999)

showed phosphorus uptake occurred anoxically with NO_3^- but at a slower rate than aerobically with oxygen. This led to the conclusion that not all PAOs are capable of denitrification and that the rates of phosphorus uptake indicated the relative fraction of dPAO. Oehmen et al. (2010) later suggested the use of total phosphorus uptake to assess the fraction of dPAO to total PAO. They also concluded that *Accumulibacter* Clade I could likely reduce NO_3^-, whereas *Accumulibacter* Clade II could likely only reduce NO_2^-. These results agreed with other findings, as Flowers et al. (2009) stated that Clade II cannot use NO_3^- and Lanham et al. (2011) found that Clade I can use NO_3^-. However, Rubio-Rincón et al. (2017) reported a sludge enriched with *Accumulibacter* Clade I could not remove phosphorus with NO_3^- but instead relied on GAO to reduce NO_3^- to NO_2^-. It is also suggested that *Accumulibacter* Clades IA and II-I may also depend on *Dechloromonas* and *Competibacter* to reduce NO_3^- to NO_2^- (Kim et al., 2013). Overall, there is conflicting reports of NO_3^- reduction by *Accumulibacter* Clade I, but sub-clade diversity may be responsible for differences in findings.

Dechloromonas was first postulated as a PAO based on anoxic phosphorus removal that occurred in its presence (Datta and Goel, 2007). *Dechloromonas* was later shown to exhibit GAO-phenotype with an absence of polyphosphate storage when formed in community with *Accumulibacter* (Ahn et al., 2007); however, a PAO-phenotype was suggested as well (Kong et al., 2007). Overall, there is conflicting evidence of *Dechloromonas*' direct contribution to EBPR; however, it is suggested that both *Dechloromonas* and *Competibacter* are key organisms for the reduction of NO_3^- to NO_2^- such that PAOs can reduce NO_2^- while removing orthophosphate (Kim et al., 2013). Zheng et al. (2013) showed denitrifying GAO could be maintained with anaerobic-anoxic cycle using NO_3^- as the electron acceptor. Therefore, flanking communities capable of

feast-famine competition have been observed in EBPR studies and may contribute to assisting or competing with PAOs. The basis for cooperation is based on the assumption that dPAOs cannot reduce NO_3^- and have a competitive advantage for NO_2^- reduction compared to dGAOs. Demonstration of dPAO or dGAO selection based on electron-acceptor competition has not been conducted over a variety of controls for pH, temperature, and electron donor.

One study has shown competition of dPAO and dGAO in granules. Bassin et al. (2012) ran reactors at 20 and 30°C to investigate denitrification performance by biomass in granular sludge. They concluded that GAO were responsible for nitrate reduction at 30°C and that Clade I *Accumulibacter* assisted in NO_3^- reduction at 20°C. Clade II *Accumulibacter* was noted as incapable of NO_3^- reduction to NO_2^- but was the mainly responsible for NO_2^- reduction. Therefore, lower temperature granular sludge reactors may have less competition by GAO if conditions exist for nitrate reducing PAO to exist.

FNA accumulation impacted the denitrifying and phosphorus removal capabilities of PAOs (Zhou et al., 2010). Zhou et al. (2010) proposed that at a pH of 7.0 and NO_2^--N of 0.22 mg/L that PAOs are inhibited. Inhibition of PAOs affects the ability of PO_4^{3-}-P removal more than the ability for PHA utilization. Zeng et al. (2016) suggested that NO_2^- reduction by PAO is a detoxification mechanism, and they saw long-term community shift more dominant in reactors with FNA, which suggested adaptation to FNA is possible and that some clades of PAO are more resistant to FNA exposure.

2.4 *Treatment Performance of PAO-NDN Granules*

Simultaneous removal of phosphorus, ammonia, and nitrogen with aerobic granular sludge was first demonstrated at the Delft University of Technology (De Kreuk et al., 2005). Full-scale implementation is commonly through the Nereda® process, which has been used to treat municipal wastewater since 2009 (Pronk et al., 2015). Lab and pilot-scale reactors have been investigated using ammonia loading rates from 0.08 to 0.45 g N/L-d and COD:NH_3-N ratios ranging from 3.4 to 39 g/g (De Kreuk et al., 2005; Figdore et al., 2018a; Iorhemen et al., 2018; Yilmaz et al., 2008). Nuanced differences between reactors—such as mixing intensity, reactor dimension, or settling time—have made it difficult to compare differences between studies and quantify the impact of operating changes on performance. However, maximum volumetric NH_3 and TIN removal rates were reported as 0.43 and 0.41 g N/L-d, respectively. (Figdore et al., 2018a; Yilmaz et al., 2008). These results provide a baseline for potential sidestream aerobic granular sludge reactor performance capacity.

When assessing treatment performance, it is important to be aware of additional removal pathways and process effects in aerobic granular sludge reactors. For example, Bassin et al. (2011) found that ammonium (NH_4^+) adsorption in aerobic granular sludge could occur at rates of 0.9 to 1.7 mg NH_4^+-N/g VSS when the pH was 7.0 and NH_3-N concentration was 30 mg/L. Granules were also found to include precipitates from real wastewater at full scale (Li et al., 2014), therefore a portion of metals are removed with biomass wasting. PO_4^{3-}-P removal was also suggested to occur within granules used for EBPR through precipitation by Ca^{2+} and PO_4^{3-} ions; however, the degree to which PO_4^{3-}-P removal by precipitation occurs is naturally dependent on pH and concentration of involved ions (Mañas et al., 2012).

2.5 *Bioaugmentation for Nitrification and Nitrogen Removal*

Leu and Stenstrom (2010) studied bioaugmentation schemes through calibrated models and found a sidestream reactor fed with centrate could decrease the SRT required for mainstream nitrification from 6 to 4 days. The effectiveness of bioaugmentation schemes were dependent on mainstream temperature, where warmer temperatures could be operated at lower SRT or could achieve greater removal. Temperature difference between the mainstream system and sidestream nitrifier-enriching reactor also affects overall mainstream nitrification performance. Head and Oleszkiewicz (2004) demonstrated that nitrifying biomass grown at elevated temperatures (e.g. 20°, 25°, or 30°C) will undergo significant decreases in nitrification rates when seeded to 10°C conditions. Therefore, acclimation of sidestream biomass to temperatures representative of mainstream flow may improve bioaugmented mainstream nitrification rates. Despite temperature differences, bioaugmentation has proven to be a successful strategy for improving nitrification rates in mainstream treatment systems. Stenström and la Cour Jansen (2016) showed sidestream bioaugmentation can increase mainstream nitrification rates by 25 to 58% at mainstream temperatures from 8 to 14°C. The sidestream reactor cultivated a different nitrifier community structure and increased nitrifier abundance, which influenced community and abundance in the augmented mainstream as well. Therefore, a nitrifier-enriching sidestream reactor has proven be a successful strategy to increase nitrification performance at full-scale.

Low SRT is still a challenge to successful bioaugmentation in existing BOD-only removal treatment systems due to retention time requirements of nitrifying organisms with slow growth rates. At lower temperatures the required SRT to achieve nitrification is higher (Tchobanoglous et al., 2014a). This exacerbates nitrification challenges for volume-limited systems. A

bioaugmentation study at low SRT and low temperature found bioaugmented nitrifiers were not adapted to colder temperatures and washed out due to the low-SRT condition (Abeysinghe et al., 2002). These results demonstrate bioaugmentation effectiveness on performance is limited by the existing system's SRT, especially at lower temperatures. Figdore et al. (2018b) suggested and demonstrated the use of aerobic granular sludge to address bioaugmentation limitations in low temperature and low SRT systems. They found that differences in morphology allowed separation of mainstream and sidestream particles after bioaugmentation and bioaugmented solids retained nitrifying populations responsible for NH_3 removal in the mainstream.

Bioaugmentation has been proven at full-scale as a viable option to improve nitrification and nitrogen removal performance. This strategy can be completed with different flow schemes, but the construction of a sidestream reactor for nitrifying bacteria production to treat anaerobic digester dewatering reject water is required. Therefore, limitations to bioaugmentation have traditionally been: 1) available construction space, 2) temperature differences between centrate stream and mainstream, and 3) low SRT of the mainstream system. A recent coupling of granular sludge and sidestream technology has the potential to uncouple SRT between bioaugmentation biomass and mainstream biomass (Figdore et al., 2018a), mitigating construction space and low SRT challenges (De Bruin et al., 2004).

3 Material and Methods

The KC WPTP consists of headworks for screening and grit removal, primary sedimentation, secondary treatment in a low-SRT, high purity oxygen activated sludge system, secondary clarification, and chlorination (hypochlorite) and dechlorination (sodium bisulfite) before discharge into the Puget Sound. Solids processing consists of belt filter thickening of blended primary and waste activated sludge, anaerobic digestion, and centrifuge biosolids dewatering. Dewatered biosolids are transported to either land application or a compost facility. The centrifuge effluent liquid stream, centrate, is returned to the plant headworks. Centrate was manually hauled from the dewatering building to the pilot area using 30 L plastic containers.

The pilot area is located in the KC WPTP testing facility building located across from the process laboratory and main control building. It is plumbed with WPTP dechlorinated secondary effluent, pressurized air, local tap water, and return heat. Return heat is exchanged from WPTP processes that generate excess heat. N_2 was supplied by Praxair in compressed gas cylinders (Guildford, United Kingdom). Cylinders were stored outside and adjacent to the pilot area and an N_2 gas line was fed into the building for pilot plant operations.

3.1 *Sidestream Treatment Reactor Description and Operation*

3.1.1 Reactor Description

The sidestream SBR (Figure 3-1) operating phases were anaerobic, aerobic, settling, decant, and idle. The reactor is a 10-ft tall, 12-in nominal diameter clear schedule 40 polyvinyl chloride column with an 8-ft liquid depth at full operating volume (176 L). The reactor column was

mounted onto a stainless-steel pedestal and had a PVC bottom; The reactor top was left open. A single metal strut channel was mounted across the top for securing probes and feed lines. A 9-in diameter EDI FlexAir^{TM} membrane disc diffuser was installed on the reactor bottom, centered with the reactor's cross-sectional area as shown in Figure 3-2 (Environmental Dynamics International, Columbia, Missouri, USA).

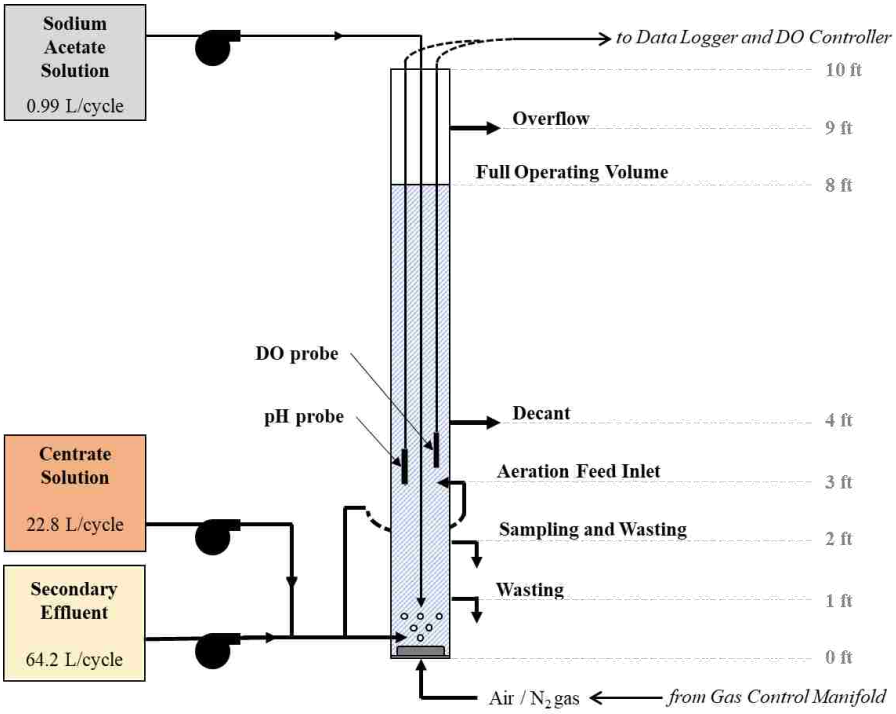

Figure 3-1. Sidestream sequencing batch reactor. Feed sources with typical feed volumes (left), installed equipment (center), and tap location and function (center/right) are shown but not-to-scale. A fine-bubble diffusser was installed on the reactor floor, and DO and pH probes were hung from the top.

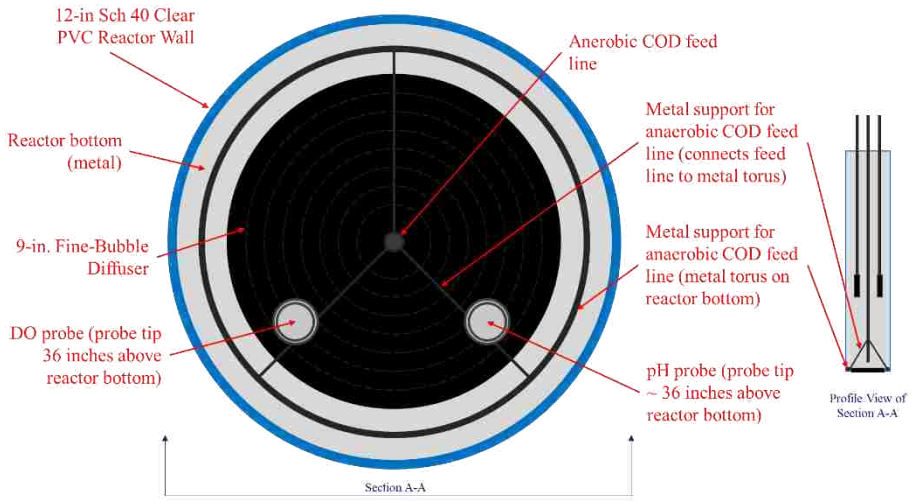

Figure 3-2. Sketch of diffuser, probes, and acetate feed line installation within sidestream reactor. The acetate feed line is installed parallel to probes and terminates above the diffuser. Three metal supports are attached to the feed line and connected to a metal torus to secure the feed line alignment at the bottom of the reactor. The feed line is also secured to a metal strut channel at the top of the reactor.

Decant and overflow taps were located 4 and 9 ft from the bottom, respectively. Half of the volume (88 L) was discharged from the reactor during decant for a 0.5 volume exchange ratio (VER). The decant flow was controlled by two values to control the time and duration of decant. One valve was controlled by a solenoid and opened fully during decant. The other valve was left open in a throttled orientation to control the decant flow rate. A float switch was installed below the 9-ft overflow tap, which if triggered stops the secondary effluent feed pump. Additional taps were installed at 1, 2, and 3 ft from the bottom of the reactor and were used for wasting, sampling, and aeration feed inlet, respectively. The 2-ft tap was occasionally used for manual wasting as well. Another aeration feed inlet tap was installed below the 1-ft tap, such that aeration feed was pumped simultaneously into the reactor via this and the 3-ft tap during centrate and secondary effluent feeding. A stainless-steel anaerobic COD feed line was plumbed into the reactor from the top and secured by the strut channel. The feed line terminated approximately 6 in above the fine-bubble diffuser and was aligned with the center of the cross-sectional area

(Figure 3-2). The acetate feed line was supported inside the reactor with three stainless steel supports connected to a torus laid flush on the reactor bottom around the diffuser.

3.1.2 Reactor Feed System

The SBR was fed 1) a sodium acetate solution for PAO growth, 2) screened anaerobic digestion dewatering centrate diluted with tap water for NH_3-N loading control, and 3) full-scale WPTP plant secondary effluent after chlorination and dechlorination. The ratio of the secondary effluent feed volume to the centrate solution feed volume was 2.8 to lower the sidestream reactor temperature to a similar range as in the mainstream system. Typical feed concentrations per cycle were 990 mL of acetate solution, 22.8 L of centrate solution, and 64.2 L of secondary effluent. Feed solutions were supplied with Masterflex® L/S® Series peristaltic pumps and tubing (Cole-Parmer® Instrument Company, Vernon Hills, Illinois, USA). Feed pumps were calibrated periodically and peristaltic Masterflex® tubing was replaced as necessary. Influent lines were a combination of flexible plastic and rigid stainless-steel tubing.

KC staff prepared and maintained the pilot reactor feed solutions. A sodium acetate solution was batched every one-to-four days in a 5-gallon plastic COD feed tank by dissolving $NaC_2H_3O_2$ into local tap water. A glacial acetic acid and sodium acetate solution, mixed at a 1:3 ratio based on acetate concentration was used from April 17 to May 9, 2019 to lower the pH during aeration phase below 8.0 to minimize AOB inhibition from free ammonia. Prior to this, the pH had rose above 8.5 when NH_3-N loading was increased to promote nitrification because higher alkalinity was added and not fully consumed by AOB. The COD feed tank was cleaned periodically to prevent growth.

Secondary effluent feed was pumped from the bottom top of a 100-gallon plastic tank. An influent tap at the top of the tank was plumbed to chlorinated and dechlorinated secondary effluent line. The tank was kept full using a float switch for filling during feed pumping into the SBR. A float switch was used to control the secondary effluent and stop the tank from overfilling. The tank was cleaned periodically.

Centrate feed solution was batched by every 1 to 7 days. Centrate was set for approximately 10-minutes to 1-hour to allow solids to settle before centrate supernatant was passed through a 0.425 mm sieve. Screened centrate was then added to a 100-gallon plastic reservoir and diluted with local tap water to achieve a desired NH_3-N concentration. After batching the centrate solution, the feed tank was mechanically mixed. Sodium bicarbonate was added to the centrate feed solution from January 18 to February 11, 2019 to account for the loss in alkalinity when local tap water was used in lieu of secondary effluent feed. Monobasic potassium phosphate (KH_2PO_4) was added to the centrate solution during startup so PAO growth would not be phosphorus limited as COD loading rates were increased to increase biomass production. This addition was continued at a dose of 50 g KH_2PO_4/100 gal after startup and was lowered incrementally to 20 g/100 gal. From October 23 to December 2, 2018 when there was no supplemental addition. The supplemental addition artificially increased the influent PO_4^{3-}-P load but accounted for less than 10% of influent PO_4^{3-}-P on average.

The centrate tank feed concentrations were based on measured concentrations from the centrate feed tank, where centrate was diluted with tap water dilution and added with KH_2PO_4 salt addition as necessary. Centrate feed samples were collected by KC after the batching of each

new centrate solution. Additional centrate and secondary effluent feed samples were collected and measured at UW once or twice a week. Averaged concentrations of centrate, prior to dilution and KH_2PO_4 salt addition, and secondary effluent feed are shown in Table 3-1. Volumetric loading rates and the ratio of COD to NH_3-N in the reactor feed are shown in Appendix A.

Table 3-1. WPTP centrate and secondary effluent concentrations for NH_3-N, PO_4^{3-}-P, and TSS measured in samples taken throughout this study.

Parameter	Units	NH_3-N	PO_4^{3-}-P	TSS	N:P Ratio
Centrate					
Average	mg/L	1200.1	164.1	1729.1	7.4
Standard Deviation	mg/L	156.3	24.2	1437.5	0.9
Number of Samples		71	71	53	71
Secondary Effluent					
Average	mg/L	31.3	2.4	4.4	13.7
Standard Deviation	mg/L	8.2	0.4	3.8	2.4
Number of Samples		129	129	105	129

3.1.3 Anaerobic Mixing, Aeration and Control

Gas Mixing. N_2 gas was sparged into the reactor fine-bubble diffuser to mix the reactor during the anaerobic phase. The fine-bubble diffuser was plumbed to a manifold used for gas control. All gas lines were constructed of stainless steel. The N_2 and air lines to a manifold had pressure regulators upstream of rotameters. Gilmont glass float rotameters with 86.95 L/min flow rate capacity at standard condition (1.0 atm and 70 °F, or 21.1°C) were used to controlled nitrogen gas and baseline air flow during the anaerobic and aeration phases, respectively (Vernon Hills, Illinois, USA). N_2 gas was directed to the reactor diffuser for mixing during the anaerobic period at 7.8 L/min (a reactor sparge rate of 2.66 m^3 N_2/hr per m^3 or superficial upflow velocity of 6.4 m/hr). Air was supplied during aeration with baseline flow typically 4-6 L/min. This equates to a

reactor sparging rate of 1.36-2.05 m^3/hr per m^3 and a superficial upflow velocity of 3.3-4.9 m/hr. Higher air flow rates were provided as needed to maintain the DO setpoint.

Aeration Control. The air supply and DO concentration was managed using a Moore Controller and proportional-integral (PI) algorithm (Moore Industries, North Hills, California, USA). DO values were averaged over a 60-second moving interval before being communicated to the More Controller algorithm. Additional air was provided at a rate proportional to the DO concentration in the bulk liquid and the DO setpoint concentration. For example, at a setpoint DO concentration of 2.0 mg/L the air flow rate was greater when the DO concentration was measured at 1.5 mg/L compared to when it was measured at 1.8 mg/L. A representative DO concentration profile during a SBR aeration phase is shown in Appendix A.

Online Monitoring. Online monitoring DO, pH, and temperature was measured using Hach® LDO® Model 2 and PHD sc probes for DO and pH, respectively (Loveland, Colorado, USA). Both probes also recorded temperature within the reactor. Probes were secured to the strut channel at the top of the reactor and hung so that sensors were approximately 3-ft from the reactor bottom. Data was communicated to a Hach® sc1000 module, which served as a data logging and control system for online measurements. The sc1000 processed data as a 60-second moving-average of instantaneous values measured by probes, then recorded moving-averages onto a secure digital (SD) card inside the sc1000 unit. The SD card was removed manually from the sc1000 and data was processed with an Excel® spreadsheet (Microsoft, Redmond, Washington). Minimum, maximum, and average values were calculated for DO, pH, and

temperature daily for anaerobic phases, aeration phases, and a full 24-hour period. Average daily values for online measurements are shown in Appendix A.

Probe Calibration. Probes used for online monitoring were calibrated according to the manufacturer's guidelines. Calibrations were checked with standards and in situ quality control checks, where Hach Intellical^{TM} LDO101 (DO) and HQD (pH) probes were inserted into the sidestream reactor to verify measurements. Quality control checks showed DO and pH measurements from online probes had a maximum variance of 15 and 2%, respectively, from calibrated LDO101 and HQD probes.

3.1.4 Sequencing Batch Reactor Operating Phases

A typical 6-hour reactor cycle is illustrated in Figure 3-3. Acetate feed occurred at the beginning of the anaerobic phase after 5 minutes of anaerobic mixing with N_2 gas. After 6 minutes of aeration diluted centrate and secondary effluent are fed for 15 minutes to bring the reactor to full volume. At the end of the aeration period a short settling time is used before decanting.

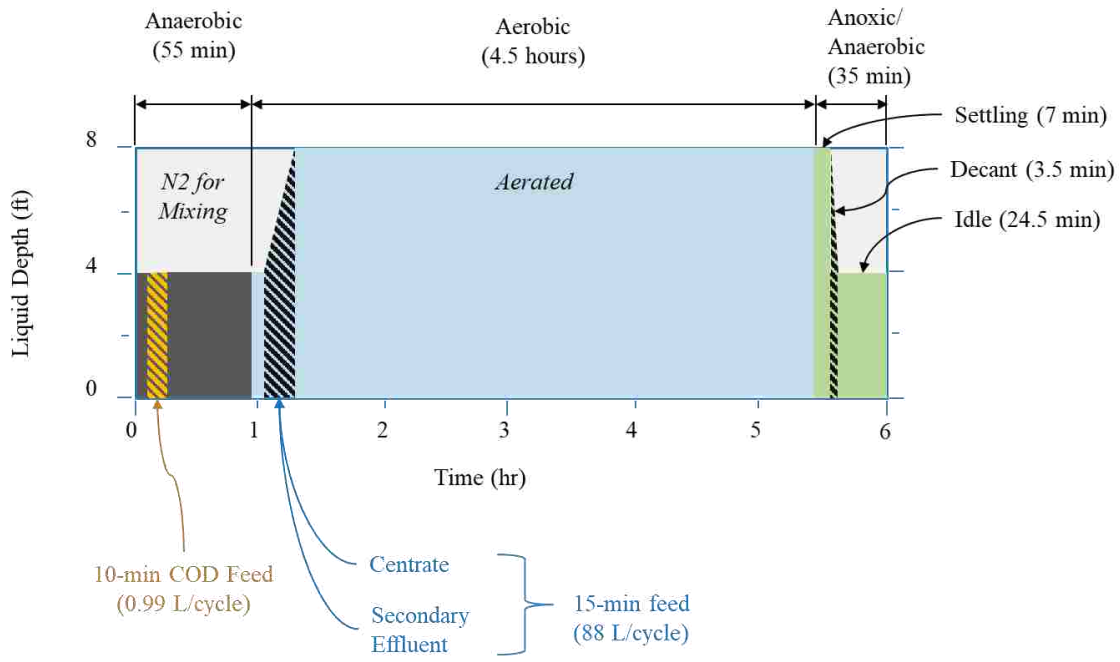

Figure 3-3. Typical 6-hour reactor cycle with phases and depths illustrated for anaerobic, aeration, settling, decant, and idle. Cycle time is shown on the x-axis in hours, and fill depth is shown on the y-axis in feet. The cycle starts half-full at the 4-foot depth. Each foot of depth is approximately 22 L.

The SBR cycle phases were controlled with ChronTrol® XT timers (San Diego, California, USA). Initially, the SBR cycle time was 4.0 hours and was increased to 6.0 hours after 74 days of operation (Table 3-2). Minor changes were made to the anaerobic phase length and COD feed duration, which was 10 minutes for most of the study (Table 3-3). The COD feed duration was temporarily increased to 30 minutes for a 40-day period to observe the effect on performance. The aeration phase was initially 2 hours per cycle (12 hours per day) but was increased by 30 minutes (15 hours per day) after a month of operations to promote nitrification. Aeration duration was increased again to 4.5 hours per cycle (18 hours per day) when the cycle length was increased to 6.0 hours. Centrate and secondary effluent feed length was 15 minutes and started 6 minutes after the start of the aeration phase. Settling time was decreased incrementally to select for larger granular particles with higher settling velocity (Table 3-4). On January 23, 2019 the

settling time was increased from 7 to 8 minutes to retain a greater portion of smaller granules during the decant phase. The settling phase was initiated after aeration when air was no longer supplied to the fine-bubble diffuser and mixing stopped. The decant phase was approximately 3.5 minutes. After decanting, the reactor remained in idle for additional denitrification to occur before the start of the next cycle.

Table 3-2. Major sequencing batch reactor cycle time changes and operating days.

Date of Change	Operation Length	Cycle Length	Anaerobic Phase	Aeration Phase	Settling, Decant, & Idle
	days	hrs	mins	mins	mins
2/24/2018	30	4	60	120	60
3/26/2018	44	4	55	150	35
5/9/2018	373	6	55	270	35

Table 3-3. Summary of time changes for the SBR anaerobic and aerobic phases.

Date of Change	Operation Length	Total Phase Length	Pre-Feed Mixing	Feed Duration	Post-Feed Reaction/Mixing
	days	mins	mins	mins	mins
Anaerobic Phase Changes (AN)					
2/24/2018	30	60	10	2	48
3/26/2018	22	55	5	2	48
4/17/2018	65	55	5	10	40
6/21/2018	40	55	5	30	20
7/31/2018	290	55	5	10	40
Aeration Phase Changes (OX)					
2/24/2018	30	120	6	15	99
3/26/2018	44	150	6	15	129
5/9/2018	373	270	6	15	249

Table 3-4. Summary of time changes for settling, decant, and idle in the SBR cycle.

Date of Change	Operation Length	Settling, Decant, & Idle	Settling	Decant	Idle
	days	mins	mins	mins	mins
2/8/2018	4	60	20	3.5	36.5
2/12/2018	9	60	18	3.5	38.5
2/21/2018	5	60	17	3.5	39.5
2/26/2018	7	60	16	3.5	40.5
3/5/2018	4	60	15	3.5	41.5
3/9/2018	7	60	14	3.5	42.5
3/16/2018	7	60	13	3.5	43.5
3/23/2018	3	60	10	3.5	46.5
3/26/2018	2	35	10	3.5	21.5
3/28/2018	2	35	9	3.5	22.5
3/30/2018	40	35	8	3.5	23.5
5/9/2018	259	35	7	3.5	24.5
1/23/2019	114	35	8	3.5	23.5

3.1.5 Reactor Startup and Seed Sludge

The KC South Treatment Plant (STP) MLSS was selected for the pilot seed sludge. Small-diameter granular-like particles were reported in EBPR continuous-flow treatment systems by Wei et al. (2019). They found granule solids in the mixed liquor in stereomicroscope observation and found that the mixed liquor contained semispherical solids greater than 0.212 mm sieve size which is the minimum sieve size defined for granular sludge (De Kreuk et al., 2007). The STP has an anaerobic/aerobic activated sludge secondary treatment process that accomplishes EBPR. The reactor was seeded to a settled sludge depth of 0.8 ft on February 8, 2018 with 0.425 mm screened recycle activated sludge from the KC STP. After a period of operating and design changes a second seeding was completed on February 24, 2018 with another batch of screened STP sludge. February 24, 2018 was considered “Day 0” of operations.

This sieving process was done on January 5, January 20, and February 24, 2018. Stereomicroscope images verified that retained particles had a semi-spherical morphology with smooth exterior (no filamentous or flocculent outgrowth on the surface area of granular particles), and 84% of the seed sludge was granular based on the 0.212 mm sieve criteria. Neisser staining, activity tests, DNA sequencing and polymerase chain reaction (PCR) analyses verified the presence of PAOs.

Initially, significant nitrification did not occur during aeration in the sidestream reactor, likely due to a lack of nitrifiers in the seed source. Thus, only the acetate COD feed concentration was increased for the first 59 days and the MLSS and net phosphorus removal increased. Monobasic potassium phosphate was added to the centrate feed tank during startup to promote PAO growth for enhanced granule formation. Supplemental phosphorus decreased as the centrate fraction in the influent feed increased. Settling time was incrementally decreased to wash out floc while increasing average granule size and MLSS.

The NH_3-N loading rate was increased more rapidly after 59 days of operation, and nitrification and nitrogen removal rates increased simultaneously. The aeration phase started at 12 hours per day on Day 0 and was increased to 15 and 18 hours per day after 30 and 74 days of operation, respectively. This strategy was implemented to first achieve desired granular sludge morphology for relatively fast settling particles before increasing nitrifier populations for desired nitrification and denitrification performance.

3.2 *Reactor Upsets and Determination of Relatively Stable Performance Periods*

Operations were adjusted as needed to maintain target loading and performance while minimizing impacts of upset events. Upsets were characterized as temporary, simultaneous decreases in nitrification, nitrogen removal, and anaerobic acetate removal. Inhibition from secondary effluent and centrate feed sources were suspected to cause irregular and uncontrollable process upsets. Two different inhibition test methods were conducted following upset periods to identify if feed solutions were responsible for the sudden decreased nitrification performance. The test methods compared relative oxygen uptake rates (OUR) or nitrification rates between sludge samples split into beakers with a control synthetic feed solution, secondary effluent solution, and centrate solution with equivalent initial NH_3-N concentration, DO, and pH. The nitrification comparison method was conducted from January 8, 2019 to January 22, 2019 and the OUR method was conducted from April 16, 2019 to May 9, 2019. These tests indicated potential for nitrification inhibition by both secondary effluent and centrate. The nitrification rate with secondary effluent was 54% of the rate with synthetic solution on January 14, which corresponded with a 55% decrease in NH_3-N oxidation in the sidestream reactor. The OUR with centrate was 52% of the rate with synthetic solution on May 2, 2019, which corresponded with only a 4% decrease in NH_3-N oxidation in the sidestream reactor. Further sampling and testing is needed to determine the main constituent(s) within influent solutions that cause upset events.

Equipment outages also created process upsets in 2018, from October 24 to November 2 (acetate pumping failure) and from December 8 to 10 (DO control failure). Following upsets, loading and solid wasting rates were decreased to minimize long-term impact of upset events on reactor

performance and granule morphology. Upsets obscured performance capacity, so a method was developed to determine periods of relatively stable operations and performance.

Operational periods where equipment outages and upset events reoccurred and impacted long-term morphology or performance were characterized as unstable. Instability was determined by assessing changes in subsequent measurements of loading rates, feed ratios, monitoring data, and removal efficiencies (Table 3-5). Stable periods are analyzed in this study and were determined as ranges where loading rates and monitoring data remained within the lower and upper bounds presented on Table 3-5. Five periods of relatively stable operations and performance were defined from this analysis. Periods of stability and upsets are shown in Table 3-6 with start and end dates, duration, and descriptions.

Table 3-5. Criteria and parameters assessed in determination of stable and unstable phases for nitrification performance.

Parameter	Units	Criteria[A]	Lower Bound	Upper Bound
Loading Rates				
Acetate-COD Loading Rate	g/L-d	% change[1]	-25%	25%
NH_3-N Loading Rate	g/L-d	% change	-25%	25%
PO_4^{3-}-P Loading Rate	g/L-d	% change	-25%	25%
Feed Ratios				
COD:NH_3-N	gCOD/gN	% change	-25%	25%
COD:PO_4^{3-}-P	gCOD/gP	% change	-25%	25%
NH_3-N:PO_4^{3-}-P	gN/gP	% change	-25%	25%
Monitoring Data (daily averages)				
Anaerobic pH		delta	-0.4	0.4
Anaerobic Temperature	°C	delta	-2.0	2.0
Aeration pH		delta	-0.4	0.4
Aeration DO	mg/L	delta	-0.2	0.2
Aeration Temperature	°C	delta	-2.0	2.0
Full Cycle pH		delta	-0.4	0.4
Full Cycle Temperature	°C	delta	-2.0	2.0
Removal Efficiency				
NH_3-N	%	% change	-10%	20%
Inorganic Nitrogen	%	% change	-10%	20%
PO_4^{3-}-P	%	% change	-10%	20%
SND	%	% change	-10%	20%
Anaerobic Acetate-COD	%	% removal	99%	100%

Notes:

[A] Relative criteria, noted by "% change" or "delta," indicates a percentage change or delta from the value of the previous day. Absolute criteria noted as "% removal" is based on individual, daily values.

Table 3-6. Periods identified during startup and long-term operation. Five periods of relatively stable operations and performance are identified. Upset and restart periods are also identified and described.

Period	Start Date	End Date	Days	Description / Notes
Initial Startup Period			*126*	
Pre-start	2/8/2018	2/23/2018	16	Reactor was seeded and operations were changed
Startup 1	2/24/2018	4/23/2018	59	MLSS increased and sludge became more granular
Startup 2	4/24/2018	5/29/2018	36	NH_3-N loading and nitrification rates increased
Restabilization	5/30/2018	6/29/2018	31	Recovery after loading-induced upset
"Full Study" Period, after Startup			*322*	
Full Study	6/30/2018	5/17/2019	322	All dates after the defined startup period
Periods of Relatively Stable Performance			*107*	
Period 1A	6/30/2018	7/30/2018	31	30-minute COD feed length; variable phosphorus removal
Period 1B	7/31/2018	9/11/2018	43	10-minute COD feed length; variable phosphorus removal
Period 1C	9/12/2018	9/27/2018	16	Performance relatively high and stable; DO variable
Period 2A	2/28/2019	3/16/2019	17	Small decrease in P & N removal from 3/4 to 3/8
Period 2B	4/26/2019	5/17/2019	22	Two minor dips in N removal performance
Periods of Unstable Operation and Performance			*137*	
Low NH_3-N	9/28/2019	10/5/2019	8	Lower NH_3-N feed due to equipment outage
Low Performance	10/8/2018	10/23/2018	16	Decreased and decreasing performance
Pump Failure	10/24/2018	11/27/2018	35	1.5 gal of acetate pumped into reactor
Re-Seeding Event	11/28/2018	1/4/2019	38	Poor performance; many filaments observed on granules
Period 2 Upset	3/17/2019	4/25/2019	40	Performance decrease and acetate leakage observed
Restart Period			*54*	
Restart	1/5/2019	2/27/2019	54	Restart

3.3 *Sampling and Analysis*

Sidestream samples for analytical measurements and batch tests were removed using the 2-ft tap. Prior to sampling, the tap was flushed with 200-300 mL of liquid from the reactor. This volume was either wasted from or returned to the sidestream reactor after the sampling period. Samples obtained from feed (centrate solution or secondary effluent) and decanted effluent tanks were grabbed with a plastic dipper. Samples from feed tanks were taken near tank outlets – directly before the influent pumping line. Effluent samples were obtained after manually mixing the effluent decant tank. An autosampler was programmed to collect samples from the effluent tank near the end of the decant period for composite effluent samples, which were used for effluent

alkalinity and composite effluent TSS measurements by the KC WPTP process laboratory. Granular particles settle rapidly and collected in the effluent tank, which was not well-mixed. Although the effluent tank was flushed regularly to remove settled solids, this may have led to sampling bias in composite effluent TSS measurements. Centrate feed tank samples were grabbed periodically after the aeration feed phase and consistently after each new centrate solution batch was mixed.

Samples that required suspended solids for analyses (metals, size distribution, TSS, VSS, and alkalinity) were stored at 4°C until analysis. Samples taken for determination of dissolved concentrations (inorganic nitrogen, orthophosphate, acetate) were filtered with a 0.45 µm syringe filter after being removed from the reactor, then stored at 4°C. A cooler and reusable frozen gel packs kept samples cold during transport to UW, where they were immediately analyzed or stored at 4°C until analysis. A UW researcher sampled from the sidestream reactor twice per week. These samples were analyzed within 24 hours. Additional filtered and centrate batch samples were collected by KC and stored on-site at 4°C until pickup by a UW researcher. These samples were stored for 24-to-72 hours before analysis. Results suggested that differences in holding times did not influence analytical measurements.

3.3.1 Sieve Analysis and Size Distribution

The distribution of particles sizes within sidestream MLSS was determined using a sieve analysis. Samples were passed through a series of 1.25-in tall, 3-in diameter sieves with various stainless-steel mesh size (Table 3-7). Sieves were stacked in order of decreasing mesh size from

top to bottom. A plastic beaker was fit to the bottom sieve to catch water and particles that passed through all meshes.

Table 3-7. List of nominal sieve sizes and the respective date each mesh was first used in the size distribution analysis.

Sieve Mesh[A]	Date	Sieve Mesh	Date	Sieve Mesh	Date
0.212 mm	2/24/2018	1.00 mm	7/9/2018	2.00 mm	3/29/2018
0.425 mm	2/24/2018	1.18 mm	3/29/2018	2.36 mm	3/29/2018
0.600 mm	2/24/2018	1.40 mm	3/29/2018	2.80 mm	11/6/2018
0.850 mm	2/24/2018	1.70 mm	7/9/2018	3.00 mm[B]	11/6/2018

Notes:

[A] Sieve mesh and body constructed in accordance with American Society for Testing and Materials Standard E11

[B] 3.00 mm mesh used from November 6 to December 8, 2018. No particles were retained on this sieve while in use for the size distribution analysis. Its use was discontinued on December 8, 2018.

A 500-mL sample was removed from the 2-ft tap into a glass beaker. Samples were removed when the reactor was half-filled and at high mixing intensity (7 to 100 L/min; 2.4 to 34.0 m^3/hr per m^3; 5.8 to 81.8 m/hr). The 500-mL sample was mixed on a stir plate and 10 to 30 mL was grabbed using a plastic pipette with a broken tip (approximately 2-cm diameter). Sample volume increased from approximately 10 mL to 30 mL as the range of particle size distributions increased to ensure at least 2.5 mg of solids would be retained on each sieve mesh during the analysis (Standard Method 2540 D).

The 10 to 30 mL sample was poured over the top of the sieve stack, onto the largest mesh. Particles on the top sieve were washed with deionized water from a wash bottle until all particles smaller than the sieve mesh were washed through to subsequent sieves. The top sieve was removed and retained particles were backwashed into a labelled plastic beaker. After completing this “wash, remove, and backwash” procedure for all sieve sizes, TSS and VSS were measured for each size range according to Standard Methods 2540 D and E. The particle size distribution

was determined by dividing the TSS of each size range by the TSS of the entire sample, as shown in Equation 3-1.

$$\text{Fraction of Mass for particle size range } (\text{FM}_n) = \frac{\text{TSS}_n}{\sum_1^n \text{TSS}_n} \quad (3\text{-}1)$$

Where:

TSS_n = mass retained on sieve n divided by total sample volume

The sum of square deviations from the mean (SSDM) was calculated to assess uniformity of granule size distributions, as shown in Equation 3-2. Smaller SSDM values correspond to more uniform size distributions and a perfectly uniform distribution is expected to have an SSDM value of zero.

$$\text{Sum of Squared Deviations from Mean (SSDM)} = \sum_1^n (\overline{\text{FM}_n} - \text{FM}_n)^2 \quad (3\text{-}2)$$

Where:

FM_n = fraction of sample total mass retained on sieve n

3.3.1.1 Average Granule Diameter and Granular Sludge Surface Density

Results from the size distribution analysis were used to compute the average granule diameter, or average size, and the surface area for particles in the sidestream reactor. The weighted average diameter was computed using the percentage of mass retained on each sieve multiplied by the average mesh size of the sieve the mass was retained on and the next larger sieve, as shown in Equation 3-3.

$$\text{Weighted average diameter of mixed liquor granules, mm} = \sum_{1}^{n} \mathrm{FM}_n(\mathrm{D_n}) \qquad (3\text{-}3)$$

Where:

n = sieve size sequence number

D_n = average size of opening of sieve n and sieve n-1, mm

The granular sludge surface area density was computed by multiplying the weighted average of surface area to volume ratios (SA/VOL) by the volume of granular sludge biomass (Equation 3-4). The SA/VOL for a given particle was calculated by simplifying particle morphology to an ideal sphere, including particles that passed through a 0.212 mm sieve. The MLSS was divided by measured granular sludge density to compute granule volume within the sidestream reactor. The granule size distribution (i.e. SA/VOL) and MLSS were measured at different frequencies, so interpolation was used to generate D_n and MLSS data such that the biofilm surface area could be calculated for any day of reactor operation.

$$\text{Granular Sludge Surface Area Density, } \frac{\mathrm{cm}^2}{L} = \left[\sum_{1}^{n} \mathrm{FM}_n \left(\frac{6}{D_n}\right)\right] \frac{\mathrm{MLSS}}{\rho} \qquad (3\text{-}4)$$

Where:

MLSS = mixed liquor concentration, g/L

ρ = average density of granular sludge MLSS, 1.03 g/cm^3

D_n = average size of opening of sieve n and sieve n-1, cm

3.3.2 Analytical Methods

The SVI, TSS, and VSS were measured according to the respective Standard Methods: 2710 D, 2540 D, and 2540 E. A 1.4-L Settleometer cylinder was used to determine SVI values at 5 and 30 minutes (Raven Environmental Products, St. Louis, Missouri, USA). Density was measured in duplicate with 25 and 16.2-mL pycnometers according to the protocol outlined in Experimental Methods in Wastewater Treatment (Van Loosdrecht et al., 2016).

Settling performance of granules was measured in situ by observing sludge blanket depth, or settled sludge volume, at 30-second intervals during the settling phase (Standard Method 2710 E). The top of the settled sludge was determined visually as the depth with greatest contrast between sludge concentration and supernatant. The sludge blanket interface was not well-defined during settling because of discrete settling characteristics of granules were such that smaller particles remained in the supernatant above the determined sludge blanket interface. The linear portion of these measurements were fit using a linear trendline in Excel® and had an $R^2 > 0.97$.

A ZEISS Stemi 508 stereomicroscope (Oberkochen, Germany) and Olympus BH-2 polarizing trinocular light microscope (Shinjuku, Tokyo, Japan) were used to view granular morphology. An axiocam ERc 5s microscope camera and ZEN lite software were used to capture and scale stereomicroscope images, and an Olympus digital camera was mounted to the light microscope for image capture. FUJI software was used to scale light microscope images from a micrometer (Schindelin et al., 2012).

Concentrations for inorganic nitrogen species (NH_3, NO_2^-, and NO_3^-) and PO_4^{3-} were measured using a Thermo Scientific™ Gallery™ Automated Photometric Analyzer. NH_3 was measured spectrophotometrically with a 660 nm wavelength and based on absorbance (ISO 7150). PO_4^{3-} and NO_2^- were measured similarly at a wavelength of 880 nm and 540 (SM 4500-P.E., SM 4500 NO2-N). NO_3^- was measured indirectly by reducing all NO_3^- to NO_2^- and measuring total oxidized nitrogen species, then subtracting the NO_2^- concentration of the same sample (SM 4500 NO3-N). A Thermo Scientific™ Dionex™ ion chromatography system (ICS) was used to measure acetate (Pfaff, 1993). Nutrient and acetate standards were batched from the appropriate salts (NH_4Cl, KH_2PO4, $NaNO_3$, $NaNO_2$, NaAc) and Milli-Q® ultrapure water (Resistivity = 18.2 MΩ-cm at 25°C). Alkalinity was measured according to Standard Method and was completed by the KC WPTP laboratory (Standard Method 2320 B).

Hach Intellical™ LDO101 and HQD probes were used to measure DO and pH, respectively, in batch activity tests. The LDO101 probe was a plastic-body laboratory model and the HQD probe was the rugged stainless steel-body model. Probes were operated and calibrated according to the manufacturer's guidelines. The DO probe was calibrated using a 1-point automatic air calibration method. The pH probe was calibrated with 3-point (4.01, 7.0, and 10.01) and 2-point (7.0 and 10.01) standard curves.

3.3.3 Relative Nitrification Activity at Saturated Dissolved Oxygen

Activity tests were conducted at saturated DO concentrations to determine maximum specific NH_3 and NO_2^- oxidation rates. MLSS was obtained from the sidestream reactor, diluted with secondary effluent, and spiked with a concentrated NH_3 solution in a 1000-mL glass beaker to

30-40 mg N/L. Compressed air was supplied via porous stone at a high rate of 4-8 L/min to ensure solids were well-mixed. DO, pH, and temperature were measured and recorded at 10 to 15-minute intervals over a 40 to 60-minute testing period. The temperature was measured with a non-mercury, spirit thermometer. Contents from the entire test beaker were blended after approximately an hour of aeration, then at least two 10-mL samples were pipetted for TSS and VSS analysis. Average testing temperatures and pH ranged from 11.6 to 20.7°C and 7.1 and 8.4, respectively. Initial NH_3 concentrations were typically between 30 and 40 mg N/L.

The NH_3 removal, NO_2^- production, and NO_3^- production rates (mg N/L-min) were determined by fitting a linear trend line (average R^2 of 0.98 ± 0.02) to data plotted in Excel®. Rates were corrected to 20°C using a temperature-activity coefficient of 1.072 (Melcer et al., 2003), then normalized to VSS concentration and reported as mg N/g VSS-hr. To compute NO_2^- production rate, the rate of NO_3^--N and NO_2^--N generation was added to account for NO_2^- produced prior to transformation to NO_3^-.

3.3.4 Effect of DO and Ammonia Concentration on Nitrification Kinetics

Batch tests were done using the pilot reactor MLSS to observe the effect of DO concentration on the nitrification kinetics. Results from these tests were used to obtain the apparent half-saturation coefficient for DO (K_{DO}). Batch tests were conducted in a 1-L glass beaker filled to approximately 500 mL. Temperature was controlled by adjusting the room's heat exchanger manually. Compressed air, carbon dioxide, and N_2 gas flows were controlled with dedicated Dwyer rotameters into a feed tube to a porous stone at the bottom of the glass beaker (Michigan City, Indiana, USA). Rotamers had 5.0, 1.0, and 0.1 L/min capacity at standard condition and

used to adjust gas flow as necessary to achieve desired DO, pH, and mixing setpoints. Carbon dioxide assisted with pH control, and N_2 and air flows were adjusted to achieve identical mixing energy at different DO concentrations. The combined gas flow rate was constant for each batch test at a rate that provided adequate mixing, determined by visual observation. Sample collection involved no gas sparging for 15-30 seconds before using a 5-mL syringe to remove approximately 3 mL of supernatant. Supernatant within the syringe was immediately filtered by a 0.45 µm filter into a 15-mL falcon tube and stored in an insulated container with ice packs.

Three bench tests were completed to determine K_{DO}. Test conditions used a constant mixed gas flow of 6 L/min with air and N_2 flows adjusted to control DO concentrations to 1.0, 2.0, 3.0, and 6.0 mg/L. The initial NH_3-N concentration ranged from 44-80 mg/L and was maintained above 20 mg/L by adding 1 g HCO_3NH_4-N/L solution between changes in DO setpoints. Sample frequency was at 10 or 20-minute intervals Test temperatures were maintained within a range of 1.1-2.7°C, with average test values of 18.2, 16.8, and 15.2°C. Batch test pH values ranged from 7.2-7.6 with a maximum range of 0.2 on any given test date. DO was controlled such that standard deviations were 0.0, 0.0, 0.1, and 0.2 mg/L for target DO values of 1.0, 2.0, 3.0, and 6.0 mg/L. Detailed recordings for one of the three K_{DO} batch tests was used to assess the standard deviation from target DO setpoints.

Data was processed by fitting a linear trendline in Excel® and using the slope to determine NH_3 removal rates. NH_3 oxidation rates were assumed as identical to NH_3 removal for simplicity. Rates were corrected to 20°C using 1.072 temperature coefficient and reported as mg N/g VSS-hr. The final VSS concentration was measured after testing and used to calculate SNRs at each

DO setpoint. Rates for each DO setpoint were averaged between tests. Average SNRs for each DO condition were used to fit a K_{DO} value and maximum SNR using the Michaelis-Menten Equation shown in Equation 2-2 (Michaelis and Menten, 1913). The Excel® solver program was used to determine these parameters.

3.3.5 Anaerobic Acetate Removal Kinetics

Acetate-COD concentrations were measured during the anaerobic phase in the sidestream reactor. In situ acetate concentrations were measured as mg COD/L in 2.5 to 10-minute intervals. Linear specific acetate uptake rates (SAURs) were determined using a linear fit in Excel® to determine the rate of COD removal and the measured MLVSS during the aeration phase. It was assumed that the anaerobic MLVSS concentration was double the concentration measured at full-volume depth during aeration. SAURs were reported as mg COD/g VSS-hr.

3.3.6 Quantitative Polymerase Chain Reactor and Sequencing

Bao Nguyen Quoc, a UW PhD Candidate, conducted all qPCR and sequencing-related analyses for this project. Samples were collected regularly to characterize relative abundance of microorganisms of interest using the quantitative polymerase chain reaction (qPCR) and microbial ecology using sequencing techniques. Samples were centrifuged at 13,200 relative centrifugal force for two minutes in an Eppendorf 5415D Centrifuge (Hamburg, Germany). A pellet was formed, supernatant was removed, and the remaining sample was frozen at -80°C until DNA extraction. DNA was extracted using DNeasy PowerBiofilm Kit in accordance with the manufacture's guidelines (Qiagen, Hilden, Germany).

qPCR was used to determine relative fractions of target organisms. Primers were selected for specific genes relevant to target organisms, which were AOB, NOB, PAOs, GAOs, and total bacteria (EUB) (Table 3-8). Abundance of AOB, NOB, PAOs, and GAOs were determined by dividing gene copy numbers from each respective group by the EUB gene copy number for each sample. Ratios of AOB to NOB and PAO to GAO were computed by dividing gene copy numbers of AOB by NOB and PAO by GAO, respectively. PCR was completed prior to qPCR to verify presence or absence of targeted organisms. The amoA gene was targeted to quantify AOB abundance, and the nxrB gene was used for *Nitrospira*, which was equated to NOB abundance (no other NOB were detected in PCR). The 16S rRNA gene of *Candidatus Accumulibacter phosphatis* and *Candidatus Competibacter phosphatis* were targeted to quantify PAO and GAO abundances, respectively. Three qPCR runs were completed for each sample, from which average values and standard deviations were calculated. Standards were prepared by Bao Nguyen Quoc, a UW PhD candidate, using TOPO™ TA Cloning™ Kit to clone genes of interest into plasmids, which were transferred into E. Coli (Waltham, Massachusetts, USA).

Sequencing was outsourced to MR DNA (Molecular Research) Laboratory (Shallowater, Texas, USA). Samples were run in a single-step 30-cycle PCR with 515F and 806R primers to target the 16S rRNA V4 gene. Sequencing was completed on an Ion Torrent™ Personal Genome Machine™. Sequencing data was processed MR DNA and prepared by Bao Nguyen Quoc. A 97% similarity was used to cluster and define operational taxonomic units.

Table 3-8. List of target organisms and primers used for qPCR. Adapted from presentation by Bao Nguyen Quoc, UW PhD Candidate.

Organism(s)	Primer Target	Primer(s)	Reference
AOB	amoA gene	amoA-1F amoA-2R	(Rotthauwe and Witzel, 1997)
NOB (*Nitrospira*)	nxrB gene	nxrB169F nxrB638R	(Pester et al., 2014)
PAOs	*Candidatus Accumulibacter* 16S rRNA gene	PAO651f PAO846r	(Fukushima et al., 2007)
GAOs	*Candidatus Competibacter* 16S rRNA gene	GAO-Gbf GAO-Gbr	(Fukushima et al., 2010)
General Bacteria (EUB)		515F-Y 926R	(Parada et al., 2016)

3.4 *Calculations*

Additional calculations were performed to determine removal efficiencies and the SRT. Removal efficiencies for NH_3-N, TIN, PO_4^{3-}-P, and Acetate-COD were calculated as displayed in Equation 3-5. The SND efficiency was calculated as shown in Equation 3-6. To calculate ammonia oxidized (NH_3-$N_{oxidized}$), ammonia removal via synthesis was subtracted from total ammonia removal as shown in Equation 3-7. Ammonia removal via synthesis was calculated as shown in Equation 3-8. Ammonia oxidation, total removal, and removal via synthesis were normalized to influent and effluent volumes for calculations.

$$\text{Removal Efficiency, \%} = \frac{(C_i \times V_i) - (C_e \times V_e)}{(C_i \times V_i)} \times 100\% \quad (3\text{-}5)$$

Where:

C_i = influent concentration of constituent, mg/L

C_e = effluent concentration of constituent (end-of-anaerobic for acetate), mg/L

V_i = corresponding influent volume, mg/L

V_e = effluent volume (or end-of-anaerobic concentration for acetate), mg/L

$$\text{SND Efficiency, \%} = \frac{\text{NH}_3\text{-N}_{\text{oxidized}} - (\text{NO}_2^-\text{-N} + \text{NO}_3^-\text{-N})}{\text{NH}_3\text{-N}_{\text{oxidized}}} \quad (3\text{-}6)$$

Where:

$NH_3\text{-}N_{oxidized}$ = ammonia oxidized during aeration phase, mg N/L

$NO_2^-\text{-}N_e$ = Effluent nitrite concentration, mg/L

$NO_3^-\text{-}N_e$ = Effluent nitrate concentration, mg/L

$$\text{NH}_3\text{-N}_{\text{oxidized}}, \text{mg N/L} = \text{NH}_3\text{-N}_{\text{i}} - \text{NH}_3\text{-N}_{\text{synthesis}} - \text{NH}_3\text{-N}_{\text{e}} \quad (3\text{-}7)$$

Where:

$NH_3\text{-}N_i$ = influent ammonia concentration, mg N/L

$NH_3\text{-}N_e$ = effluent ammonia concentration, mg N/L

$$\text{NH}_3\text{-N}_{\text{synthesis}}, \text{mg N/L} = \text{COD}_{\text{i}} \times 0.12 \frac{\text{mg N}}{\text{mg VSS}} \times 0.12 \frac{\text{mg VSS}}{\text{mg COD}} \quad (3\text{-}8)$$

Where:

COD_i = influent COD concentration, normalized to 88 L/cycle influent flow rate, mg/L

Weekly averages were necessary to observe meaningful SRT trends because manual wasting was not conducted on weekends, therefore a seven-day moving average was used to monitor SRT. The SRT was calculated as shown in Equation 3-9.

$$\mathrm{SRT}_n,\ \mathrm{days} = \frac{\frac{1}{n}\sum_{i=1}^{n}(\mathrm{MLSS}_i)}{\frac{1}{n}\sum_{i=1}^{n}\left(\mathrm{WAS}_{\mathrm{full,i}}(\mathrm{MLSS}_i) + \mathrm{WAS}_{\mathrm{half,i}}(\mathrm{MLSS}_i \times 2) + Q_{\mathrm{out,i}}(C_{\mathrm{out,i}})\right)} \quad (3\text{-}9)$$

Where:

SRT_n = n-day moving-average solids retention time, days

$MLSS_i$ = mixed liquor suspended solids, mg/L

$WAS_{full,i}$ = waste activated sludge volume at full reactor volume, L

$WAS_{half,I}$ = waste activated sludge volume at half-volume, L

$Q_{out,I}$ = Effluent flow per day, L/d

$C_{out,I}$ = Effluent concentration, mg/L

The P/C ratio was computed to compare the amount of phosphorus released during the anaerobic phase to the amount of carbon stored by PAOs and GAOs. This calculation accounted for carbon used by residual NO_X-N and is shown in Equation 3-10.

$$\text{P/C Ratio} = \frac{\left((\mathrm{PO_{4i}} - \mathrm{PO_{4f}}) \times \mathrm{V_r} \times 0.5\right) / \left(30.973 \frac{\mathrm{mgP}}{\mathrm{mmolP}}\right)}{\left(\mathrm{NaAc_{feed}} \times \frac{0.99\mathrm{L}}{\mathrm{cycle}} \times 0.78 - \left(COD_f + \mathrm{NO_X\text{-}N_{AN}} \times 6\right) \times \left(\frac{88\mathrm{L}}{\mathrm{cycle}}\right)\right) / \left(0.78 \times 82.03 \frac{\mathrm{mgNaAc}}{\mathrm{mmolNaAc}} \times \frac{1\ \mathrm{mmolNaAc}}{2\ \mathrm{mmolC}}\right)} \quad (3\text{-}10)$$

Where:

P/C Ratio = ratio of phosphorus released, and carbon stored, mol P/mol C

PO_{4i} = PO_4^{3-}-P concentration during anaerobic phase before feed, mg P/L

PO_{4f} = PO_4^{3-}-P concentration at the end of the anaerobic phase, mg P/L

$NaAc_{feed}$ = feed concentration of sodium acetate tank, mg NaAc/L

COD_f = acetate concentration at the end of the anaerobic phase, mg COD/L

NO_X-N_{AN} = NO_2^- and NO_3^- concentration at start of anaerobic phase, mg N/L

Ratios of COD to nitrogen are compared as metrics for the system supplemental COD addition, performance efficiency, and denitrification efficiency. These ratios are the COD:N feed ratio (COD:N), COD:TIN removed ratio (COD:Nr), and COD:NO_X-N removed ratio (COD:NOr) and are displayed in Equations 3-11, 3-12 and 3-13, respectively. The ratios are based only on inorganic nitrogen and assumes that conversion of organic nitrogen in the centrate and secondary effluent feeds is minimal. The TIN removed is equal to the influent NH_3-N in g/d minus the sum of the effluent NH_3-N, NO_3-N and NO_2-N in g/d. For the COD:NOr ratio the amount of NO_X removed is based on an estimate of the NO_X produced (NH_3-N oxidized) minus the amount of NO_X in the effluent. The amount of NH_3-N oxidized is equal to the difference between the influent and effluent NH_3-N minus the amount of NH_3-N used for biomass synthesis. The amount NH_3-N estimated to be used for biomass synthesis as shown by Equation 3-8 is equal to an assumed net biomass yield for the PAOs/GAOs consuming the influent acetate in g VSS/g COD and an assumed nitrogen content of the biomass of 0.12 g N/g VSS. A ratio of 0.78 grams COD per 1-gram sodium acetate was used to convert the sodium acetate feed solution into units of COD and 6 grams of COD were assumed for utilization of the sodium acetate feed by denitrification of each gram of residual NO_X-N during the anaerobic phase.

$$\text{COD:NH}_3\text{-N Feed Ratio, g COD/g N} = \frac{\text{NaAc}_{\text{feed}} \times \left(\frac{0.99\text{L}}{\text{cycle}}\right) \times 0.78}{\text{NH}_3\text{-N}_{\text{i}} \times \left(\frac{88\text{L}}{\text{cycle}}\right)} \qquad (3\text{-}11)$$

$$\text{COD:TIN Removed (COD:Nr) Ratio, g COD/g N} = \frac{\text{NaAc}_{\text{feed}} \times (\frac{0.99\text{L}}{\text{cycle}}) \times 0.78}{\left(\text{NH}_3\text{-N}_i - \left(\text{NH}_3\text{-N}_e + \text{NO}_x\text{-N}_e\right)\right) \times (\frac{88\text{L}}{\text{cycle}})} \quad (3\text{-}12)$$

Where:

NO_X-N_e = effluent NO_2-N and NO_3-N concentration, mg N/L

$$\text{COD:NO}_X\text{-N Removed Ratio (COD:NOr Ratio), g COD/g N} = \frac{\text{NaAc}_{\text{feed}} \times \left(\frac{0.99\text{L}}{\text{cycle}}\right) \times 0.78 \times (\frac{88\text{L}}{\text{cycle}})}{\left(\text{NH}_3\text{-N}_{\text{oxidized}} - \left(\text{NO}_X\text{-N}_{\text{eff}}\right)\right) \times (\frac{88\text{L}}{\text{cycle}})} \quad (3\text{-}13)$$

4 Sidestream Treatment Operation and Performance

The sidestream reactor operation and performance period addressed in this document summarizes the continuously operational reactor performance over a duration of about 10.5 months from June 30, 2018 to May 17, 2019. This duration is referred to as the full operating period and does not include data from the 126-day start up period from February 24, 2018 to June 29, 2018. For 6 weeks prior to February 24, 2018 the reactor operation was tested, and modifications were made for the feed system, decant time, sample taps, and cycle step times. A summary of operating conditions and performance, including upset and stable conditions, is shown in Table 4-1 for the 10.5-month period.

Table 4-1. Average of operation and performance parameters for the approximately 10.5-month continuous operating period from June 30, 2018 to May 17, 2019 (standard deviations shown in parenthesis).

Parameter	Units	Average and Std. Dev.
MLSS	g/L	11.4 (1.9)
MLVSS/MLSS		0.76 (0.05)
SVI_{30}	mL/g	32 (5)
SVI_5/SVI_{30}		1.05 (0.10)
7-day Moving Average SRT	days (d)	34 (12)
Loading		
Acetate as COD	g/L-d	1.34 (0.37)
NH_3-N	g/L-d	0.38 (0.07)
PO_4^{3-}-P	g/L-d	0.06 (0.01)
Feed COD:N Ratio	g/g	3.7 (1.1)
Removal Efficiency		
NH_3-N	%	84 (19)
TIN	%	78 (16)
SND	%	94 (6)
PO_4^{3-}-P	%	51 (99)
Effluent		
NH_3-N	mg/L	30.2 (36.0)
NO_2^--N	mg/L	2.8 (5.2)
NO_3^--N	mg/L	7.0 (8.7)
PO_4^{3-}-P	mg/L	13 (26)
pH		7.4 (0.3)
Alkalinity	mg $CaCO_3$/L	592.7 (140.0)
COD:Nr Ratio	g/g	4.3 (2.9)
Dissolved Oxygen, pH, and Temperature		
Aeration Phase DO	mg/L	2.6 (0.6)
Aeration Phase pH		7.5 (0.2)
Anaerobic Phase pH		7.3 (0.2)
Temperature	°C	20.1 (2.4)
Granule Characteristics		
Average Diameter	mm	1.4 (0.2)
Density	g/cm^3	1.03 (0.00)

The average pH was 7.5 ± 0.2 during the aeration phase. The pH values in the anaerobic phase were about 0.2 units lower. Different DO concentration aeration control set points were used at different operating times in attempts to optimize nitrification and SND efficiency. These set points ranged from 1.5 mg/L to 2.5 mg/L, and the average DO concentration for the entire 10.5-month period was 2.6 ± 0.6 mg/L. Due to seasonal changes the reactor temperature ranged from 11.3 to 24.8°C and averaged 20.1 ± 2.4°C.

The NH_3-N loading rate averaged 0.38 ± 0.07 g/L-d and the acetate COD loading averaged 1.34 ± 0.37 g/L-d. The average COD:N feed ratio was 3.7 ± 1.1 g/g and the average COD:Nr ratio was 4.3 ± 2.9 g/g. The NH_3-N and TIN removal efficiencies averaged 84 ± 19% and 78 ± 16%, respectively. The average SND efficiency was higher at 94 ± 6% and more consistent than NH_3-N and TIN removal performance. Only inorganic nitrogen was measured in this study and it is likely that total nitrogen removal was higher due to possible release of organic nitrogen in the centrate feed.

Effluent alkalinity averaged 592.7 ± 140.0 mg $CaCO_3$/L, which was well above the threshold value of 60 mg $CaCO_3$/L (Tchobanoglous et al., 2014a) considered adequate to provide a pH of at least 6.8 and uninhibited nitrification with respect to pH. No supplemental alkalinity was required throughout the study because of the good SND performance. The high SND efficiencies also resulted in a relatively low average effluent NO_X-N concentration of 9.7 ± 10.1 mg/L. Minimizing effluent reactor NO_X-N was an objective to minimize the recycle impact on performance of the mainstream.

The average long-term PO_4^{3-}-P removal efficiency was 51 ± 99%. Compared to nitrogen removal, PO_4^{3-}-P removal was lower and more variable than inorganic nitrogen removal, but this did not appear to impact nitrogen removal, which remained stable through periods of variable PO_4^{3-}-P removal. The high standard deviation in PO_4^{3-}-P removal was affected, in part, by days with higher anaerobic PO_4^{3-}-P release than aerobic uptake and thus a higher effluent than influent concentration, and negative removal. This was observed ten times during long-term operation.

Unexpected performance upsets characterized by a decrease in EBPR and/or nitrification efficiency occurred periodically during the 10.5-month period and more notably from October 24, 2018 to January 4, 2019. Most upsets were suspected to be caused by inhibiting substances in the centrate and/or the chlorinated and dechlorinated secondary effluent. However, on two occasions it was related to equipment failures that occurred on October 24 and December 8, 2018. A typical consequence of an upset was incomplete acetate consumption in the anaerobic phase and leakage to the aeration phase causing filamentous organisms to grow on granules and an increase in flocculent particles. Manual wasting and SRT control were stopped in response to upsets until performance was returned to loading rates and removal efficiencies prior to the upset. Considering only average values obtained during the long-term operation results in an incomplete assessment of the sidestream aerobic granular sludge reactor treatment characteristics and capacity. Five stable performance periods were determined based on the operational and performance stability analysis described in the methods section.

These periods are designated as 1A, 1B, 1C, 2A and 2B. Periods 1A, 1B, and 1C occurred consecutively and before a 93-day low-performance and upset period from September 28, 2018 to January 4, 2019. Periods 2A and 2B followed a 55-day restart period from January 5 to February 27, 2019, and a 40-day period of decreased performance occurred due to upsets between periods 2A and 2B. A chronology of the reactor operation and different periods is listed below in Table 4-2.

Table 4-2. Chronological list of operating periods with start and end dates and total duration in days.

Period	Start Date	End Date	Length (days)
Startup	February 24, 2018	May 29, 2018	95
Stabilization	May 30, 2018	June 29, 2018	31
Period 1A	June 30, 2018	July 30, 2018	31
Period 1B	July 31, 2018	September 11, 2018	43
Period 1C	September 12, 2018	September 27, 2018	16
Upset	September 28, 2018	January 4, 2019	99
Restart	January 5, 2019	February 27, 2019	54
Period 2A	February 28, 2019	March 16, 2019	17
Upset	March 17, 2019	April 25, 2019	40
Period 2B	April 26, 2019	May 17, 2019	22

Distinct operating conditions between periods was useful to assess reactor performance at different feeding durations, loading rates, and DO setpoints. Period 1A had a 30-minute COD feed duration while every other period was fed for 10 minutes. Period 1B is operated at a similar DO (2.0 compared to 1.9 mg/L) and NH_3-N loading rate (0.36 compared to 0.36 g NH_3-N/L-d) compared to Period 1A, but with a shorter feed duration and seven percent higher COD:N feed ratio (4.5 compared to 4.2 g/g). In Period 1C, the average DO was more variable (0.3 compared to 0.1 mg/L standard deviation) and higher (2.8 compared to 1.9-2.0 mg/L average) than Periods 1A and 1B, yet relatively stable NH_3-N and TIN removal was achieved at an average NH_3-N loading rate of 0.40 g/L-d. Periods 2A and 2B had 10-28% higher NH_3-N loading rates and 10-78% lower COD:N feed ratios compared to Periods 1A, 1B, and 1C. In addition to the operating changes noted, SRT, PO_4^{3-}-P removal efficiency, and average granule diameter varied between these stable performance periods.

A summary of the average operating conditions and performance or these five defined stable operating periods is shown in Table 4-3. Average removal efficiencies for NH_3-N and TIN during stable periods were at least 12% and 8% higher, respectively, than average values for the 10.5-month period. The SND efficiency varied between 85 and 96% during the stable periods,

compared to the average SND efficiency of 94 ± 6% for the full period. Therefore, it appears decreased nitrification was the limiting factor for TIN removal during upset events and not denitrification or SND efficiency. Key differences between operations and performance from the periods in Table 4-3 are discussed further in later Results sections. A summary of average operating conditions and performance during upset periods is provided below in Table 4-4.

Table 4-3. Average operation and performance values for five defined stable operating periods (standard deviations displayed in parenthesis).

Parameter	Units	Period 1A	Period 1B	Period 1C	Period 2A	Period 2B
Duration	days (d)	31	43	16	17	22
MLSS	g/L	13.6 (0.6)	12.4 (0.3)	12.6 (1.2)	13.0 (0.8)	12.8 (1.0)
MLVSS/MLSS		0.73 (0.01)	0.74 (0.02)	0.76 (0.02)	0.67 (0.02)	0.71 (0.01)
SVI_{30}	mL/g	38 (2)	30 (3)	26 (2)	31 (2)	26 (2)
SVI_5/SVI_{30}		1.01 (0.01)	1.01 (0.01)	1.00 (0.00)	1.01 (0.00)	1.02 (0.02)
7-day Moving Average SRT	d	40 (12)	31 (3)	26 (1)	23 (3)	27 (8)
Loading						
Acetate as COD	g/L-d	1.49 (0.00)	1.62 (0.08)	1.67 (0.00)	1.76 (0.00)	1.28 (0.06)
NH_3-N	g/L-d	0.36 (0.04)	0.36 (0.03)	0.40 (0.02)	0.46 (0.01)	0.44 (0.02)
PO_4^{3-}-P	g/L-d	0.06 (0.01)	0.06 (0.01)	0.07 (0.00)	0.06 (0.00)	0.06 (0.00)
COD:N Feed Ratio	g/g	4.2 (0.4)	4.5 (0.3)	4.2 (0.2)	3.8 (0.1)	2.9 (0.2)
Removal Efficiency						
NH_3-N	%	99 (2)	98 (3)	96 (5)	98 (3)	96 (5)
TIN	%	86 (4)	94 (3)	88 (6)	88 (4)	90 (6)
SND	%	85 (3)	96 (3)	91 (6)	89 (4)	93 (4)
PO_4^{3-}-P	%	70 (24)	57 (43)	29 (75)	98 (2)	95 (11)
Effluent						
NH_3-N	mg/L	2.1 (3.2)	3.8 (6.7)	8.8 (9.9)	4.7 (6.5)	9.9 (11.2)
NO_2^--N	mg/L	12.1 (10.7)	0.2 (0.2)	0.6 (0.3)	2.1 (2.8)	2.5 (2.0)
NO_3^--N	mg/L	11.2 (7.8)	6.3 (4.7)	14.9 (11.3)	21.2 (7.1)	10.4 (9.2)
PO_4^{3-}-P	mg/L	8.3 (6.3)	13.5 (14.0)	24.0 (26.6)	0.09 (0.00)	0.07 (0.00)
pH		7.3 (0.3)	7.8 (0.2)	7.3 (0.4)	7.2 (0.1)	7.2 (0.2)
Alkalinity	mg CaCO3/L	483.8 (82.1)	565.5 (55.7)	572.0 (116.1)	542.9 (39.3)	547.4 (39.0)
COD:Nr Ratio	g/g	5.0 (0.3)	4.8 (0.4)	4.7 (0.3)	4.3 (0.2)	3.2 (0.3)
Dissolved Oxygen, pH, and Temperature						
Aeration Phase DO	mg/L	1.9 (0.1)	2.0 (0.1)	2.8 (0.3)	3.1 (0.2)	2.3 (0.2)
Aeration Phase pH		7.5 (0.2)	7.7 (0.0)	7.5 (0.1)	7.4 (0.1)	7.4 (0.1)
Anaerobic Phase pH		7.1 (0.2)	7.5 (0.0)	7.5 (0.1)	7.1 (0.0)	7.1 (0.1)
Temperature	°C	22.8 (1.3)	21.7 (1.1)	19.2 (0.6)	20.9 (1.9)	20.5 (1.1)
Granule Characteristics						
Average Granule Diameter	mm	1.3 (0.1)	1.1 (0.1)	1.3 (N/A[A])	1.5 (N/A)	1.4 (N/A)
Density	g/cm^3	N/A	1.03 (0.00)	1.03 (0.00)	1.03 (N/A)	N/A

Note: [A] Standard deviation not available (N/A) when only one data point was acquired

Table 4-4. Average operation and performance values for four upset and unstable performance periods (standard deviations in parenthesis).

Parameter	Units	Upset Period 1	Upset Period 2	Idle Operations	Restart Period
Duration	d	61	40	38	54
MLSS	g/L	10,900 (1,500)	11,500 (1,000)	10,300 (1,800)	8,900 (1,600)
MLVSS/MLSS		0.83 (0.02)	0.76 (0.04)	0.78 (0.06)	0.76 (0.05)
SVI_{30}	mL/g	29 (3)	30 (2)	36 (4)	38 (3)
SVI_5/SVI_{30}		1.01 (0.01)	1.00 (0.01)	1.19 (0.20)	1.13 (0.12)
7-day Moving Average SRT	d	32 (12)	29 (10)	44 (17)	40 (10)
Loading					
Acetate as COD	g/L-d	1.46 (0.25)	1.41 (0.35)	0.78 (0.32)	1.06 (0.33)
NH_3-N	g/L-d	0.40 (0.09)	0.43 (0.06)	0.29 (0.04)	0.33 (0.07)
PO_4^{3-}-P	g/L-d	0.06 (0.01)	0.06 (0.01)	0.04 (0.01)	0.05 (0.01)
COD:N Feed Ratio	g/g	4.0 (1.7)	3.4 (1.2)	2.6 (0.9)	3.3 (0.5)
Removal Efficiency					
NH_3-N	%	73 (19)	79 (13)	67 (24)	82 (18)
TIN	%	67 (15)	76 (12)	63 (21)	77 (16)
SND	%	98 (3)	96 (4)	92 (9)	94 (5)
PO_4^{3-}-P	%	32 (160)	55 (67)	0 (176)	61 (47)
Effluent					
NH_3-N	mg/L	59.9 (46.8)	47.0 (29.9)	49.6 (40.2)	27.6 (27.3)
NO_2^--N	mg/L	1.4 (2.0)	4.5 (7.1)	1.9 (1.7)	2.0 (2.5)
NO_3^--N	mg/L	1.5 (3.1)	2.0 (3.2)	6.1 (7.9)	6.5 (9.8)
PO_4^{3-}-P	mg/L	21.8 (49.6)	13.2 (18.4)	17.7 (28.9)	9.5 (11.1)
pH		7.7 (0.2)	7.3 (0.3)	7.2 (0.2)	7.3 (0.2)
Alkalinity	mg CaCO3/L	691.5 (180.9)	663.7 (139.2)	519.9 (196.5)	596.2 (127.7)
COD:Nr Ratio	g/g	5.3 (1.2)	4.4 (1.6)	2.6 (7.3)	4.5 (1.4)
Dissolved Oxygen, pH, and Temperature					
Aeration Phase DO	mg/L	2.9 (0.6)	2.3 (0.4)	3.1 (1.0)	2.9 (0.2)
Aeration Phase pH		7.7 (0.1)	7.4 (0.1)	7.3 (0.2)	7.5 (0.1)
Anaerobic Phase pH		7.5 (0.1)	7.1 (0.1)	7.2 (0.2)	7.2 (0.1)
Cycle Temperature	°C	17.9 (1.6)	18.5 (0.8)	18.3 (2.9)	21.6 (1.7)
Granule Characteristics					
Average Granule Diameter	mm	1.5 (0.1)	1.6 (0.2)	1.60 (0.1)	1.3 (0.1)
Density	g/cm^3	1.03 (0.00)	1.02 (N/A)	N/A	1.02 (N/A)

4.1 *Mixed Liquor and Granule Characteristics*

The reactor had an average MLSS of 11.4 ± 1.9 g/L and SVI_5/SVI_{30} ratio of 1.05 ± 0.10 during the full 10.5-month period. Growing a high fraction (> 90%) of fast-settling granules was an important goal for the bioaugmentation process. The average granule percentage of the mixed liquor for the 10.5-month period was of 96 ± 2% based on a cut off sieve size of 0.212 mm. A semi-spherical morphology was maintained for the granules through different operational conditions and upset events, with no signs of performance-inhibiting disintegration (Figure 4-1). Granular morphology consisted of nodule-like growth, as shown in Figure 4-2. Smooth white-colored outgrowth was observed in October 2018, as shown in Figure 4-3, and was a different color from the apparent existing granule that the outgrowth surrounded.

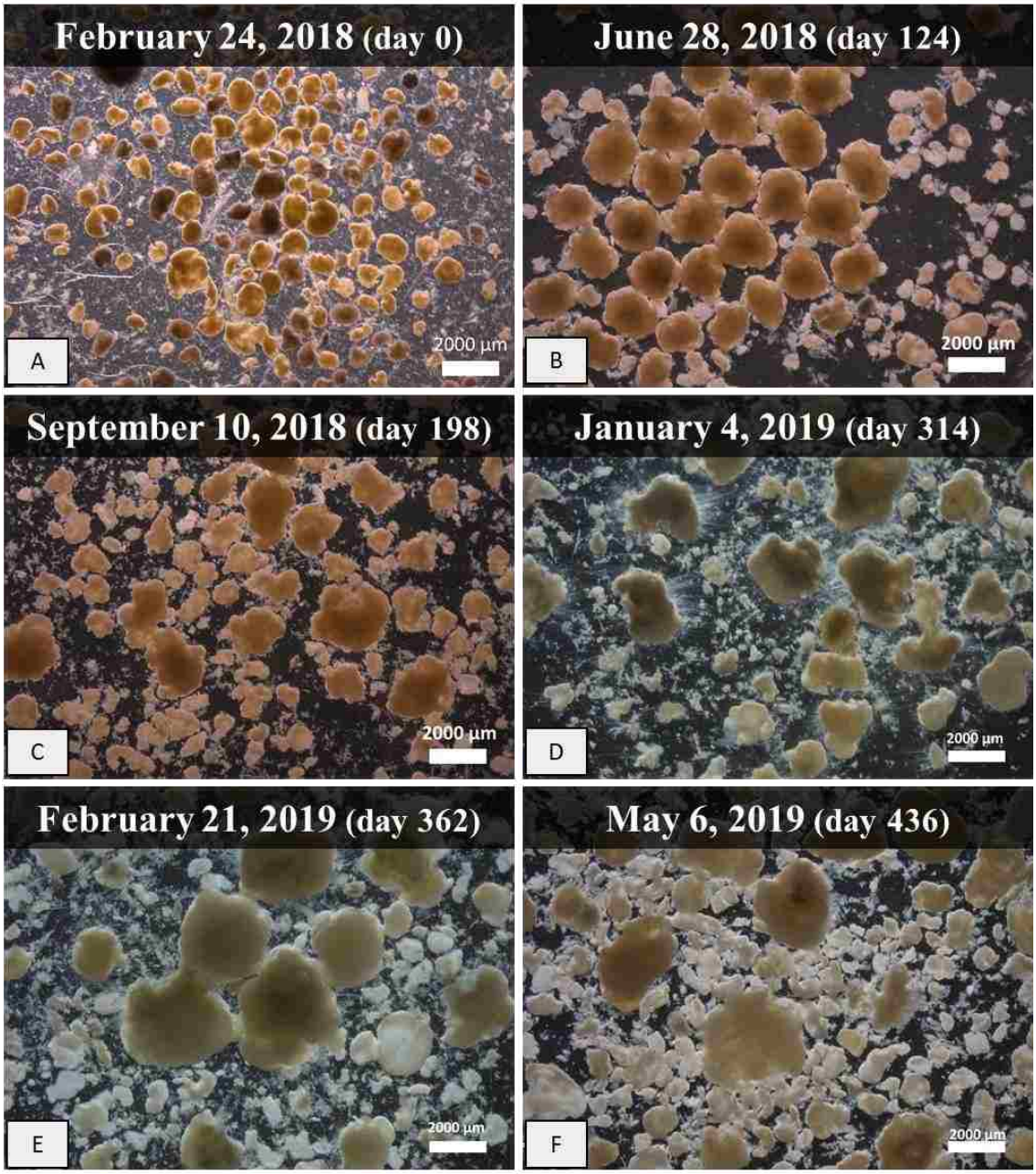

Figure 4-1. Aerobic granular sludge images from stereomicroscope-mounted camera. Initial MLSS was rich with small granules from selective seed source (a) and by the end of startup granule size had increased significantly (b). The size distribution became more uniform over time (c). Following a series of upset events, acetate leakage, and a re-seeding event, filaments were observed on the outer layer of granules. Following the restart, granule sizes ranged between 0.212 mm and 3.0 mm and had a uniform distribution.

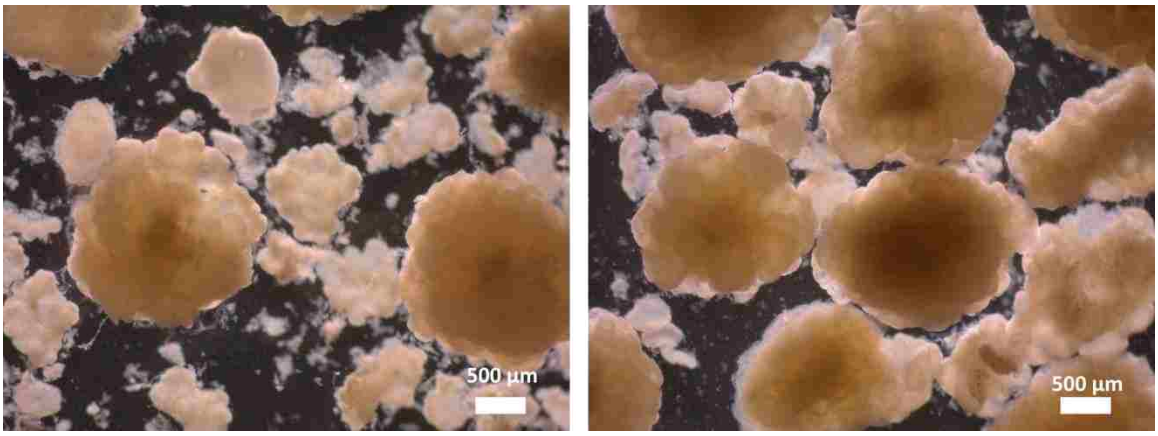

Figure 4-2. Stereomicroscope images from July 2, 2018 (left) and August 16, 2018 (right).

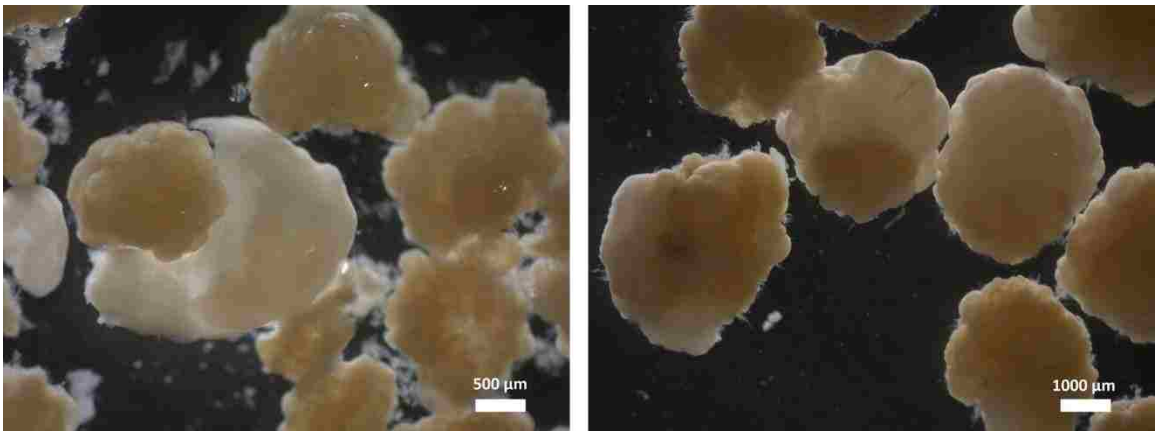

Figure 4-3. Stereomicroscope images of outgrowth around granules on October 18, 2018 (left) and October 22, 2018 (right).

Average settling velocity of the mixed liquor blanket were measured at 15.9 ± 4.3 m/hr from July 2, 2018 to April 11, 2019 (Figure 4-4). Settling velocities during the upset and restart periods were measured from October 25, 2018 to February 7, 2019 and averaged 18.5 ± 4.2 m/hr. Average settling velocities measured during stable performance periods were 12.5 ± 1.4 m/hr.

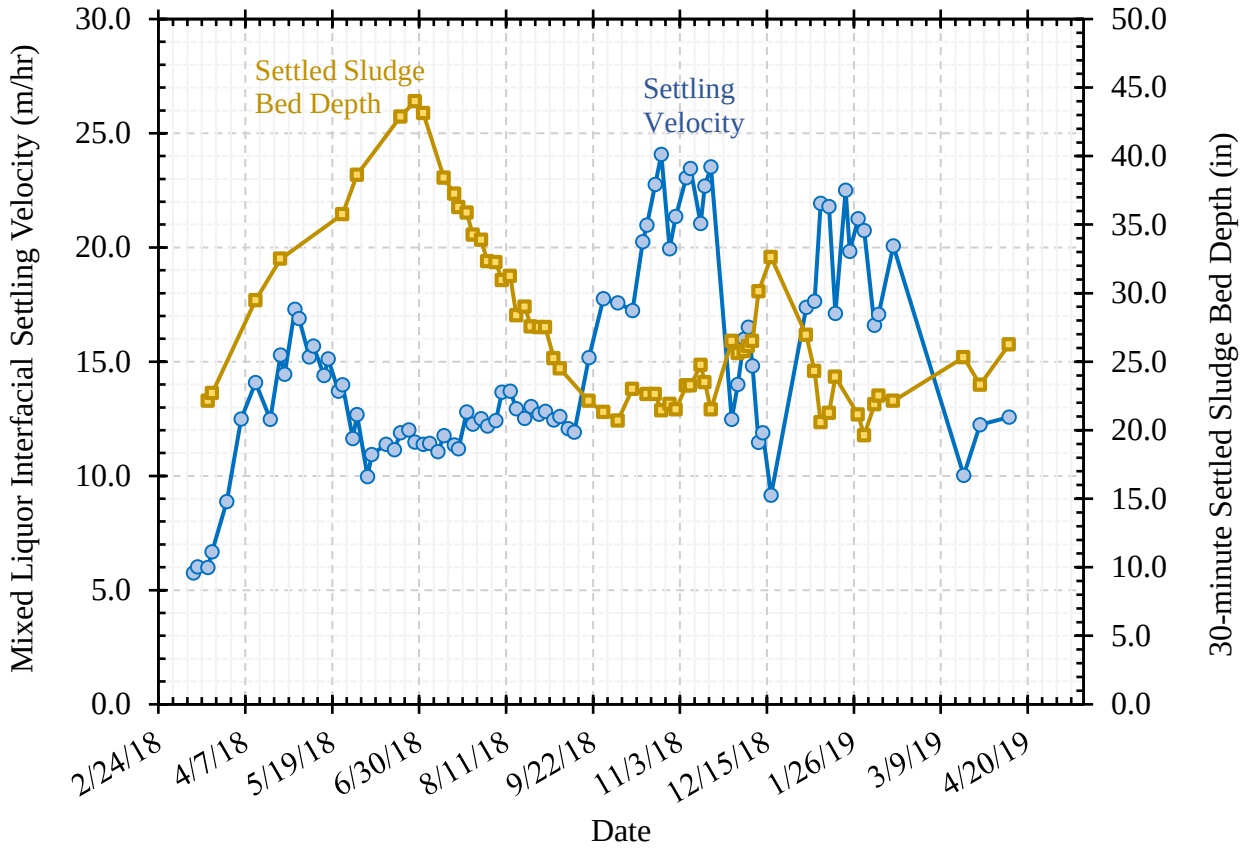

Figure 4-4. Sidestream granular MLSS settling velocity and 30-minute settles sludge bed depth measured in the sidestream reactor.

Average granule size and SVI_5/SVI_{30} ratio were monitored to track changes in morphology and settling performance of granular MLSS. Average granule diameter increased rapidly during startup as the settling time was decreased from 17 minutes to 8 minutes from February 24 to March 31, 2018 (Figure 4-5). Average size continued to increase throughout startup, then varied between 1.0 to 1.8 mm over the full period. Average sizes appeared to change in response to operational changes, such as the COD feed duration or DO setpoint, but the scope and time available did not allow for a systematic study of factors that could affect the average size.

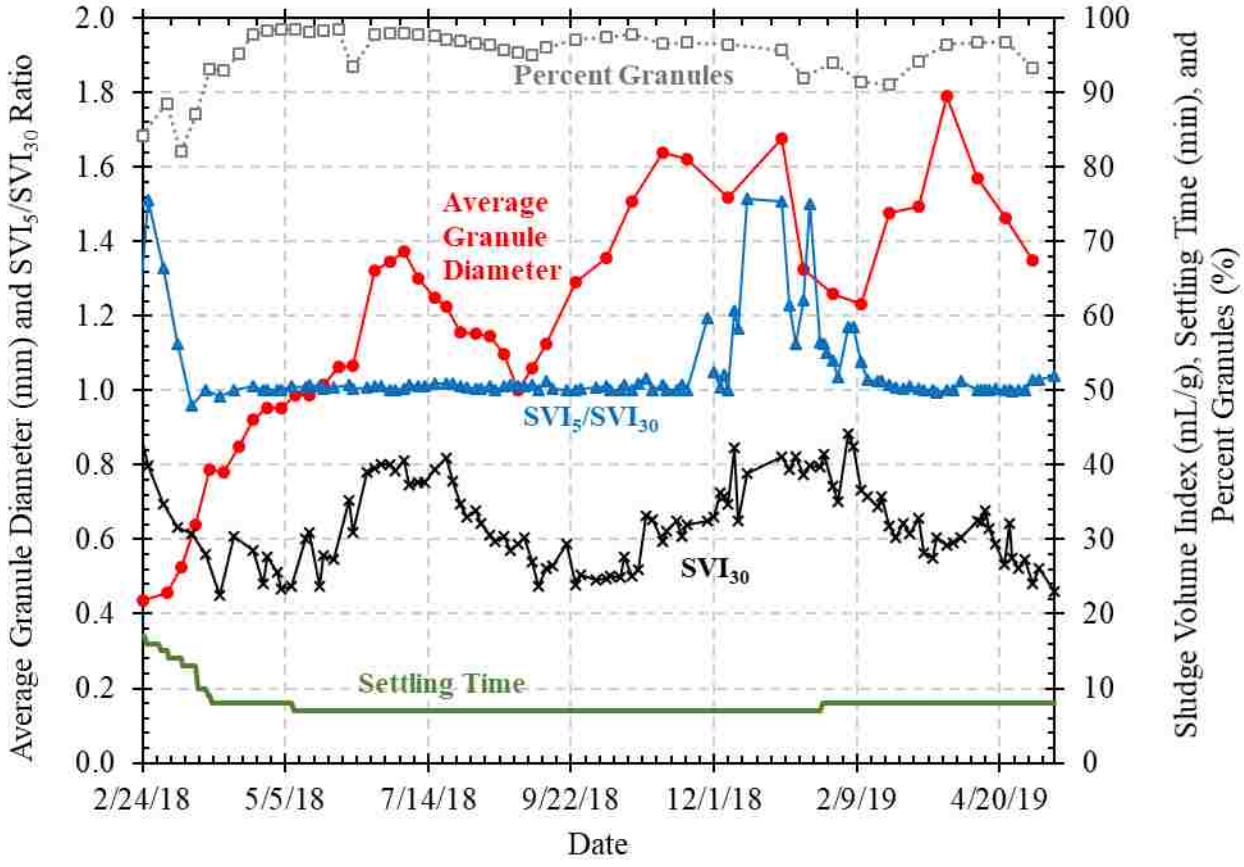

Figure 4-5. Average granule diameter, SVI_5, SVI_{30}, SVI_5/SVI_{30}, and settling time from February 24, 2018 to May 17, 2019.

The average SVI_{30} value was 32 ± 5 mL/g during the full period. The SVI_5/SVI_{30} ratio remained below 1.05 from March 20, 2018 to November 18, 2019. Following a reseeding on November 28, 2018, filamentous outgrowth was observed on granules (Figure 4-1D) and the SVI_5/SVI_{30} increased to 1.5 mL/g on December 17, 2018. Despite the growth of filaments, SVI_{30} values remained below 45 mL/g and settling velocities (Figure 4-4) were higher than 9 m/hr. Resumption of manual sludge wasting removed filamentous granules, which eventually disappeared from stereomicroscope observations. Regular manual wasting resumed on January 4, 2019 and the SVI_5/SVI_{30} ratio dropped below 1.05 within a month. It appeared that an observable presence of filaments had greater impact on SVI_5/SVI_{30} ratios than the fraction of

flocculent particles, which increased in abundance from January 3 to February 25, 2019 as the SVI_5/SVI_{30} simultaneously decreased. MLSS settling velocities were much faster than typical flocculent sludge settling rates, ranging from 9.2 to 21.4 m/hr.

Granule size distributions were analyzed during the full period and are shown in Figure 4-6 at the beginning of startup (February 24, 2018) and end of startup (June 25, 2018), during stable Period 1B (September 10, 2018), at beginning of restart (January 3, 2019) and during stable Period 2B (May 6, 2019). Granule diameters ranged from 0.212 to 0.850 mm at startup and increased to a maximum range of 0.212 to 3.0 mm. The initial MLSS had a normal distribution centered around particles retained on the 0.425 mm sieve, which was used when screening for the initial seed source. Initially the distribution became less uniform as loading rates and average granule size increased; however, over the course of the study the size distribution became increasingly uniform as the range of average particle sizes increased. Uniformity was quantified using the SSDM value for each distribution. Lower SSDM values indicate more uniform size distributions. Over time, the SSDM approached zero and distribution uniformity increased. The long term changes in size distribution (Figure 4-6) and distribution uniformity (Figure 4-7) demonstrate that size distribution stability may take longer to achieve than operation and performance stability.

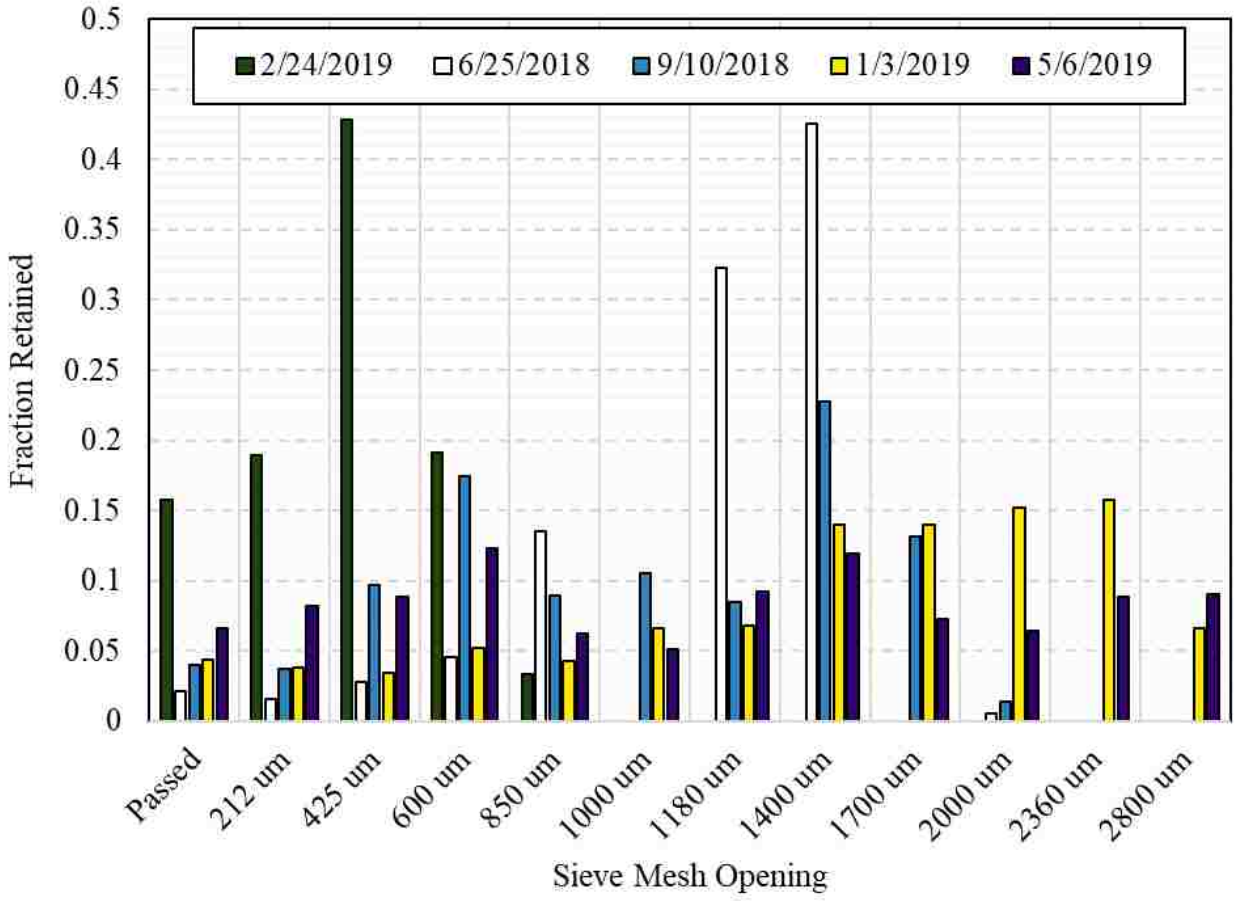

Figure 4-6. Fraction of total mass retained on different sieve sizes for reactor granular size distribution analysis.

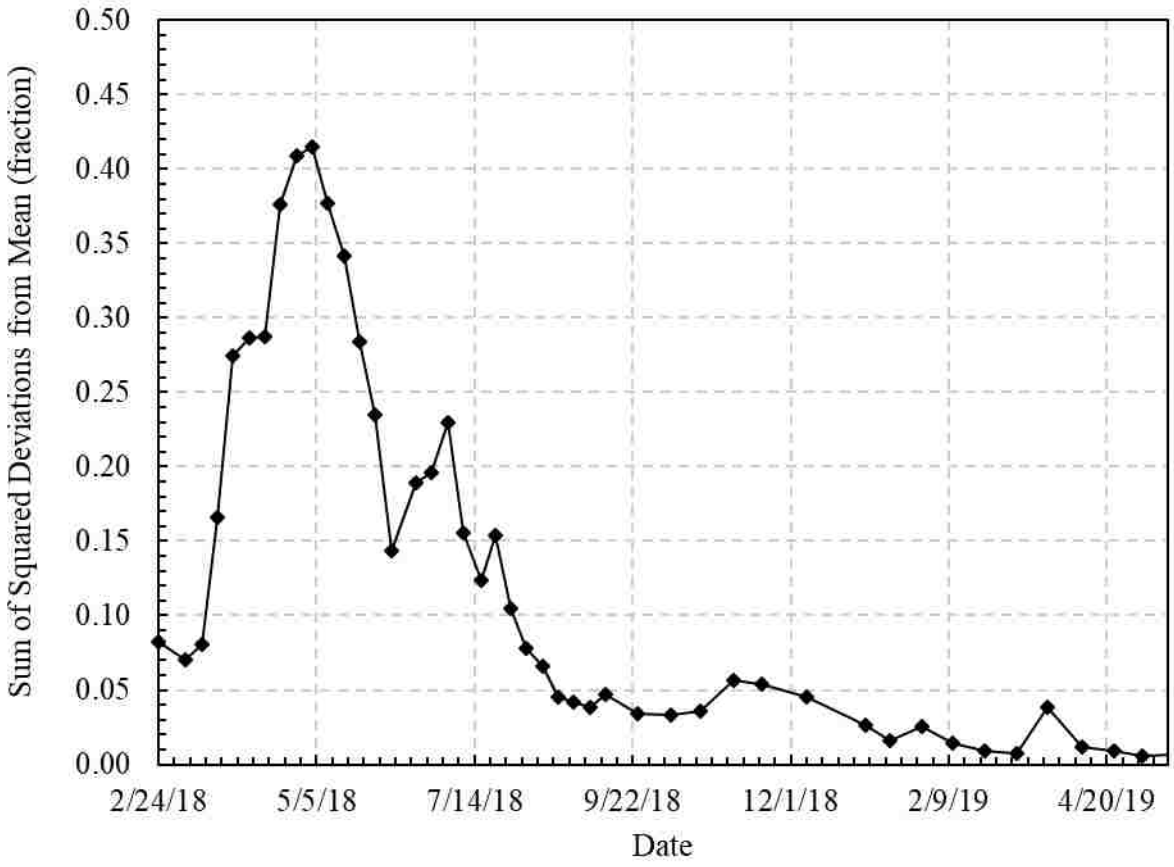

Figure 4-7. Sum of squared deviations from mean (SSDM) were calculated for size distribution data as a proxy for uniformity, where a fraction of 0.0 indicates a perfectly uniform distribution. Size distribution become less uniform during startup until May 4, 2018. After startup, manual wasting was implemented, and particle size distribution trended toward uniformity.

4.2 *Microbial Characterization*

The abundance of PAOs, GAOs, AOB, and NOB relative to the total bacteria population measured by qPCR (i.e. relative abundance) was measured over the full operating period (Figure 4-8). After seeding, the relative abundance of PAOs was 10.6 ± 0.6% and GAOs were measured below 0.2 ± 0.0%. The AOB and NOB relative abundance were below 0.1%. These results were expected because the seed sludge was taken from a non-nitrifying treatment plant with EBPR. The relative abundance of GAOs remained below 1% and PAO relative abundance remained relatively stable at 9.4 ± 0.8% throughout startup and into stable operations. On September 5, 2018, relative abundance of GAOs was measured at 11.6 ± 1.1% and as a result the GAO/PAO ratio increased to 1.0 ± 0.1 after ranging from a factor of 12.0 to 55.3 from March 6 to July 26, 2018. Following September 5, 2019, the GAO population fraction decreased, and the GAO/PAO ratio decreased steadily from 1.0 to 0.1. Results show that PAOs were enriched in the sidestream reactor and were maintained at equal or greater abundance than GAOs throughout the study. Both the relative abundance of PAO and GAO populations declined during the upset period from September 6 to November 13, 2018; however, following the restart, relative abundance of PAOs was enriched as GAOs continued to decrease.

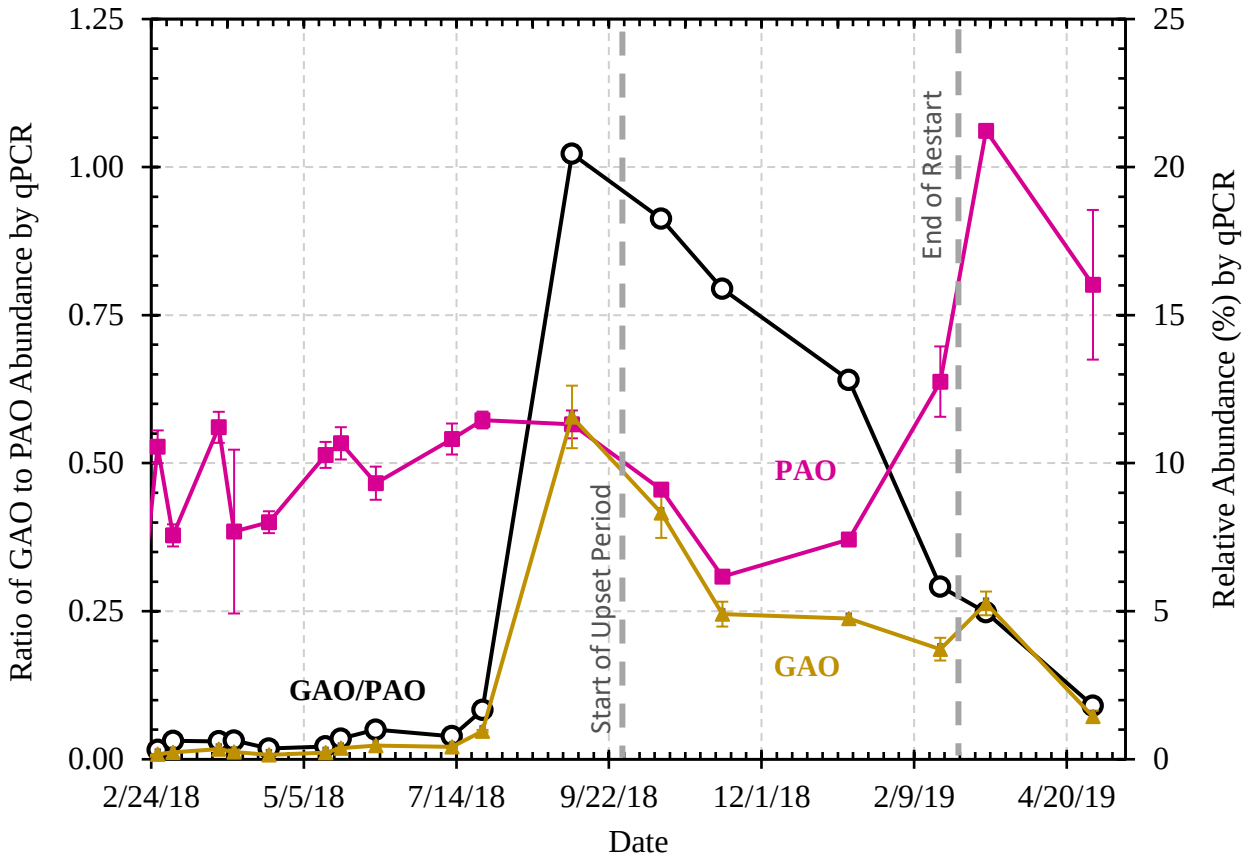

Figure 4-8. Relative abundance of PAO and GAO (right y-axis) and GAO/PAO ratio (left y-axis) over time. Error bars are displayed for each data point. Plots were generated with qPCR data provided by Bao Nguyen Quoc, UW PhD candidate.

Nitrifiers were measured in relatively low concentration during startup (AOB < 0.11% and NOB < 0.06% relative abundance) before the NH_3-N loading rates were increased (Figure 4-9). On May 15, 2018, relative abundances of AOB and NOB increased to 1.10% and 0.42%, respectively. Relative abundances of AOB and NOB varied from 1.06 to 3.16% and 0.24 to 0.79%, respectively, during the full study. The AOB abundance followed a similar trend to PAOs, where the population reached a minimum during the upset period and rose to a maximum near the end of restart. The AOB/NOB ratio ranged from 2.6 to 4.4, which is greater than an expected value for systems with full nitrification.

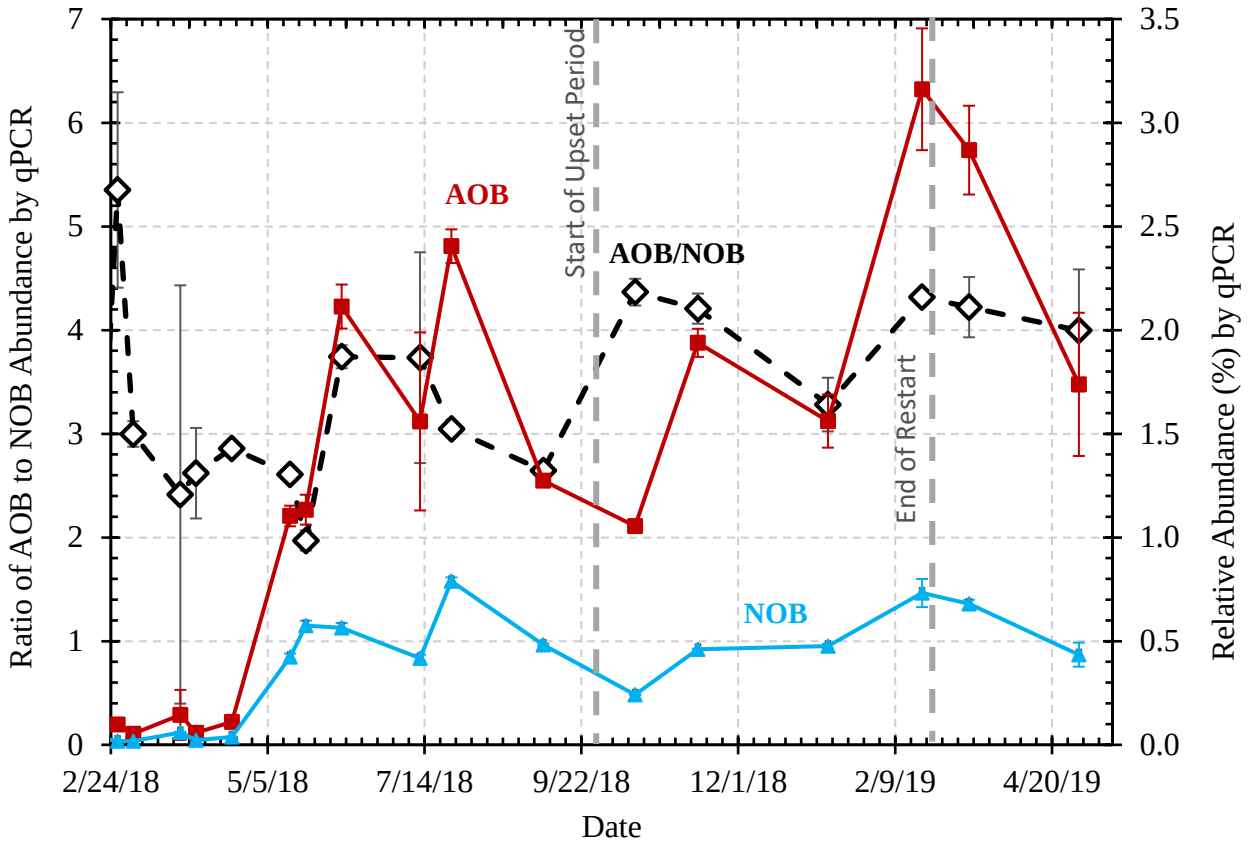

Figure 4-9. Relative abundance of AOB and NOB (right y-axis) and the ratio of AOB/NOB (left y-axis) versus time. Error bars are displayed for each data point. Plots were generated with qPCR data provided by Bao Nguyen Quoc, UW PhD candidate.

Sequencing analyses for nitrifiers were done with a reactor mixed liquor sample on May 8, 2018, near the end of startup and after a sustained period of relatively stable operations and performance for a sample on September 6, 2018. 16S rRNA sequencing was also completed for a sample collected on May 22, 2018. Microorganisms are classified by genus from genomic sequencing and results are shown in Table 4-5. *Nitrosomonas* was the dominant AOB (over 65% of the AOB population), and *Nitrospira* was the dominant NOB (over 80% of the NOB population). AOA were detected at very low concentrations (less than 0.2%) and were split between two genera: *Nitrososphaeraceae* and *Nitrosopumilus*. The presence of AOA may

suggest an environment with low ammonia exists within the granule biofilm. GAOs were detected in 16S rRNA (Figure 4-10) but not shotgun metagenomic (Table 4-5) sequencing. *Candidatus Accumulibacter phosphatis* and *Dechloromonas* were both detected at relatively high abundances (greater than 20%, combined), demonstrating an enrichment in PAOs. Sulfate reducing and sulfur oxidizing organisms were detected at relatively low abundance in genome sequencing results. The presence of these organisms may be influenced by occasional salt-water intrusion from the Puget Sound into WPTP during high tide events.

Table 4-5. Genomic sequencing data for sidestream reactor samples collected on May 8 and September 6, 2018. The relative abundance of populations, group by genus, are displayed in percentages. Table adapted from presentation by Bao Nguyen Quoc, UW PhD candidate.

Genus	**Abundance (%)**	
	5/8/2018	**9/6/2018**
Candidatus Accumulibacter phosphatis	17.35	12.54
Dechloromonas	20.36	9.95
Pseudomonas	1.63	2.15
Flavobacteriales	3.18	1.79
Dokdonella	0.14	1.62
Chitinophagales	1.24	1.59
Sulfur oxidization		
Sulfuritalea	2.09	1.60
Sulfate reducing bacteria		
Desulfovibrionaceae	0.23	0.28
Desulfobacteraceae	0.12	0.24
AOB		
Nitrosomonas	1.28	1.58
Nitrosococcus	0.11	0.52
Nitrosospira	0.24	0.28
AOA		
Nitrososphaeraceae	0.002	0.01
Nitrosopumilus	0.001	0.002
NOB		
Nitrospira	0.13	0.21
Nitrobacter	0.03	0.04

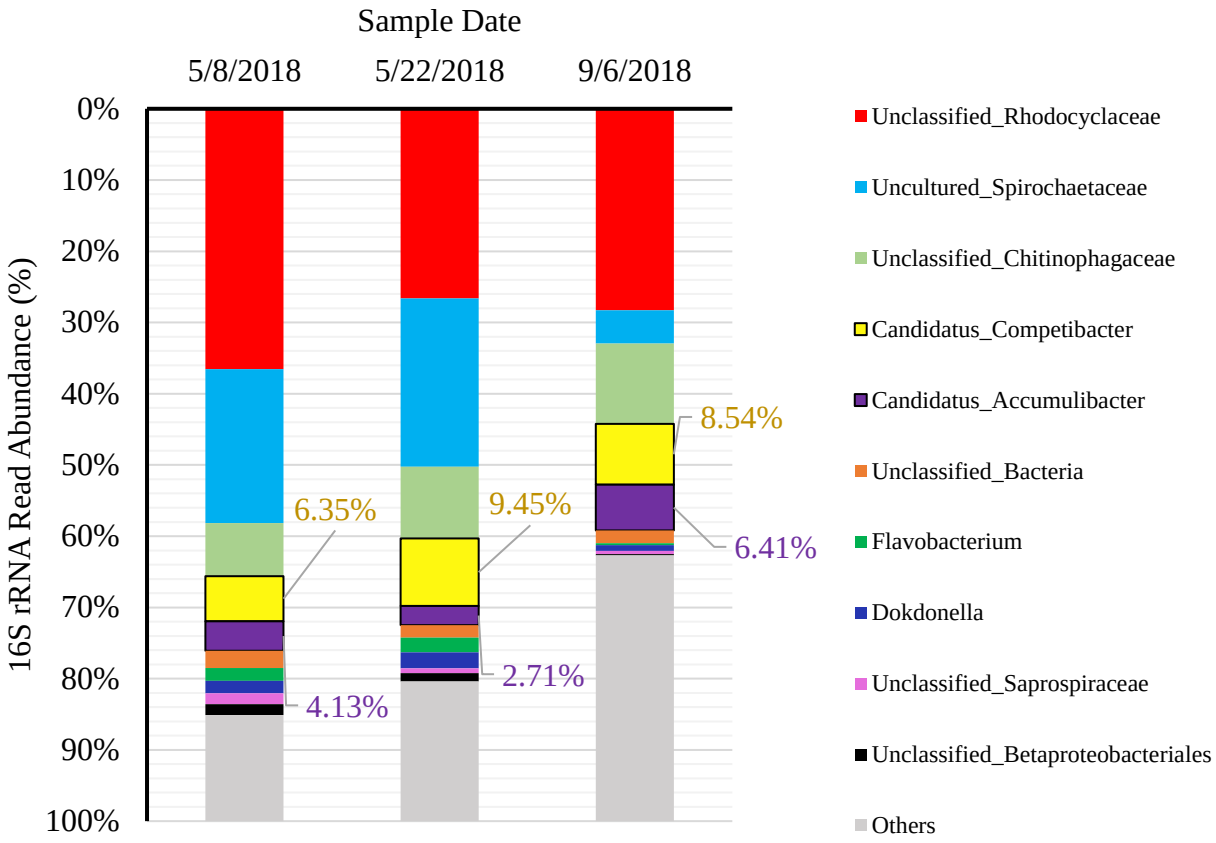

Figure 4-10. 16S rRNA gene sequencing data for sidestream reactor samples collected on May 8, 22, and September 6, 2018. The abundance of gene reads is displayed, which is not equivalent to population abundance. Figure adapted from presentation by Bao Nguyen Quoc, UW PhD candidate.

4.3 *Ammonia Removal*

NH_3-N removal efficiencies ranged from 96 to 99% at NH_3-N loadings from 0.36 to 0.46 g/L-d on average during stable periods (Table 4-6). The estimated amount of the NH_3-N via removal for biomass growth from acetate COD was 7 to 11%. Thus, the amount of influent NH_3-N that was oxidized ranged from 86 to 89%. In general, higher loading rates corresponded with greater volumetric NH_3-N removal rates during performance periods. The highest volumetric NH_3-N removal rates were achieved at loading rates of 0.46 ± 0.01 and 0.44 ± 0.02 g/L-d and were

equivalent to volumetric removal rates of 0.45 ± 0.02 and 0.42 ± 0.01 g/L-d during Periods 2A and 2B, respectively.

Table 4-6. NH_3-N loading rates and removal efficiency during stable performance periods. The fraction of NH_3-N removal via synthesis and oxidation is shown as a percentage of the total NH_3-N removed and is not based on influent NH_3-N.

Parameter	Units	Period				
		1A	1B	1C	2A	2B
NH_3-N Loading Rate	g/L-d	0.36 (0.04)	0.36 (0.03)	0.40 (0.02)	0.46 (0.01)	0.44 (0.02)
NH_3-N Removal Efficiency	%	99 (2)	98 (3)	96 (5)	98 (3)	96 (5)
NH_3-N Removed via Synthesis	%	10 (1)	11 (1)	10 (1)	9 (0)	7 (0)
NH_3-N Removed via Oxidation	%	90 (1)	89 (1)	90 (1)	91 (0)	93 (0)

4.3.1 Nitrification Kinetics

The average volumetric NH_3-N removal rate and specific nitrification rate (SNR) for each stable performance period ranged from 15.4 to 22.2 mg NH_3-N/L-hr and 1.76 to 2.60 mg NH_3-N/g VSS-hr, respectively, and were based on in situ profiles of NH_3-N concentration versus time (Table 4-7). Higher NH_3-N loading correlated with higher SNRs, as shown in Figure 4-11. Higher COD:N ratios correlated with lower SNR during stable performance periods, and higher SNRs were generally observed at higher DO concentrations as well (Figure 4-12).

Table 4-7. Bulk and specific NH_3-N removal and nitrification rates measured in the sidestream aerobic granular sludge reactor during stable performance periods.

Parameter	Units	Period				
		1A	1B	1C	2A	2B
NH_3-N Loading Rate	g/L-d	0.36 (0.04)	0.36 (0.03)	0.40 (0.02)	0.46 (0.01)	0.44 (0.02)
Aeration Phase DO	mg/L	1.9 (0.1)	2.0 (0.1)	2.8 (0.3)	3.1 (0.2)	2.3 (0.2)
Bulk Removal Rates						
NH_3-N Removal Rate	mg/L-hr	17.4 (1.7)	18.3 (1.1)	18.7 (1.7)	21.2 (N/A)	23.9 (6.4)
Specific NH_3-N Removal Rate	mg/g VSS-hr	1.76 (0.23)	1.99 (0.17)	2.05 (0.26)	2.52 (N/A)	2.60 (0.64)
Nitrification Rates						
NH_3-N Oxidation Rate	mg/L-hr	15.4 (1.7)	16.2 (1.1)	16.4 (1.7)	18.9 (N/A)	22.2 (6.4)
Specific NH_3-N Oxidation Rate	mg/g VSS-hr	1.56 (0.22)	1.76 (0.17)	1.81 (0.25)	2.24 (N/A)	2.41 (0.65)

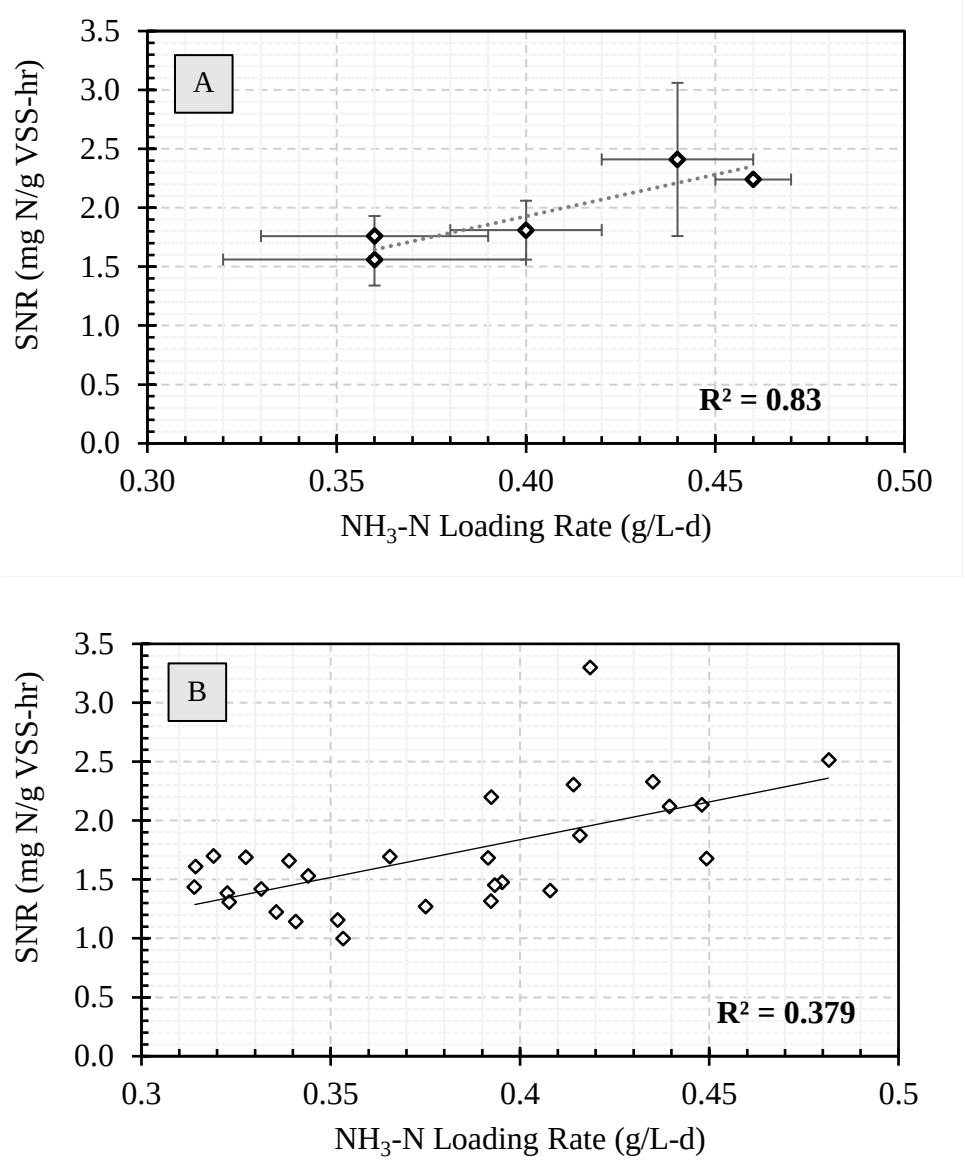

Figure 4-11. (A) Higher specific nitrification rate (SNR) correlated with higher average NH_3-N loading rates of stable performance periods (R^2=0.83). Daily data points also show higher SNRs observed at greater frequency when the NH_3-N loading rate is increased.

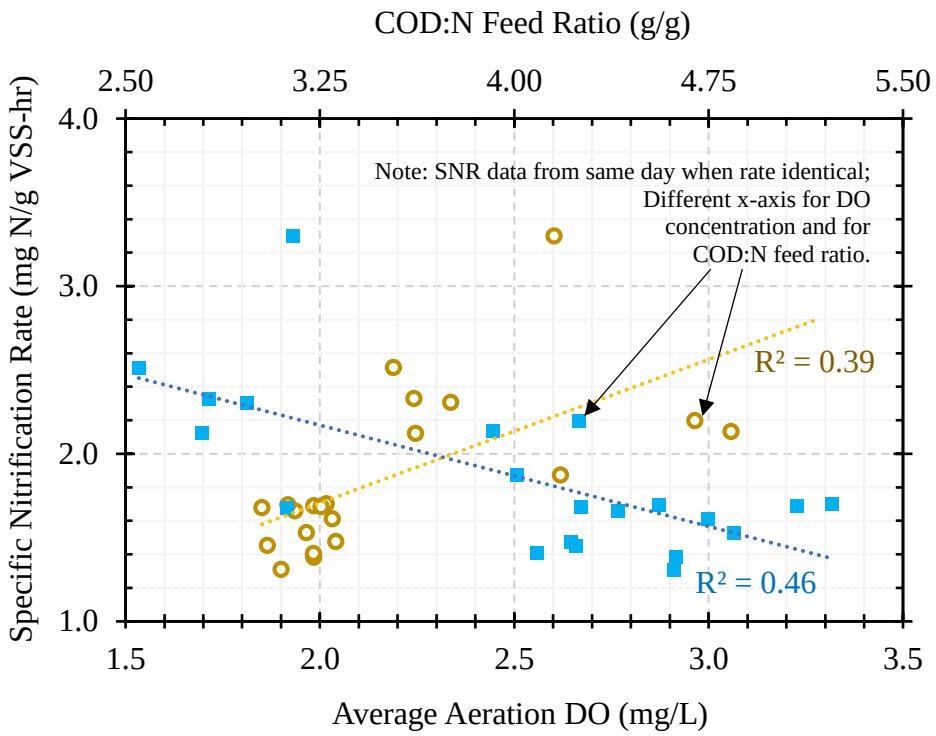

Figure 4-12. Specific nitrification rate versus average aeration DO (gold circle) and COD:N feed ratio (blue square). Black arrows serve to indicate that SNRs from the same day of operation are plotted against two x-axes.

Correlations between SNR and DO concentration (positive; R^2=0.39), COD:N feed ratio (negative; R^2=0.46), and NH_3-N loading rate (positive; R^2=0.38) were relatively weak (Figure 4-12) It is likely that all three factors affected the SNR. The highest SNR achieved in the sidestream reactor was 2.41 ± 0.65 mg NH_3-N/g VSS-hr at an average loading rate of 0.44 ± 0.2 g NH_3-N/L-d during the 22-day Period 2B with a COD:N feed ratio of 2.9 ± 0.2 g/g and average DO concentration of 2.3 ± 0.2 mg/L.

4.3.2 Effect of Bulk Liquid Dissolved Oxygen Concentration

Nitrification kinetics were assessed in activity tests at the pilot facility using reactor MLSS to determine apparent maximum SNR and half-saturation constant for DO (K_{DO}). These tests were done on April 16, April 25, and May 2, 2019 during a period with NH_3-N loading of 0.44 ± 0.02 g/L-d to the sidestream reactor. As described in the Methods section, the SNRs were obtained at NH_3-N concentrations above 20 mg/L and controlled DO concentrations ranging from 1.0 mg/L to 7.5 mg/L. The observed SNRs were corrected to a temperature of 20°C. The SNR increased with DO concentration and ranged from 3 mg NH_3-N/g VSS-hr at a DO concentration of 1 mg/L to 7 mg NH_3-N/g VSS-hr at a DO concentration of 7.5 mg/L (Figure 4-13). The experimental data were best fit with the Michaelis-Menten Equation using a maximum SNR of 7.9 mg NH_3-N/g VSS-hr and K_{DO} of 1.5 mg/L.

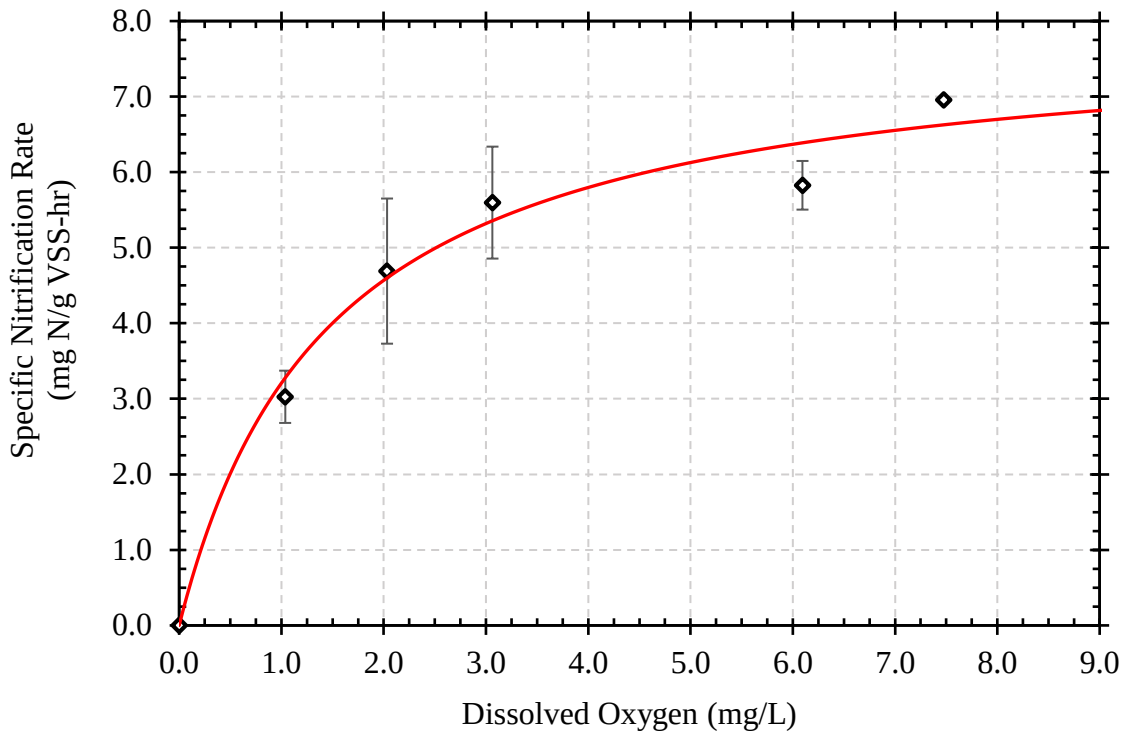

Figure 4-13. Specific nitrification rate versus dissolved oxygen concentration at unlimiting NH_3-N concentration. Data points represent average values from bench tests with standard deviations shown for both parameters (DO standard deviations are hidden by data point markers). DO of 7.5 mg/L was obtained during one batch test. Red line represents Michaelis-Menten Equation model with maximum SNR of 7.9 mg N/g VSS-hr and K_{DO} of 1.5 mg N/L.

The SNRs obtained in bench activity tests were higher than in situ SNRs measured at similar average DO concentrations. In the sidestream reactor, the SNR was 2.4 g NH_3-N/g VSS-hr during Period 2B when the average DO was 2.3 mg/L. During batch activity tests at a DO concentration of 2.0 mg/L the SNR was 4.7 mg NH_3-N/g VSS-hr. Therefore a 96% increase in SNR was measured in batch activity tests at approximately the same average DO concentration as the sidestream reactor.

4.3.3 Relative Nitrifier Activity at Saturated Dissolved Oxygen Concentration

Relative activity of NOB and AOB was assessed by comparing conversion rates of NH_3-N to NO_2^--N and NO_2^--N to NO_3^--N in weekly bench activity tests. These tests were conducted with the sidestream reactor MLSS at saturated DO, which inhibited denitrification during tests and allowed for both NO_2^--N and NO_3^--N production rates to be measured (Figure 4-14). The NO_2^--N production rate accounted for all NO_2^--N that was produced and converted to NO_3^--N during the test.

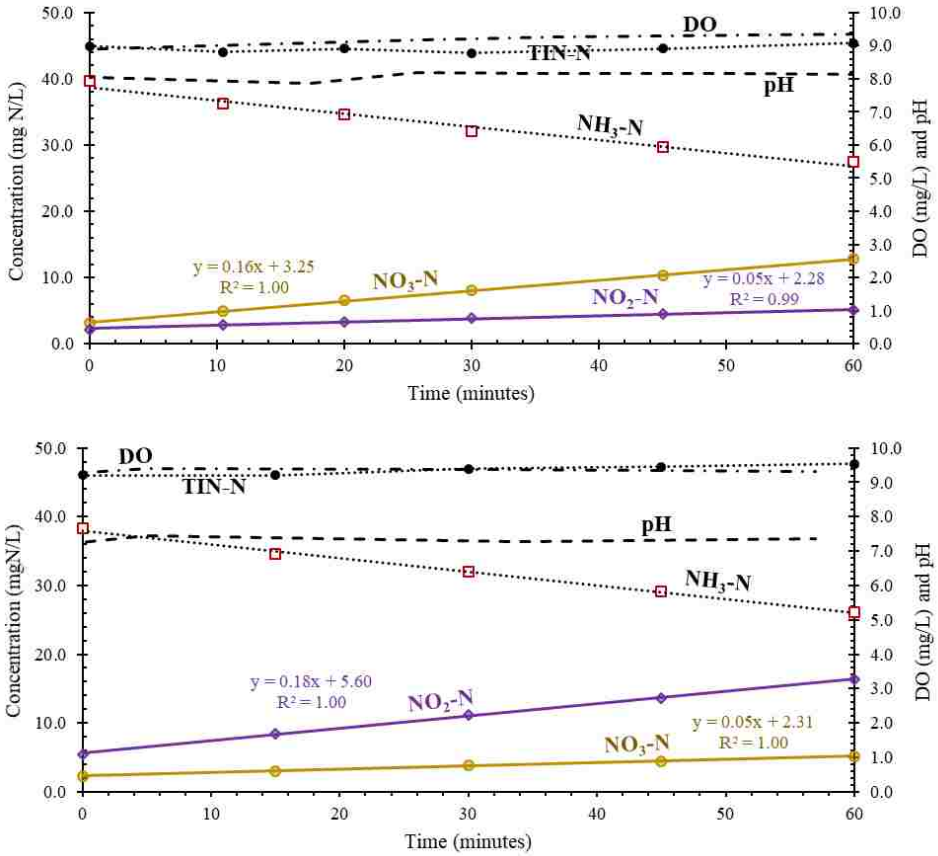

Figure 4-14. Concentration profiles of NH_3-N, NO_2^--N, and NO_3^--N from bench activity tests at saturated DO. The TIN remained relatively constant, demonstrating no SND occurred at saturated DO concentration. The top plot was for a test completed on September 6, 2018 and the bottom plot is for a test completed on May 6, 2019.

Nitrifier activity was monitored by comparing the ratio of the NO_3^--N production rate to the NO_2^--N production rate. The NO_3^--N/NO_2^--N production rate ratio, has a theoretical maximum value of 1.0 for a mixed liquor capable of full nitrification and minimum of 0.0 for a sample with no NOB activity and thus full nitritation. Examples of these results are shown in Figure 4-14. The NO_3^--N/NO_2^--N production rate ratio for the September 6, 2018 sample was 0.8 and for May 6, 2019 it was 0.2. Measured NO_3^--N/NO_2^--N production rate ratios ranged from 0.1 to 0.9 during the full operating period (Figure 4-15). These ratios indicate that nitritation was achieved in the sidestream reactor. Evidence of partial nitritation was corroborated by accumulation of NO_2^- in effluent samples as shown in Figure 4-15.

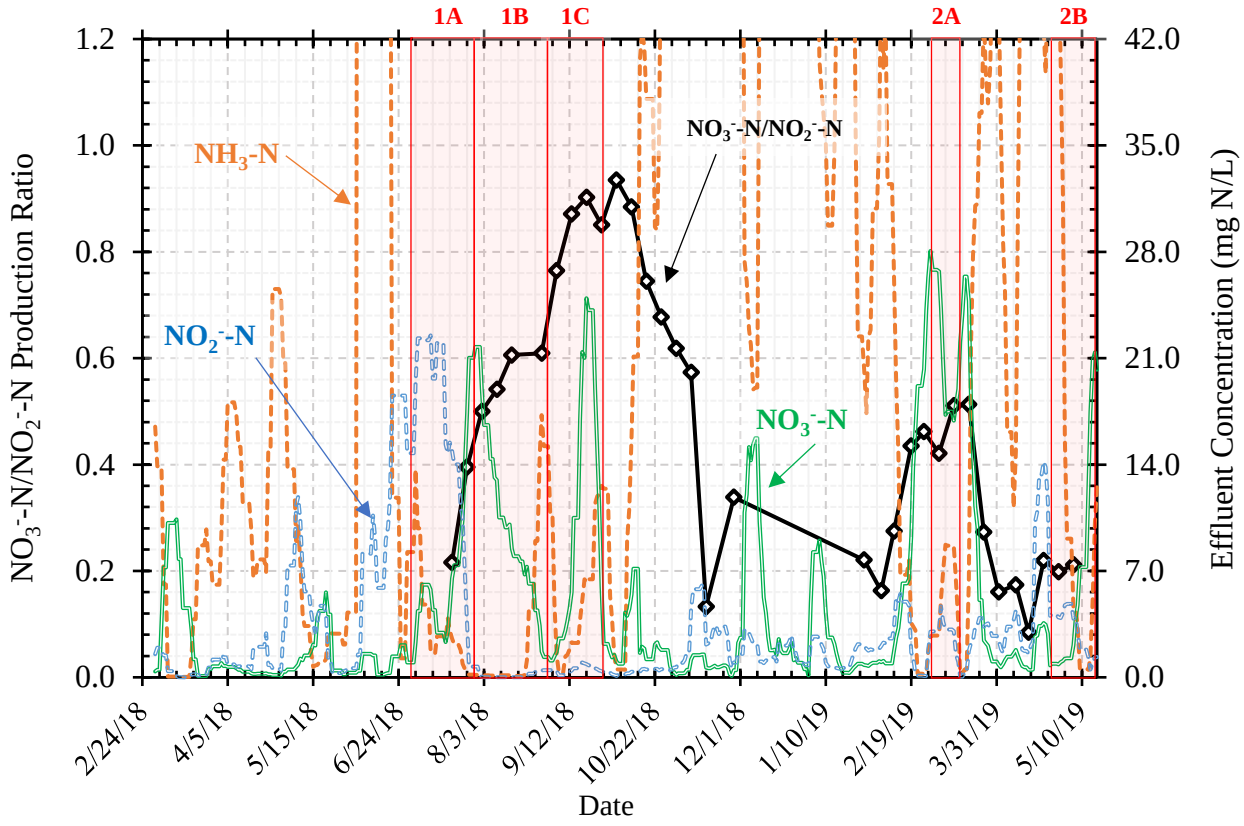

Figure 4-15. NO_3^--N/NO_2^--N production rate ratio (left y-axis) and effluent inorganic nitrogen concentrations (NH_3-N, NO_2^--N, and NO_3^--N; right y-axis) over time. Effluent concentrations are plotted as a 7-day average for clarity.

A low NO_3^--N/NO_2^--N Production Ratio of 0.2 was first measured on July 19, 2018. This value an effluent NO_X-N of 21.9 mg/L with approximately 60% NO_2^-. The NO_3^--N/NO_2^--N production rates ratios increased steadily for 63 days until a 0.9 ratio was measured on September 20, 2018. Low NH_3-N and decreasing NO_3^--N concentrations were measured in the sidestream reactor effluent during the steady rise in the NO_3^--N/NO_2^--N production ratios from July 19 to September 20, 2018 (Figure 4-15). Virtually no NO_2^- was measured in the sidestream effluent during this period as well. The high NO_3^--N/NO_2^--N production ratio of 0.9 was maintained from September 20 to October 4, 2018, then began decreasing steadily until November 8, 2018. While the ratio decreased, the sidestream reactor effluent NH_3-N concentrations increased due to decreased sidestream reactor nitrification rates. During the extended upset period from November 8, 2018 to January 4, 2019 the NO_3^--N/NO_2^--N production ratios were below 0.4 and effluent NH_3-N concentrations remained high above 10 mg/L as a result of poor nitrification performance (Figure 4-15).

After restarting the reactor on January 5, 2019, the NO_3^--N/NO_2^--N production ratios were maintained at or below 0.5 and two distinct values were observed. The first set of values occurred from February 19 to March 18, 2019 the ratio ranged from 0.4 to 0.5. During this period the effluent NO_3^--N concentrations were above 9 mg/L in the sidestream effluent (Figure 4-15) with relatively low NO_2^--N in comparison. Therefore, although bench activity tests indicated an equal ratio of NO_2^- and NH_3 oxidation by NOB and AOB, the sidestream effluent showed an accumulation of primarily NO_3^-. A brief upset occurred on March 18, 2019, which was accompanied by a decrease in the NO_3^--N/NO_2^--N production ratio. Sidestream reactor

nitrification rates also dropped during this period, and the sidestream effluent NH_3-N concentration increased to concentrations ranging from 16.9 to 66.0 mg/L.

A brief plateau in the NO_3^--N/NO_2^--N production ratio at 0.6 near the end of Period 1B and at 0.9 near the end of Period 1C. These plateaus corresponded with brief spikes in the effluent NH_3-N concentration that rose above 4.0 mg/L from August 23 to 31 and above 7.0 mg/L from September 17 to 19. The NO_3^--N/NO_2^--N production ratio decreased after Period 1C, which corresponded to upset events in the sidestream reactor. During this period, effluent NH_3-N concentrations were relatively high and NO_3^--N/NO_2^--N production ratios remained below 0.4.

Overall, it appeared that higher effluent NH_3-N concentrations corresponded with lower NO_3^--N/NO_2^--N production rate ratios. When comparing performance periods highlighted in Figure 4-15 and summarized in Table 4-8, it is apparent that the relative nitrifier activity was changing during Periods 1A, 1B, and 1C, whereas relative nitrifier activity was more stable during Periods 2A and 2B. Compared to Period 2A, the NOB activity declined relative to AOB activity in Period 2B. Key differences between these performance periods were differences in average DO concentration and effluent NH_3-N concentration. At lower DO concentration and higher effluent NH_3-N concentration a lower NO_3^--N/NO_2^--N production ratio was measured (Table 4-8). In Period 2A the average DO concentration was 3.2 ± 0.2 mg/L and the effluent NH_3-N concentration was 4.7 ± 6.5 mg/L. The NO_3^--N/NO_2^--N production ratio was measured at 0.47 ± 0.06 during this period. In contrast, in Period 2B the average DO concentration was 2.3 ± 0.2 mg/L and the effluent NH_3-N concentration was 9.9 ± 11.2 mg/L. This resulted in a NO_3^--N/NO_2^--N production ratio of 0.20 ± 0.01.

Overall, Period 2B had the lowest NO_3^--N/NO_2^--N production ratio and relative NOB activity, which was achieved at an average aeration DO concentration of 2.3 ± 0.2 mg/L and NH_3-N loading rate of 0.44 ± 0.2 g/L-d. This period also had a relatively high average NH_3-N effluent concentrations, high average AOB/NOB abundance ratio, and low GAO/PAO abundance ratio compared to other performance periods (Table 4-8).

Table 4-8. Specific NO_2^--N and NO_3^--N production rates from bench tests at saturated DO. Reactor mixed liquor for tests was taken during the aeration phase. An upward arrow (↑) symbolized an increasing trend during the periods, and a dash (--) symbolizes parameter stability.

Parameter	Unit	1A	1B	1C	2A	2B
Specific NO_2^--N Production Rate (Nitrification Rate)	mgN/gVSS-hr	12.70 (3.79)	7.36 (1.06)	6.47 (0.49)	11.23 (0.44)	9.76 (0.83)
Specific NO_3^--N Production Rate	mgN/gVSS-hr	3.64 (0.45)	4.45 (1.05)	5.67 (0.60)	5.22 (0.51)	2.00 (0.26)
NO_3^--N/NO_2^--N Production Rate Ratio	mg/hr / mg/hr	0.31 (0.13)	0.60 (0.10)	0.87 (0.03)	0.47 (0.06)	0.20 (0.01)
NO_3^--N/NO_2^--N Production Rate Ratio Trend		↑[A]	↑	↑	--	--
Nitrite Accumulation Ratio	mg NO_2-N/ mg NO_3-N	0.5 (0.4)	0.1 (0.2)	0.1 (0.1)	0.1 (0.1)	0.3 (0.3)
Operation and Performance Parameter						
Average Aeration DO	mg/L	1.9 (0.1)	2.0 (0.1)	2.8 (0.3)	3.1 (0.2)	2.3 (0.2)
NH_3-N Loading Rate	g/L-d	0.36 (0.04)	0.36 (0.03)	0.40 (0.02)	0.46 (0.01)	0.44 (0.02)
Effluent NH_3-N	mg/L	2.1 (3.2)	3.8 (6.7)	8.8 (9.9)	4.7 (6.5)	9.9 (11.2)
Effluent Free Ammonia	mg N/L	0.01 (0.02)	0.08 (0.16)	0.09 (0.13)	0.03 (0.04)	0.07 (0.08)
GAO/PAO Ratio by qPCR	gene copy number / gene copy number	0.06 (0.00)	1.02 (0.00)	N/A (N/A)	0.27 (0.00)	0.09 (0.00)
AOB/NOB Ratio by qPCR	gene copy number / gene copy number	3.39 (0.94)	2.65 (0.12)	NA (N/A)	4.27 (0.44)	4.00 (0.06)

Note: [A] Trends of NO_3^--N/NO_2^--N Production Ratio can be seen in Figure 4-15. Measurements showed an increasing ratio during stable periods 1A, 1B, and the beginning of 1C.

4.3.4 Effect of Surface Area on Specific Nitrification Rates

As described in the methods section, the size distribution for mixed liquor samples was determined and used to calculate weighted average surface area per unit mass in the reactor (cm^2/g TSS), which was then multiplied by MLSS to calculate the granular sludge surface area density (cm^2/L). The SNR determined from NH_3 profiles was matched to calculated granular sludge surface area density values, but interpolation for the weighted surface area to volume ratio (SA/VOL) and MLSS were required because size distribution analyses were usually conducted every other week. Enough data was collected during performance periods 1A, 1B, and 2B for the evaluation of SNR against granular sludge surface area density.

Both the MLSS and the SA/VOL affect the granular sludge surface area density value, so both variables were plotted against the SNR (Figure 4-16) to first assess whether SA/VOL or MLSS had an individual effect on nitrification. Data plotted was from all stable performance periods. Neither parameter was found to impact the SNR within the sidestream reactor. Figure 4-17 shows the SNR plotted against granular sludge surface area density for Periods 1A, 1B, and 2B. There was no apparent trend between the SNR and granular sludge surface area density for any performance period. Thus, changes in surface area did not affect the SNR.

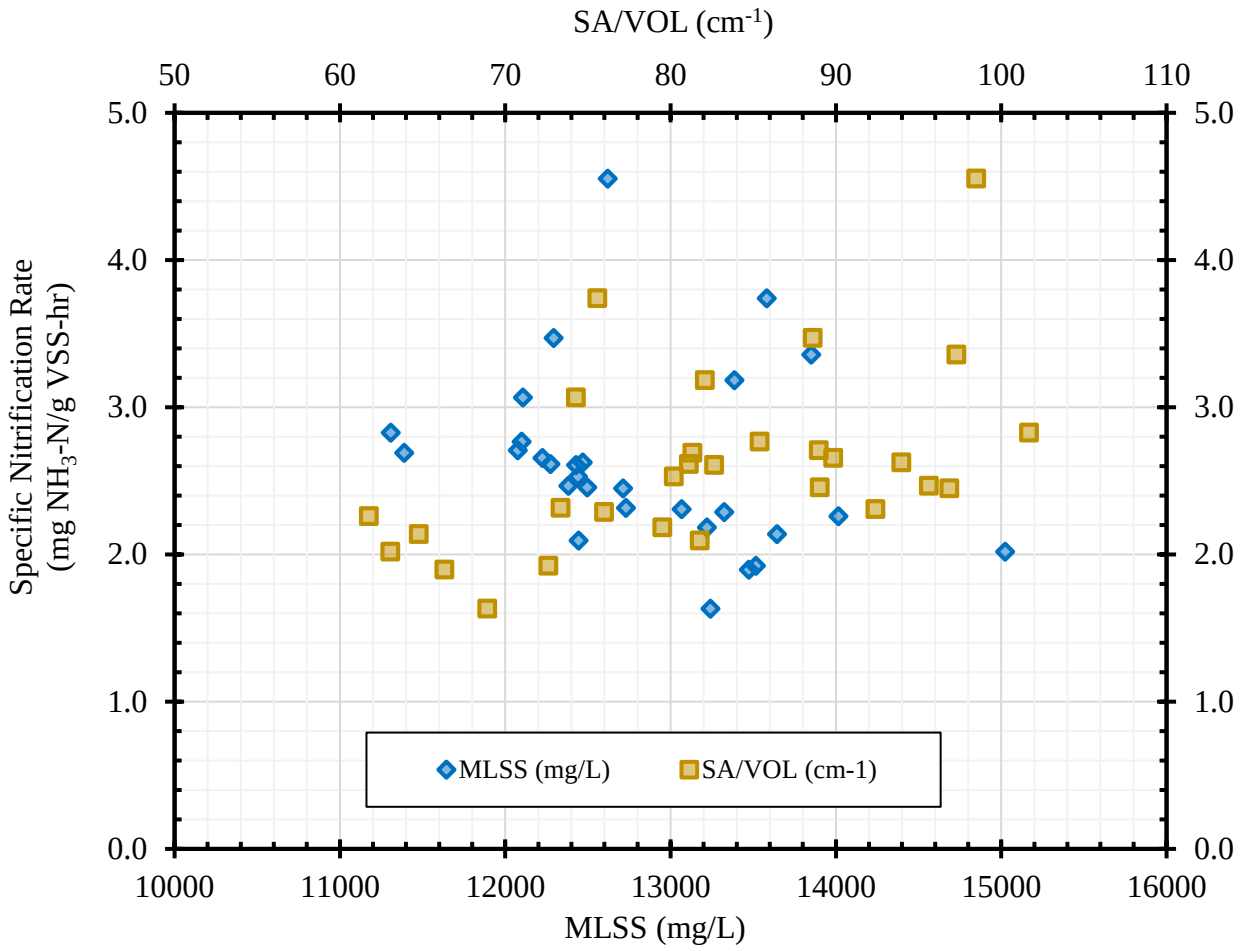

Figure 4-16. Specific Nitrification Rate (g NH_3-N/g VSS-hr) versus weighted average granular surface area to volume (SA/VOL) ratio and MLSS concentration for measurements during stable performance periods.

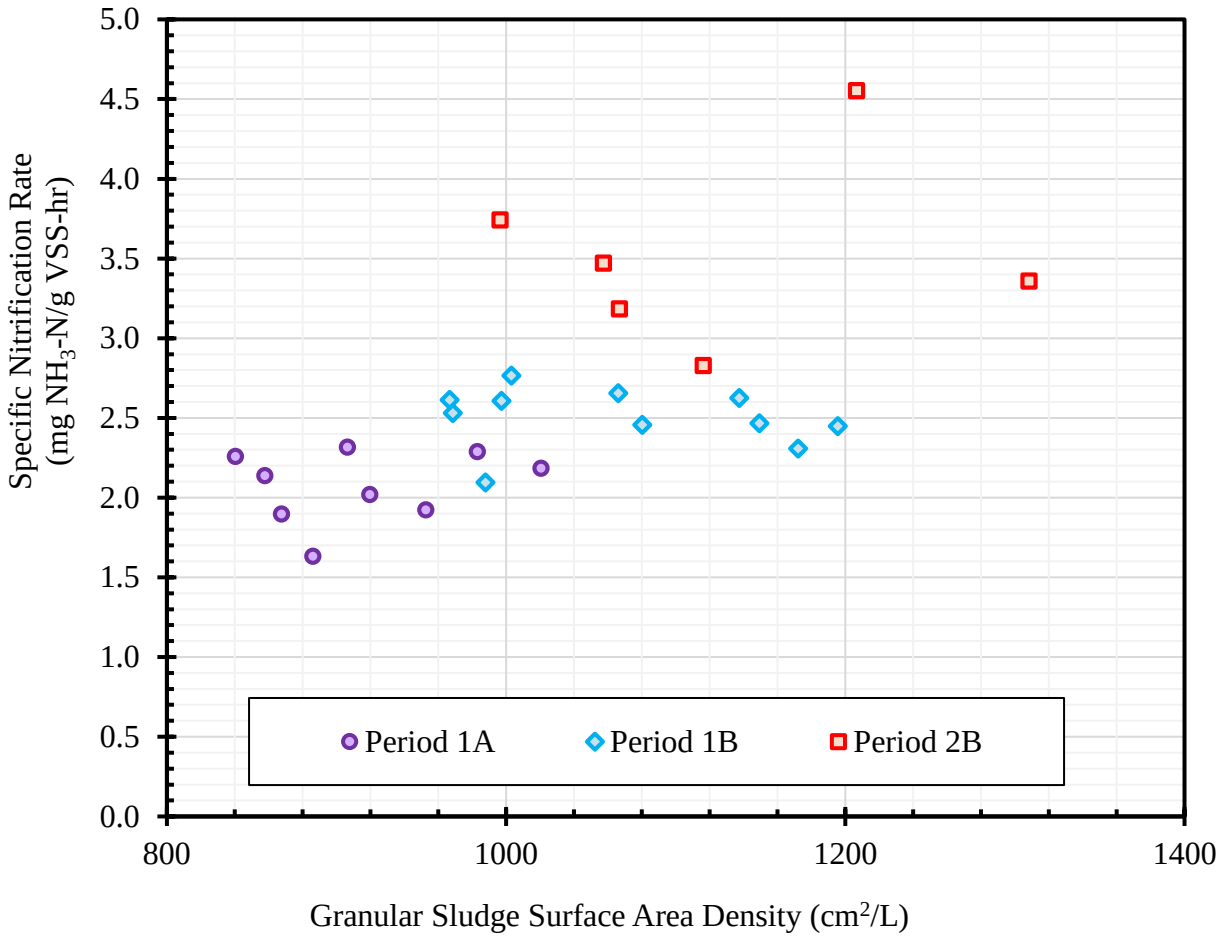

Figure 4-17. Specific nitrification rate (SNR) versus granular sludge surface area density for Period 1A (purple circle), Period 1B (blue diamond), and Period 2B (red square). Data from Periods 1C and 2A not shown due to a lack of data points for SNR during these periods.

4.4 *Simultaneous Nitrification and Denitrification*

The SND efficiency was consistently above 80% throughout the full operating period, as shown in Figure 4-18A. As a result, nitrification inhibition from low pH was not a concern for the sidestream operation (Figure 4-18B), and no supplemental alkalinity was needed. The denitrification, or SND, rate was approximately equivalent to the nitrification rate during the first half of aeration, which is demonstrated by non-detectable NO_2^--N and NO_3^--N concentrations in sidestream profiles (Figure 4-19 and Figure 4-20). NO_X-N accumulation typically occurred at greater rates during the last one to two hours of aeration. This accumulation was a result of a decreased denitrification rate near the end of the cycle and affected the TIN removal efficiency.

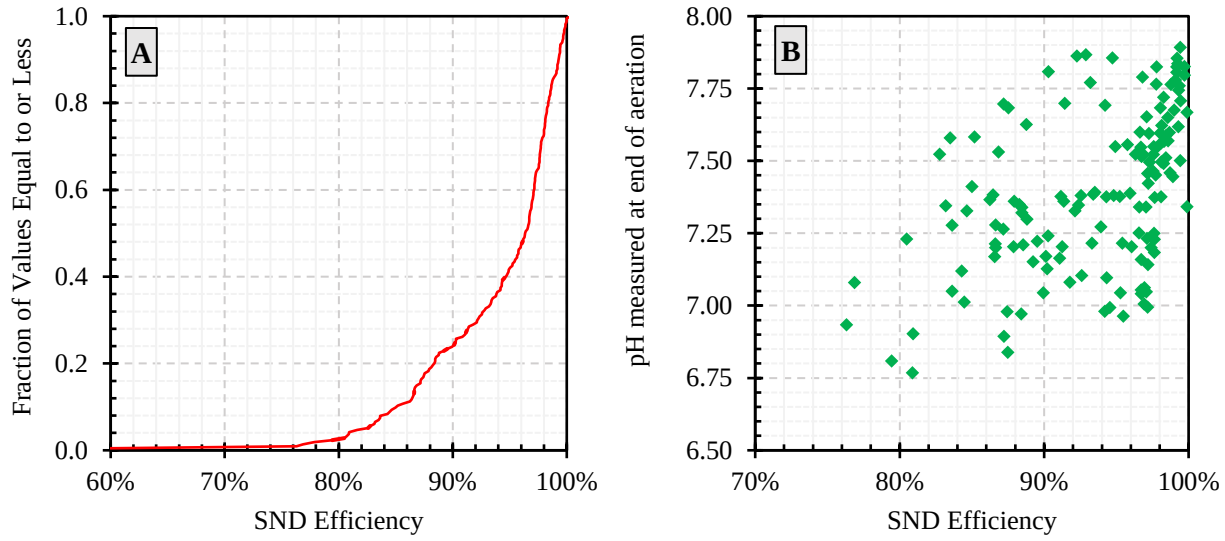

Figure 4-18. Cumulative distribution function of SND efficiency for values recorded from the start of nitrification performance (April 24, 2018) until May 17, 2019. The SND efficiency was maintained above 95% for 60% of the measurements (A), and the pH measured in the sidestream reactor at the end of aeration versus SND efficiency (B).

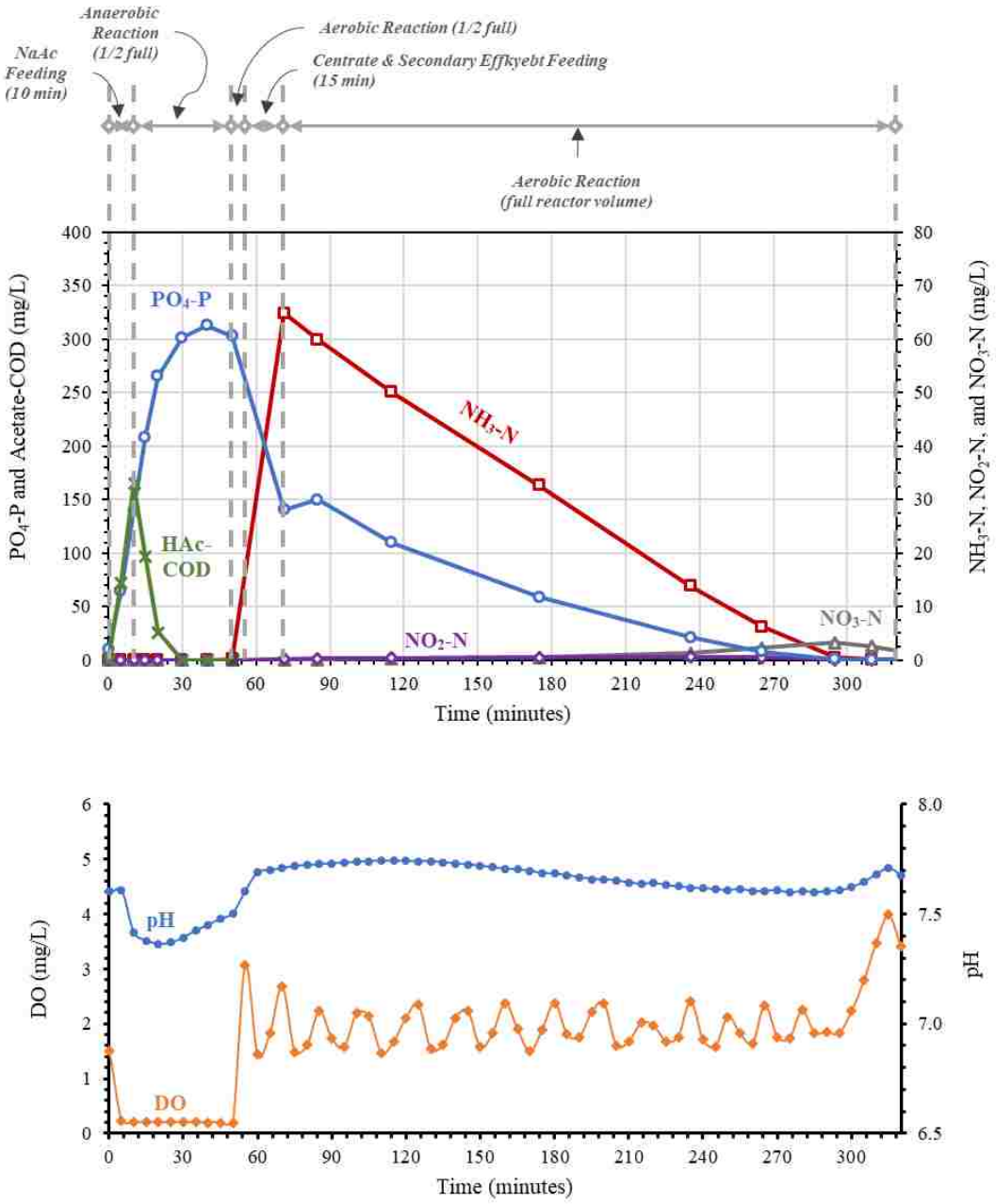

Figure 4-19. COD and nutrient profile for anaerobic and aeration phases on September 3, 2018 in sidestream reactor (top) with corresponding DO and pH changes versus time (bottom). The average temperature was 21.0°C for the cycle displayed. Zero minutes indicated the start of anaerobic acetate feeding.

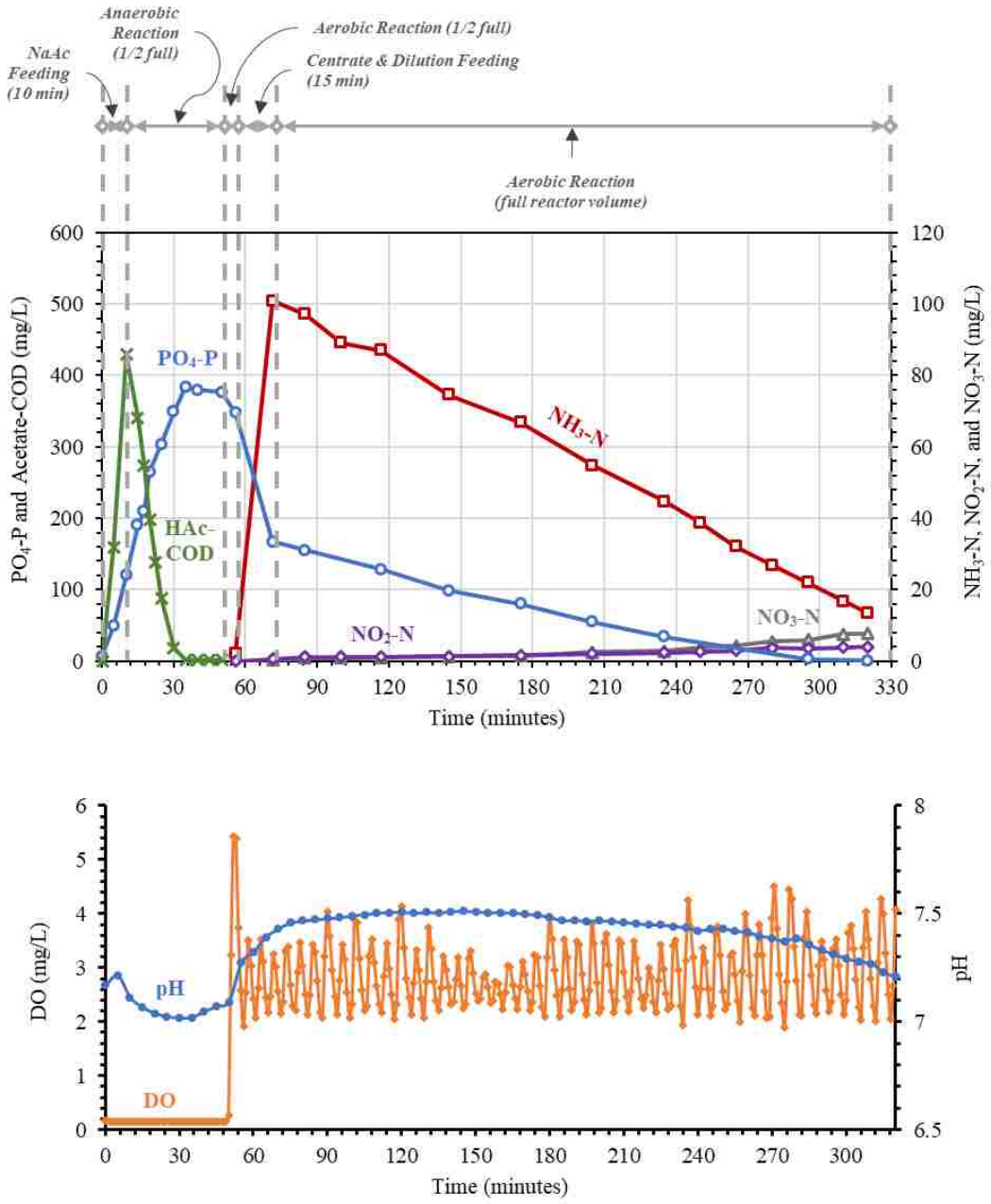

Figure 4-20. COD and nutrient profile for anaerobic and aeration phases on March 7, 2019 in sidestream reactor (top) with corresponding DO and pH changes versus time (bottom). The average temperature was 20.5°C for the cycle displayed. Zero minutes indicated the start of anaerobic acetate feeding.

The average SND efficiency was above 85% for all the performance periods. Differences in SND efficiency between performance periods demonstrated the impact of anaerobic COD feed duration and average aeration DO concentration. The effect of COD feed duration and bulk liquid COD concentration in the anaerobic phase were demonstrated in Periods 1A and 1B. After decreasing the COD feed duration from 30 minutes in Period 1A to 10 minutes in Period 1B, the SND efficiency started to increase and reached the full operation average of 94% within 8 days (Figure 4-21). This showed that while the COD feed duration and anaerobic acetate concentration affected the SND efficiency, a change in these parameters did not lead to an instantaneous increase in SND performance. Overall, the average SND efficiency was noticeably higher during Period 1B when the COD feed duration was 10 minutes compared to Period 1A when the COD feed duration was 30 minutes (Figure 4-22).

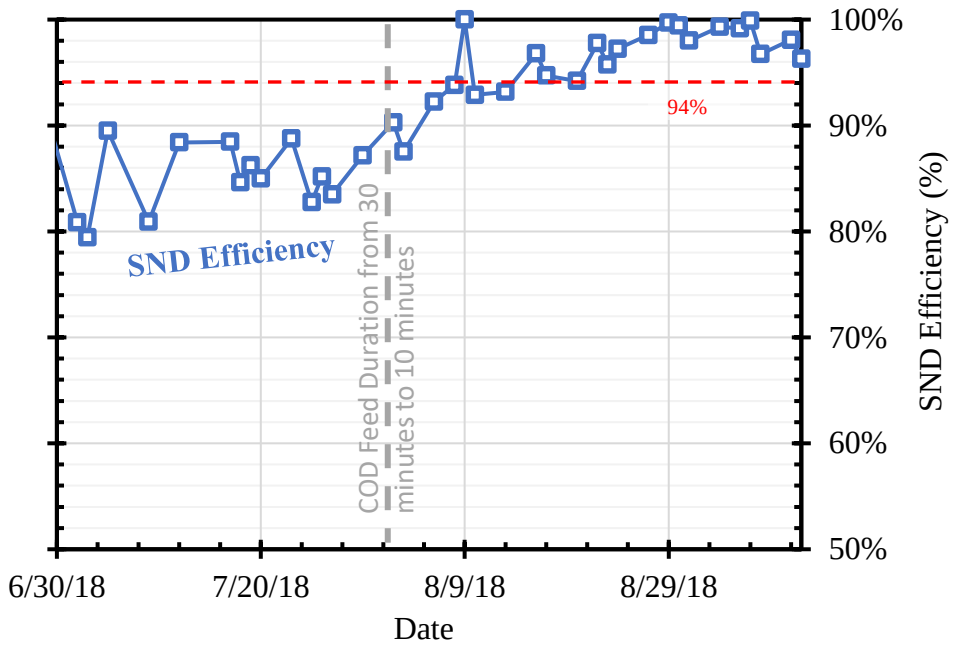

Figure 4-21. SND efficiency versus time from June 30 to September 11, 2018. On July 31, 2018 the COD feed duration was decreased from 30 to 10 minutes. A 94% SND efficiency was the average value during the full operating period and drawn as a benchmark using a horizontal red dashed line.

The DO concentration also affected SND efficiency, which was demonstrated in Periods 2A and 2B, where Period 2A had an average DO concentration of 3.2 ± 0.2 mg/L and 2B had an average DO concentration of 2.3 ± 0.2 mg/L. During these periods the NH_3-N loading was similar at a rate 0.46 ± 0.01 g/L-d during Period 2A and 0.44 ± 0.02 g/L-d during Period 2B. The COD:N feed ratio was lowered in Period 2B to 2.9 ± 0.2 g/g from a ratio of 3.8 ± 0.1 g/g in Period 2B, and a lower COD:N feed ratio could have cause a decreased SND efficiency during Period 2B. Instead, higher SND efficiencies were observed at the lower operating DO concentrations in Period 2B, as shown in Figure 4-23. Although not a controlled study, lowering the average aeration phase DO from 3.2 to 2.3 mg/L between Periods 2A and 2B resulted in an increased average SND efficiency in Period 2B by 4%, despite Period 2B being operated at a lower COD:NH_3-N ratio and similar NH_3-N loading rate compared to Period 2A.

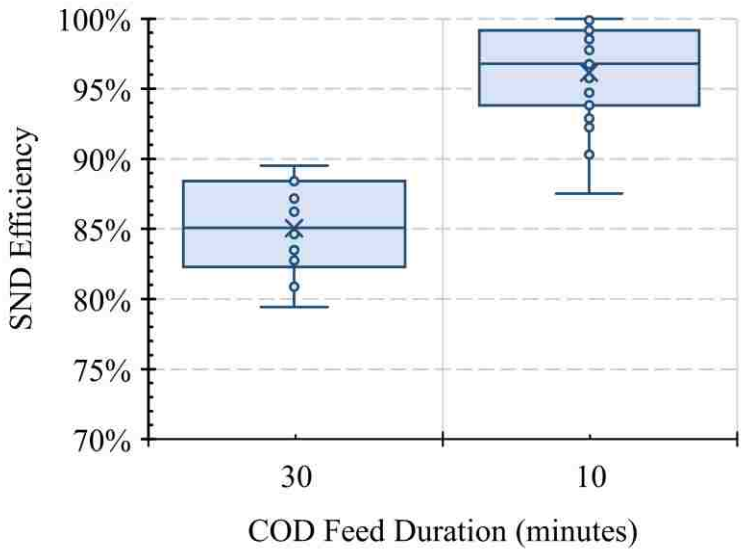

Figure 4-22. Operations with a shorter COD feed duration in Period 1B versus 1A had a higher SND efficiency.

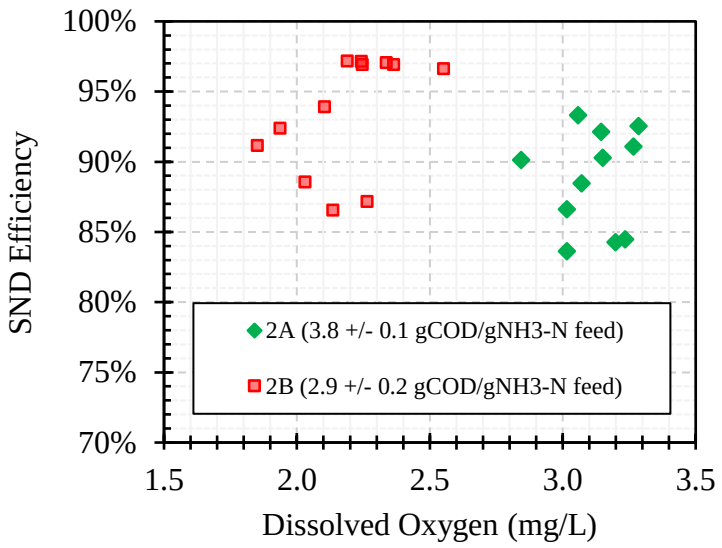

Figure 4-23. Higher aeration phase average DO concentrations corresponded with lower SND efficiencies. Performance Periods 2A and 2B are operated at different DO concentrations and COD:N feed ratios.

4.4.1 Carbon to Nitrogen Removal Ratio

Three ratios of carbon to nitrogen were assessed during the full operating period: 1) the ratio of COD to NH_3-N in feed sources (COD:N feed ratio), 2) the ratio of COD fed to TIN removed (COD:Nr ratio), and 3) the ratio of COD fed to NO_X-N reduced (COD:NOr ratio).

The COD:N feed ratio was adjusted during the full operating period and ranged from 0.6 to 8.7 g/g. Maximum and minimum values occurred briefly due to temporary dilutions of either the centrate or supplemental COD feed solutions to mitigate excess nitrification or acetate leakage, respectively. The COD:Nr ratio was higher than COD:N feed ratio due to incomplete TIN removal efficiency. The COD:NOr ratio accounted for NH_3-N assimilated by heterotrophs and was thus higher than the COD:Nr ratio. Organic carbon from endogenous decay, centrate or secondary effluent feed solutions was not measured or considered in the carbon to nitrogen ratios

reported during the full operating period. Organic carbon in centrate and secondary effluent was considered negligible.

During stable operating periods, the COD:N feed ratio was highest in Periods 1A, 1B, and 1C, with the highest ratio in Period 1B at 4.5 ± 0.3 g/g (Table 4-9). During these periods, the average COD:Nr ratio ranged from 4.7 to 5.0 g/g and the average COD:NOr ratio ranged from 5.3 to 5.7 g/g. In general, these ratios were relatively constant in comparison to each other and higher compared to the carbon to nitrogen ratios in Periods 2A and 2B.

In Period 2A the COD:N feed ratio decreased to 3.8 ± 0.1 g/g due to an increase in the NH_3-N loading rate. In Period 2B the feed ratio decreased again to 2.9 ± 0.2 g COD/g NH_3-N due to a decrease in the COD loading rate. Lower COD:N feed ratios did not limit denitrification and a SND efficiency of 93 ± 4% was achieved with a feed ratio of 2.9 ± 0.2 g COD/g NH_3-N. Lower COD:N feed ratios also corresponded with lower COD:NOr ratios. The COD:NOr ratios in Periods 2A and 2B were 4.7 ± 0.3 and 3.4 ± 0.4 g COD fed per g NO_X-N removed.

Table 4-9. Average values for COD:N feed and removal ratios with relevant sidestream reactor operation and performance parameters for stable operating periods.

Parameter	Units	1A	1B	1C	2A	2B
NH_3-N Loading Rate	g/L-d	0.36 (0.04)	0.36 (0.03)	0.40 (0.02)	0.46 (0.01)	0.44 (0.02)
Aeration DO	mg/L	1.9 (0.1)	2.0 (0.1)	2.8 (0.3)	3.1 (0.2)	2.3 (0.2)
SND Efficiency	%	85 (3)	96 (3)	91 (6)	89 (4)	93 (4)
TIN Removal Efficiency	%	86 (4)	94 (3)	88 (6)	88 (4)	90 (6)
Effluent pH		7.3 (0.3)	7.8 (0.2)	7.3 (0.4)	7.2 (0.1)	7.2 (0.2)
COD:N Feed Ratio	g/g	4.2 (0.4)	4.5 (0.3)	4.2 (0.2)	3.8 (0.1)	2.9 (0.2)
COD:Nr Ratio	g/g	5.0 (0.3)	4.8 (0.4)	4.7 (0.3)	4.3 (0.2)	3.2 (0.3)
COD:NOr Ratio	g/g	5.7 (0.23)	5.4 (0.5)	5.3 (0.5)	4.7 (0.3)	3.4 (0.4)

4.5 *Phosphorus Removal*

PO_4^{3-}-P removal was not a direct objective of this study; however, maintaining a stable PAO population was desired to maintain granules with good settling characteristics and SND capability. PO_4^{3-}-P removal performance did not correlate well with NH_3-N or TIN removal during stable performance periods. As noted in Section 4, average NH_3-N and TIN removal efficiency was greater than 96 and 86% during performance periods; however, the average PO_4^{3-}-P removal efficiency during these periods ranged from 29 to 98% (Table 4-10). A noticeable deterioration in PO_4^{3-}-P removal performance occurred from Period 1A to Period 1C. During this time, the PO_4^{3-}-P removal efficiency dropped from an average of 70 ± 24% in Period 1A to 57 ± 43% in Period 1B and to 29 ± 75% in Period 1C. High standard deviations were a result of variable and negative removal performance. Negative PO_4^{3-}-P removal occurred when anaerobic PO_4^{3-}-P release by PAOs was greater than subsequent PO_4^{3-}-P uptake during aeration. The P/C ratio decreased from Period 1A to 1C along with the decreased PO_4^{3-}-P removal performance.

However, the P/C ratio did not appear to be an absolute measure of removal performance or capacity because similar ratios in Period 1B (0.48 ± 0.11) and 2A (0.45 ± 0.03) were measured, yet removal performance was much higher in Period 2A at a removal efficiency of 98 ± 3%.

Overall, the PO_4^{3-}-P removal efficiency was highest during Periods 2A and 2B at 98 ± 2% and 95 ± 11%, respectively. These removal efficiencies corresponded with PO_4^{3-}-P removal per MLVSS of 3.26 ± 0.22 and 3.61 ± 0.21 mg P/g VSS, respectively, and an average effluent concentration below 2.0 mg P/L. These performances were done at loading rates of 0.056 ± 0.002 and 0.064 ± 0.002 g PO_4^{3-}-P/L-d.

Table 4-10. Average PO_4^{3-}-P loading and removal efficiency and other relevant parameters.

Parameter	Units	1A	1B	1C	2A	2B
PO_4^{3-}-P Loading Rate	g/L-d	0.058 (0.006)	0.058 (0.006)	0.066 (0.004)	0.056 (0.002)	0.064 (0.002)
PO_4^{3-}-P Removal Efficiency	%	70 (24)	57 (43)	29 (75)	98 (2)	95 (11)
NH_3-N Removal Efficiency	%	99 (2)	98 (3)	96 (5)	98 (3)	96 (5)
TIN Removal Efficiency	%	86 (4)	94 (3)	88 (6)	88 (4)	90 (6)
Effluent PO_4^{3-}-P	mg/L	8.3 (6.3)	13.5 (14.0)	24.0 (26.6)	0.5 (0.5)	1.6 (3.4)
Anaerobic Phase pH		7.1 (0.2)	7.5 (0.0)	7.5 (0.1)	7.1 (0.0)	7.1 (0.1)
GAO/PAO Abundance Ratio by qPCR	gene copy number / gene copy number	0.06 (0.00)	1.02 (0.00)	N/A (N/A)	0.27 (0.00)	0.09 (0.00)
P/C Ratio	mol P/ mol C	0.62 (0.05)	0.48 (0.11)	0.37 (0.05)	0.45 (0.03)	0.58 (0.04)
PO_4^{3-}-P removed per MLVSS	mg P/g VSS	2.13 (0.74)	1.70 (1.36)	1.24 (3.78)	3.26 (0.22)	3.61 (0.21)
COD fed to PO_4^{3-}-P removed	g/g	44.3 (22.4)	16.4 (70.3)	74.5 (111.1)	30.8 (1.4)	21.0 (4.9)
PO_4^{3-}-P removed per NO_X-N removed	g/g	0.15 (0.06)	0.12 (0.08)	-0.09 (0.33)	0.13 (0.01)	0.17 (0.01)

4.5.1 Acetate Removal Kinetics

Acetate removal kinetics were measured from sidestream reactor profiles of COD concentration versus time during the anaerobic phase after acetate feeding (Figure 4-24). Measured removal kinetics remained relatively linear, even at bulk COD concentrations near 20 mg/L. This was apparent from the high coefficients of determination ($R^2 > 0.98$) obtained while using linear regression to measure acetate removal rates, as shown in Figure 4-24.

Anaerobic acetate removal kinetics provided enough time for complete acetate removal within the 50-minute anaerobic feed and reaction phases. The exception to this was during upset periods when acetate removal rates decreased and resulted in acetate leakage into the aeration phase. The average acetate removal rate and specific acetate removal rate (SAUR) were measured 10 times during acetate leakage events (acetate removal efficiency below 98%) and 50 times when acetate removal efficiencies were greater than 98% (Table 4-11). The average SAUR during acetate leakage events was 32.0 ± 9.5 mg COD/g VSS-hr, whereas during the full operating period, excepting leakage events, the average SAUR was 70.4 ± 24.8 mg COD/g VSS-hr.

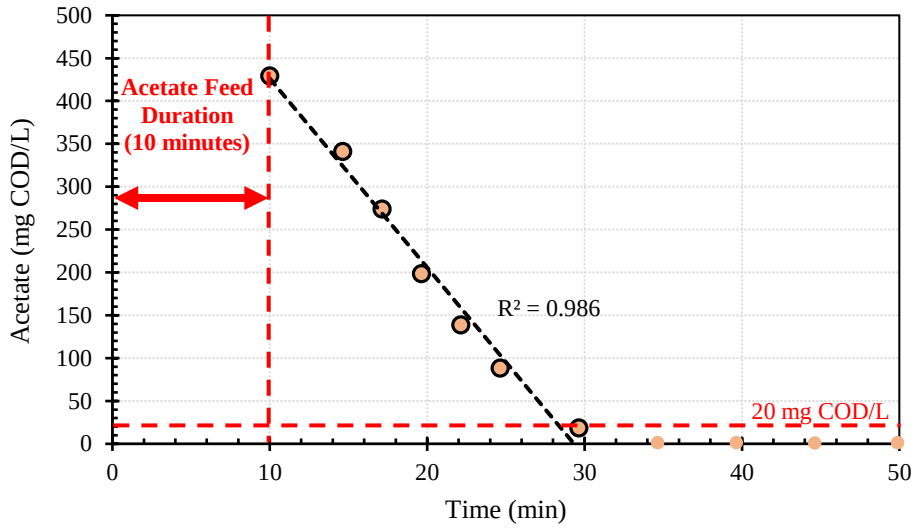

Figure 4-24. Example of sidestream reactor profile of COD concentration versus time during anaerobic phase after feeding. A linear trend line was fit to data points outlined with black circles ($R^2 > 0.98$), where acetate concentration ranged from 29 to 429 mg COD/L.

Table 4-11. Statistics of specific acetate uptake rates measured during upset events and anaerobic acetate breakthrough (< 98%) and during non-breakthrough performance (> 98%).

	Anaerobic Acetate Removal Efficiency	
	< 98%	≥ 98%
Specific Acetate Uptake Rate (mg COD/g VSS-hr)		
Maximum	44.2	119.6
Minimum	12.0	32.2
Average	32.0	70.4
Standard Deviation	9.5	24.8
Median	33.2	66.0

During stable performance periods, the SAUR was higher and ranged from 84.0 ± 20.4 to 98.9 ± 0.6 mg COD/g VSS-hr during performance periods with 10-minute acetate feed durations, as shown in Table 4-12. Period 1A had a 30-minute acetate feed phase compared to the 10-minute feed phase in Period 1B. Therefore, instead of a direct comparison of acetate uptake rates, the concentration at 30 minutes after the start of anaerobic feeding was measured and compared, as

shown in Figure 4-25. Higher anaerobic acetate concentrations at 30 minutes after feeding in Period 1A show slower SAURs when the COD feed duration was longer.

Table 4-12. Acetate removal kinetics parameters for stable performance periods.

Parameter	Units	1A	1B	1C	2A	2B
Acetate Loading Rate	g COD/L-d	1.49 (0.00)	1.62 (0.08)	1.67 (0.00)	1.76 (0.00)	1.28 (0.06)
7-day average SRT	days	40 (12)	31 (3)	26 (1)	23 (3)	27 (8)
F/M (sodium acetate)	g COD/g VSS-d	0.15 (0.01)	0.18 (0.01)	0.18 (0.02)	0.20 (0.01)	0.14 (0.02)
COD Feed Duration	min	30	10	10	10	10
Acetate Uptake Rate	mg COD/L-min	12.4[A] (1.2)	25.4 (6.1)	28.7 (0.8)	24.2 (6.1)	25.1 (N/A)
Specific Acetate Uptake Rate	mg COD/g VSS-hr	37.9 (4.9)	84.0 (20.4)	98.9 (0.6)	84.1 (19.9)	86.3 (N/A)

Note: [A] Acetate uptake rate, and specific acetate uptake rate, were measured from in situ reactor profiles and were measured after the end of the COD feed phase, which was 20 minutes later in the anaerobic phase during Period 1A compared to Periods 1B, 1C, 2A, and 2B.

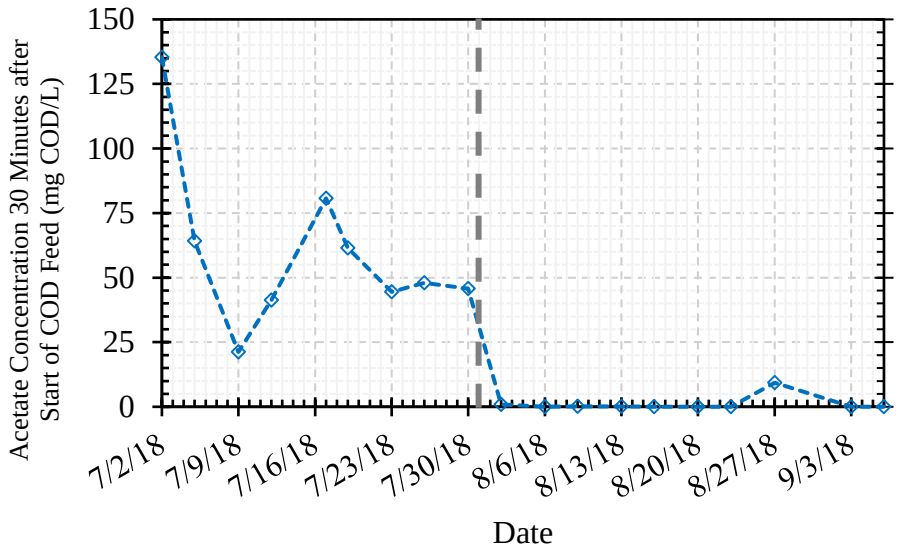

Figure 4-25. Acetate bulk liquid concentration measured 30 minutes after the start of the anaerobic COD feed phase in the sidestream reactor. Vertical line indicates when COD feed duration was changed from 30 minutes to 10 minutes on July 31, 2018 at 1:00 PM.

4.5.2 Phosphorus Removal Kinetics

PO_4^{3-}-P removal kinetics were assessed from profiles measured during the aeration phase from July 2, 2018 to September 6, 2018. The PO_4^{3-}-P removal rates demonstrated an exponential decay behavior in July 2018 when the anaerobic feed duration was 30-minutes in length, and when the COD feed duration was shortened to 10 minutes a more linear PO_4^{3-}-P removal profile was observed, as shown in Figure 4-26. To quantify these changes the initial and final rates of PO_4^{3-}-P removal were measured using linear portions of the PO_4^{3-}-P removal profile during the first and last hour of aeration, respectively (Figure 4-27). The average ratio of initial and final PO_4^{3-}-P removal rates was 11.7 when the COD feed duration was 30 minutes and the ratio dropped to 1.9 during the period of a 10-minute COD feed duration. When considering the profiles from 10-minute COD feed periods, the average initial specific PO_4^{3-}-P uptake rate was 5.9 mg P/g VSS-hr and the average final specific phosphorus uptake rate was 3.3 mg P/g VSS-hr.

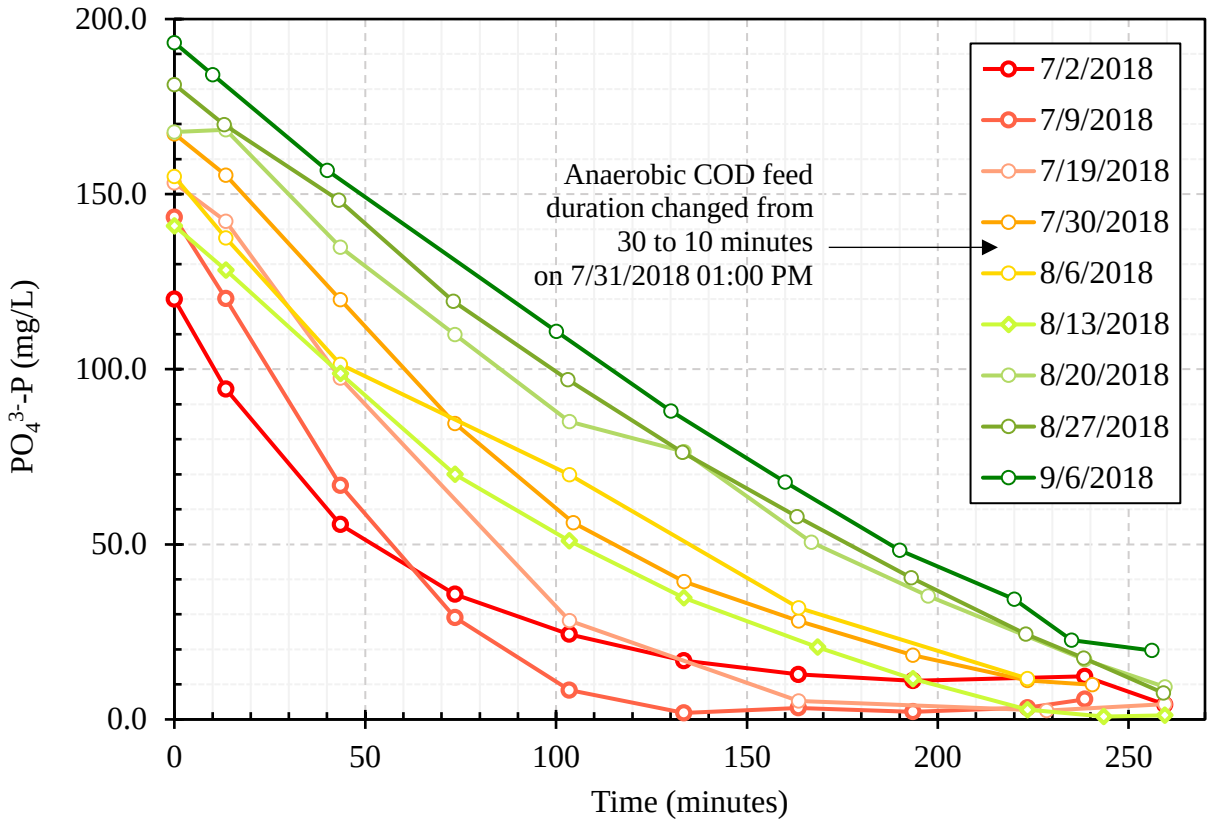

Figure 4-26. PO_4^{3-}-P removal profiles during aeration demonstrates a change in removal behavior from an exponential decay trend to linear profile. The COD feed duration was decreased from 30 to 10 minutes on July 31, 2018 at 01:00 PM and profiles appear to become more linear after this date.

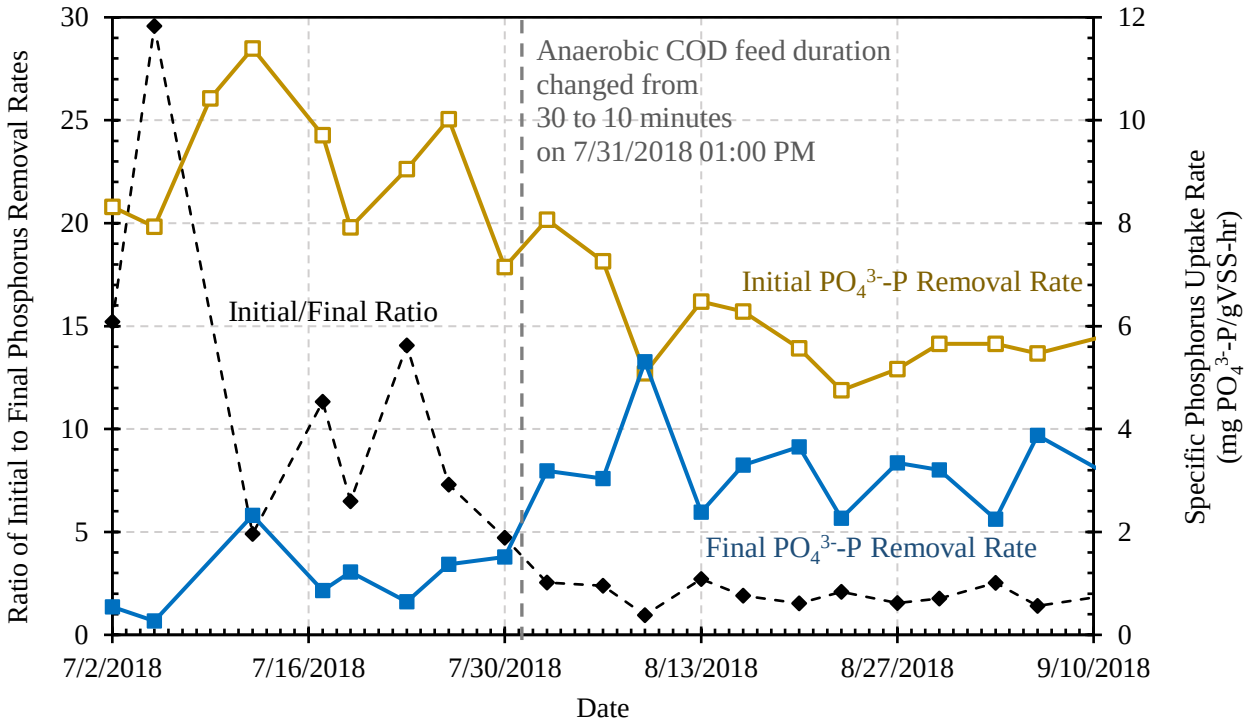

Figure 4-27. Initial and final specific PO_4^{3-}-P uptake rates and the ratio of the initial and final removal/uptake rates. The COD feed duration was decreased from 30 to 10 minutes on July 31, 2018 at 01:00 PM and profiles appear to become more linear after this date.

5 Discussion

5.1 *Operating Conditions and Reactor Performance*

The overall performance for the pilot plant 10.5-month operation showed nitrification, TIN, and SND removal efficiencies of 84, 78, and 94%, respectively, but during the stable period without upsets these efficiencies were 96, 90, and 93%, respectively. The treatment capability is best illustrated by performance during stable periods 2A and 2B, without PAO and nitrification inhibition and is used here for comparison to results from SBR granular reactor bench-scale studies by Figdore et al. (2018a) and Yilmaz et al. (2008) in Table 5-1.

All operations in Table 5-1 had PAO-NDN granules and were operated at similar NH_3-N loadings. Figdore et al. (2018a) simulated sidestream centrate treatment bioaugmentation, while Yilmaz et al. (2008) evaluated aerobic granular sludge treatment of an anaerobic pond effluent for pretreatment of abattoir wastewater. The SBR cycle for the bench-scale study by Figdore et al. (2018a) was similar to the pilot plant reactor, but the VFA feed consisted of 75% acetate and 25% propionate and the centrate was diluted with tap water. The Yilmaz et al. (2008) SBR was fed anaerobic pond effluent with acetate addition in the anaerobic feed phase. The pond effluent soluble COD (sCOD) concentration averaged 270 mg/L, which was 40% biodegradable sCOD and 25% VFA. The SBR cycle and aeration time was longer at 8 hours and 315 minutes versus the 6-hour and 249-minute operations by this study and Figdore et al. (2018a). Yilmaz et al. (2008) also had a longer 80-minute mixed postanoxic period before settling compared to Figdore et al. (2018a) and this study at 41.8 and 23.5 minutes after decanting.

Table 5-1. Operating conditions and performance comparison of Period 2A and 2B to Figdore et al. (2018a) and Yilmaz et al. (2008).

Parameter	Units	Period 2A	Period 2B	Figdore et al. (2018a)	Yilmaz et al. (2008)
Feed		centrate/ secondary effluent	centrate/ secondary effluent	centrate/ tap water	anaerobic pond effluent
Supplemental Carbon		sodium acetate	sodium acetate	sodium acetate/ sodium propionate	sodium acetate
Reactor Volume	L	176	176	2	5
Cycle Time	hr	6	6	6	8
Selector Settling Velocity	m/hr	9.1	9.1	10.1	10.4
Operating Conditions					
NH_3-N loading	g/L-d	0.46 (0.01)	0.44 (0.02)	0.45 (0.03)	0.44 (0.01)
VFA-COD:N feed	g/g	3.8 (0.1)	2.9 (0.2)	3.4	3.7
SRT	d	23 (3)	27 (8)	16 (2)	15-20
Average Aeration DO	mg/L	3.1 (0.2)	2.3 (0.2)	1.8-2.2	3.3 (3.0-3.5)
Temperature	°C	20.9 (1.9)	20.5 (1.1)	18.0 (N/A)	18.0-22.0
pH		7.3 (0.1)	7.3 (0.1)	8.0 (0.1)	7.0-8.5
Performance					
Avg. Granule Diameter	mm	1.5	1.4	1.3 (0.6)	1.0
SVI_5	mL/g	31 (2)	26 (1)	22 (4)	N/A
NH_3-N removal	%	98.0 (2.8)	95.8 (4.6)	95.0 (6.0)	99.7
TIN removal	%	88.0 (3.9)	89.6 (5.6)	90.1	95.8
SND N removal	%	88.8 (3.5)	93.5 (4.2)	94.2	80.0-85.0

The granular sludge reactor nitrification efficiency performance is affected by the SRT, aeration DO concentration, and total granular surface area. All three reactors had high nitrification efficiency of 95.0 to 99.7% at average SRTs from 16 to 27 days and average DO concentrations of 2.0 to 3.3 mg/L. The TIN removal efficiency is related to the nitrification efficiency and SND efficiency. This study and Figdore et al. (2018a) had similar TIN and SND efficiency, ranging from 88 to 90% and 89 to 94%, respectively. Yilmaz et al. (2008) had a higher TIN removal efficiency of 96% but lower SND efficiency. The higher TIN efficiency was due to the longer postanoxic period after aeration and before decanting.

The SND efficiency is affected by the COD:N feed ratio, granular size, SRT, and aeration DO concentration. The granular size is affected by the selective settling velocity, which is the particle settling velocity needed to reach a depth below the decant depth at a given settling time. Based on decant depth and settling times used, the selective settling velocities were within 10% for all three studies at 9.1 to 10.4 m/hr. However, the granular size of 1.0 mm for Yilmaz et al. (2008) was significantly smaller than the 1.3 to 1.5 mm sizes for this study and Figdore et al. (2018a). The lower SND efficiency for Yilmaz et al. (2008) compared to Figdore et al. (2018a) was likely due to the higher aeration DO concentration and smaller granular size because their COD:N feed ratios and SRTs were similar.

The slightly higher SND efficiency by Figdore et al. (2018a) compared to Periods 2A and 2B may have been related to more NOB suppression. Denitrification of NO_2^- requires less COD than for NO_3^-. Figdore et al. (2018a) and Period 2B had similar effluent NO_X-N concentration, but 84% of the effluent NO_X-N was NO_2^- in Figdore et al. (2018a) compared to 19% for Period 2B.

5.2 *Granule Size and Size Distribution*

A predominantly granular sludge was maintained in the sidestream reactor. Based on a minimum size of 0.212 mm to define a granule (De Kreuk et al., 2007), the reactor mixed liquor consisted of over 90% granules. Over 85% of the mixed liquor was retained on a 0.425 mm sieve. Sidestream mixed liquor contained granules of varying size and the granule size reported herein is a weighted average size for the mass retained on up to 11 sieves ranging from 0.212 mm to 2.80 mm for a mixed liquor sample.

The granular sludge morphology and size result in a much higher settling velocity than for flocculent sludge. The settling time of 7 or 8 minutes was selected to retain particles with settling velocity from 9.1 to 10.5 m/hr or more. As shown in Figure 5-1, the mixed liquor interfacial settling velocity was higher than the required settling velocity for particle retention when the granule size was greater than 0.8 mm and generally increased with larger granule size. The settled sludge blanket after 10 minutes of settling and decant was generally at about a third of the reactor volume, much lower than the 50% VER for the SBR. The settled volume depth is a result of the rapid thickening rate and low SVI of the granular sludge.

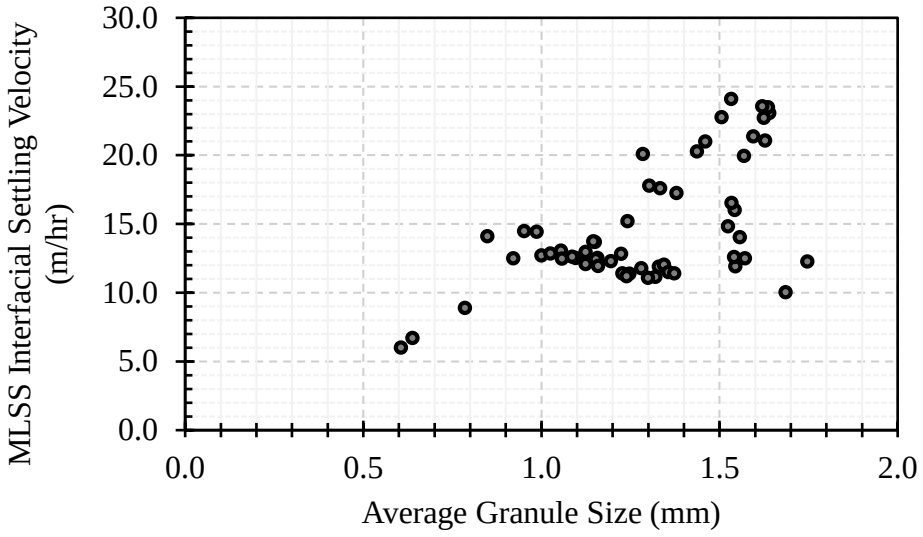

Figure 5-1. Initial mixed liquor interfacial settling velocity versus average granule size. Full-volume reactor MLSS concentrations ranged from 9.0 to 15.0 g/L during the operating period for plotted data.

The higher interfacial settling velocity compared to the selective settling velocity suggests other factors may have affected granule size. One possibility is the high bulk liquid acetate substrate gradient during the anaerobic phase to enable substrate diffusion into deeper granule biofilm depth. By the end of the 10-minute anaerobic feeding period under stable operations the bulk liquid acetate COD concentration ranged from 170 to 430 mg/L.

During stable performance periods the granule size ranged from 1.1 to 1.5 mm. In addition to settling velocity, granule size and size distribution is important with respect to nitrification and SND capacity and efficiency. Smaller granules have a greater surface area to volume and thus would have higher SNR. Larger granules have a greater anoxic volume which would increase SND efficiency. As shown in Figure 4-17, the SNR was not limited by the reactor granular sludge surface area density (cm^2/L). The average size was also large enough to promote over 90% SND efficiency at the controlled DO concentration average of 2.0 to 3.2 mg/L. Thus, granules size of 1.1 to 1.5 mm for the reactor SRT and MLSS concentration during stable operating periods met both nitrification and nitrogen removal needs.

Theoretically, there would need to be a lower reactor SRT that resulted in lower MLSS concentration and lower reactor granular sludge surface area density to decrease the nitrification efficiency from that observed at our operating conditions. Nitrification limitation could also occur at the SRT used in this study if the reactor had much larger granule size. This may have been possible if a much shorter settling time was used.

Typically, only the average granule diameter is reported when quantifying granular MLSS morphology, but this study showed the importance of including size distribution to characterize a granular sludge system and the biofilm surface area density. A granule size of about 1.4 mm was measured five times from July 7, 2018 to May 17, 2019. During this time the size distribution changed, becoming more uniform at longer reactor operating times as was shown in Figure 4-5 and Figure 4-7. Granular size distribution characterization may be done by plotting the percent

by weight equal to or less versus the sieve sizes used and then reporting the 10, 50, and 90 percentile sizes.

5.3 *Shortcut Nitrogen Removal*

Minimizing the COD:N feed ratio was an operating objective for the pilot reactor along with maximizing the SND efficiency. Subject to variations in the centrate feed NH_3-N concentration and reactor upsets, the COD:N feed ratio was adjusted with an aim towards a minimum value while sustaining high SND efficiency. The average COD:N feed ratio during the stable operating periods ranged from 2.9 to 4.5 g/g with the lowest values in the last two periods, Periods 2A and 2B, of 3.8 and 2.9 g/g, respectively. These are within the range of the 3.4 g COD/g NH_3-N value reported by Figdore et al. (2018a). The COD:NOr ratios for Period 2A, Period 2B, and Figdore et al. (2018a) are 4.7, 3.4, and 4.2 g/g, respectively.

The COD:N needed for high SND efficiency is affected by the degree of NOB suppression and shortcut nitrogen removal. Figdore et al. (2018a) attributed their relatively low COD:N ratio to the presence of NOB suppression and shortcut nitrogen removal based on a higher effluent NO_2^--N concentration of 9.5 mg/L versus 2.0 mg/L for NO_3^--N and an AOB/NOB abundance ratio of 6.4. The ratio of AOB to NOB biomass for complete oxidation of NH_3 to NO_3^- is proportional to their respective synthesis yield coefficients per unit of nitrogen oxidized, assuming equal specific endogenous decay rates. AOB/NOB yield ratios of 2.1 to 2.5 have been reported by Fang et al. (2009). Assuming that the AOB and NOB biomass is equally proportional to their qPCR abundance, a qPCR AOB/NOB abundance ratio greater than 2.5 indicates some level of NOB suppression with higher values at greater NOB suppression.

NOB suppression was claimed by Figdore et al. (2018a) to be due to a free ammonia (FA) concentration of 1.6 mg/L at the start of aeration from the elevated NH_3-N concentration and pH. A threshold value for FA inhibition has not been established in studies with flocculent sludge due to varying observed inhibition concentrations from 0.10 to 10.0 mg/L (Anthonisen et al., 1976; Simm et al., 2006; and Ushiki et al., 2017). The differences appear to be related to the NOB species involved.

There have not been any studies showing FA inhibition of NOB for granular sludge, and Poot et al. (2016) claimed that FA inhibition is unlikely in granular sludge due to the NH_3-N and pH gradients in the granule biofilm. They and others, in studies with laboratory air lift granular sludge reactors, have shown that the bulk liquid DO:NH_3-N concentration ratio controls NOB suppression. These studies were not done with PAO-NDN granules and no denitrification by the granules during aeration was apparent. NOB suppression was observed at a DO:NH_3-N ratios of 0.25 or less by Bartrolí et al. (2010) at 30°C and a ratio of 0.41 at 20°C by Soler-Jofra et al. (2019). Based on effluent NO_2^- and NO_3^- concentrations results shown by Poot et al. (2016) there was 80% NOB suppression at a DO:NH_3-N ratio of 0.10 or less and about 60% NOB suppression at a DO:NH_3-N ratio of 2.0 to 2.5.

The mechanism for the effect of the bulk liquid DO and NH_3-N concentration on NOB suppression is related to the spatial distribution of AOB and NOB in the granule and the DO and NH_3-N gradient from the bulk liquid. At elevated bulk liquid NH_3-N concentration, AOB may be dominant on the outer layer because it can grow faster than NOB. The consumption of DO by AOB in the outer granule aerobic layers results in lower DO concentration and thus lower NOB

activity and thus NO_2^- diffuses to the bulk liquid at a higher concentration than and NO_3^-. A higher DO concentration for the same bulk liquid NH_3-N concentration increases NOB activity. The NOB suppression may be compounded with PAO-NDN granules because the PAOs and possibly GAOs may compete with the NOB for NO_2^- in the inner granule layers.

The effluent nitrogen species and FA concentrations, maximum DO:NH_3-N ratios, AOB/NOB ratios, and batch test NO_3^--N/ NO_2^--N production ratios are examined for results in Figure 5-2 and Figure 5-3 for Periods 2A and 2B, respectively, to discuss the presence and cause of NOB suppression. The DO:NH_3-N ratio is lowest at the start of the aeration phase when NH_3 concentration is highest. As NH_3 is oxidized, the DO:NH_3-N ratio decreases and the maximum DO:NH_3-N ratio is reached at the end of the aeration phase (Figures A-6 to A-8). The results show a strong dependency on the DO:NH_3-N ratio and no significant effect of the FA concentration. Results in Figure 5-2A show variable and elevated NO_3^--N concentrations above 10 mg/L. On February 27, 2019 the DO:NH_3-N ratio dipped from above 1.0 to 0.4 and the NO_3^--N concentration decreased and NO_2^--N concentration increased. A similar effect of the decline in DO:NH_3-N ratio is seen for March 5, 2019. When the DO:NH_3-N ratio decreased to 0.2, the NO_3^--N decreased to 10 mg/L and the NO_2^--N increased to above 5 mg/L. Changes in FA concentration were not related to changes in effluent NO_2^--N concentration in a manner that would suggest NOB inhibition by FA. When the DO:NH_3-N ratio increased on February 29, 2019 and March 8, 2019, the FA concentration increased but the NO_2^--N concentration decreased.

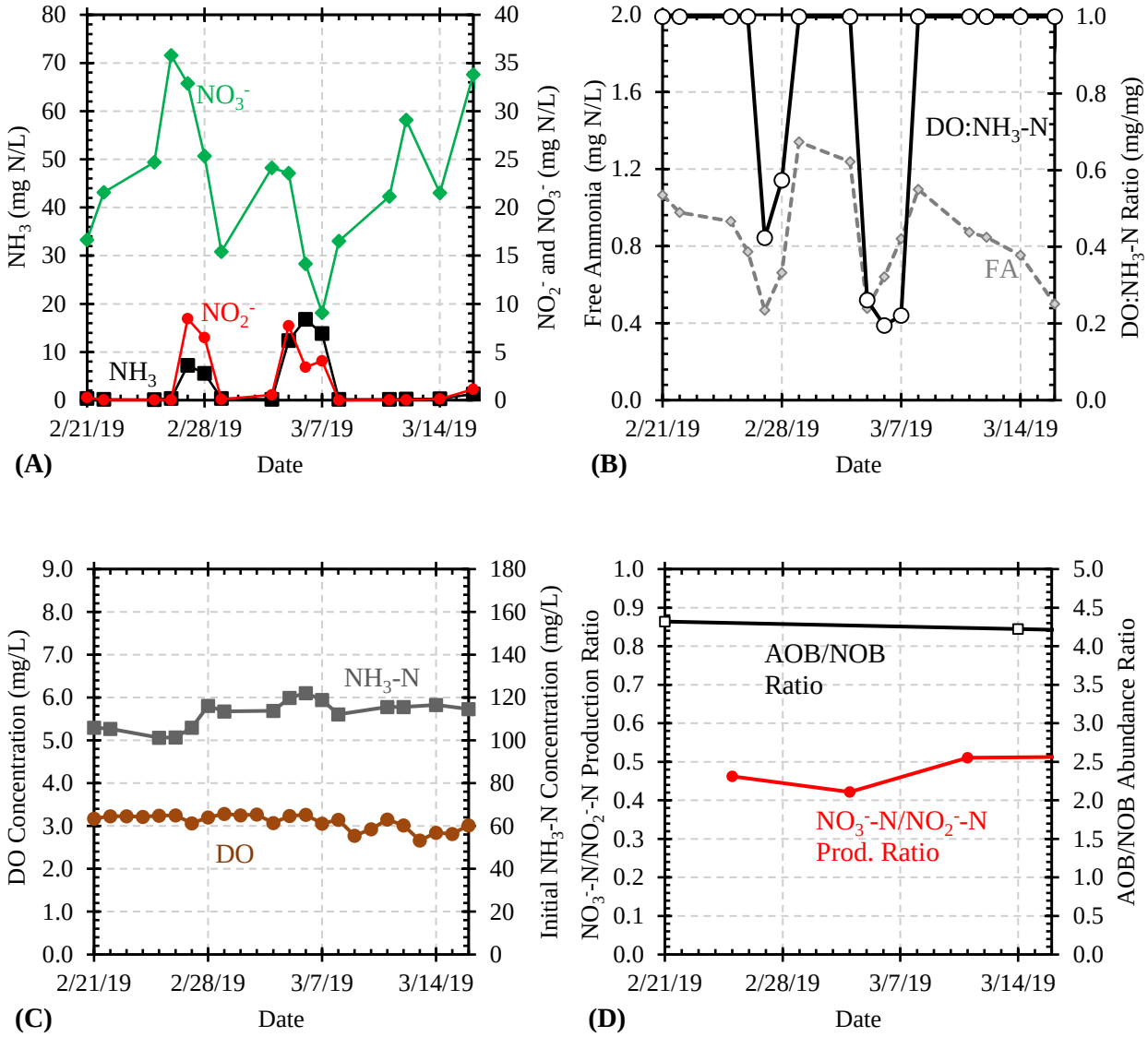

Figure 5-2. Operations and performance before and during Period 2A, from February 28, 2019 to March 17, 2019. A) Effluent NH_3, NO_2^-, and NO_3^- concentrations versus time, B) the initial free ammonia (FA) concentration and maximum DO:NH_3-N concentration ratio versus time, C) average aeration phase DO concentration and initial NH_3-N concentration versus time, and D) the NO_3^--N/NO_2^--N production rate ratio and AOB/NOB abundance ratio versus time. Any DO:NH_3-N ratio of or above 1.0 is displayed as 1.0 in (B).

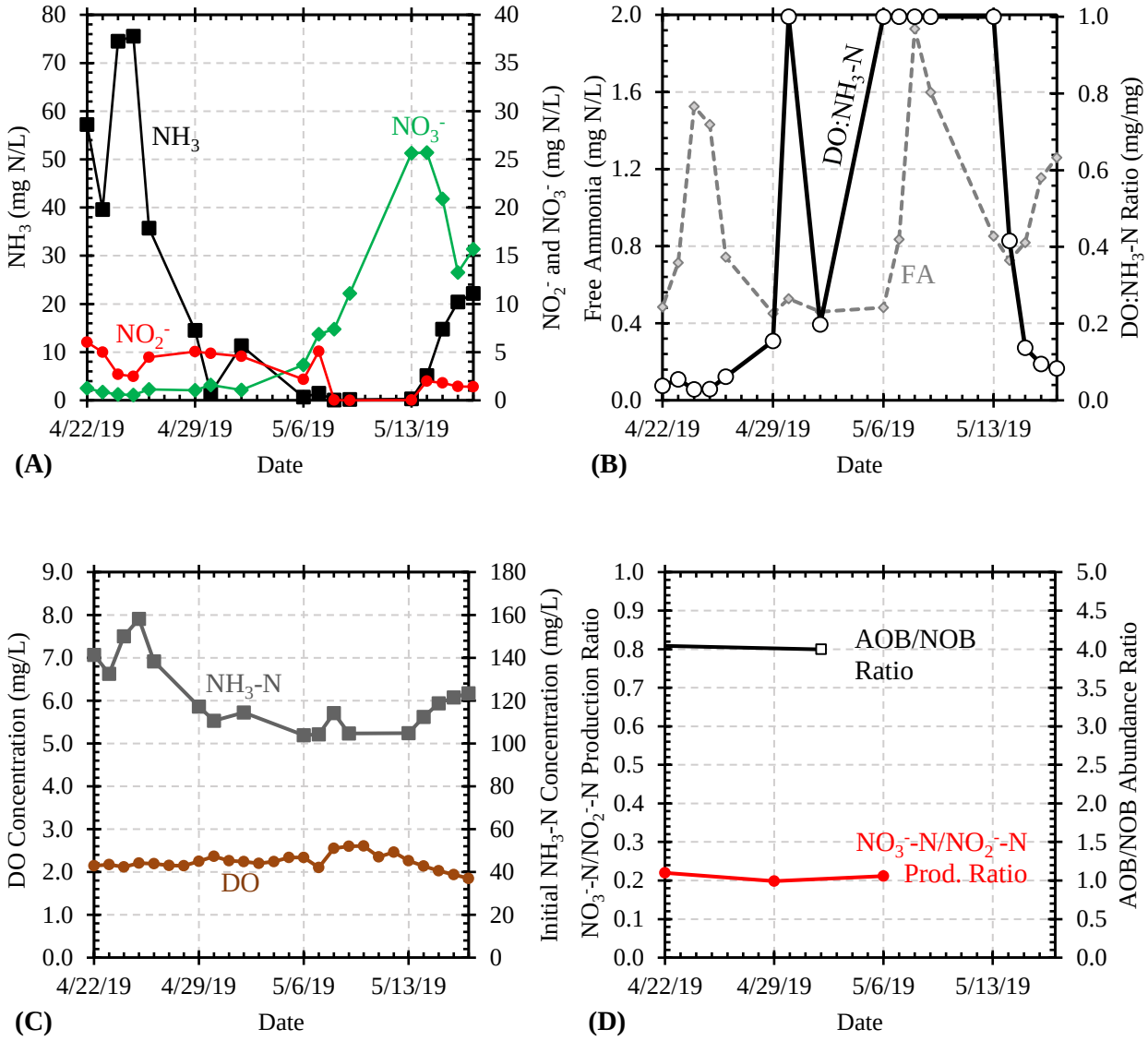

Figure 5-3. Operations and performance before and during Period 2B, from April 26, 2019 to May 16, 2019. A) Effluent NH_3, NO_2^-, and NO_3^- concentrations versus time, B) the initial free ammonia (FA) concentration and maximum DO:NH_3-N concentration ratio versus time, C) average aeration phase DO concentration and initial NH_3-N concentration versus time, and D) the NO_3^--N/NO_2^--N production rate ratio and AOB/NOB abundance ratio versus time. Any DO:NH_3-N ratio of or above 1.0 is displayed as 1.0 in (B).

The impact of DO:NH_3-N ratio and FA concentration is more dramatic for the results in Figure 5-3. With the exception of a high value on April 30, 2019, the DO:NH_3-N ratio was less 0.20 until May 2, 2019 and the NO_3^--N concentration was well below the NO_2^--N concentration to

indicate high NOB suppression. As the reactor improved its nitrification efficiency to low NH_3-N concentration by May 6, 2019 the DO:NH_3-N ratio increased to above 1.0, the NO_3^--N concentration increased to 25 mg/L and the NO_2^--N concentration declined to below 0.5 mg/L. These results show that for the PAO-NDN granular sludge reactor a DO:NH_3-N ratio of 0.20 or less was necessary for high NOB suppression. Figdore et al. (2018a) also operated with an average DO:NH_3-N ratio below 0.2 mg/mg and achieved a shortcut nitrogen removal. This compares to a value of 0.10 by Poot et al. (2016) at 20°C. Differences may be related to differences in spatial distribution of the AOB and NOB as a function of their operating history. Another possibility is that a higher DO:NH_3-N ratio could be tolerated by the PAO-NDN granular sludge reactor because of the competition for NO_2^- by the PAOs in the inner granule layers.

Shortcut nitrogen removal in this study is also supported by the AOB/NOB abundance ratios in Figure 5-2D and Figure 5-3D, which are in the range of 4.0 to 4.2, greater than the ratio of 2.5 for complete oxidation of NH_3 to NO_3^-. Because of the long SRT for the reactor of 23 to 40 days the AOB/NOB ratio reflects the history of NOB suppression under variable reactor operating conditions over time. The higher AOB/NOB ratios indicate a modest level of NOB suppression was occurring over time. The lower NO_3^- production rate in the batch tests at high DO also support the observation of an AOB/NOB ratio affected by NOB suppression.

This study and the lab study by Figdore et al. (2018a) had dPAOs present within the granule to compete for NO_2^- utilization with NOB. The NO_2^- and NO_3^- accumulation is minimal for the first half of the aeration phase, and the SDNR is nearly as fast as SNR. Therefore, dPAOs are likely

competitive for NO_2^- and are potentially a contributing factor in the suppression of NOB in PAO-NDN granules. The role of dPAO competition for NOB suppression in PAO-NDN granules is not well reported because most studies on NOB suppression have been completed for nitritation reactors used in a two-step process for shortcut nitrogen removal with anammox.

The importance of DO:NH_3-N ratio and NOB suppression should be an important consideration in the operation of the mainstream system for nitrogen removal and efficient carbon utilization. Methods to provide nitrification with DO:NH_3-N ratio to maximize SND and minimize carbon needed for nitrogen removal must be considered. This could involve using staged aerobic reactors with different DO control concentrations and/or varying the DO concentration during aeration from near zero to elevated values.

5.4 *Reactor Specific Nitrification Rates and Effect of DO*

Profiles of changes in bulk liquid concentrations for acetate, PO_4^{3-}-P, NH_3-N, NO_2^--N, NO_3^--N were obtained every 1 to 3 weeks during the reactor anaerobic/aerobic phases in the SBR cycle. In many cases the nitrification rate remained linear but for some days when the effluent NH_3-N concentration was below 5 to 10 mg/L, the rate also became limited by the bulk liquid NH_3-N concentration. However, there were insufficient data points available at lower NH_3-N concentrations to obtain an apparent NH_3-N half-saturation coefficient from the profile results.

The observed relatively constant NH_3-N removal rates at NH3-N concentrations above 10-20 mg/L were corrected for the estimated amount of NH_3-N used for biomass synthesis and normalized to the reactor MLVSS concentration to obtain a specific nitrification rate (SNR) as

mg NH_3-N/g VSS-hr. These SNRs were not limited by NH_3-N concentration but by the bulk liquid DO concentration. The average SNR for the stable operating periods ranged from 1.8 to 2.6 mg/g VSS-hr. The SNR value in the bench-scale sidestream treatment reactor by Figdore at al. (2018a) with PAO-NDN granules was about 4.1 mg NH_3-N/g VSS-hr at an average DO concentration of 2.0 mg/L.

The effect of changes in the relative populations of heterotrophs and AOB on the SNR is evaluated by comparing the SNRs between operation periods 1B and 2B in Table 5-2. The SNR for period 2B was 37% higher than for period 1B. The average bulk liquid DO concentration was 15% higher for period 2B and the average feed COD:N feed ratio was 35% less, which results in a higher fraction of AOB in the VSS for period 2B. If most of the AOB growth is in the outer aerobic layers of the granules as expected due to its proximity to the higher bulk liquid NH_3-N and DO concentration, the higher SNR for period 2B can be expected to be related to the higher granule AOB fraction due to SNR being normalized to the VSS concentration.

Table 5-2. Average operating conditions, SNR and AOB to total bacteria fraction from qPCR results for periods 1B and 2B.

Period	**Temp.**	**NH_3-N Loading**	**COD:N Feed Ratio**	**DO**	**Granule Size**	**SNR**	**qPCR AOB/EUB Abundance**
	°C	**g/L-d**	**g/g**	**mg/L**	**mm**	**mg N/g VSS-hr**	
1B	21.7	0.36	4.54	2.0	1.10	1.76	0.0127
2B	20.5	0.44	2.93	2.3	1.35	2.41	0.0174
% Change	*-6%*	*22%*	*-35%*	*15%*	*23%*	*37%*	*37%*

Results of qPCR analysis of reactor mixed liquor samples showed a greater relative abundance of AOB compared to the total bacteria qPCR (EUB) for period 2B. The AOB fraction in Period 2B was 1.74% compared to 1.27% in Period 1B, which is 37% higher. The average bulk liquid DO

concentration in Period 2 was 15% higher and would contribute to the higher SNR but it appears that the higher fraction of AOB in the granules is also a significant factor behind the higher SNR. Thus, the SNR was affected by the feed COD:N ratio. At higher COD:N feed ratios, a lower SNR value can be expected.

Other factors should affect SNR values for a given granular sludge system. These include AOB, NOB, and heterotrophic bacteria concentrations and spatial distribution in the outer aerobic layers of the granules, granule size, reactor SRT, diffusion rates of DO and NH_3-N, and temperature. Even though SNR values are very dependent on specific granular sludge characteristics and system operating conditions, it is a useful parameter to quantify the nitrification capacity of a granular sludge reactor. The SNR value is dependent on the DO concentration. Knowledge of the system half-saturation coefficient value for DO (K_{DO}) allows the maximum SNR to be defined for a given system.

The effect of DO concentration on the granular sludge nitrification rate was determine from batch tests at high NH_3-N concentration with DO control at different levels and an apparent NH_3-N oxidation half-saturation coefficient value of a 1.5 mg/L was determined (Figure 4-13). A modeling procedure was used to evaluate granular sludge process kinetics by Baeten et al. (2018) and an apparent NH_3-N oxidation half-saturation coefficient value of a 4.0 mg DO/L was determined using process performance results for the Nereda® PAO-NDN granular sludge SBR system in Garmerwolde, the Netherlands. There were obvious major differences between the Garmerwolde Nereda® system and our sidestream reactor process including wastewater characteristics of a soluble and particulate BOD carbon source versus mainly acetate feeding,

biodegradable COD:N feed ratio, and anaerobic feeding method that would result in different granular sludge morphology, microbial population and relative fractions and spatial distribution. Stereomicroscope images of granules from the Nereda® granular sludge system showed flocculent-like biomass growth on the granules (outgrowth), presumably due to biodegradation of particulate BOD during the aeration phase. The mixed liquor also had a greater amount of floc compared to our sidestream reactor. Baeten et al. (2018) pointed out the importance of OHO, PAO, AOB, and NOB population concentration and spatial distribution and granular morphology on apparent K_{DO} values.

Outgrowth was also seen in a bench-scale SBR reactor bioaugmented with sidestream granular sludge and fed soluble synthetic wastewater by Figdore et al. (2018a). Therefore, the nitrification kinetics for bioaugmented granules during the pilot mainstream system operation phase of this study are expected to be different than the sidestream reactor granules.

5.5 *Simultaneous Nitrification and Denitrification*

During a large portion of aeration phase of the sidestream operation little NO_3^--N and NO_2^--N was present as NH_3-N was being removed and oxidized, and thus the SNR and specific denitrification rates (SDNR) were equal. The SDNR is dependent on the amount and type of carbon and electron acceptor available for denitrification in the anoxic granule layers. Stored carbon by dPAOs and dGAOs is assumed to be the primary electron donor for denitrification, OHO could also contribute to SDNR by using carbon released from biomass endogenous decay in anoxic granule layers. An example of similar SNR and SDNR during aeration was shown in Figure 4-19 and Figure 4-20. The SNR remained constant during the aerobic phase but the

SDNR decreased toward the end of aeration as indicted by an increased in NO_2^--N and NO_3^--N concentration in the bulk liquid. The decrease in SDNR is due to the decline in stored carbon concentration within the granules.

If desired, the system SND efficiency could be optimized by an operating strategy using online DO control and NO_2^--N and NO_3^--N monitoring. When increased NO_X-N is detected above a desired value the DO control set point could be lowered to decrease the SNR. A greater nitrogen removal efficiency would occur, and less NO_X-N would be recycled to the mainstream process, but the lower DO concentration would increase the final NH_3-N concentration due to the effect of DO on the nitrification kinetics. Alternatively, a mixed anoxic phase using endogenous decay carbon could be implemented after aeration to polish remaining NO_X-N. However, this would increase the cycle time and lower the overall NH_3-N loading for the system.

Comparison of the SND efficiencies for Periods 1A and 1B in Figure 4-22 showed that anaerobic phase feed time was an important factor. The same amount of acetate was fed for each cycle, but feed duration was 30 minutes for Period 1A and 10 minutes for Period 1B. For the 30-minute COD feed duration the SND efficiency was 85% SND efficiency and for 10-minutes it was 96%. The bulk liquid COD concentrations was higher for the shorter feed time and the acetate uptake rate was higher as indicated by concentrations after 30 minutes in the anaerobic phase shown in Figure 4-25. A higher COD concentration is expected to drive the COD deeper into the biofilm by diffusion and the greater uptake rate observed may have been due to more PAO and GAO biomass being used for COD uptake. This suggests a greater percentage of the COD fed anaerobically was stored in deeper granule layers during shorter COD feed duration.

The PO_4^{3-}-P uptake profiles in the aeration phase were different for the two feed conditions. As shown in Figure 5-4, the initial P uptake rate was higher and declined much sooner for the longer COD feed time. The slower initial P uptake rate and more linear removal behavior with time for the shorter feed period suggests that stored carbon was being utilized primarily for NO_X-N reduction during aeration and that some DO was used for the operation at the longer feed time, because anoxic PO_4^{3-}-P uptake rates are slower than aerobic PO_4^{3-}-P uptake rates.

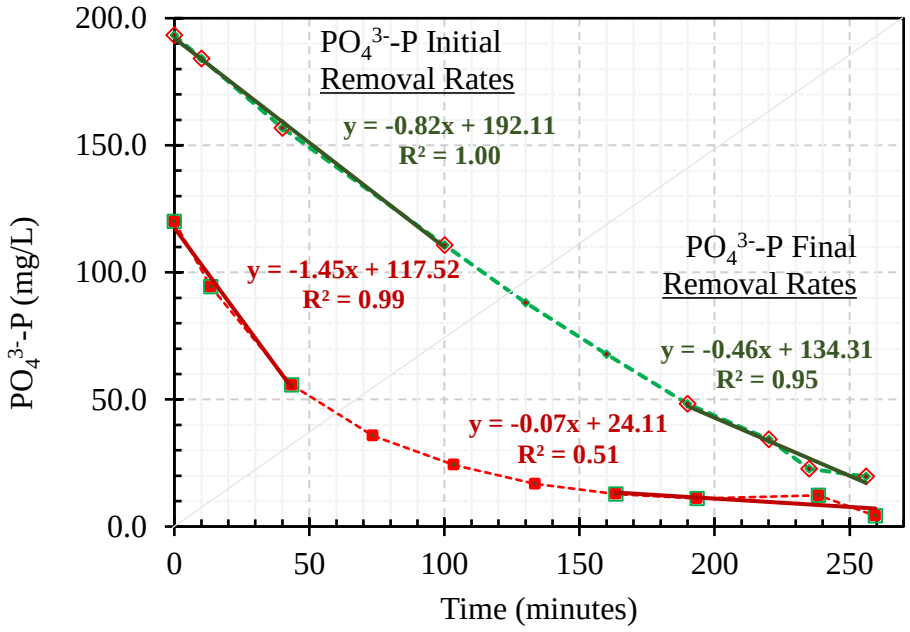

Figure 5-4. Example of how initial and final PO_4^{3-}-P removal rates were measured, based on 3 to 4 data points in linear regions of the PO_4^{3-}-P removal trends. The green profile (diamond marker) is from the period with shorter acetate feed duration, and the red profile (square markers) is from the period with longer acetate feed.

5.6 *Process Upsets*

Process upsets caused unstable and undesired performance for over 60% of the time in the 10.5-month period. Understanding the cause of upsets is necessary to mitigate and possibly prevent

them. Two main types of upsets were observed in this study: operation-induced and feed source inhibition. Operation-induced upsets occurred when reactor operations created an environment that allowed the growth of NOB and GAOs. These conditions appeared detrimental in the long-term for nitrification and EBPR process stability. The second cause of process upsets was feed source inhibition. Feed solutions to the sidestream reactor were obtained from two individual sources and blended within the reactor during aeration feed. Therefore, testing of each source individually was necessary to identify if and which feed source was inhibiting nitrification performance.

As described in the Methods Section 3.2, feed sources inhibition was tested to evaluate the individual effect of secondary effluent and centrate on nitrification rates. Secondary effluent samples collected on January 14 and 16, 2019 tested positive for nitrification inhibition. These dates corresponded with decreased nitrification performance in the sidestream reactor as well; From January 14 to 17, 2019 the NH_3-N removal performance decreased by approximately 25%. The dilution feed source was changed from secondary effluent to tap water on January 18, 2019 and performance was recovered within 3 days. Therefore, both test results and reactor performance suggested secondary effluent to be a cause of periodic inhibition.

The secondary effluent feed solution to the sidestream is received after the WPTP chlorination and dechlorination process. Disinfection products can form during chlorination but it was not possible in this study to determine if inhibition was being caused by disinfection products and what compounds.

The centrate also tested positive for inhibition on May 2, 2019. However, the corresponding performance in the sidestream reactor on May 2, 2019 was relatively high at 95 % NH_3-N removal efficiency. Therefore, centrate may have caused inhibition during activity tests but it appears the dilution of this feed solution to only 9% of total reactor volume was enough to make inhibition on sidestream performance negligible. Figdore et al. (2018a) also used dewatered centrate as a feed source and did not report process inhibition, although the centrate used in this study was collected about two years prior. The evidence of centrate inhibition is less strong than evidence for secondary effluent inhibition.

An operation-induced upset appears to have occurred after Period 1C. Long-term operating conditions in the sidestream reactor provided the environment for NOB growth, which led eventually to GAO growth in the sidestream MLSS. Both the NOB/AOB ratio and GAO/PAO ratio were measured at their highest values on September 5, 2018 (Figure 4-8 and Figure 4-9) suggesting that conditions for their growth were present leading up to this date. Operations and performance starting in July appeared to promote an accumulation of NOB and GAO in the granular MLSS. NOB require DO and NO_2^- for energy production and growth. GAO may have a competitive substrate utilization and growth advantage over PAO with NO_3^- versus NO_2^- (Rubio-Rincón et al., 2017). In July and August 2018, the reactor was operated with low effluent NH_3-N that decreased below 0.5 mg/L (Figure 5-5). Incomplete SND during this period led to an accumulation of NO_2^--N in the effluent. Therefore, in Period 1A during July there was approximately 30 to 60 minutes of reaction time during the aeration phase when NO_2^- and DO were simultaneously available for NOB growth. During August, the effluent NO_2^--N concentration decreased and effluent NO_3^--N concentration increased. This corresponded with an

increase in NOB activity that was measured in batch activity tests (Figure 4-15). The accumulation of NO_3^--N may have provided dGAO a competitive advantage for growth, as their propagation began after high effluent NO_3^--N was observed.

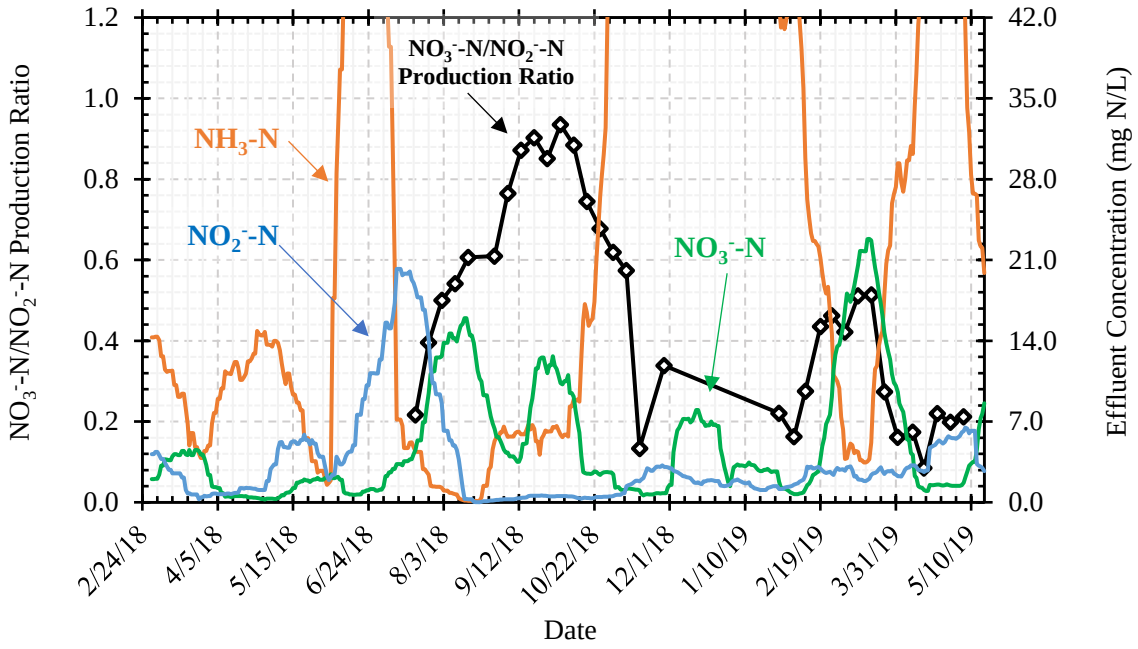

Figure 5-5. The NO_3^--N/NO_2^--N production rate ratio and 25-day averaged NH_3-N, NO_2^--N, and NO_3^--N effluent concentrations.

Outgrowth around the granule biofilm was observed around the time dGAO growth started. Prior to GAO growth, granules had outgrowth that occurred in nodule clusters, as shown in Figure 4-2. Gonzalez-Gil and Holliger (2014) used thin sections of granule cross sections and FISH to show that PAOs grow in clusters around granules and that GAO do not. Therefore, the outgrowth observed surrounding granule surfaces shown in Figure 4-3 is likely not PAO growth. The correspondence of this growth with an increase in GAO abundance after NO_3^--N accumulation suggests that the growth is dGAOs/GAOs.

Excessive outgrowth of organisms that are not AOB is detrimental to nitrification rates because it competes for available aerobic surface area. Furthermore, GAOs compete for acetate with PAOs. This competition limits the denitrifying activity of dPAO, assumed as primarily NO_2^--N reduction. The NO_2^--N reduction rates by dPAO provides competition against NOB for NO_2^--N. Therefore, maintaining operating conditions that limit NOB and dGAO growth appear important for maintaining long-term process stability for the sidestream reactor.

6 Conclusions

A pilot plant sidestream treatment granular sludge SBR with anaerobic/aerobic phase for growth of PAO-NDN granules for 10.5 months and fed centrate diluted with secondary effluent during aeration and sodium acetate in the anaerobic phase. The NH_3-N loading rate ranged from 0.31 to 0.46 g/L-d during stable performance periods. DO was controlled to maximize SND during aeration, and operating conditions to minimize the acetate COD:N feed ratio were pursued. Periodic inhibition of PAO and nitrification activity was encountered. The following conclusions were made.

- The average performance over the 10.5-month period with upsets was 85% NH_3-N removal, 90% TIN removal, and 94% SND efficiency.
- Without upsets the removal efficiency averaged 96% NH_3-N removal, 90% TIN removal, and 93% SND efficiency.
- High SND efficiency was achieved with COD:N feed ratios from 2.9 to 4.5 g/g.
- The SVI_{30} ranged from 26 to 38 mL/g and SVI_5/SVI_{30} from 1.00 to 1.02 during stable performance. Upset conditions had no significant effect on the granular sludge morphology, SVI, or size.
- Granule size ranged from 1.0 to 1.8 mm and the granule size distribution varied over time with a 3.0 mm maximum size.
- The granular sludge surface area density, in cm^2/L, is a function of the size distribution and MLSS concentration.
- The granular sludge size of 1.0 to 1.5 mm provided more than enough surface area density needed for nitrification and these granules had a large enough inner anoxic volume for high SND efficiency.

- The COD:N feed ratio, anaerobic phase COD concentration, and DO concentration affected apparent nitrification kinetics and/or SND efficiency.
    - A higher COD:N feed ratio decreased SNR.
    - A higher anaerobic phase COD concentration increased SND efficiency.
    - A higher DO concentration increased SNR and decreased SND efficiency.
- Specific nitrification rate was constant over most of the aeration time and SNRs ranged from 1.6 to 2.4 mg NH_3-N/g VSS-hr. The SNR increased with AOB abundance.
- Shortcut nitrogen removal was evident by high AOB/NOB abundance ratio based on qPCR, low NO_3^--N/NO_2^--N production ratio in batch tests, and lower COD:N feed ratio.
- Bulk liquid DO:NH_3-N concentration ratio at 0.20 mg/mg and lower resulted in almost complete NOB suppression.
- Free ammonia concentration did not affect NOB suppression.

7 Future Work

The mainstream bioaugmentation pilot plant study will continue from this work. The project has separate, predefined objectives and is expected to be summarized in future reports, master's thesis, and journal publications. Mainstream bioaugmentation will start during 2019.

The sidestream reactor study has demonstrated the ability to achieve high removal efficiencies with low supplemental carbon due to operating conditions that promoted shortcut nitrogen removal. The effect of NH_3-N loading, COD:N feed ratio, and DO concentration on nitrification was demonstrated and populations of AOB, NOB, PAO, and GAO were identified and compared to process performance. Changes in granular sludge morphology and settling performance was also assessed. Further work can be done to 1) identify reasons for inhibition events that caused upset periods, 2) refine operating strategies and optimize shortcut nitrogen removal performance, 3) quantify the effect of SRT on microbial populations and process performance, 4) assess performance at lower reactor temperature, 5) further quantify apparent kinetics of PAO-NDN granules, 6) measure N_2O emissions from SND during aeration, and 7) further characterize microbial communities.

7.1 *Identify Cause of Reactor Upsets*

Two approaches can be considered. The first is to use tap water with necessary cation addition in place of secondary effluent. This then allows isolating the centrate feed as the possible cause of upsets. The second is intensive sampling of each centrate batch and frequent secondary effluent samples for use in the nitrification inhibition testing.

7.2 *Refine Operating Strategies and Optimize Shortcut Nitrogen Removal*

Shortcut nitrogen removal was achieved in the sidestream reactor. This allowed a low COD:N feed ratio for operations, simulating an ideal scenario where operating costs are minimized by requiring less supplemental COD while maintaining target sidestream reactor performance. Shortcut nitrogen removal was demonstrated only during the last fraction of the full operating period, and stable performance at an average COD:N feed ratio as low as 2.9 g/g was only achieved for 17 days. This demonstrated the capacity of the system; however, future work should aim to sustain shortcut nitrogen removal for at least three SRTs for a more convincing demonstration of steady state operations and performance, and to assess duration required for a relatively steady state microbial population to be achieved. The effect of the NO_2^--N demand by the PAO/GAO population on NOB suppression is not understood.

In this study, it appeared that the aeration DO:NH_3-N ratio and FA concentration contributed to NOB suppression. The literature points more strongly to the importance of the DO:NH_3-N ratio then FA. Tests could be done with more constant centrate NH_3-N concentration by adding NH_3-N to the feed tank when the batch NH_3-N concentration is lower. Then, the DO:NH_3-N ratio could be varied to assess AOB and NOB activity based on performance and qPCR measurements.

Additional experiment could also be done to assess the influent of the PAO/GAO biomass on NO_2 competition with NOBs. For a given operation the fate of NO_3^--N, NO_2^--N and NOB activity

7.3 *Effect of SRT on Nitrification, SND Efficiency, and COD:N Ratio*

The SRT during this study was controlled between 20 and 40 days. This range is practical for full scale control and performance, but lacks precision required to quantify the effect of SRT on operations and performance. In addition, the bench-scale pilot reactor was operated at a lower average SRT of 16 days. Therefore, future work should focus on maintaining tighter control of SRT and adjusting SRT to study the effect of this parameter on nitrification, SND efficiency, and the COD:NOr ratio.

Lower SRTs are expected to decrease the SNR by decreasing the abundance of AOB. However, the effect of lower SRTs on NOB, PAO, GAO, or OHO populations should be studied, especially for the relative populations of 1) NOB to AOB and 2) GAOs to PAOs. Longer SRTs provide additional COD from endogenous decay and this may have contributed to the low COD:NOr ratios in this study. Assessing the effect of SRT on the required COD:N feed ratio to maintain target performance should be included in future work.

7.4 *Effect of Temperature on Operations and Performance*

Stable performance periods in this study were conducted at average temperatures ranging from 19 to 24°C. Temperature was artificially raised during the restart period in January 2019 following the extended upset events from October to December 2018. Thus, the reactor was not studied in a relatively stable performance conditions at target loading and performance at temperatures below 19°C. In general, lower temperatures are suspected to favor PAO over GAO and NOB over AOB. Stable reactor performance should be compared when operated at lower temperatures compared to the performance at operating temperatures in this study. Assessing the

effect of temperature on the ability to achieve desired nitrification, SND efficiency, and shortcut nitrogen removal will be beneficial for future process design and operations.

7.5 *Kinetics of PAO-NDN Granules*

Batch kinetic tests quantified the effect of DO concentration on SNRs of sidestream granular mixed liquor during Period 2B. Apparent nitrification kinetics is expected to change depending on the operating conditions. Therefore, the effect of DO concentration on granular sludge should also be assessed if size or size distribution is changed due to any future changes in settling time or wasting strategy.

Apparent kinetics also should be assessed for the maximum denitrification rate and apparent half-saturation constant of both NO_2^- and NO_3^-. These parameters should be assessed for granules with near-full PHA storage removed from the sidestream reactor near the start of aeration phase and for granules removed at the end of aeration phase. Identifying these rates and how they compare at the start and end of aeration could provide better process control to maximize SND efficiency.

7.6 *N_2O Emissions*

N_2O is a potent greenhouse gas that contributes to approximately 5% of annual human greenhouse gas emissions (U.S. Environmental Protection Agency, 2013). This is largely from agricultural processes, but there is a contribution from wastewater treatment processes as well. Understanding the greenhouse gas emissions contribution of this sidestream treatment process is important because future process decisions may be motivated by environmental stewardship as

well as economic considerations. It is apparent that N_2O emissions may be generated in both the nitrification and denitrification processes, and that low COD:N ratios can contribute to relatively higher emissions (Law et al., 2012). Therefore, future work should quantify how operations of the sidestream reactor also affects N_2O emissions.

7.7 *Microbial Characterization*

Samples were regularly collected and preserved during startup and the full operating period for DNA, RNA, and FISH analyses. Samples were selected for qPCR to broadly represent changes in AOB, NOB, PAO, and GAO populations. However, only *Accumulibacter* and *Competibacter* have been assessed in terms of the PAO and GAO populations, respectively. Also, clade-level information for *Accumulibacter* has not yet been identified. Sequencing was completed in May and September of 2018, but not in 2019. Sequencing results had indicated a significant population of *Dechloromonas*, which has a proposed PAO-phenotype; however, it has not been confirmed whether *Dechloromonas* has contributed to EBPR or SND in this process.

Future work should sequence samples from May 2019 when shortcut nitrogen removal was achieved. Identifying clade-level information for the *Accumulibacter* population will also contribute to understanding which dPAOs are present in PAO-NDN granules. Samples collected during the operating period from July to September of 2018 could be used to quantify changes in PAO and GAO populations and AOB and NOB populations. These changes could then be matched to changes in operations and performance, and transcriptomics could be used on stored samples to directly measure microbial activity during the aeration phase. A high frequency samples preserved for DNA, RNA, and FISH have been collected and are stored for this period.

Overall, there is a lot of potential to further analyze and match operations and performance with the structure of microbial communities.

8 References

Abeysinghe, D.H., De Silva, D.G.V., Stahl, D.A., Rittmann, B.E., 2002. The Effectiveness of Bioaugmentation in Nitrifying Systems Stressed by a Washout Condition and Cold Temperature. Water Environ. Res. 74, 187–199. https://doi.org/10.2175/106143002x139901

Ahn, J., Schroeder, S., Beer, M., McIlroy, S., Bayly, R.C., May, J.W., Vasiliadis, G., Seviour, R.J., 2007. Ecology of the microbial community removing phosphate from wastewater under continuously aerobic conditions in a sequencing batch reactor. Appl. Environ. Microbiol. 73, 2257–2270. https://doi.org/10.1128/AEM.02080-06

Anthonisen, A.C., Loehr, R.C., Prakasam, T.B., Srinath, E.G., 1976. Inhibition of nitrification by ammonia and nitrous acid. J. Water Pollut. Control Fed. 48, 835–52.

APHA, 2012. Standard Methods for the Examination of Water and Wastewater, 20th ed. Washington DC. https://doi.org/10.1002/9780470087800

Baeten, J.E., Van Loosdrecht, M.C.M., Volcke, E.I.P., 2018. Modelling aerobic granular sludge reactors through apparent half-saturation coefficients. Water Res. 146, 134–145. https://doi.org/10.1016/j.watres.2018.09.025

Barnard, J.L., 1975. Biological nutrient removal without the addition of chemicals. Water Res. 9, 485–490.

Bartrolí, A., Pérez, J., Carrera, J., 2010. Applying ratio control in a continuous granular reactor to achieve full nitritation under stable operating conditions. Environ. Sci. Technol. 44, 8930–8935. https://doi.org/10.1021/es1019405

Bassin, J.P., Kleerebezem, R., Dezotti, M., Van Loosdrecht, M.C.M., 2012. Simultaneous nitrogen and phosphate removal in aerobic granular sludge reactors operated at different temperatures. Water Res. 46, 3805–3816. https://doi.org/10.1016/j.watres.2012.04.015

Bassin, J.P., Pronk, M., Kraan, R., Kleerebezem, R., Van Loosdrecht, M.C.M., 2011. Ammonium adsorption in aerobic granular sludge, activated sludge and anammox granules. Water Res. 45, 5257–5265. https://doi.org/10.1016/j.watres.2011.07.034

Bowden, G., Tsuchihashi, R., Stensel, H.D., 2016. Technologies for Sidestream Nitrogen Removal, Water Environment Reserch Foundation. https://doi.org/10.2166/9781780407890

Daims, H., Lebedeva, E. V., Pjevac, P., Han, P., Herbold, C., Albertsen, M., Jehmlich, N., Palatinszky, M., Vierheilig, J., Bulaev, A., Kirkegaard, R.H., Von Bergen, M., Rattei, T., Bendinger, B., Nielsen, P.H., Wagner, M., 2015. Complete nitrification by Nitrospira bacteria. Nature 528, 504–509. https://doi.org/10.1038/nature16461

Datta, T., Goel, R., 2007. Evidence of non-Candidatus A. Phosphatis population participating in enhanced biological removal in carrousel activated sludge process, in: Proceedings of the Water Environment Federation. pp. 4944–4955. https://doi.org/10.2175/193864707787969045

De Bruin, L.M.M., De Kreuk, M.K., Van Der Roest, H.F.R., Uijterlinde, C., Van Loosdrecht, M.C.., 2004. Aerobic granular sludge technology: an alternative to activated sludge? Water Sci. Technol. 49, 1–7.

De Kreuk, M.K., Heijnen, J.J., Van Loosdrecht, M.C.M., 2005. Simultaneous COD, nitrogen, and phosphate removal by aerobic granular sludge. Biotechnol. Bioeng. 90, 761–769. https://doi.org/10.1002/bit.20470

De Kreuk, M.K., Kishida, N., Van Loosdrecht, M.C.M., 2007. Aerobic granular sludge – state of the art. Water Sci. Technol. 55, 75. https://doi.org/10.2166/wst.2007.244

De Kreuk, M. K., Picioreanu, C., Hosseini, M., Xavier, J.B., Van Loosdrecht, M.C.M., 2007. Kinetic model of a granular sludge SBR: Influences on nutrient removal. Biotechnol. Bioeng. 97, 801–815. https://doi.org/10.1002/bit.21196

Erdal, U.G., Erdal, Z.K., Randall, C.W., 2003. The Competition Between PAOs and GAOs in EBPR Systems at Different Temperatures and the Effects on System Performance. Water Sci. Technol. 47, 1–8.

Fang, F., Ni, B.J., Li, X.Y., Sheng, G.P., Yu, H.Q., 2009. Kinetic analysis on the two-step processes of AOB and NOB in aerobic nitrifying granules. Appl. Microbiol. Biotechnol. 83, 1159–1169. https://doi.org/10.1007/s00253-009-2011-y

Figdore, B.A., Stensel, H.D., Winkler, M.K.H., 2018a. Bioaugmentation of sidestream nitrifying-denitrifying phosphorus-accumulating granules in a low-SRT activated sludge system at low temperature. Water Res. 135, 241–250. https://doi.org/10.1016/j.watres.2018.02.035

Figdore, B.A., Winkler, M.K.H., Stensel, H.D., 2018b. Bioaugmentation with Nitrifying Granules in Low-SRT Flocculent Activated Sludge at Low Temperature. Water Environ. Res. 90, 343–354. https://doi.org/10.2175/106143017x15054988926488

Filipe, C.D.M., Daigger, G.T., Grady, C.P.L., 2001a. A metabolic model for acetate uptake under anaerobic conditions by glycogen accumulating organisms: Stoichiometry, kinetics, and the effect of pH. Biotechnol. Bioeng. 76, 17–31. https://doi.org/10.1002/bit.1022

Filipe, C.D.M., Daigger, G.T., Grady, C.P.L., 2001b. Stoichiometry and kinetics of acetate uptake under anaerobic conditions by an enriched culture of phosphorus-accumulating organisms at different pHs. Biotechnol. Bioeng. 76, 32–43. https://doi.org/10.1002/bit.1023

Filipe, C.D.M., Daigger, G.T., Grady, C.P.L., 2001c. Effects of pH on the Rates of Aerobic Metabolism of Phosphate-Accumulating and Glycogen-Accumulating Organisms. Water Environ. Res. 73, 213–222. https://doi.org/10.2175/106143001x139191

Filipe, C.D.M., Daigger, G.T., Grady, C.P.L.J., 2001d. pH as a Key Factor in Competition Between Glycogen-Accumulating Organisms and Phosphorus-Accumulating Organisms. Water Environ. Res. 73, 223–232.

Flowers, J.J., He, S., Yilmaz, S., Noguera, D.R., McMahon, K.D., 2009. Denitrification capabilities of two biological phosphorus removal sludges dominated by different "Candidatus Accumulibacter" clades. Environ. Microbiol. Rep. 1, 583–588. https://doi.org/10.1111/j.1758-2229.2009.00090.x

Fukushima, T., Onuki, M., Satoh, H., Mino, T., 2010. Effect of pH reduction on polyphosphate- and glycogen-accumulating organisms in enhanced biological phosphorus removal processes. Water Sci. Technol. 62, 1432–1439. https://doi.org/10.2166/wst.2010.361

Fukushima, T., Uda, N., Onuki, M., Satoh, H., Mino, T., 2007. Development of the Quantitative PCR Method for Candidatus 'Accumulibacter phosphatis' and Its Application to Activated

Sludge. J. Water Environ. Technol. 5, 37–43. https://doi.org/10.2965/jwet.2007.37

Gonzalez-Gil, G., Holliger, C., 2014. Aerobic granules: Microbial landscape and architecture, stages, and practical implications. Appl. Environ. Microbiol. 80, 3433–3441. https://doi.org/10.1128/AEM.00250-14

Head, M.A., Oleszkiewicz, J.A., 2004. Bioaugmentation for nitrification at cold temperatures. Water Res. 38, 523–530. https://doi.org/10.1016/j.watres.2003.11.003

Hu, Z., Wentzel, M.C., Ekama, G.A., 2002. Anoxic growth of phosphate-accumulating organisms (PAOs) in biological nutrient removal activated sludge systems. Water Res. 36, 4927–4937. https://doi.org/10.1016/S0043-1354(02)00186-0

Hwang, J.H., Oleszkiewicz, J.A., 2007. Effect of Cold-Temperature Shock on Nitrification. Water Environ. Res. 79, 964–968. https://doi.org/10.2175/106143007x176022

Iorhemen, O.T., Hamza, R.A., Zaghloul, M.S., Tay, J.H., 2018. Simultaneous organics and nutrients removal in side-stream aerobic granular sludge membrane bioreactor (AGMBR). J. Water Process Eng. 21, 127–132. https://doi.org/10.1016/j.jwpe.2017.12.009

Isanta, E., Reino, C., Carrera, J., Pérez, J., 2015. Stable partial nitritation for low-strength wastewater at low temperature in an aerobic granular reactor. Water Res. 80, 149–158. https://doi.org/10.1016/j.watres.2015.04.028

Kent, T.R., Bott, C.B., Wang, Z.W., 2018. State of the art of aerobic granulation in continuous flow bioreactors. Biotechnol. Adv. 36, 1139–1166. https://doi.org/10.1016/j.biotechadv.2018.03.015

Kent, T.R., Sun, Y., An, Z., Bott, C.B., Wang, Z.-W., 2019. Mechanistic understanding of the NOB suppression by free ammonia inhibition in continuous flow aerobic granulation bioreactors. Environ. Int. 131, 105005. https://doi.org/10.1016/j.envint.2019.105005

Kim, J.M., Lee, H.J., Lee, D.S., Jeon, C.O., 2013. Characterization of the denitrification-associated phosphorus uptake properties of "Candidatusaccumulibacter phosphatis" clades in sludge subjected to enhanced biological phosphorus removal. Appl. Environ. Microbiol. 79, 1969–1979. https://doi.org/10.1128/AEM.03464-12

Kong, Y., Xia, Y., Nielsen, J.L., Nielsen, P.H., 2007. Structure and function of the microbial community in a full-scale enhanced biological phosphorus removal plant. Microbiology 153, 4061–4073. https://doi.org/10.1099/mic.0.2007/007245-0

Kouba, V., Catrysse, M., Stryjova, H., Jonatova, I., Volcke, E.I.P., Svehla, P., Bartacek, J., 2014. The impact of influent total ammonium nitrogen concentration on nitrite-oxidizing bacteria inhibition in moving bed biofilm reactor. Water Sci. Technol. 69, 1227–1233. https://doi.org/10.2166/wst.2013.757

Lancaster, K.M., Caranto, J.D., Majer, S.H., Smith, M.A., 2018. Alternative Bioenergy: Updates to and Challenges in Nitrification Metalloenzymology. Joule 2, 421–441. https://doi.org/10.1016/j.joule.2018.01.018

Lanham, A.B., Moita, R., Lemos, P.C., Reis, M.A.M., 2011. Long-term operation of a reactor enriched in Accumulibacter clade I DPAOs : performance with nitrate , nitrite and oxygen 352–360. https://doi.org/10.2166/wst.2011.063

Law, Y., Ye, L., Pan, Y., Yuan, Z., 2012. Nitrous oxide emissions from wastewater treatment processes. Philos. Trans. R. Soc. B Biol. Sci. 367, 1265–1277. https://doi.org/10.1098/rstb.2011.0317

Leu, S.-Y., Stenstrom, M.K., 2010. Bioaugmentation to Improve Nitrification in Activated Sludge Treatment. Water Environ. Res. 82, 524–535. https://doi.org/10.2175/106143009x12487095237071

Li, J., Ding, L.-B., Cai, A., Huang, G.-X., Horn, H., 2014. Aerobic Sludge Granulation in a Full-Scale Sequencing Batch Reactor. Biomed Res. Int. 2014, 1–12. https://doi.org/10.1155/2014/268789

Mañas, A., Pocquet, M., Biscans, B., Sperandio, M., 2012. Parameters influencing calcium phosphate precipitation in granular sludge sequencing batch reactor. Chem. Eng. Sci. 77, 165–175. https://doi.org/10.1016/j.ces.2012.01.009

Meinhold, J., Filipe, C.D.M., Daigger, G.T., Isaacs, S., 1999. Characterization of the denitrifying fraction of phosphate accumulating organisms in biological phosphate removal. Water Sci. Technol. 39, 31–42.

Melcer, H., Dold, P.L., Jones, R.M., Bye, C.M., Takacs, I., Stensel, H.D., Wilson, A.W., Sun, P., Bury, S., 2003. Methods for Wastewater Characterization in Activated Sludge Modeling.

Michaelis, L., Menten, M.L., 1913. Die Kinetic der Invertinwirkung (The Kinetics of Invertase Action translated by Roger S. Goody and Kenneth A. Johnson. Biochemistry 49, 333–368. https://doi.org/10.1021/bi201284u

Nguyen, H.T.T., Kristiansen, R., Vestergaard, M., Wimmer, R., Nielsen, P.H., 2015. Intracellular accumulation of glycine in polyphosphate-accumulating organisms in activated sludge, a novel storage mechanism under dynamic anaerobic-aerobic conditions. Appl. Environ. Microbiol. 81, 4809–4818. https://doi.org/10.1128/AEM.01012-15

Nor Anuar, A., Ujang, Z., van Loosdrecht, M.C.M., de Kreuk, M.K., 2007. Settling behaviour of aerobic granular sludge. Water Sci. Technol. 56, 55–63. https://doi.org/10.2166/wst.2007.671

Oehmen, A., Carvalho, G., Freitas, F., Reis, M.A.M., 2010. Assessing the abundance and activity of denitrifying polyphosphate accumulating organisms through molecular and chemical techniques. Water Sci. Technol. 61, 2061–2068. https://doi.org/10.2166/wst.2010.976

Oehmen, A., Saunders, A.M., Vives, M.T., Yuan, Z., Keller, J., 2006. Competition between polyphosphate and glycogen accumulating organisms in enhanced biological phosphorus removal systems with acetate and propionate as carbon sources. J. Biotechnol. 123, 22–32. https://doi.org/10.1016/j.jbiotec.2005.10.009

Oehmen, A., Yuan, Z., Blackall, L.L., Keller, J., 2005. Comparison of acetate and propionate uptake by polyphosphate accumulating organisms and glycogen accumulating organisms. Biotechnol. Bioeng. 91, 162–168. https://doi.org/10.1002/bit.20500

Parada, A.E., Needham, D.M., Fuhrman, J.A., 2016. Every base matters: Assessing small subunit rRNA primers for marine microbiomes with mock communities, time series and global field samples. Environ. Microbiol. 18, 1403–1414. https://doi.org/10.1111/1462-2920.13023

Pester, M., Maixner, F., Berry, D., Rattei, T., Koch, H., Lücker, S., Nowka, B., Richter, A.,

Spieck, E., Lebedeva, E., Loy, A., Wagner, M., Daims, H., 2014. NxrB encoding the beta subunit of nitrite oxidoreductase as functional and phylogenetic marker for nitrite-oxidizing Nitrospira. Environ. Microbiol. 16, 3055–3071. https://doi.org/10.1111/1462-2920.12300

Pfaff, J.D., 1993. Method 300.0 Determination of Inorganic Anions By Ion Chromatography. Cincinnati, Ohio.

Picioreanu, C., Pérez, J., Van Loosdrecht, M.C.M., 2016. Impact of cell cluster size on apparent half-saturation coefficients for oxygen in nitrifying sludge and biofilms. Water Res. 106, 371–382. https://doi.org/10.1016/j.watres.2016.10.017

Poot, V., Hoekstra, M., Geleijnse, M.A.A., van Loosdrecht, M.C.M., Pérez, J., 2016. Effects of the residual ammonium concentration on NOB repression during partial nitritation with granular sludge. Water Res. 106, 518–530. https://doi.org/10.1016/j.watres.2016.10.028

Pronk, M., De Kreuk, M.K., De Bruin, B., Kamminga, P., Kleerebezem, R., Van Loosdrecht, M.C.M., 2015. Full scale performance of the aerobic granular sludge process for sewage treatment. Water Res. 84, 207–217. https://doi.org/10.1016/j.watres.2015.07.011

Reino, C., Suárez-Ojeda, M.E., Pérez, J., Carrera, J., 2016. Kinetic and microbiological characterization of aerobic granules performing partial nitritation of a low-strength wastewater at 10 °C. Water Res. 101, 147–156. https://doi.org/10.1016/j.watres.2016.05.059

Rotthauwe, J., Witzel, K., 1997. The Ammonia Monooxygenase Structural Gene amoA as a Functional Marker: Molecular Fine-Scale Analysis of Natural Ammonia-Oxidizing Populations ammonia-oxidizing populations.pdf. Appl. Environ. Microbiol. 63, 4704–4712.

Rubio-Rincón, F.J., Lopez-vazquez, C.M., Welles, L., van Loosdrecht, M.C.M., Brdjanovic, D., Loosdrecht, M.C.M. Van, 2017. Cooperation between Candidatus Competibacter and Candidatus Accumulibacter clade I, in denitrification and phosphate removal processes. Water Res. 120, 156–164. https://doi.org/10.1016/j.watres.2017.05.001

Schindelin, J., Arganda-Carreras, I., Frise, E., Kaynig, V., Longair, M., Pietzsch, T., Preibisch, S., Rueden, C., Saalfeld, S., Schmid, B., Tinevez, J.Y., White, D.J., Hartenstein, V., Eliceiri, K., Tomancak, P., Cardona, A., 2012. Fiji: An open-source platform for biological-image analysis. Nat. Methods 9, 676–682. https://doi.org/10.1038/nmeth.2019

Serralta, J., Ferrer, J., Borras, L., Seco, A., 2006. Effect of pH on Biological Phosphorus Uptake. Biotechnol. Bioengingeering 95, 875–882. https://doi.org/10.1002/bit.21040

Simm, R.A., Mavinic, D.S., Ramey, W.D., 2006. A targeted study on possible free ammonia inhibition of Nitrospira. J. Environ. Eng. Sci. 5, 365–376. https://doi.org/10.1139/S05-044

Soler-Jofra, A., Wang, R., Kleerebezem, R., Van Loosdrecht, M.C.M., Pérez, J., 2019. Stratification of nitrifier guilds in granular sludge in relation to nitritation. Water Res. 148, 479–491. https://doi.org/10.1016/j.watres.2018.10.064

Stenström, F., la Cour Jansen, J., 2016. Promotion of nitrifiers through side-stream bioaugmentation: A full-scale study. Water Sci. Technol. 74, 1736–1743. https://doi.org/10.2166/wst.2016.340

Tchobanoglous, G., Stensel, H.D., Tsuchihashi, R., Burton, F.L., 2014a. Chapter 7 Fundamentals of Biological Treatment, in: Metcalf and Eddy, Inc. Wastewater Engineering: Treatment

and Resource Recovery 5th Edition. pp. 551–696.

Tchobanoglous, G., Stensel, H.D., Tsuchihashi, R., Burton, F.L., 2014b. Chapter 8 Suspended Growth Biological Treatment Processes, in: Metcalf and Eddy, Inc. Wastewater Engineering: Treatment and Resource Recovery 5th Edition. pp. 697–940.

Tu, Y., Schuler, A.J., 2013. Low acetate concentrations favor polyphosphate-accumulating organisms over glycogen-accumulating organisms in enhanced biological phosphorus removal from wastewater. Environ. Sci. Technol. 47, 3816–3824. https://doi.org/10.1021/es304846s

United States Environmental Protection Agency, 2013. Overview of Greenhouse Gases [WWW Document]. EPA. URL epa.gov/climatechange/ghgemissions (accessed 8.22.19).

Ushiki, N., Jinno, M., Fujitani, H., Suenaga, T., Terada, A., Tsuneda, S., 2017. Nitrite oxidation kinetics of two Nitrospira strains: The quest for competition and ecological niche differentiation. J. Biosci. Bioeng. 123, 581–589. https://doi.org/10.1016/j.jbiosc.2016.12.016

Vadivelu, V.M., Keller, J., Yuan, Z., 2006. Effect of Free Ammonia and Free Nitrous Acid Concentration on the Anabolic and Catabolic Processes of an Enriched Nitrosomonas Culture. Biotechnol. Bioeng. 95, 830–839. https://doi.org/10.1002/bit

Van Loosdrecht, M.C.M., Nielsen, P.H., Lopez-Vazquez, C.M., Brdjanovic, D., 2016. Experimental Methods in Wastewater Treatment, Water Intelligence Online. https://doi.org/10.2166/9781780404752

Wei, S., Stensel, H.D., Nguyen Quoc, B., Lee, P., Huang, X., Winkler, M.K.H., 2019. 2019 Water Environment Federation Technical Exhibition and Conference, in: What's in Your Sludge? Hunting for Baby Granules in Full-Scale Activated Sludge Treatment Plants. pp. 1–6.

Weissbrodt, D.G., Schneiter, G.S., Fürbringer, J.M., Holliger, C., 2013. Identification of trigger factors selecting for polyphosphate- and glycogen-accumulating organisms in aerobic granular sludge sequencing batch reactors. Water Res. 47, 7006–7018. https://doi.org/10.1016/j.watres.2013.08.043

Whang, L., Park, J.K., 2006. Competition between Polyphosphate- and Glycogen-Accumulating Organisms in Systems : Effect of Temperature and Sludge Age. Water Environ. Res. 78, 4–11. https://doi.org/10.2175/106143005X84459

Winkler, M.K.H., Bassin, J.P., Kleerebezem, R., De Bruin, L.M.M., Van Den Brand, T.P.H., Van Loosdrecht, M.C.M., 2011. Selective sludge removal in a segregated aerobic granular biomass system as a strategy to control PAO-GAO competition at high temperatures. Water Res. 45, 3291–3299. https://doi.org/10.1016/j.watres.2011.03.024

Yilmaz, G., Lemaire, R., Keller, J., Yuan, Z., 2008. Simultaneous nitrification, denitrification, and phosphorus removal from nutrient-rich industrial wastewater using granular sludge. Biotechnol. Bioeng. 100, 529–541. https://doi.org/10.1002/bit.21774

Zeng, W., Wang, A., Zhang, J., Zhang, L., Peng, Y., 2016. Enhanced biological phosphate removal from wastewater and clade-level population dynamics of "Candidatus Accumulibacter phosphatis" under free nitrous acid inhibition: Linked with detoxication.

Chem. Eng. J. 296, 234–242. https://doi.org/10.1016/j.cej.2016.03.063

Zhang, F., Yang, H., Wang, J., Liu, Z., Guan, Q., 2018. Effect of free ammonia inhibition on NOB activity in high nitrifying performance of sludge. RSC Adv. 8, 31987–31995. https://doi.org/10.1039/c8ra06198j

Zheng, X., Sun, P., Lou, J., Fang, Z., Guo, M., Song, Y., Tang, X., Jiang, T., 2013. The long-term effect of nitrite on the granule-based enhanced biological phosphorus removal system and the reversibility. Bioresour. Technol. 132, 333–341. https://doi.org/10.1016/j.biortech.2013.01.042

Zhou, Y., Ganda, L., Lim, M., Yuan, Z., Kjelleberg, S., Ng, W.J., 2010. Free nitrous acid (FNA) inhibition on denitrifying poly-phosphate accumulating organisms (DPAOs). Appl. Microbiol. Biotechnol. 88, 359–369. https://doi.org/10.1007/s00253-010-2780-3

Appendix A: Supplemental Figures

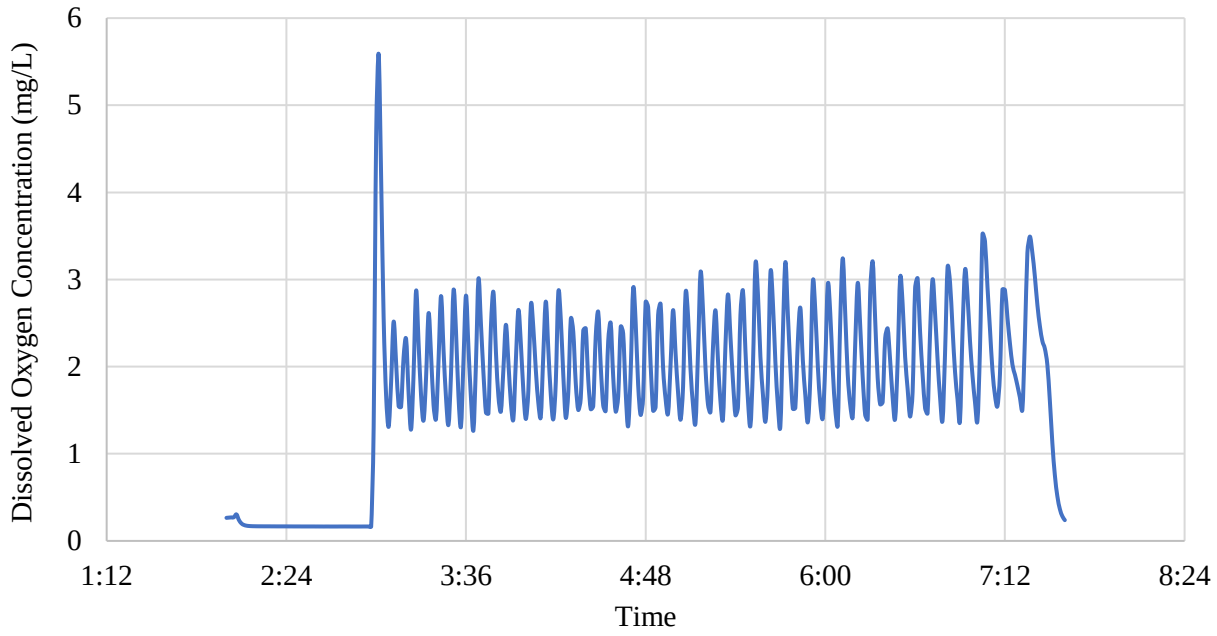

Figure A-1. Example of dissolved oxygen concentration for a 6-hour cycle in the sequencing batch reactor, starting with the anaerobic phase, on May 14, 2019 at 2:00 AM.

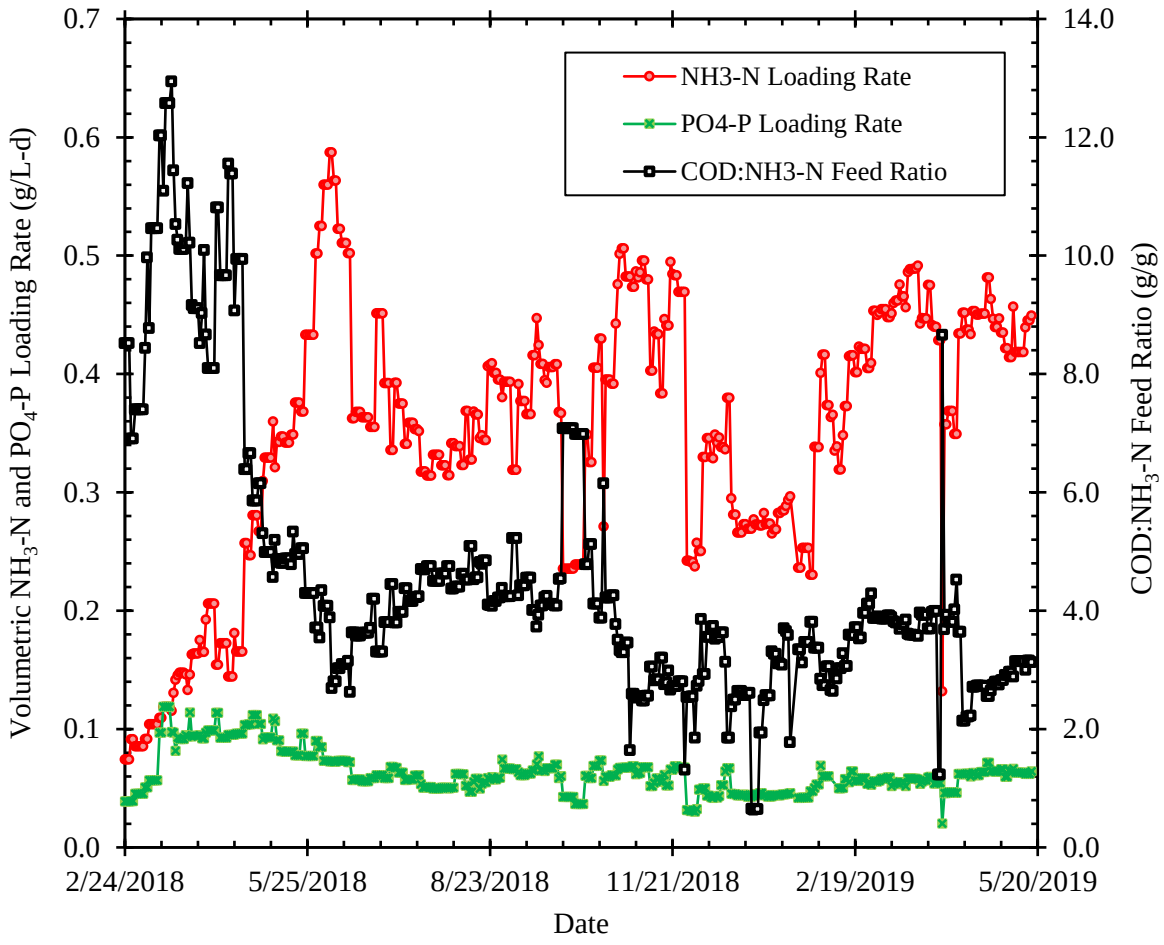

Figure A-2. Volumetric loading rate for NH_3-N and PO_4^{3-}-P (left y-axis) and COD:N feed ratio (right y-axis) versus time.

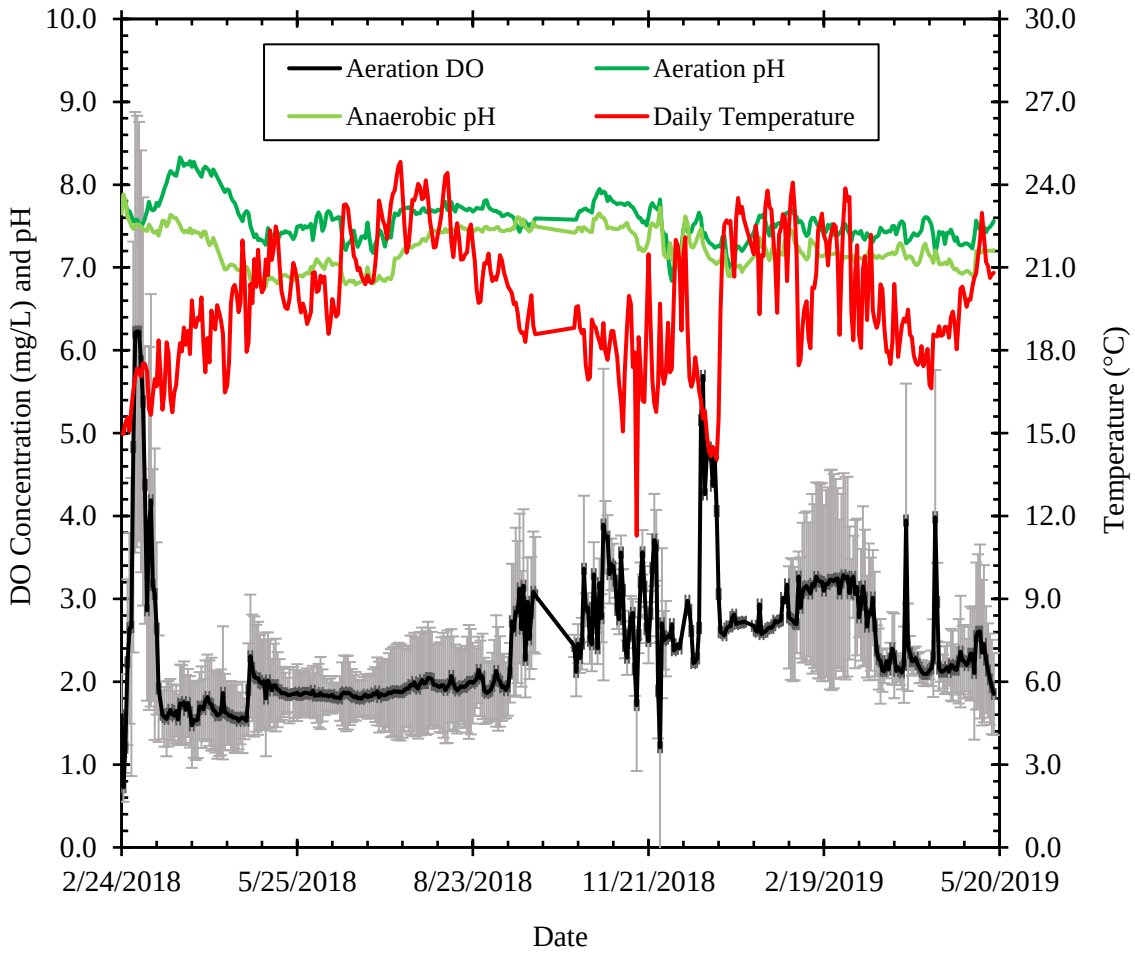

Figure A-3. Online monitoring data for average aeration DO, average anaerobic phase pH, average aeration phase pH, and average cycle temperature. Averages are conducted on a daily basis. Error bars are shown for DO concentration averages and represent the standard deviation of DO concentration measurements during aeration phase.

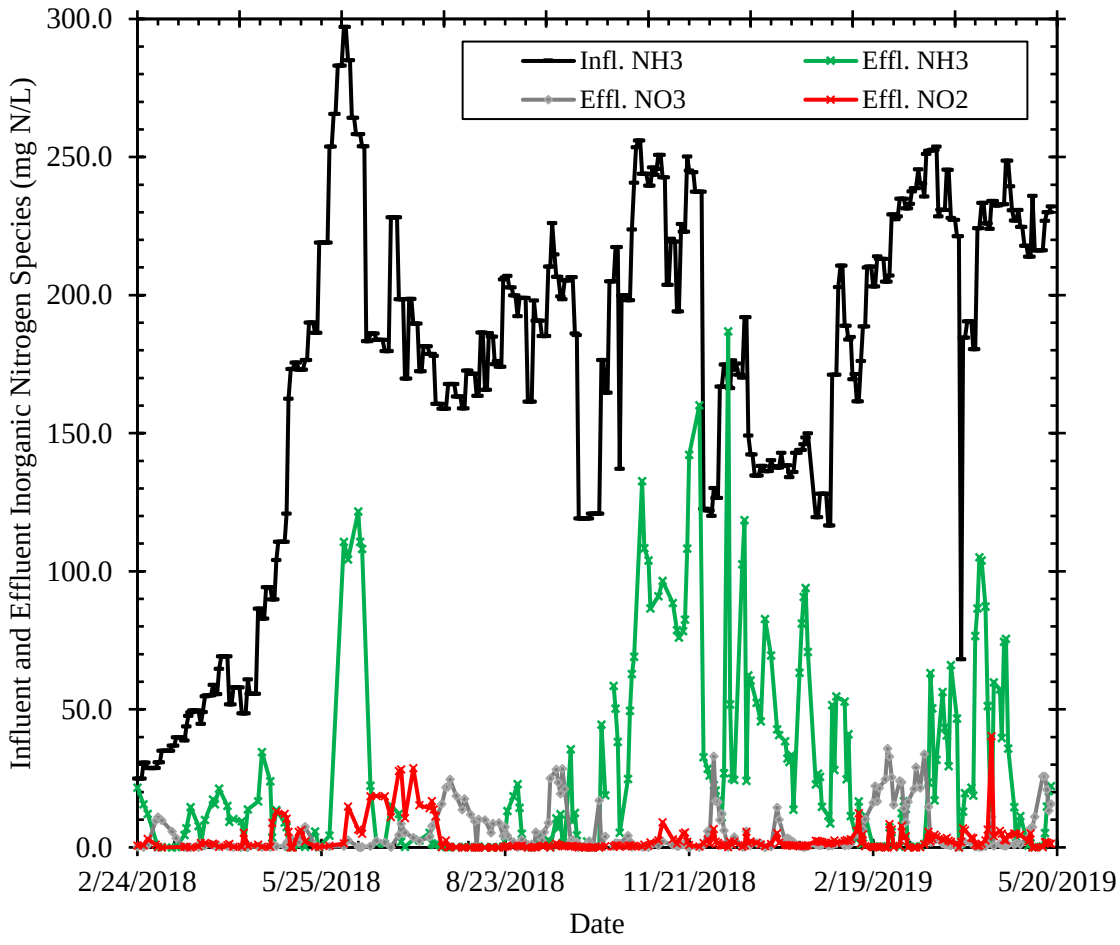

Figure A-4. Influent NH_3, effluent NH_3, effluent NO_2^-, and effluent NO_3^- concentrations in mg N/L versus time.

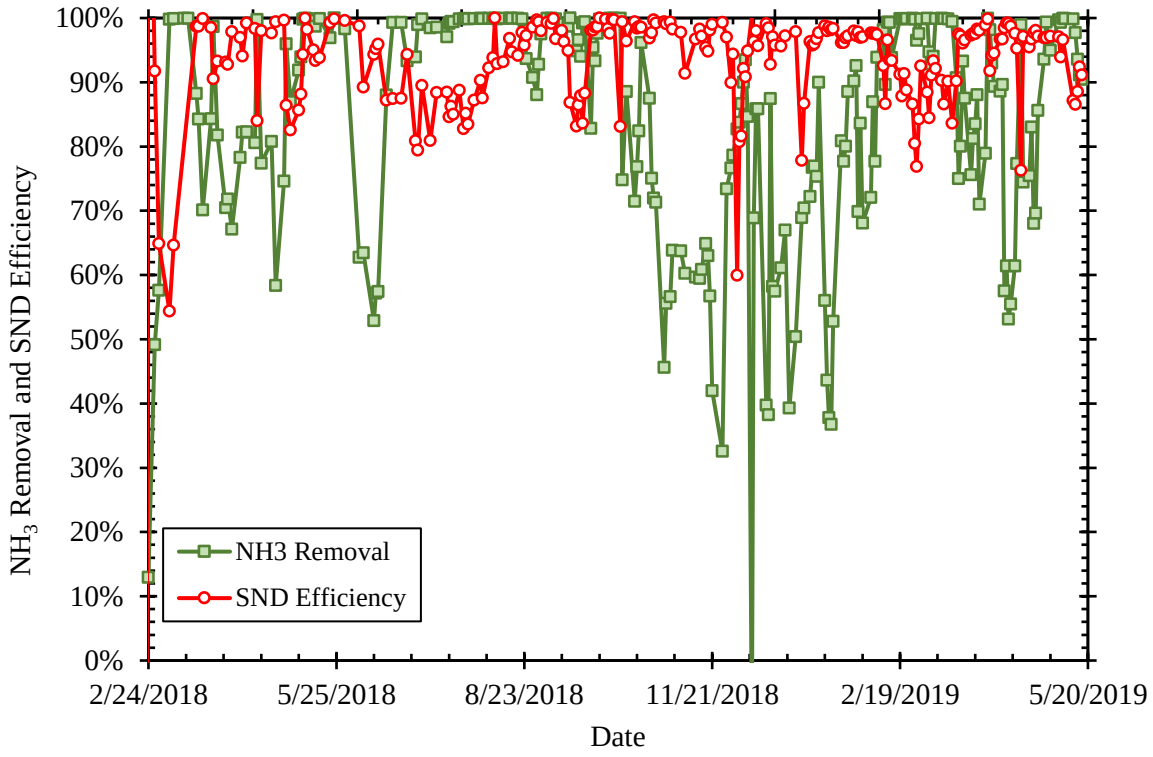

Figure A-5. NH_3 removal efficiency and SND efficiency versus time.

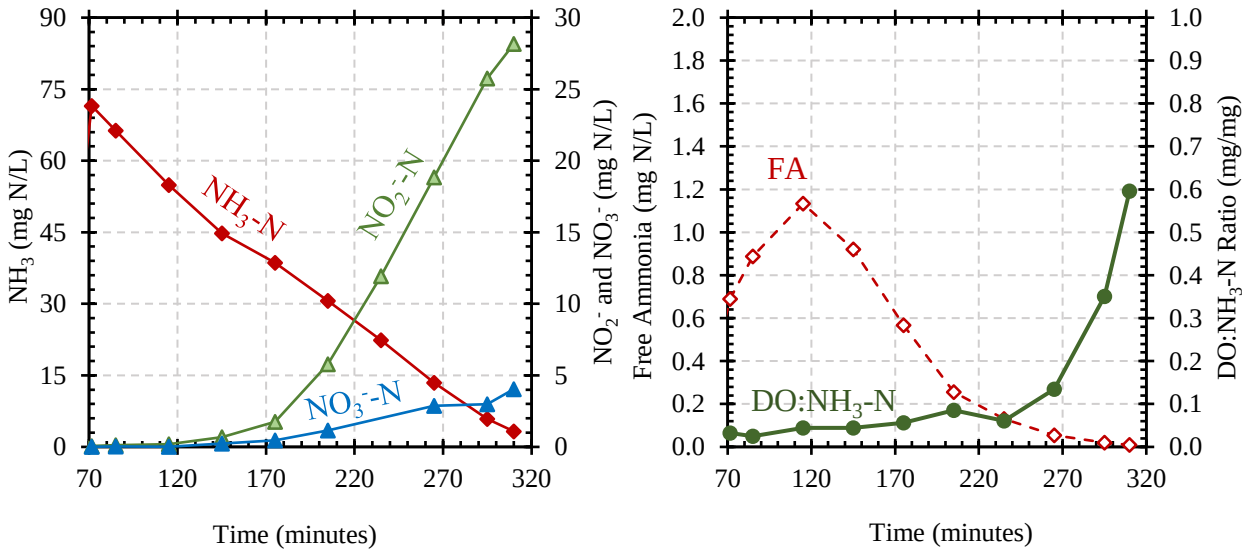

Figure A-6. NH_3-N, NO_2^--N, and NO_3^--N concentration profiles on July 9, 2018 during Period 1A (left) and the corresponding FA and DO:NH_3-N Ratio profiles (right).

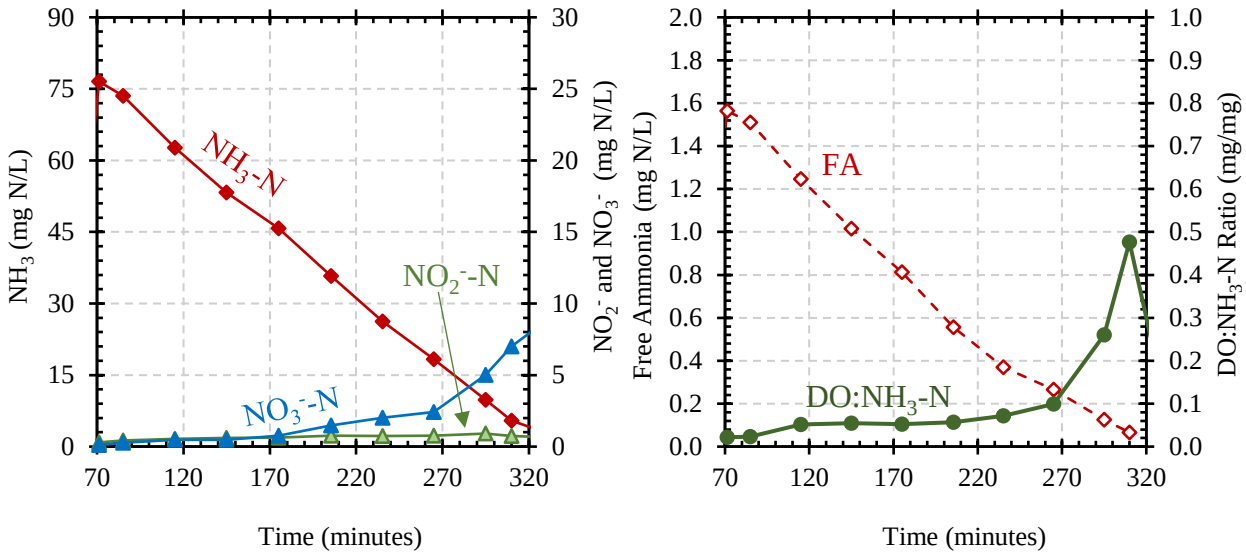

Figure A-7. NH_3-N, NO_2^--N, and NO_3^--N concentration profiles on September 13, 2018 during Period 1B (left) and the corresponding FA and DO:NH_3-N Ratio profiles (right).

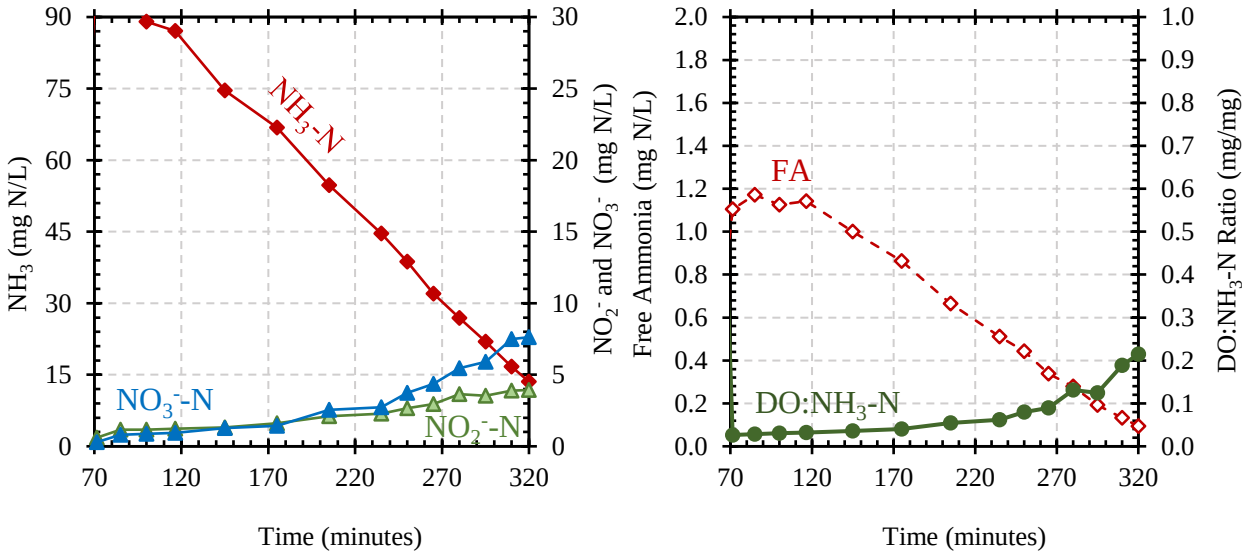

Figure A-8. NH_3-N, NO_2^--N, and NO_3^--N concentration profiles on March 7, 2019 during Period 2A (left) and the corresponding FA and DO:NH_3-N Ratio profiles (right).

Appendix B: Sidestream Cycle Profiles

Cycle profiles are shown in this section with nutrient (NH_3-N, NO_2^--N, NO_3^--N, PO_4^{3-}-P) and acetate (as COD) concentrations on the left-side y-axis and pH values on the right-side y-axis. The MLSS, MLVSS, average daily temperature, and average daily aeration-phase DO concentration are displayed in the table below. The standard deviation of DO concentrations was also calculated based on 5-minute DO concentration recordings in 2018 and 1-minute DO concentration recordings in 2019. Anaerobic phase is from minutes 0-50 and aeration feeding phase is from minutes 61-75. Labels provided on plots.

Table B-1. MLSS, MLVSS, temperature, DO concentration, influent NH_3-N concentration, and COD:N feed ratio information for Cycle Profiles displayed in Appendix B.

Date	MLSS	MLVSS	Average Temperature	Average DO	DO Standard Deviation	Influent NH_3-N	COD:N Feed Ratio
	g/L	g/L	°C	mg/L	mg/L	mg/L	g/g
6/14/2018	14.0	11.5	19.2	1.8	0.2	254	3.15
6/18/2018	14.0	11.2	23.3	1.9	0.4	186	3.58
6/28/2018	14.9	11.0	20.5	1.8	0.2	228	3.31
7/2/2018	14.0	10.5	20.4	1.8	0.3	198	3.80
7/5/2018	15.0	11.0	22.0	1.9	0.4	170	4.44
7/9/2018	13.6	10.1	22.5	1.8	0.4	190	3.98
7/12/2018	13.5	9.9	23.3	1.9	0.5	172	4.38
7/17/2018	13.2	9.8	24.8	1.9	0.6	179	4.22
7/19/2018	13.5	10.0	22.6	1.9	0.5	178	4.24
7/23/2018	12.7	9.0	23.4	2.0	0.6	159	4.75
7/26/2018	13.2	9.8	24.0	1.9	0.6	168	4.50
7/30/2018	13.2	9.6	24.2	2.0	0.6	163	4.62
8/2/2018	12.4	9.1	22.3	2.0	0.6	159	4.75
8/6/2018	12.3	8.8	22.5	1.9	0.5	171	4.40
8/9/2018	12.4	9.3	24.3	1.9	0.6	163	4.62
8/13/2018	12.4	9.0	21.4	2.0	0.6	166	5.09
8/16/2018	12.1	8.9	22.1	1.9	0.5	185	4.56
8/20/2018	12.5	9.2	21.6	2.0	0.6	174	4.85
8/23/2018	13.1	9.6	21.8	2.0	0.5	206	4.09
8/27/2018	12.7	9.7	19.8	2.0	0.5	200	4.22
8/30/2018	12.4	9.4	21.1	1.9	0.4	199	4.24
9/3/2018	12.5	9.3	20.7	2.0	0.5	161	5.23
9/6/2018	12.2	9.0	21.4	2.0	0.5	198	4.26
9/13/2018	11.4	8.7	19.7	2.6	0.8	210	4.01
9/20/2018	12.1	8.9	19.0	3.0	0.5	198	4.25
1/3/2019	7.9	5.9	21.5	2.8	N/A	137	1.94
3/7/2019	12.1	8.4	20.8	3.1	0.9	231	3.92
4/11/2019	11.6	9.4	17.4	2.1	0.1	224	3.64
5/30/2019	12.1	8.8	20.8	1.9	0.5	159	3.46

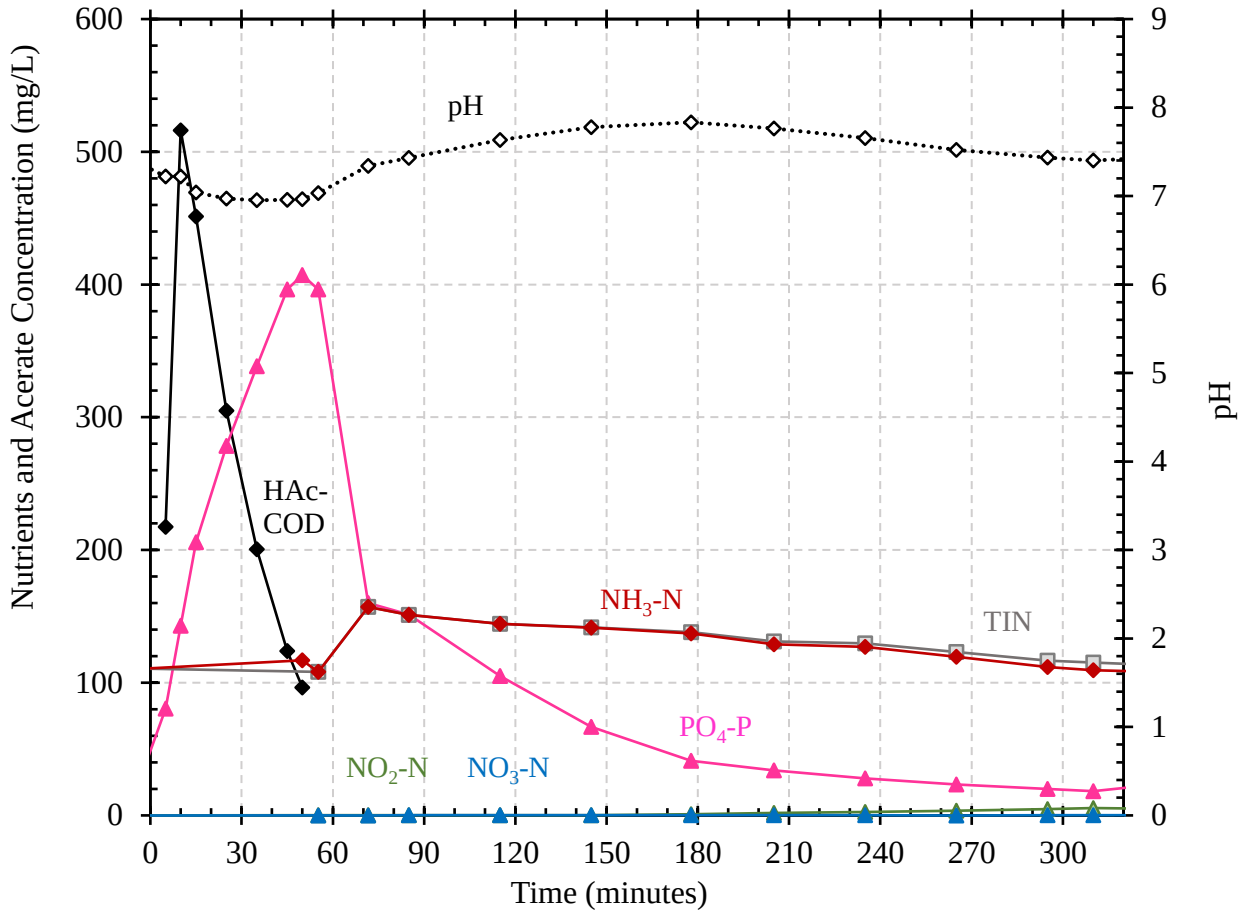

Figure B-1. Acetate-COD and nutrient profile for anaerobic (0-50 min) and aeration (50-320 min) phases on June 14, 2018 with acetate feeding from 0-10 min and diluted centrate feeding from 61-75 min. The MLVSS was 11.5 g/L, average temperature was 19.2 C, average DO concentration was 1.8 mg/L, influent NH_3-N concentration was 254 mg/L, and COD:N feed ratio was 3.15 g/g.

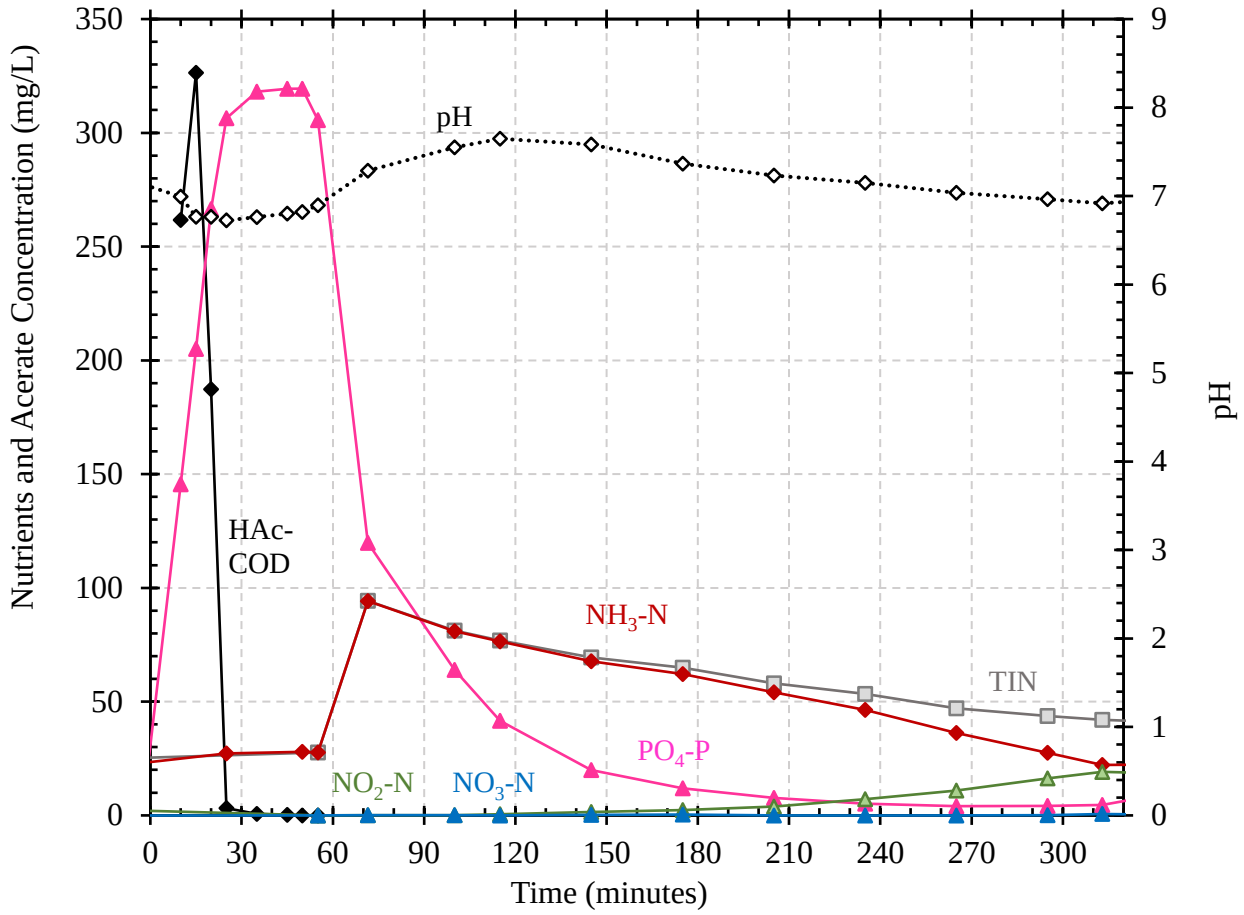

Figure B-2. Acetate-COD and nutrient profile for anaerobic (0-50 min) and aeration (50-320 min) phases on June 18, 2018 with acetate feeding from 0-10 min and diluted centrate feeding from 61-75 min. The MLVSS was 11.2 g/L, average temperature was 23.3°C, average DO concentration was 1.9 mg/L, influent NH_3-N concentration was 186 mg/L, and COD:N feed ratio was 3.58 g/g.

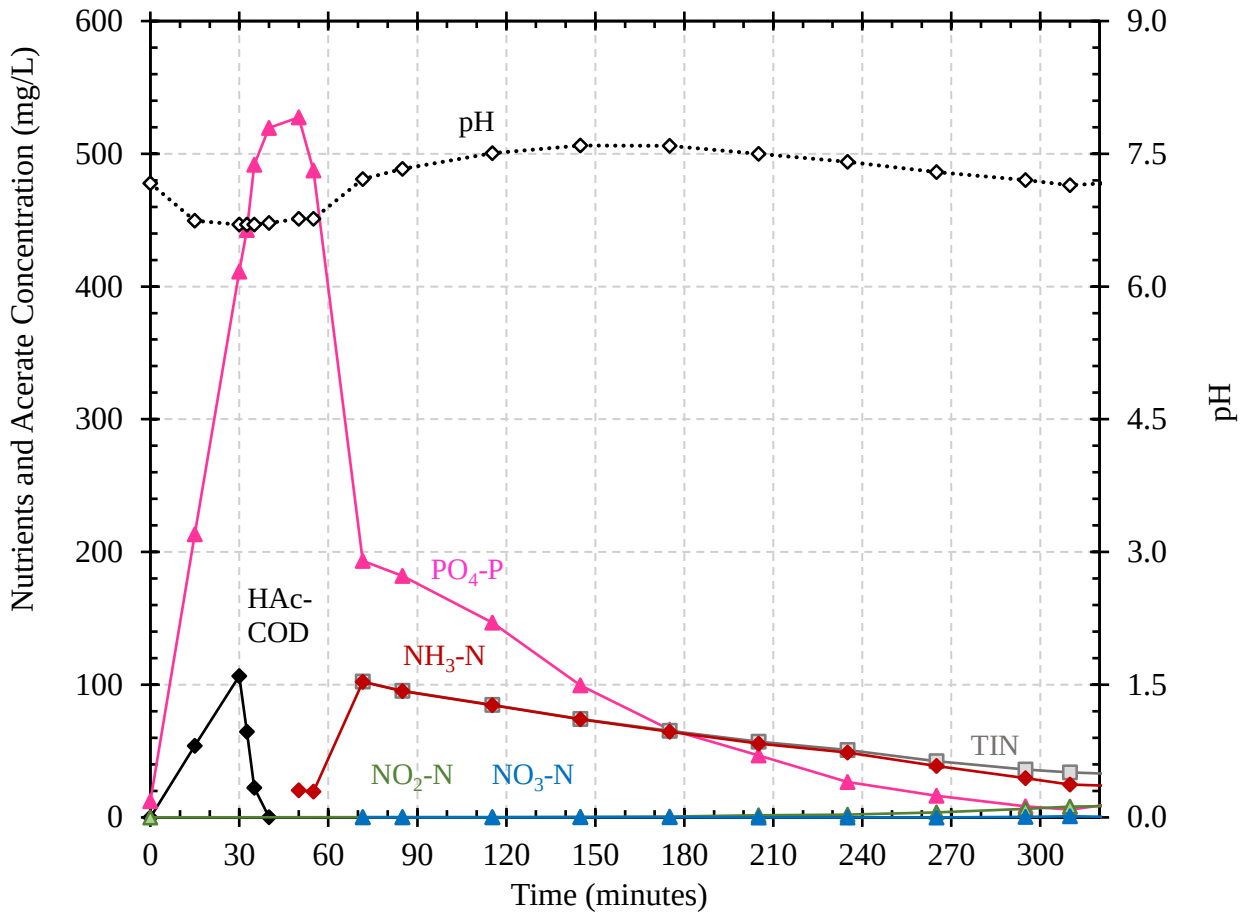

Figure B-3. Acetate-COD and nutrient profile for anaerobic (0-50 min) and aeration (50-320 min) phases on June 28, 2018 with acetate feeding from 0-30 min and diluted centrate feeding from 61-75 min. The MLVSS was 11.0 g/L, average temperature was 20.5°C, average DO concentration was 1.8 mg/L, influent NH_3-N concentration was 228 mg/L, and COD:N feed ratio was 3.31 g/g.

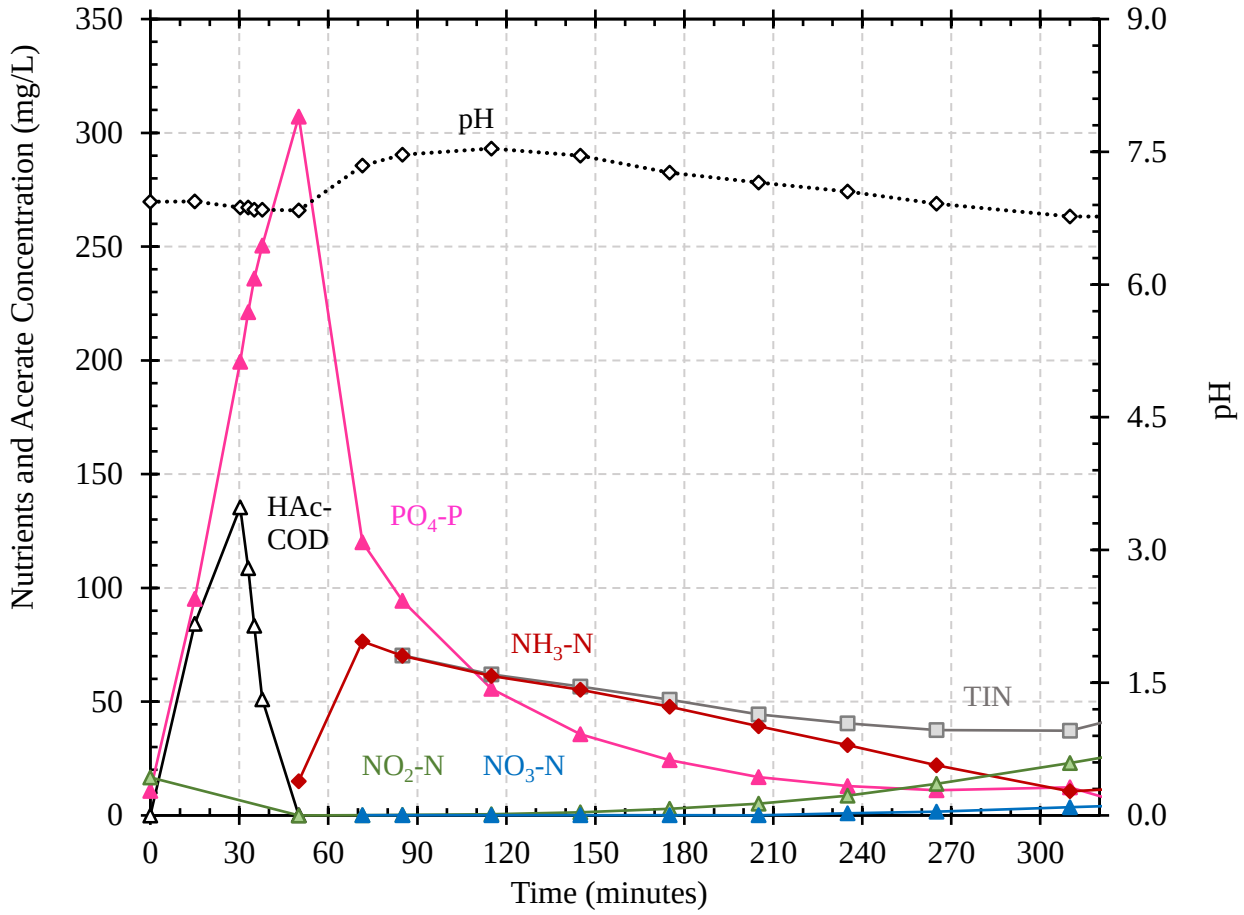

Figure B-4. Acetate-COD and nutrient profile for anaerobic (0-50 min) and aeration (50-320 min) phases on July 2, 2018 with acetate feeding from 0-30 min and diluted centrate feeding from 61-75 min. The MLVSS was 10.5 g/L, average temperature was 20.4°C, average DO concentration was 1.8 mg/L, influent NH_3-N concentration was 198 mg/L, and COD:N feed ratio was 3.80 g/g.

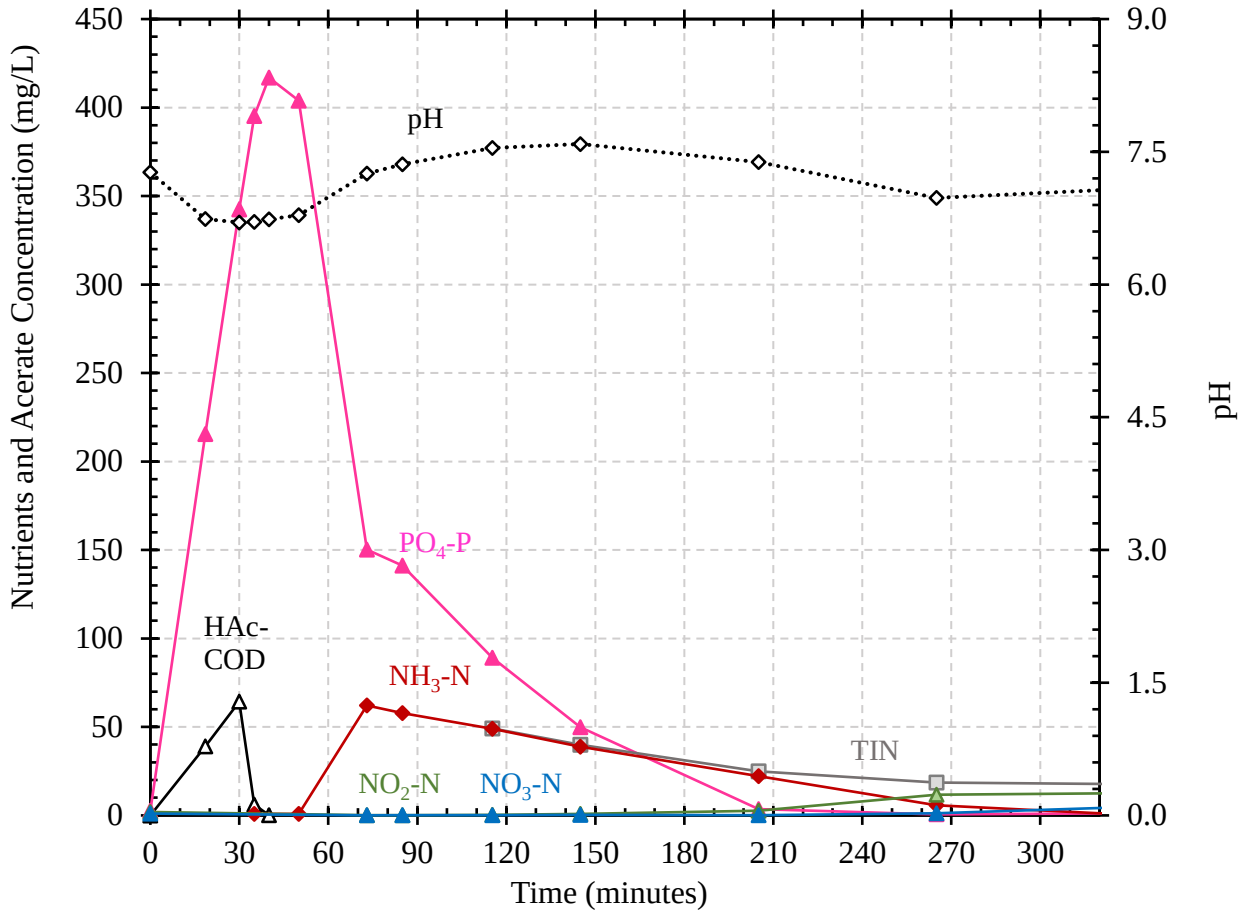

Figure B-5. Acetate-COD and nutrient profile for anaerobic (0-50 min) and aeration (50-320 min) phases on July 5, 2018 with acetate feeding from 0-30 min and diluted centrate feeding from 61-75 min. The MLVSS was 11.0 g/L, average temperature was 22.0°C, average DO concentration was 1.9 mg/L, influent NH_3-N concentration was 170 mg/L, and COD:N feed ratio was 4.44 g/g.

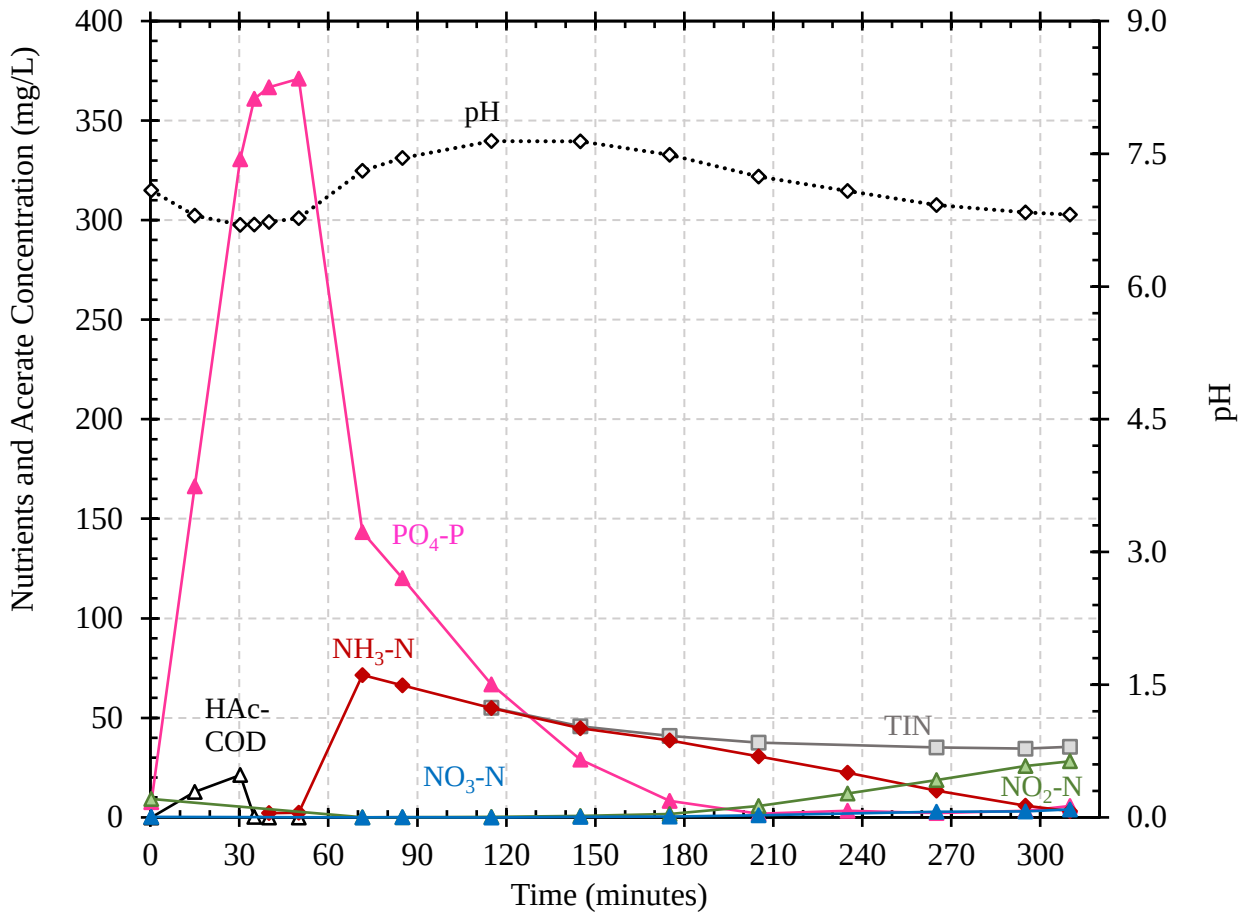

Figure B-6. Acetate-COD and nutrient profile for anaerobic (0-50 min) and aeration (50-320 min) phases on July 9, 2018 with acetate feeding from 0-30 min and diluted centrate feeding from 61-75 min. The MLVSS was 10.1 g/L, average temperature was 22.5°C, average DO concentration was 1.8 mg/L, influent NH_3-N concentration was 190 mg/L, and COD:N feed ratio was 3.98 g/g.

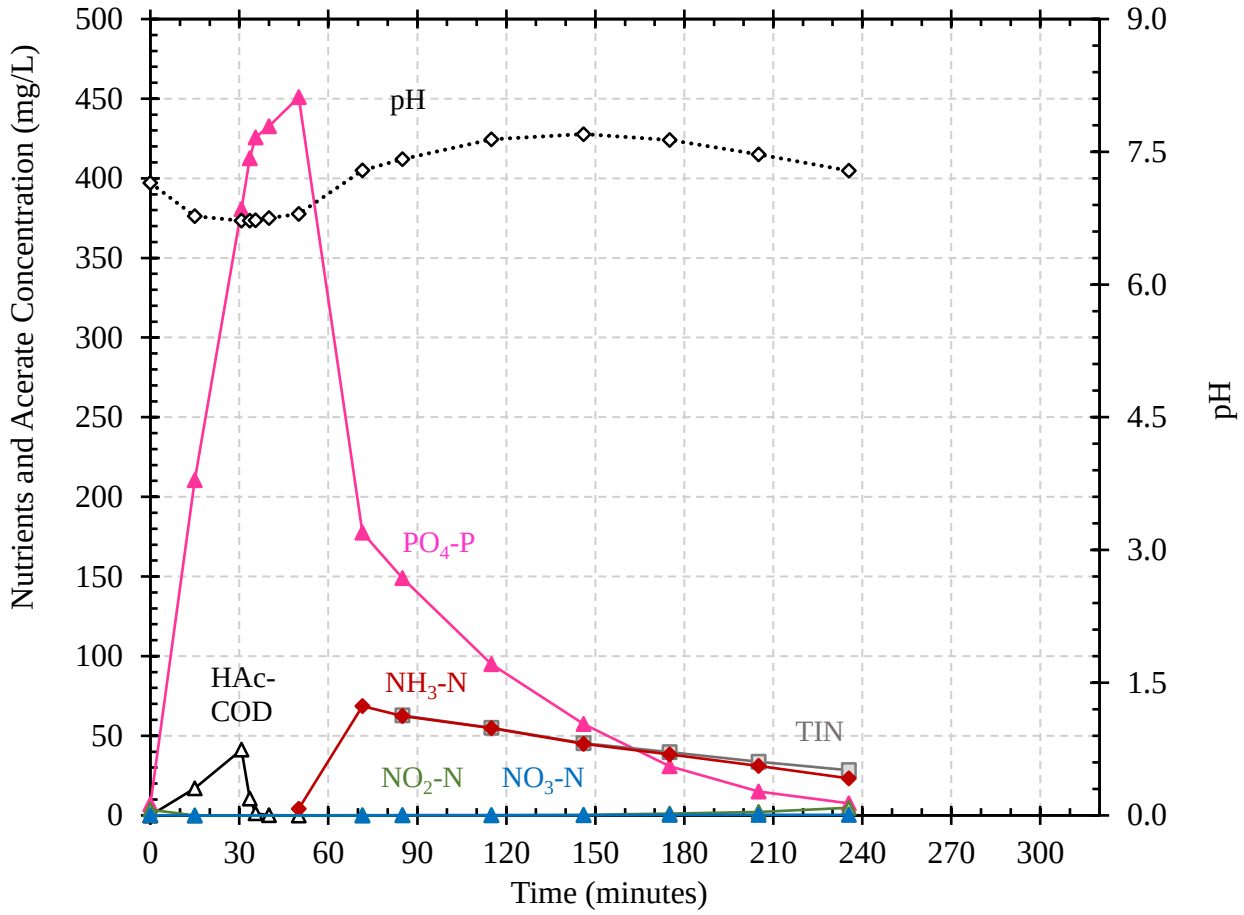

Figure B-7. Acetate-COD and nutrient profile for anaerobic (0-50 min) and aeration (50-320 min) phases on July 12, 2018 with acetate feeding from 0-30 min and diluted centrate feeding from 61-75 min. The MLVSS was 9.9 g/L, average temperature was 23.3°C, average DO concentration was 1.9 mg/L, influent NH_3-N concentration was 172 mg/L, and COD:N feed ratio was 4.38 g/g.

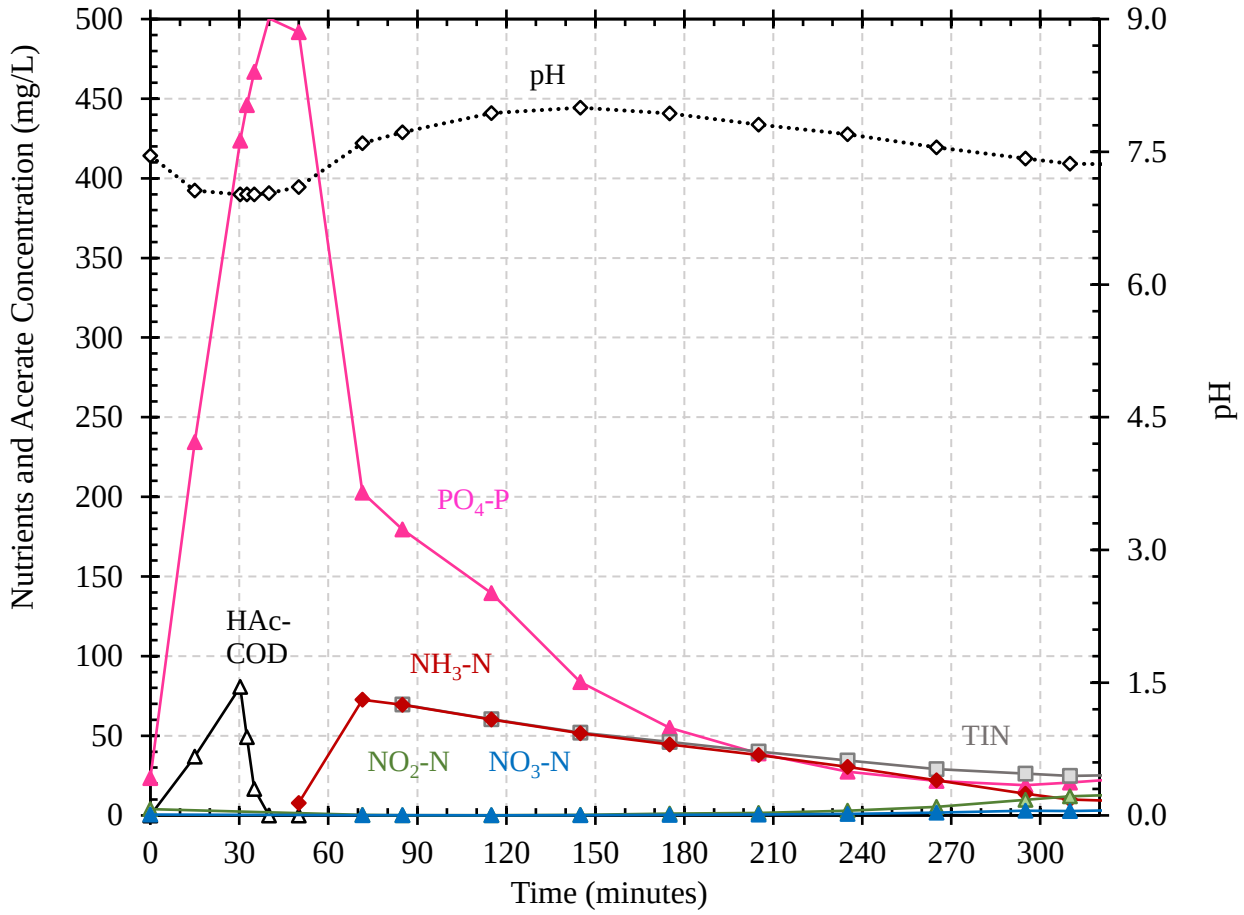

Figure B-8. Acetate-COD and nutrient profile for anaerobic (0-50 min) and aeration (50-320 min) phases on July 17, 2018 with acetate feeding from 0-30 min and diluted centrate feeding from 61-75 min. The MLVSS was 9.8 g/L, average temperature was 24.8°C, average DO concentration was 1.9 mg/L, influent NH_3-N concentration was 179 mg/L, and COD:N feed ratio was 4.22 g/g.

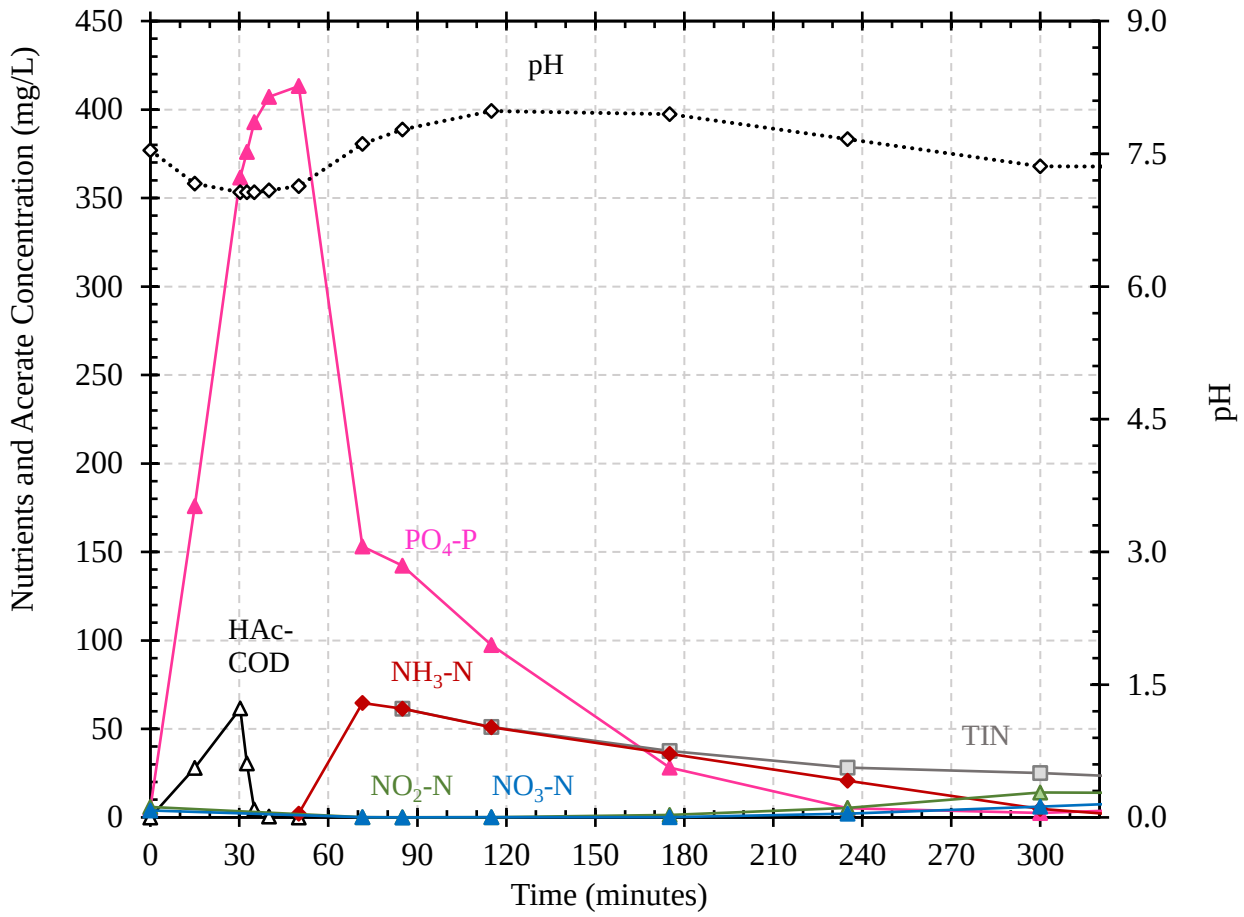

Figure B-9. Acetate-COD and nutrient profile for anaerobic (0-50 min) and aeration (50-320 min) phases on July 19, 2018 with acetate feeding from 0-30 min and diluted centrate feeding from 61-75 min. The MLVSS was 10.0 g/L, average temperature was 22.6°C, average DO concentration was 1.9 mg/L, influent NH_3-N concentration was 178 mg/L, and COD:N feed ratio was 4.24 g/g.

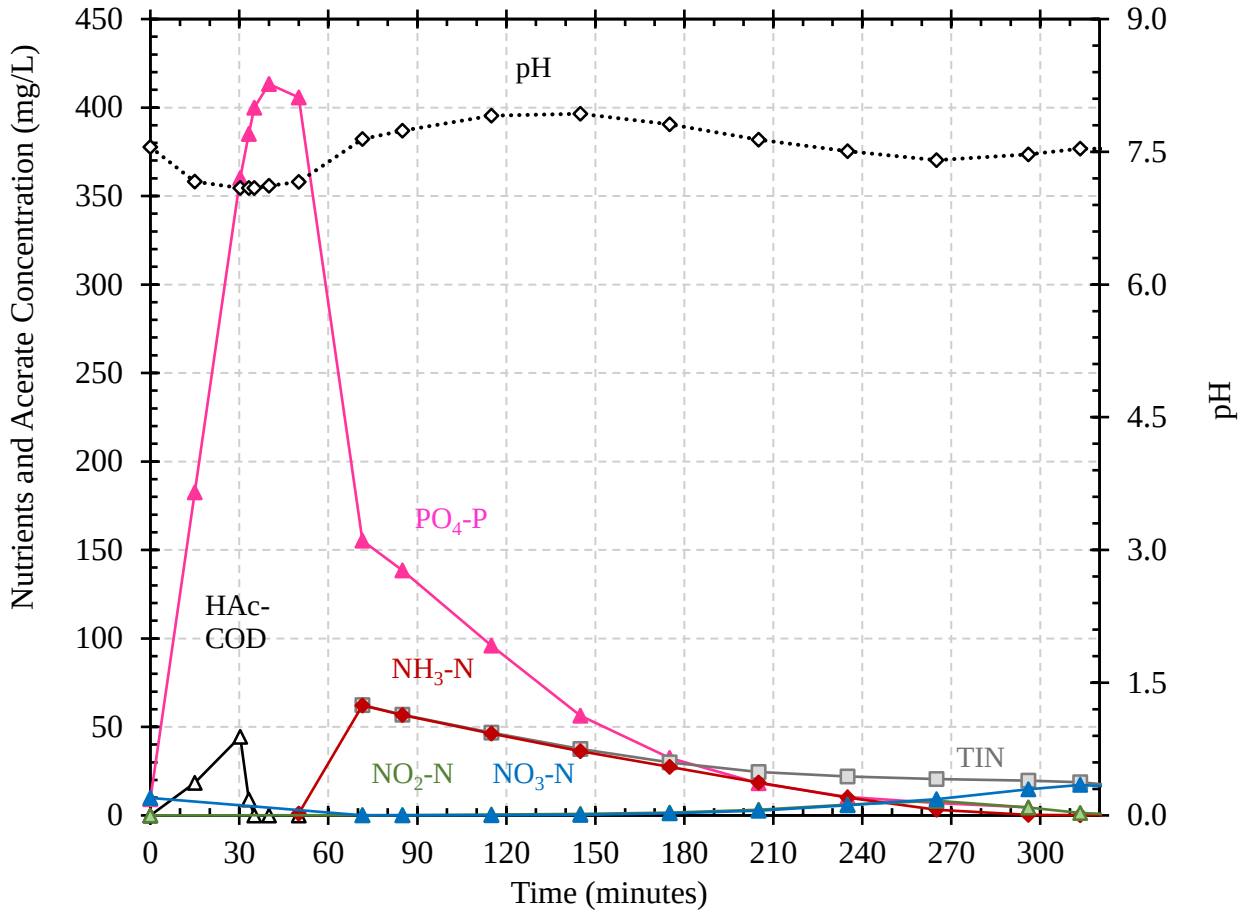

Figure B-10. Acetate-COD and nutrient profile for anaerobic (0-50 min) and aeration (50-320 min) phases on July 23, 2018 with acetate feeding from 0-30 min and diluted centrate feeding from 61-75 min. The MLVSS was 9.0 g/L, average temperature was 23.4°C, average DO concentration was 2.0 mg/L, influent NH_3-N concentration was 159 mg/L, and COD:N feed ratio was 4.75 g/g.

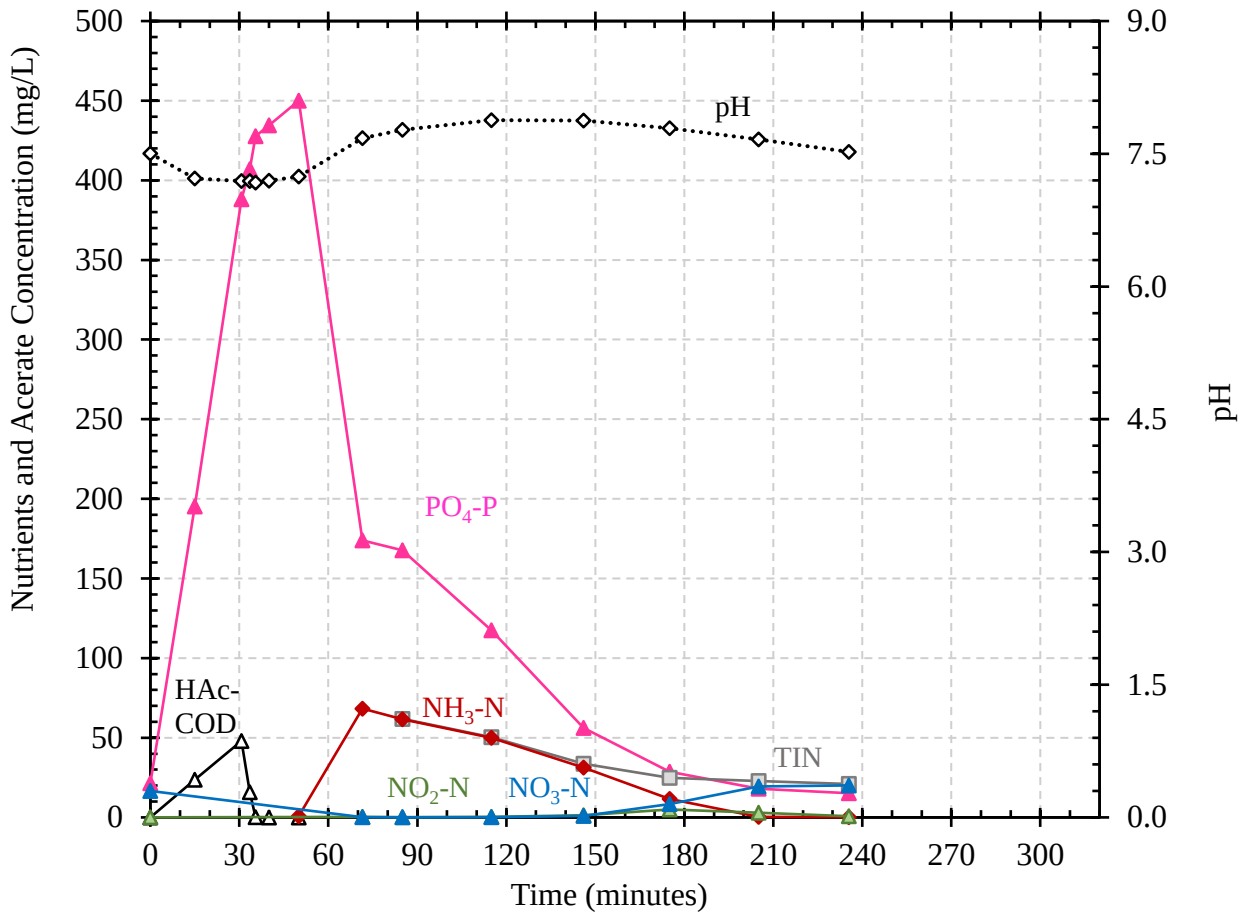

Figure B-11. Acetate-COD and nutrient profile for anaerobic (0-50 min) and aeration (50-320 min) phases on July 26, 2018 with acetate feeding from 0-30 min and diluted centrate feeding from 61-75 min. The MLVSS was 9.8 g/L, average temperature was 24.0°C, average DO concentration was 1.9 mg/L, influent NH_3-N concentration was 168 mg/L, and COD:N feed ratio was 4.50 g/g.

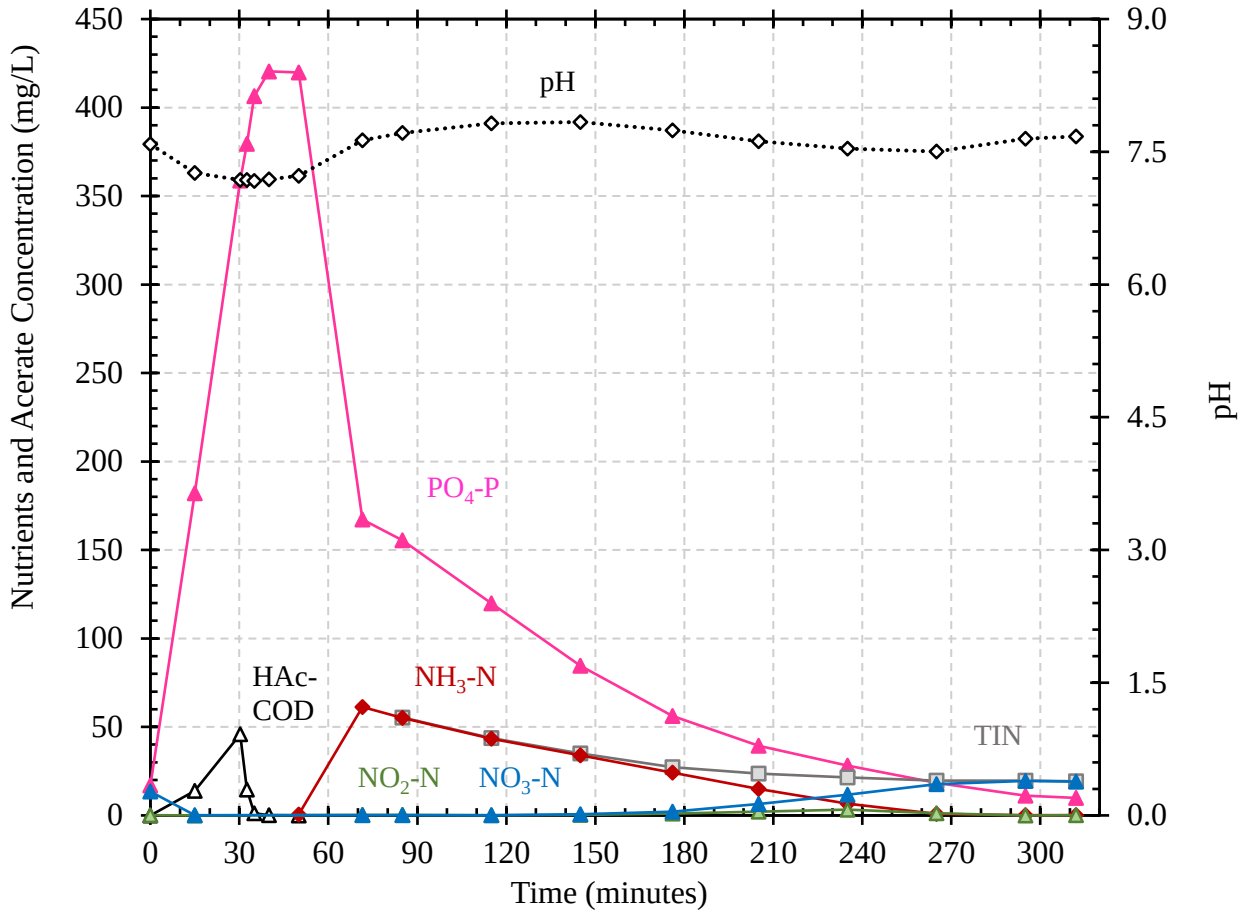

Figure B-12. Acetate-COD and nutrient profile for anaerobic (0-50 min) and aeration (50-320 min) phases on July 30, 2018 with acetate feeding from 0-30 min and diluted centrate feeding from 61-75 min. The MLVSS was 9.6 g/L, average temperature was 24.2°C, average DO concentration was 2.0 mg/L, influent NH_3-N concentration was 163 mg/L, and COD:N feed ratio was 4.62 g/g.

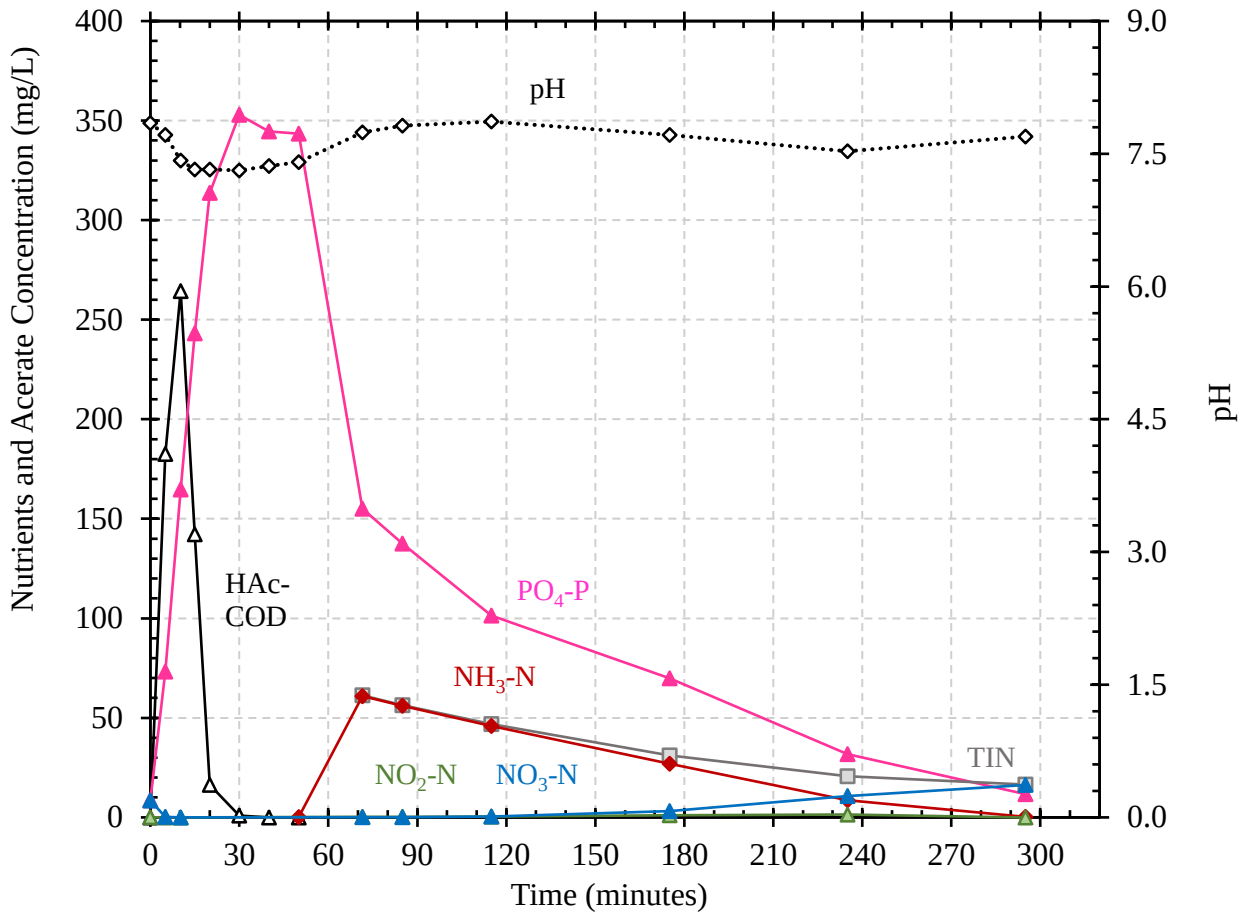

Figure B-13. Acetate-COD and nutrient profile for anaerobic (0-50 min) and aeration (50-320 min) phases on August 2, 2018 with acetate feeding from 0-10 min and diluted centrate feeding from 61-75 min. The MLVSS was 9.1 g/L, average temperature was 22.3°C, average DO concentration was 2.0 mg/L, influent NH_3-N concentration was 159 mg/L, and COD:N feed ratio was 4.75 g/g.

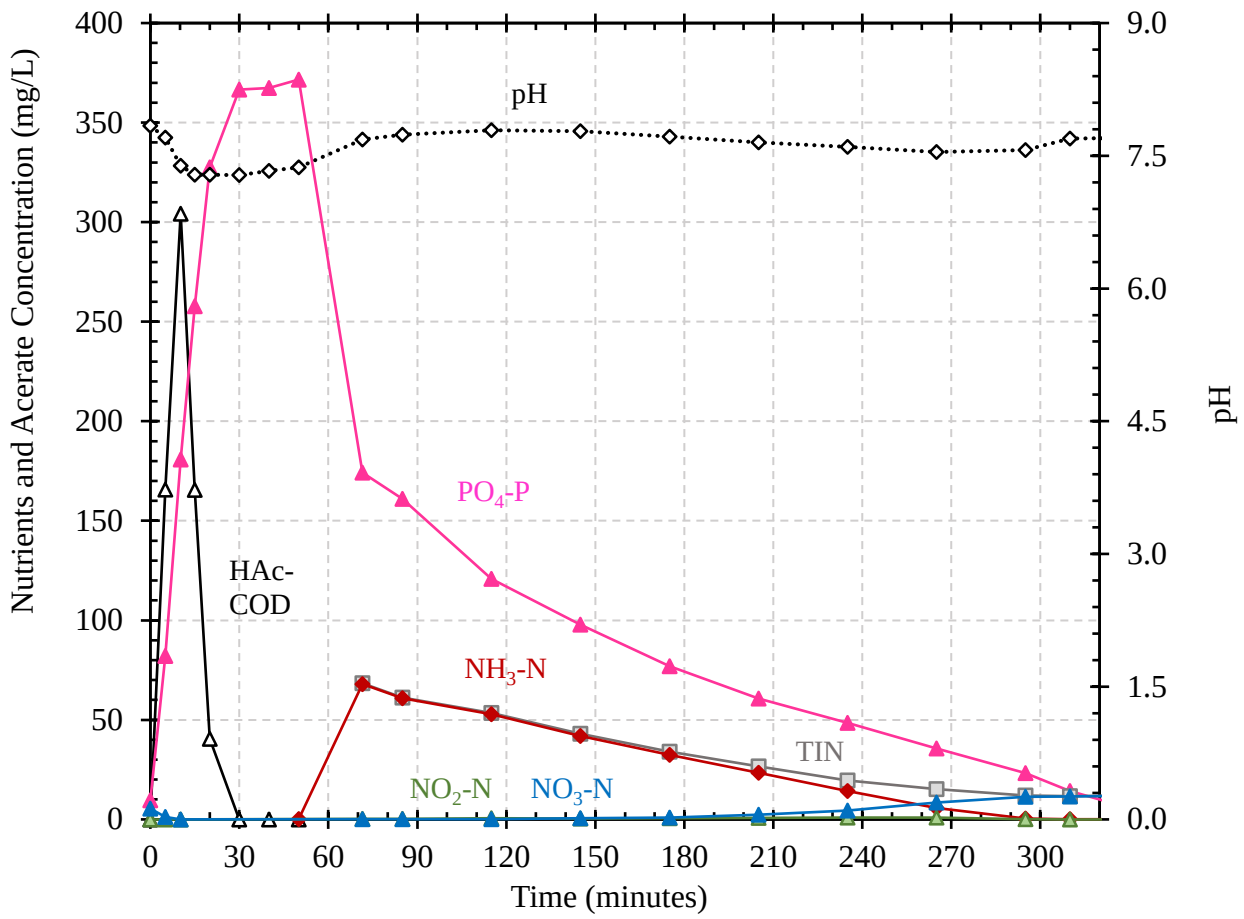

Figure B-14. Acetate-COD and nutrient profile for anaerobic (0-50 min) and aeration (50-320 min) phases on August 6, 2018 with acetate feeding from 0-10 min and diluted centrate feeding from 61-75 min. The MLVSS was 8.8 g/L, average temperature was 22.5°C, average DO concentration was 1.9 mg/L, influent NH_3-N concentration was 171 mg/L, and COD:N feed ratio was 4.40 g/g.

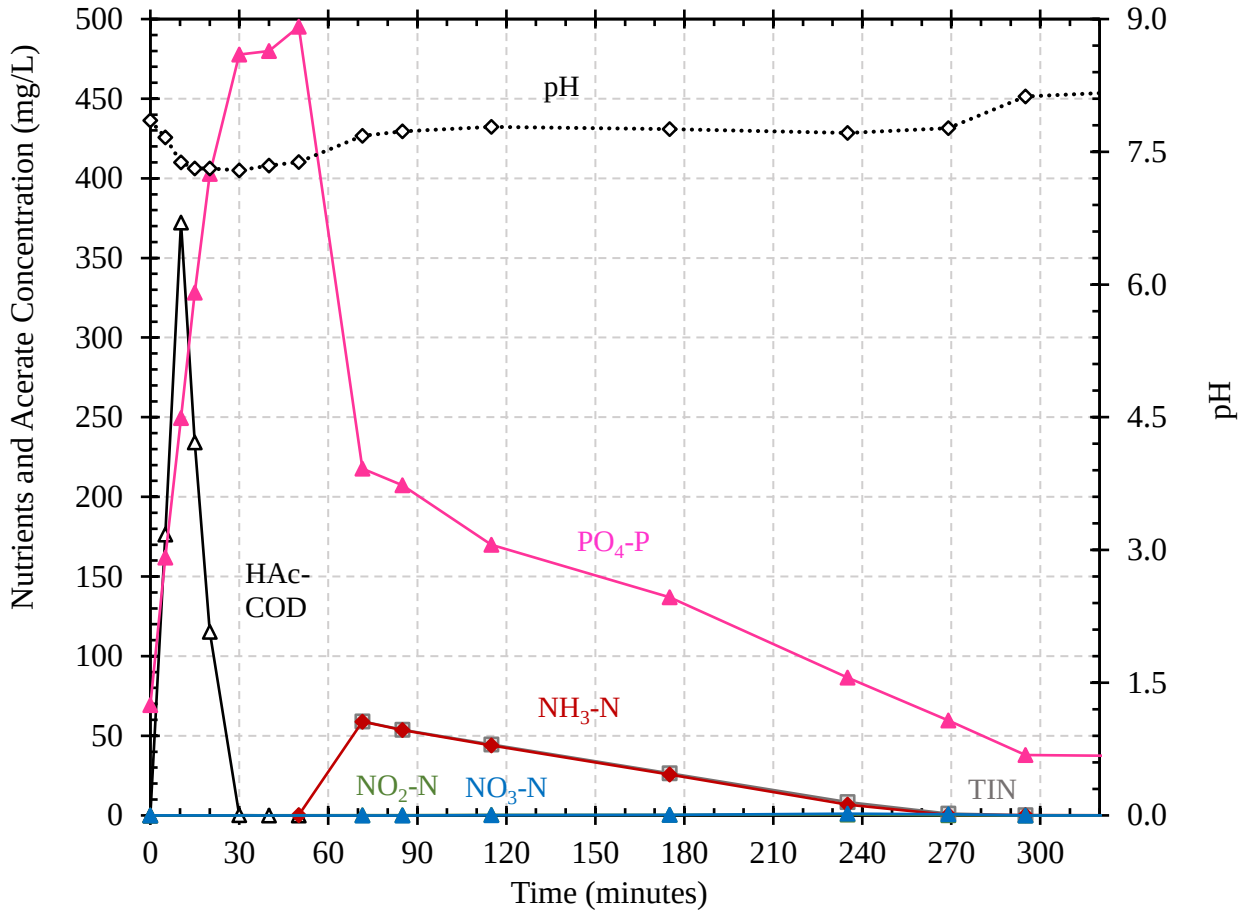

Figure B-15. Acetate-COD and nutrient profile for anaerobic (0-50 min) and aeration (50-320 min) phases on August 9, 2018 with acetate feeding from 0-10 min and diluted centrate feeding from 61-75 min. The MLVSS was 9.3 g/L, average temperature was 24.3°C, average DO concentration was 1.9 mg/L, influent NH_3-N concentration was 163 mg/L, and COD:N feed ratio was 4.62 g/g.

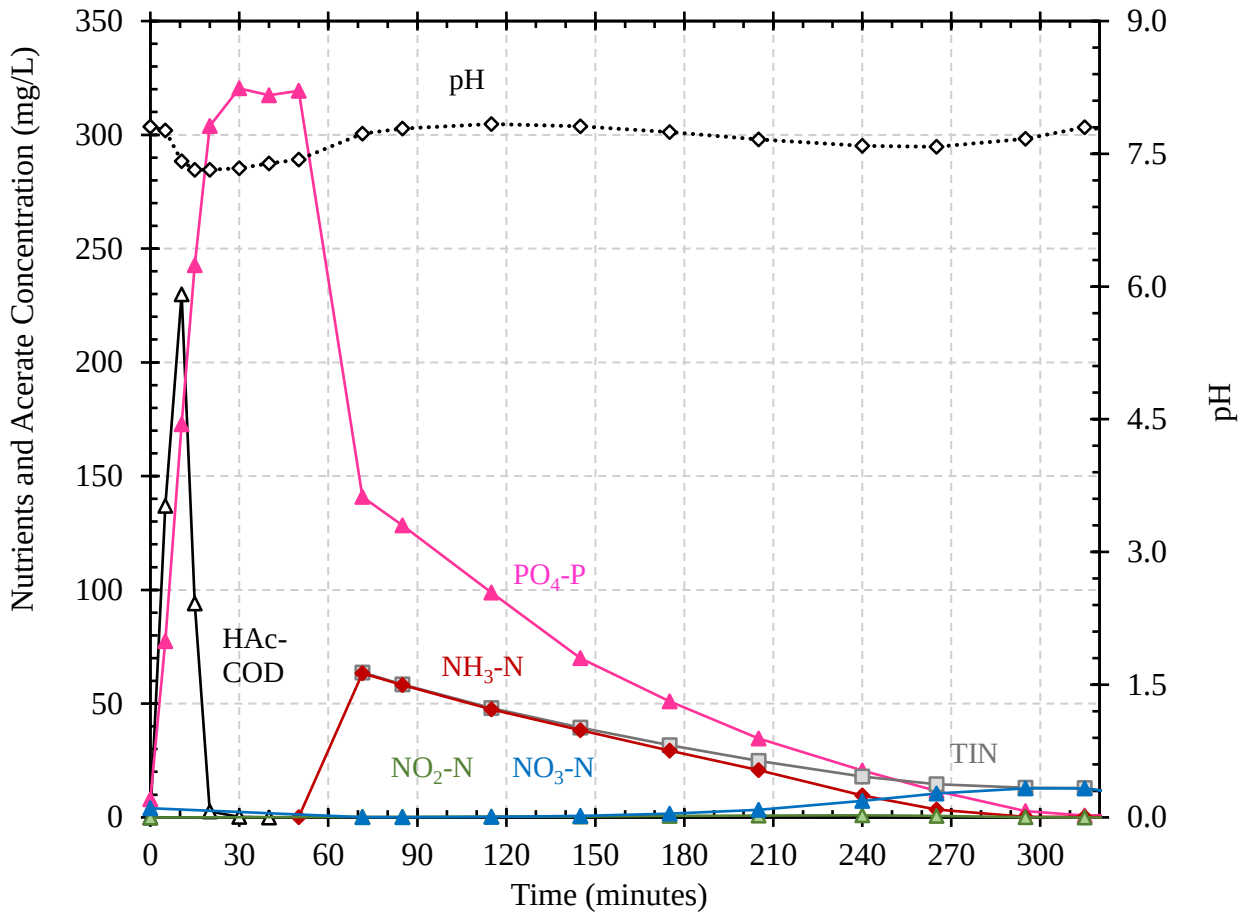

Figure B-16. Acetate-COD and nutrient profile for anaerobic (0-50 min) and aeration (50-320 min) phases on August 13, 2018 with acetate feeding from 0-10 min and diluted centrate feeding from 61-75 min. The MLVSS was 9.0 g/L, average temperature was 21.4°C, average DO concentration was 2.0 mg/L, influent NH_3-N concentration was 166 mg/L, and COD:N feed ratio was 5.09 g/g.

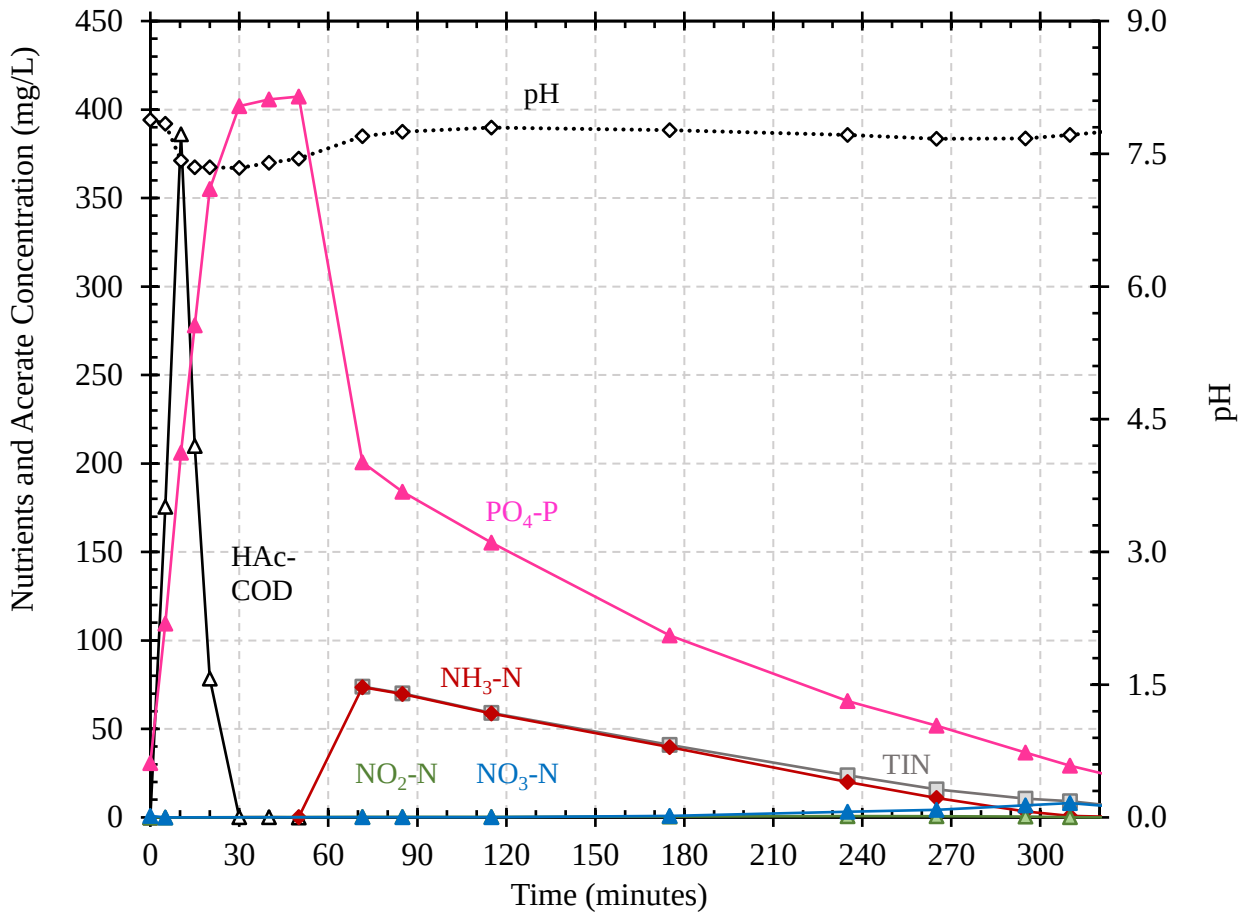

Figure B-17. Acetate-COD and nutrient profile for anaerobic (0-50 min) and aeration (50-320 min) phases on August 16, 2018 with acetate feeding from 0-10 min and diluted centrate feeding from 61-75 min. The MLVSS was 8.9 g/L, average temperature was 22.1°C, average DO concentration was 1.9 mg/L, influent NH_3-N concentration was 185 mg/L, and COD:N feed ratio was 4.56 g/g.

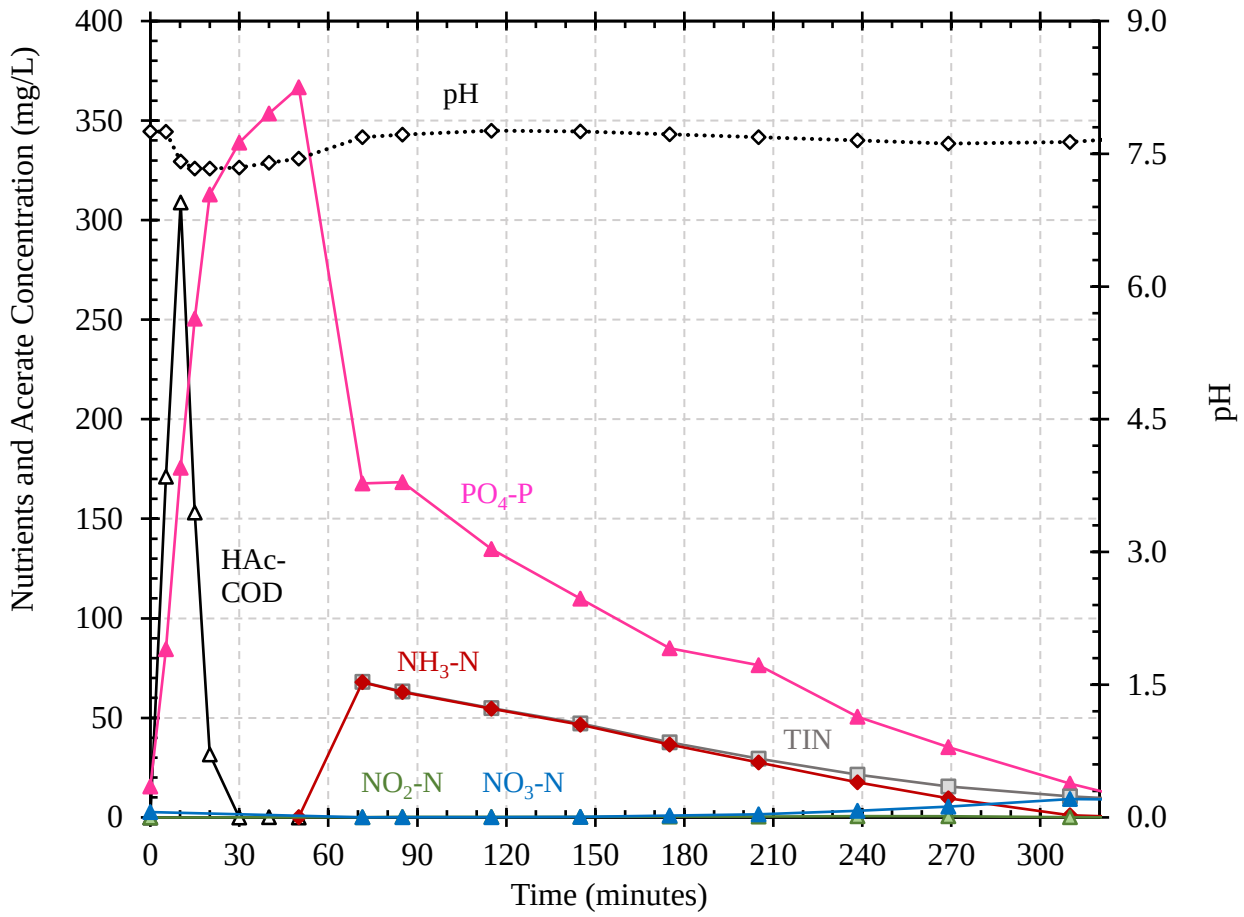

Figure B-18. Acetate-COD and nutrient profile for anaerobic (0-50 min) and aeration (50-320 min) phases on August 20, 2018 with acetate feeding from 0-10 min and diluted centrate feeding from 61-75 min. The MLVSS was 9.2 g/L, average temperature was 21.6°C, average DO concentration was 2.0 mg/L, influent NH_3-N concentration was 174 mg/L, and COD:N feed ratio was 4.85 g/g.

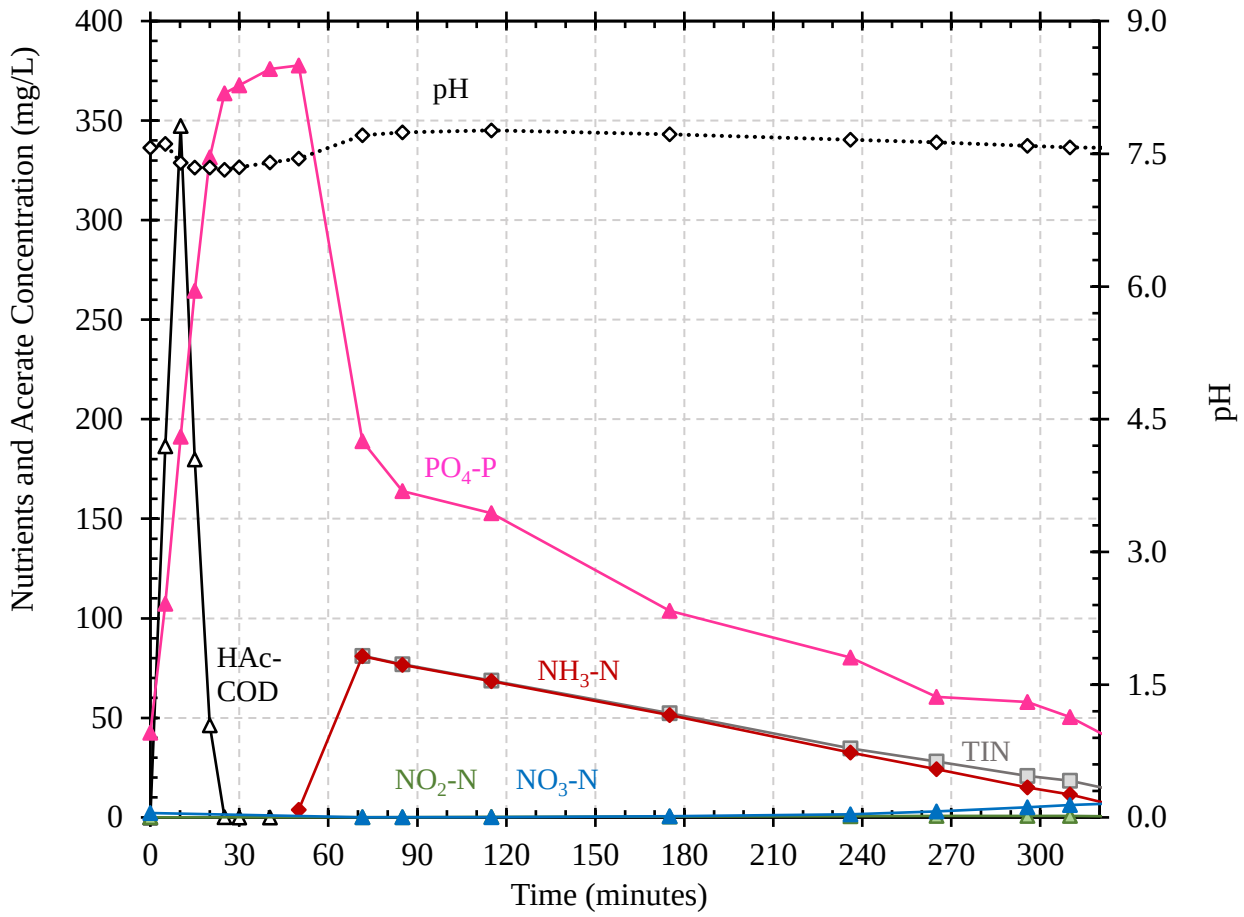

Figure B-19. Acetate-COD and nutrient profile for anaerobic (0-50 min) and aeration (50-320 min) phases on August 23, 2018 with acetate feeding from 0-10 min and diluted centrate feeding from 61-75 min. The MLVSS was 9.6 g/L, average temperature was 21.8°C, average DO concentration was 2.0 mg/L, influent NH_3-N concentration was 206 mg/L, and COD:N feed ratio was 4.09 g/g.

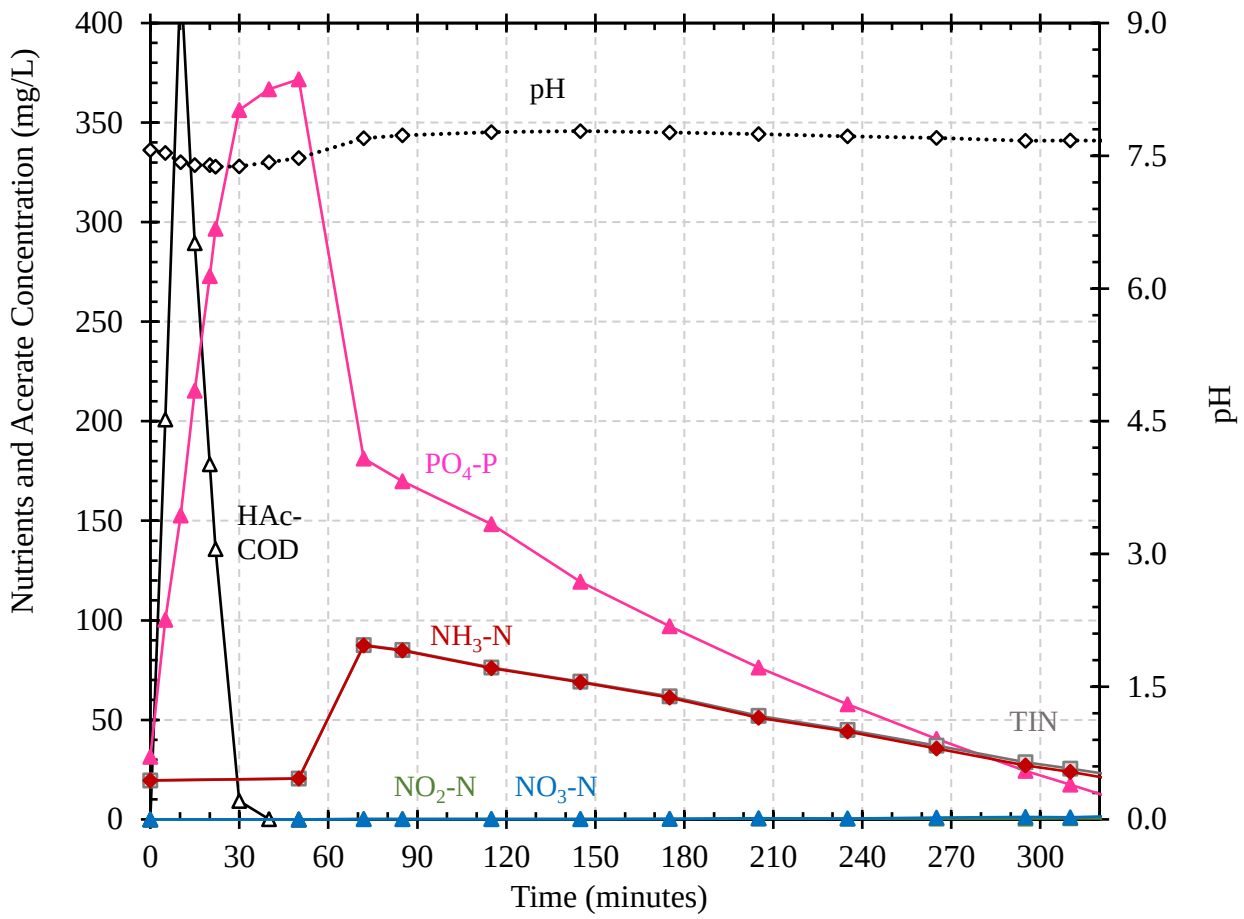

Figure B-20. Acetate-COD and nutrient profile for anaerobic (0-50 min) and aeration (50-320 min) phases on August 27, 2018 with acetate feeding from 0-10 min and diluted centrate feeding from 61-75 min. The MLVSS was 9.7 g/L, average temperature was 19.8°C, average DO concentration was 2.0 mg/L, influent NH_3-N concentration was 200 mg/L, and COD:N feed ratio was 4.22 g/g.

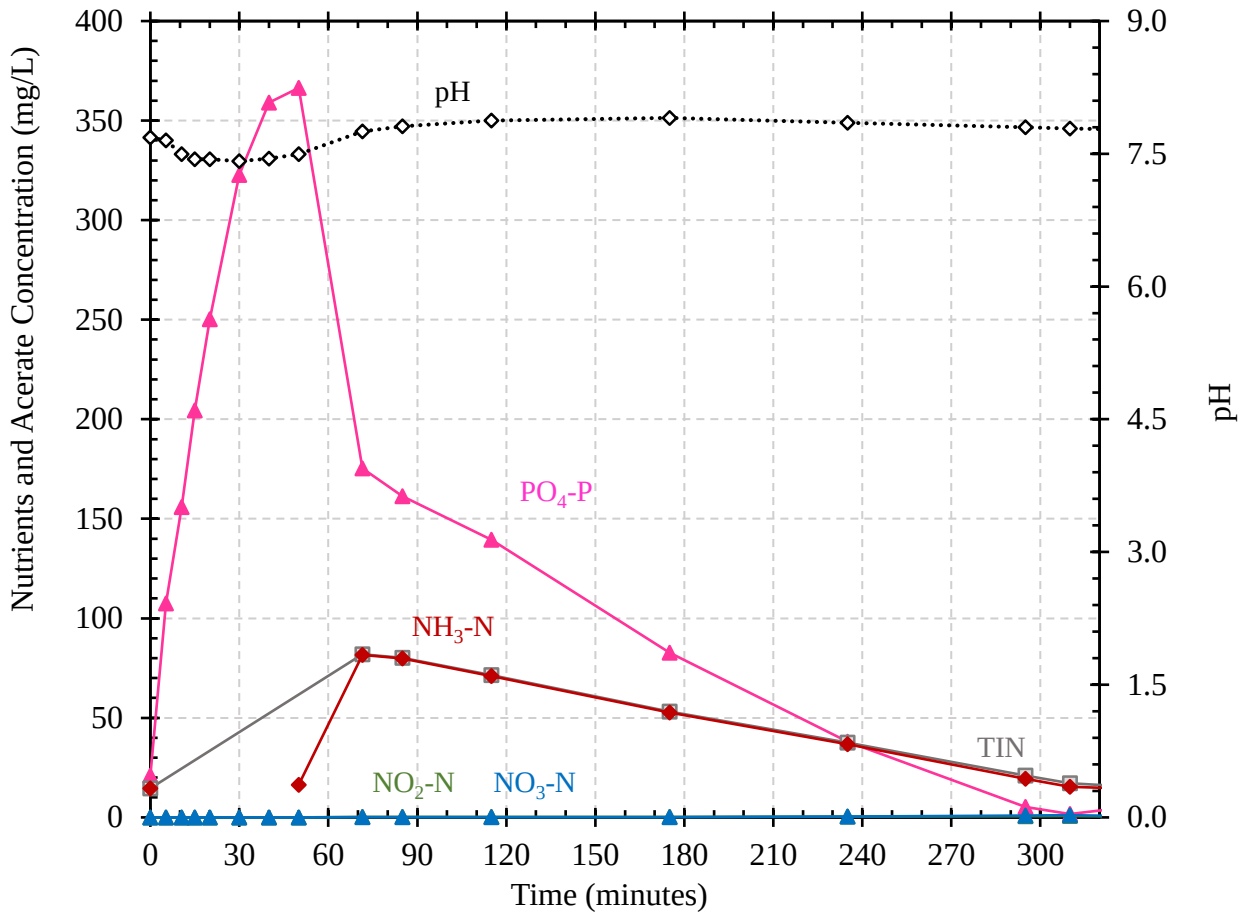

Figure B-21. Acetate-COD and nutrient profile for anaerobic (0-50 min) and aeration (50-320 min) phases on August 30, 2018 with acetate feeding from 0-10 min and diluted centrate feeding from 61-75 min. The MLVSS was 9.4 g/L, average temperature was 21.1°C, average DO concentration was 1.9 mg/L, influent NH_3-N concentration was 199 mg/L, and COD:N feed ratio was 4.24 g/g.

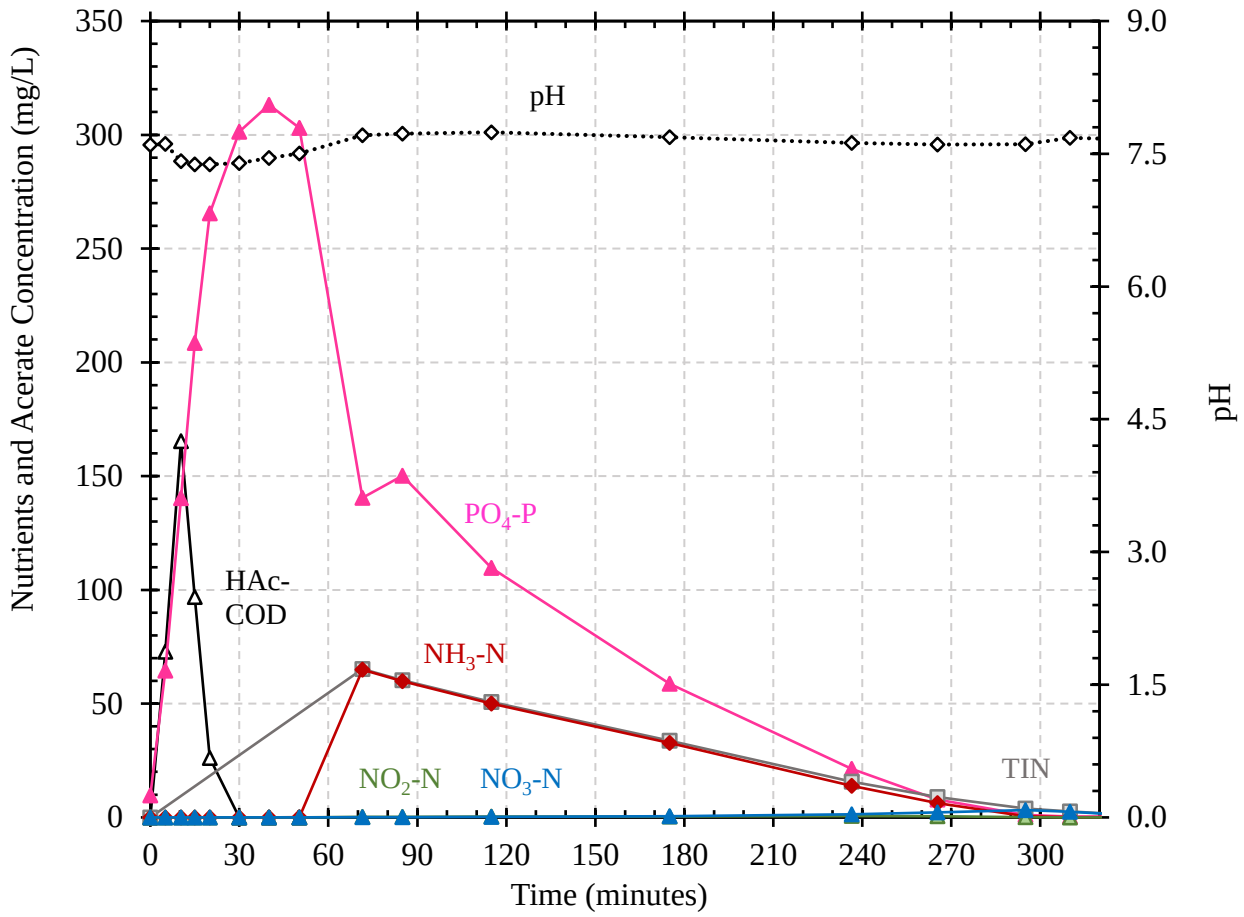

Figure B-22. Acetate-COD and nutrient profile for anaerobic (0-50 min) and aeration (50-320 min) phases on September 3, 2018 with acetate feeding from 0-10 min and diluted centrate feeding from 61-75 min. The MLVSS was 9.3 g/L, average temperature was 20.7°C, average DO concentration was 2.0 mg/L, influent NH_3-N concentration was 161 mg/L, and COD:N feed ratio was 5.23 g/g.

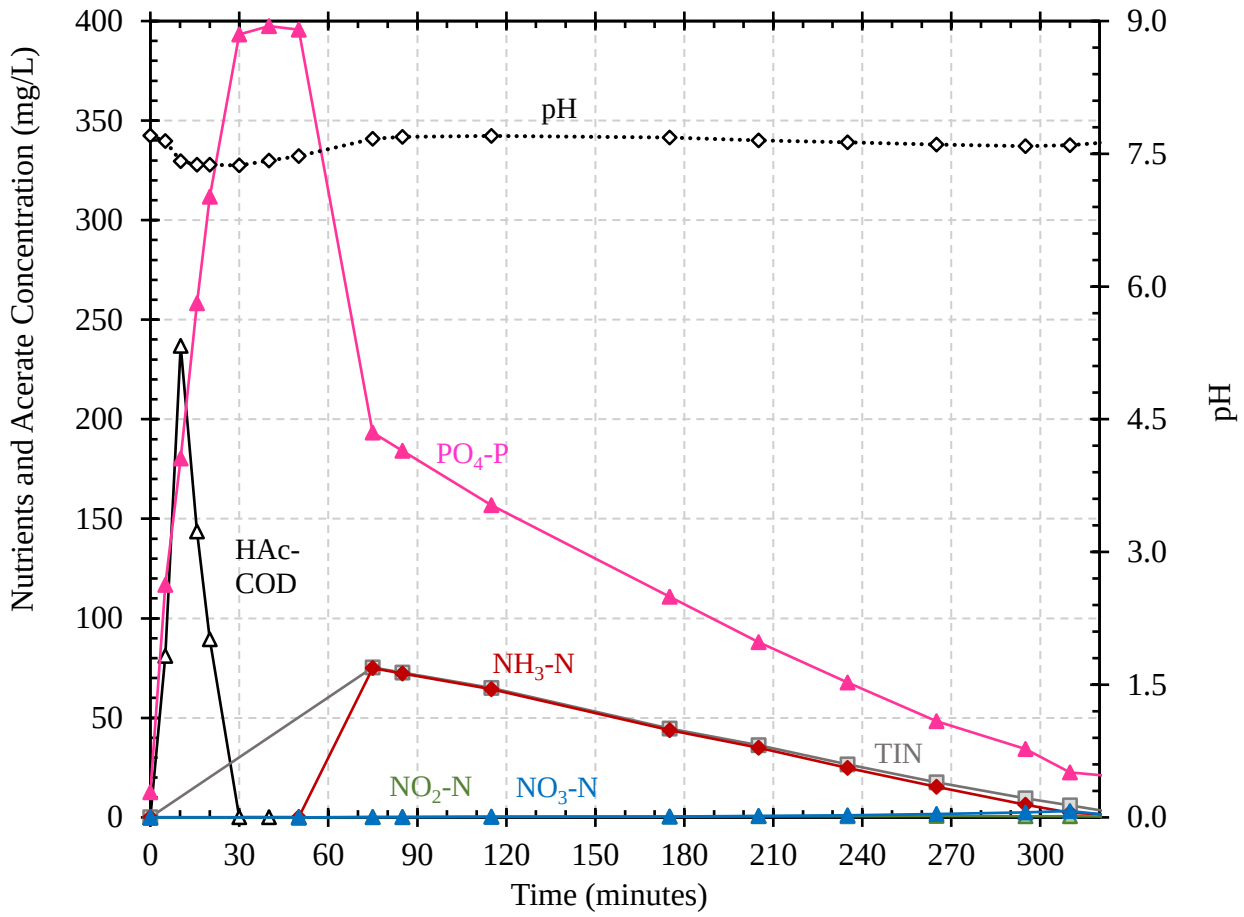

Figure B-23. Acetate-COD and nutrient profile for anaerobic (0-50 min) and aeration (50-320 min) phases on September 6, 2018 with acetate feeding from 0-10 min and diluted centrate feeding from 61-75 min. The MLVSS was 9.0 g/L, average temperature was 21.4°C, average DO concentration was 2.0 mg/L, influent NH_3-N concentration was 198 mg/L, and COD:N feed ratio was 4.26 g/g.

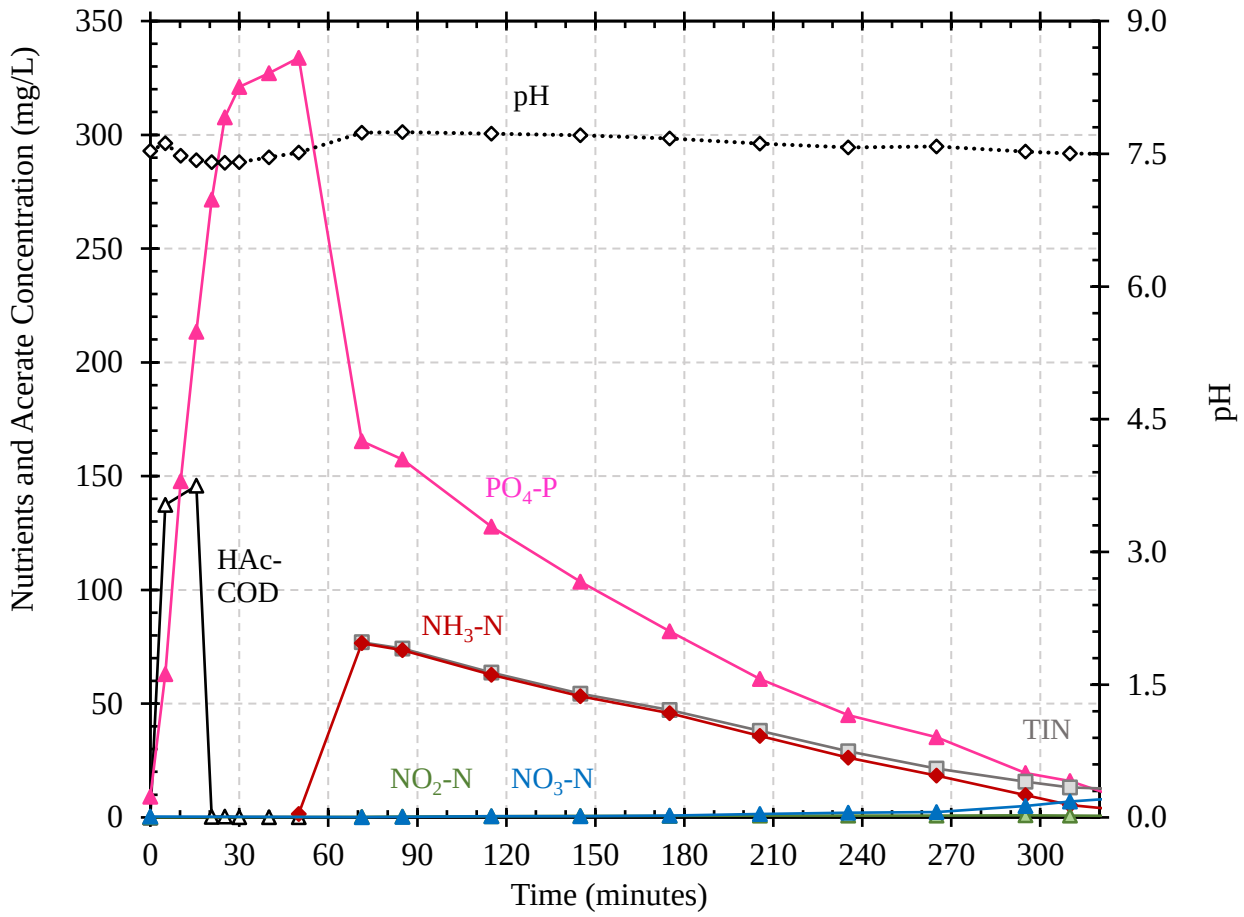

Figure B-24. Acetate-COD and nutrient profile for anaerobic (0-50 min) and aeration (50-320 min) phases on September 13, 2018 with acetate feeding from 0-10 min and diluted centrate feeding from 61-75 min. The MLVSS was 8.7 g/L, average temperature was 19.7°C, average DO concentration was 2.6 mg/L, influent NH_3-N concentration was 210 mg/L, and COD:N feed ratio was 4.01 g/g.

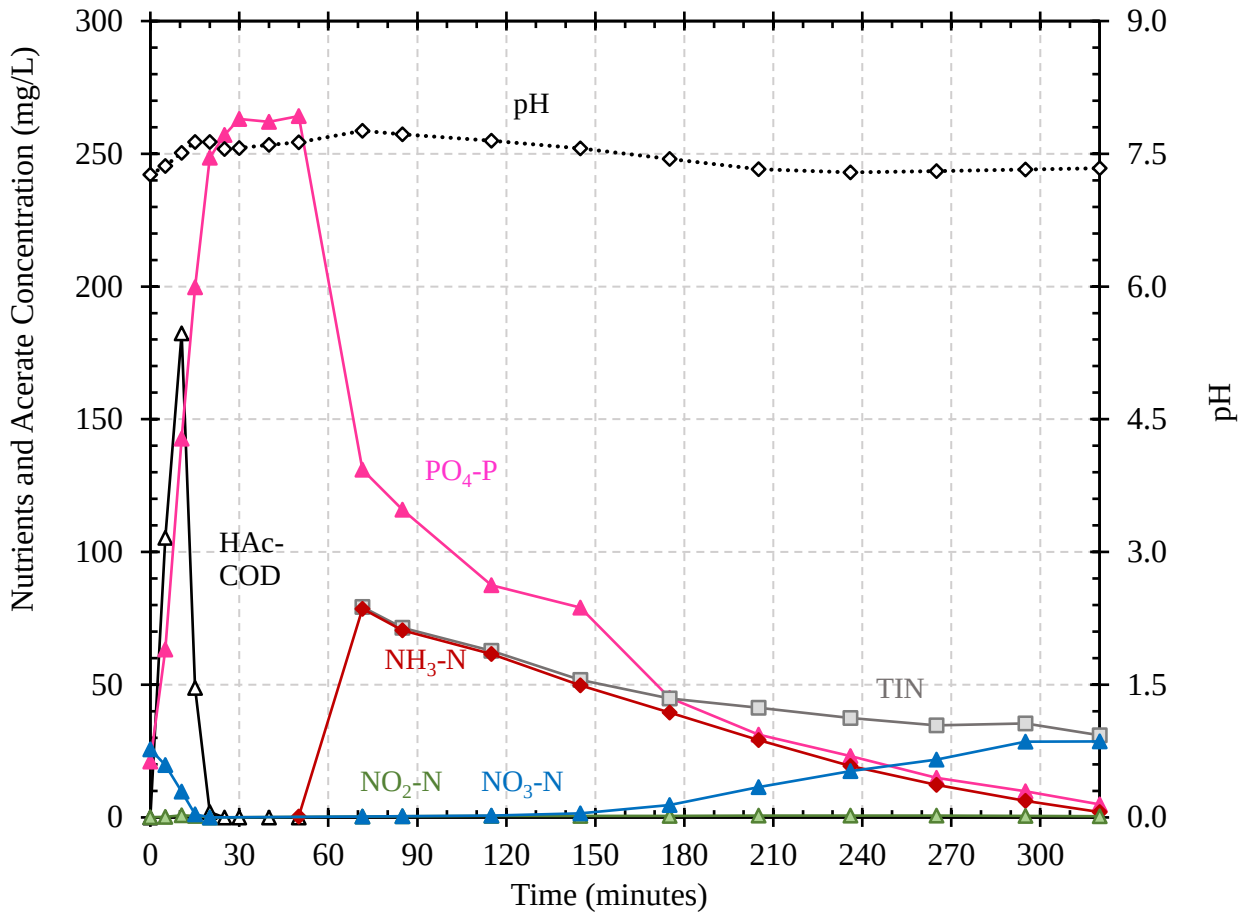

Figure B-25. Acetate-COD and nutrient profile for anaerobic (0-50 min) and aeration (50-320 min) phases on September 20, 2018 with acetate feeding from 0-10 min and diluted centrate feeding from 61-75 min. The MLVSS was 8.9 g/L, average temperature was 19.0°C, average DO concentration was 3.0 mg/L, influent NH_3-N concentration was 198 mg/L, and COD:N feed ratio was 4.25 g/g.

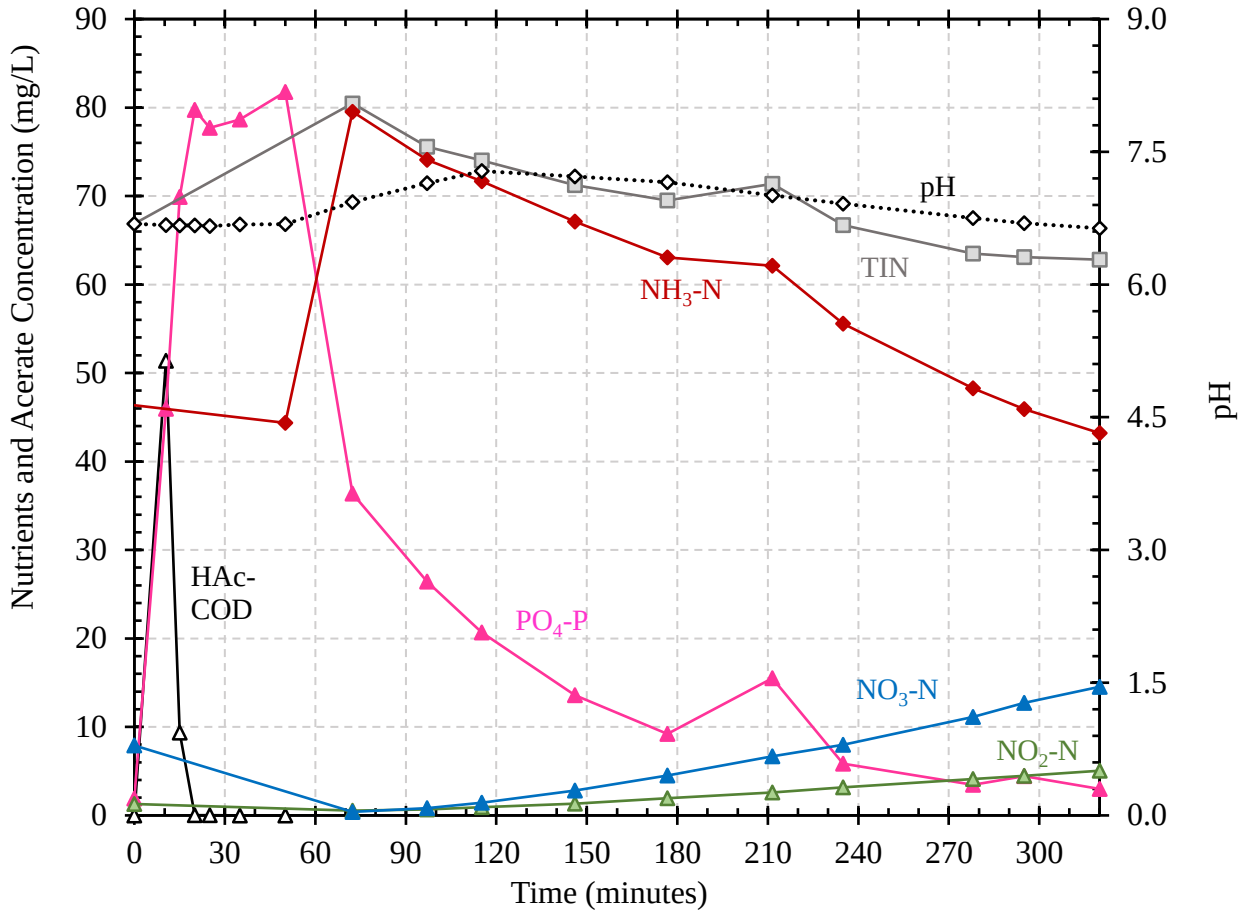

Figure B-26. Acetate-COD and nutrient profile for anaerobic (0-50 min) and aeration (50-320 min) phases on January 3, 2019 with acetate feeding from 0-10 min and diluted centrate feeding from 61-75 min. The MLVSS was 5.9 g/L, average temperature was 21.5°C, average DO concentration was 2.8 mg/L, influent NH_3-N concentration was 137 mg/L, and COD:N feed ratio was 1.94 g/g.

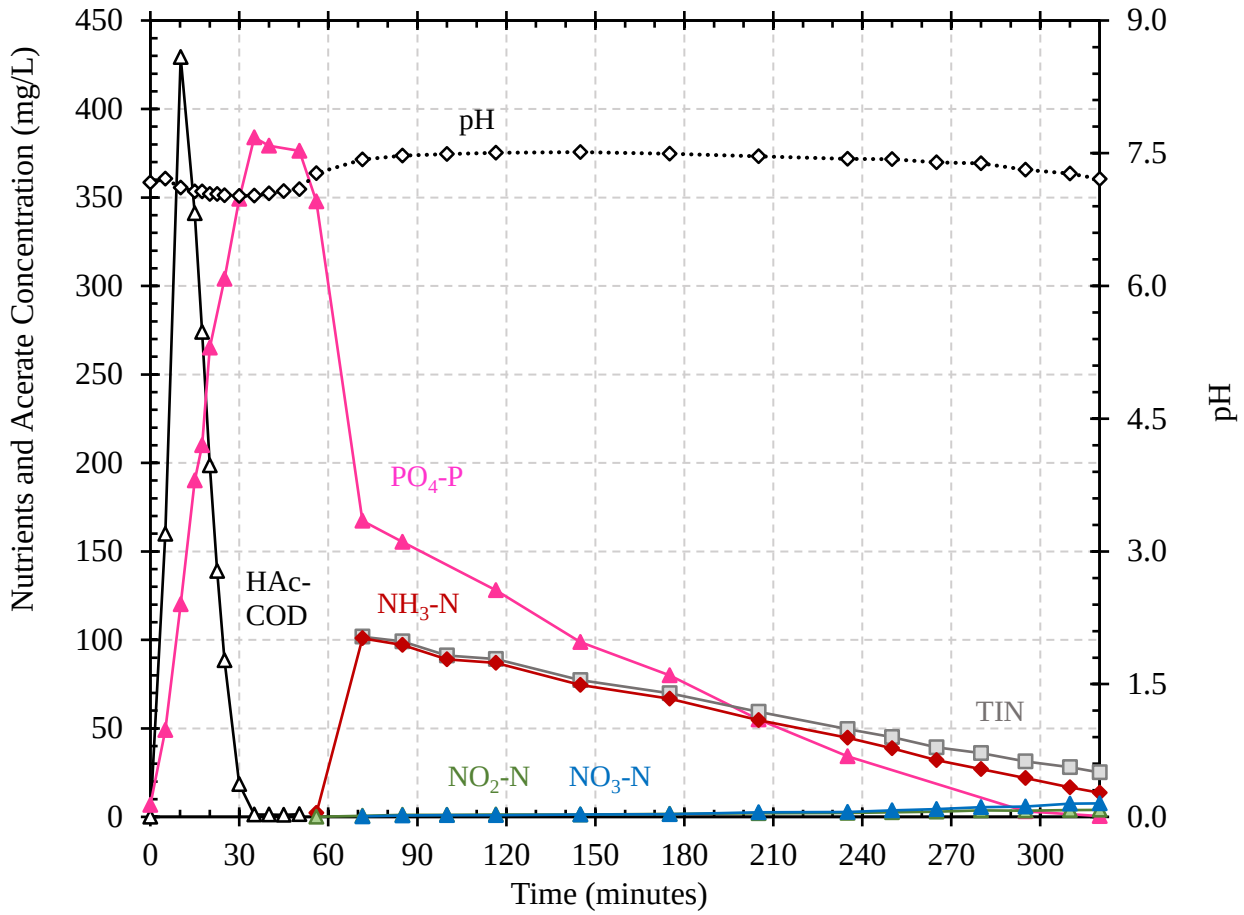

Figure B-27. Acetate-COD and nutrient profile for anaerobic (0-50 min) and aeration (50-320 min) phases on March 7, 2019 with acetate feeding from 0-10 min and diluted centrate feeding from 61-75 min. The MLVSS was 8.4 g/L, average temperature was 20.8°C, average DO concentration was 3.1 mg/L, influent NH_3-N concentration was 231 mg/L, and COD:N feed ratio was 3.92 g/g.

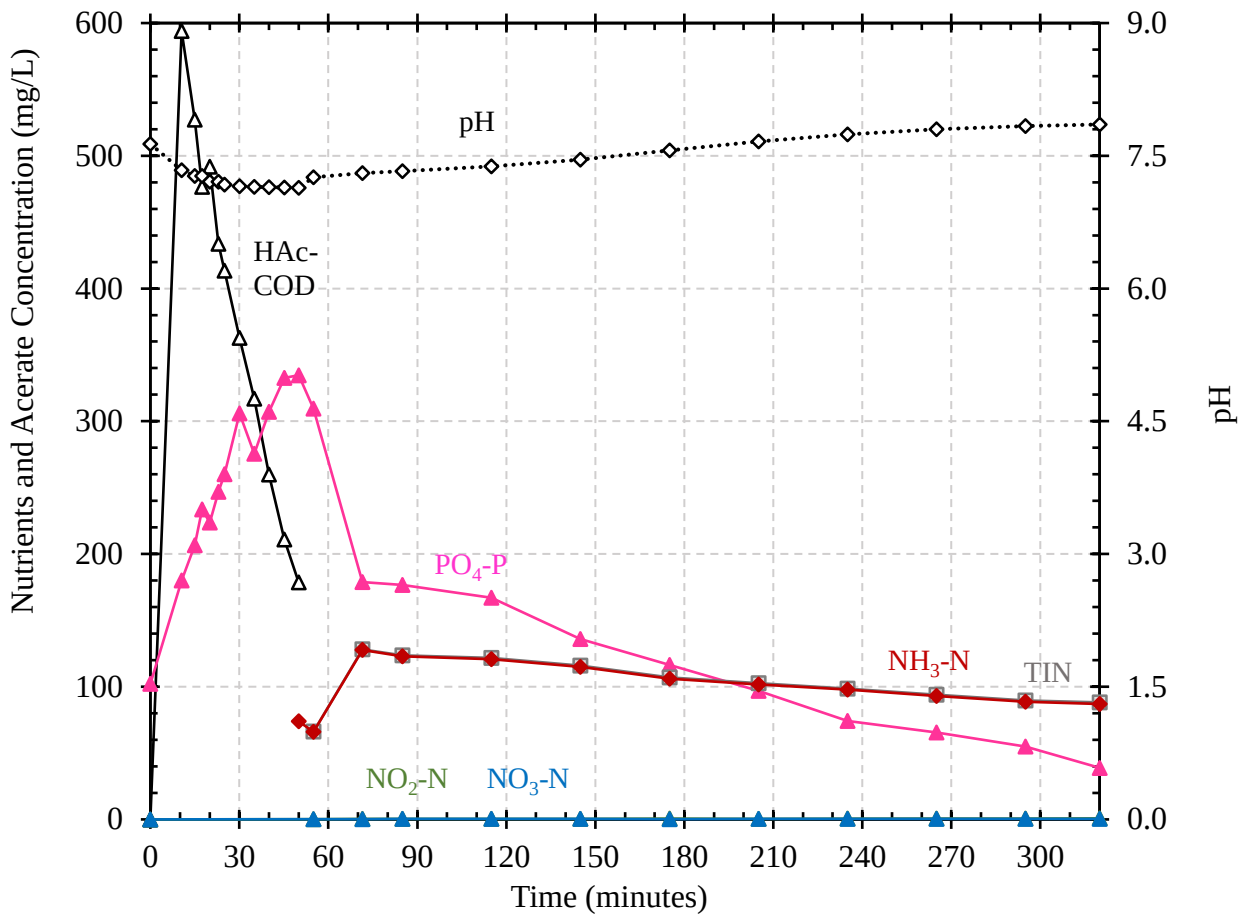

Figure B-28. Acetate-COD and nutrient profile for anaerobic (0-50 min) and aeration (50-320 min) phases on April 11, 2019 with acetate feeding from 0-10 min and diluted centrate feeding from 61-75 min. The MLVSS was 9.4 g/L, average temperature was 17.4°C, average DO concentration was 2.1 mg/L, influent NH_3-N concentration was 224 mg/L, and COD:N feed ratio was 3.64 g/g.

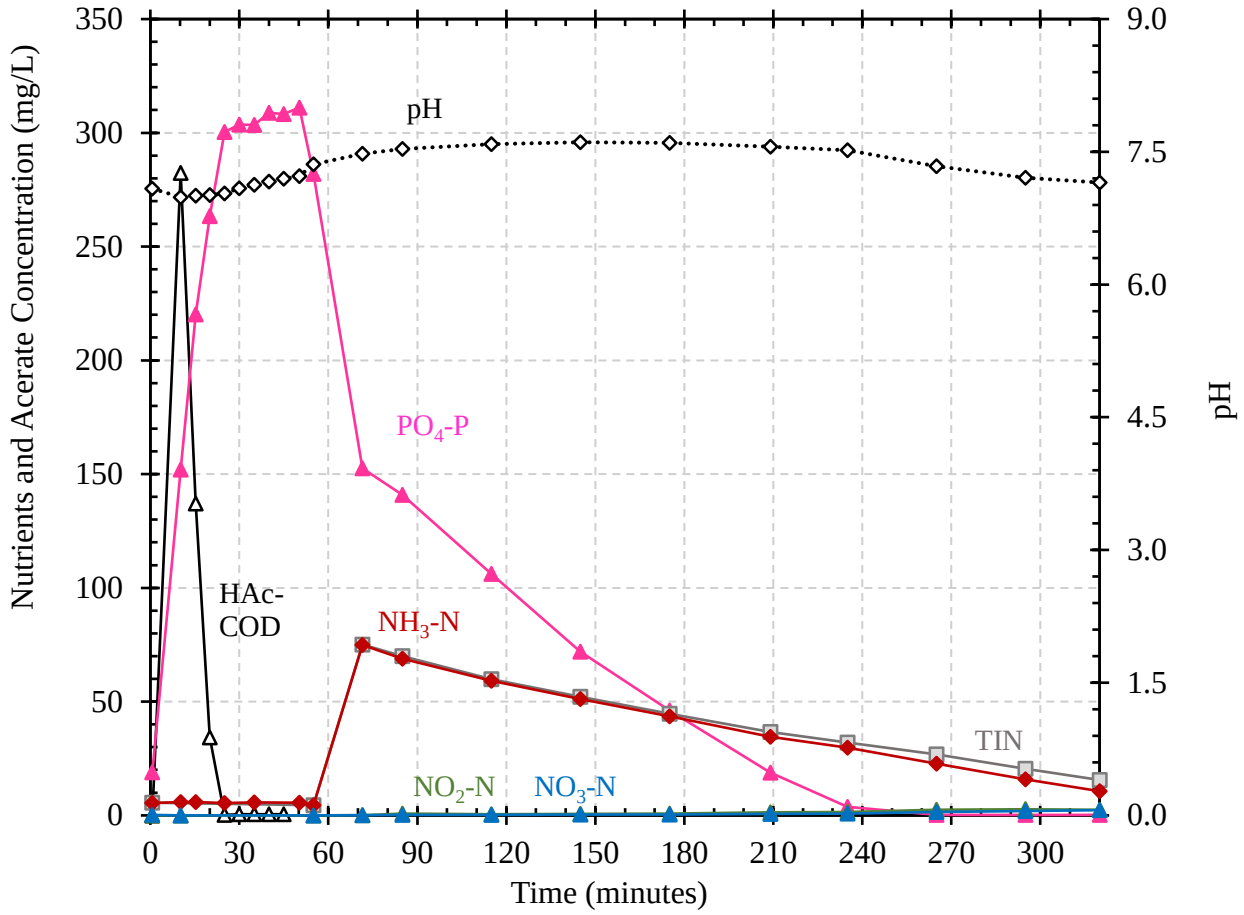

Figure B-29. Acetate-COD and nutrient profile for anaerobic (0-50 min) and aeration (50-320 min) phases on May 30, 2019 with acetate feeding from 0-10 min and diluted centrate feeding from 61-75 min. The MLVSS was 8.8 g/L, average temperature was 20.8°C, average DO concentration was 1.9 mg/L, influent NH_3-N concentration was 159 mg/L, and COD:N feed ratio was 3.46 g/g.

Appendix C: Sidestream MLSS Stereomicroscope Images

Sidestream MLSS was imaged regularly using a stereomicroscope. Images additional from those presented in the Results and Discussion sections are included here at a frequency of approximately one image per month. The table below lists dates of images included in this section.

Table C-1. Stereomicroscope image contents in Appendix C.

Date	Notes	Date	Notes
Feb 24, 2018	imaged Apr 1, 2018	Nov 15, 2018	
Mar 22, 2018	imaged Apr 1, 2018	Nov 28, 2018	after re-seed
Apr 26, 2018		Dec 18, 2018	
May 24, 2018		Jan 4, 2019	start of restart period
Jun 25, 2018	near start of Period 1A	Jan 25, 2019	
Jul 23, 2018		Feb 28, 2019	start of Period 2A
Aug 23, 2018		Mar 25, 2019	
Sep 24, 2018	near end Period 1C	Apr 25, 2019	start of Period 2B
Oct 25, 2018	acetate pump event	May 10, 2019	

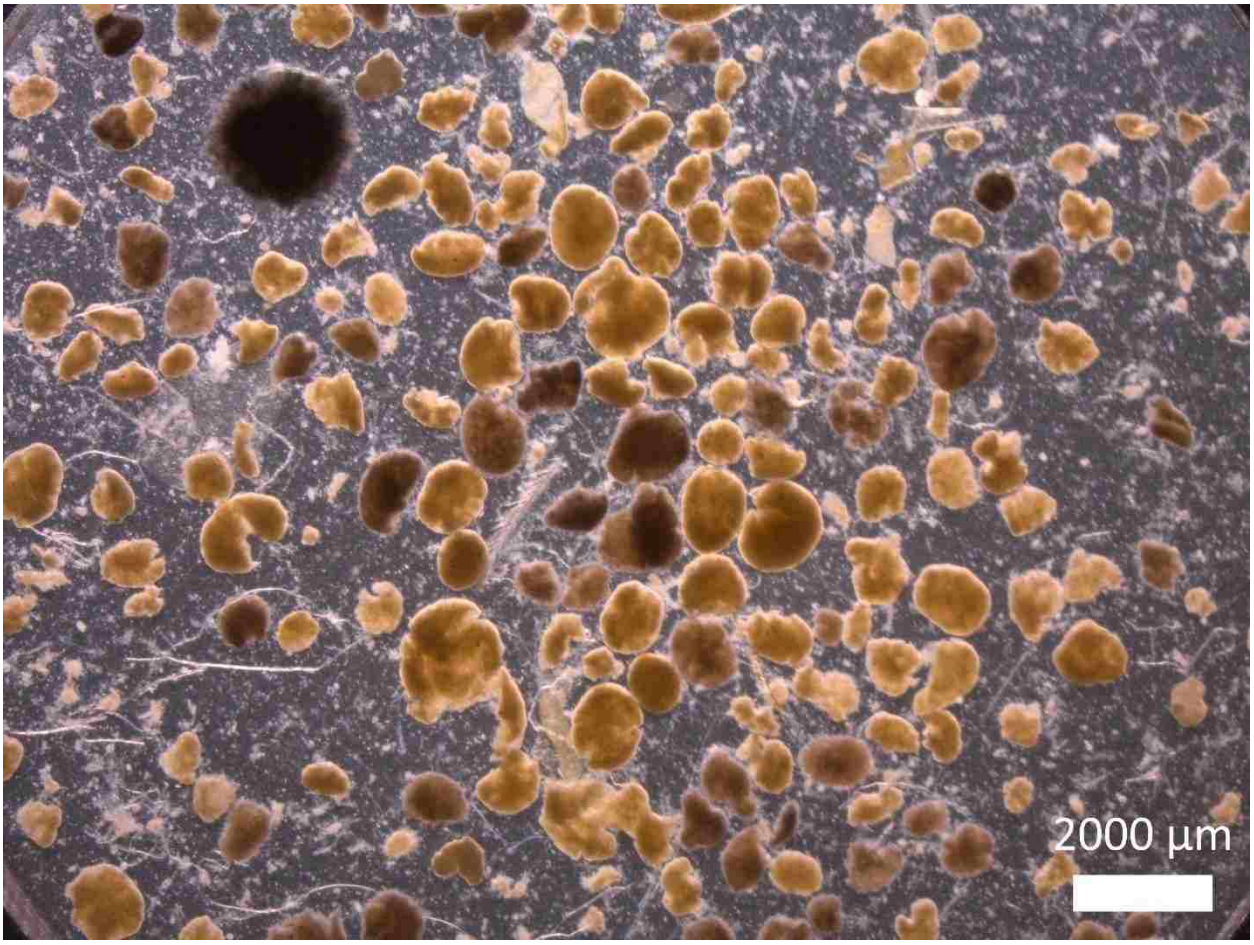

Figure C-1. February 24, 2018 Stereomicroscope Image with Scalebar

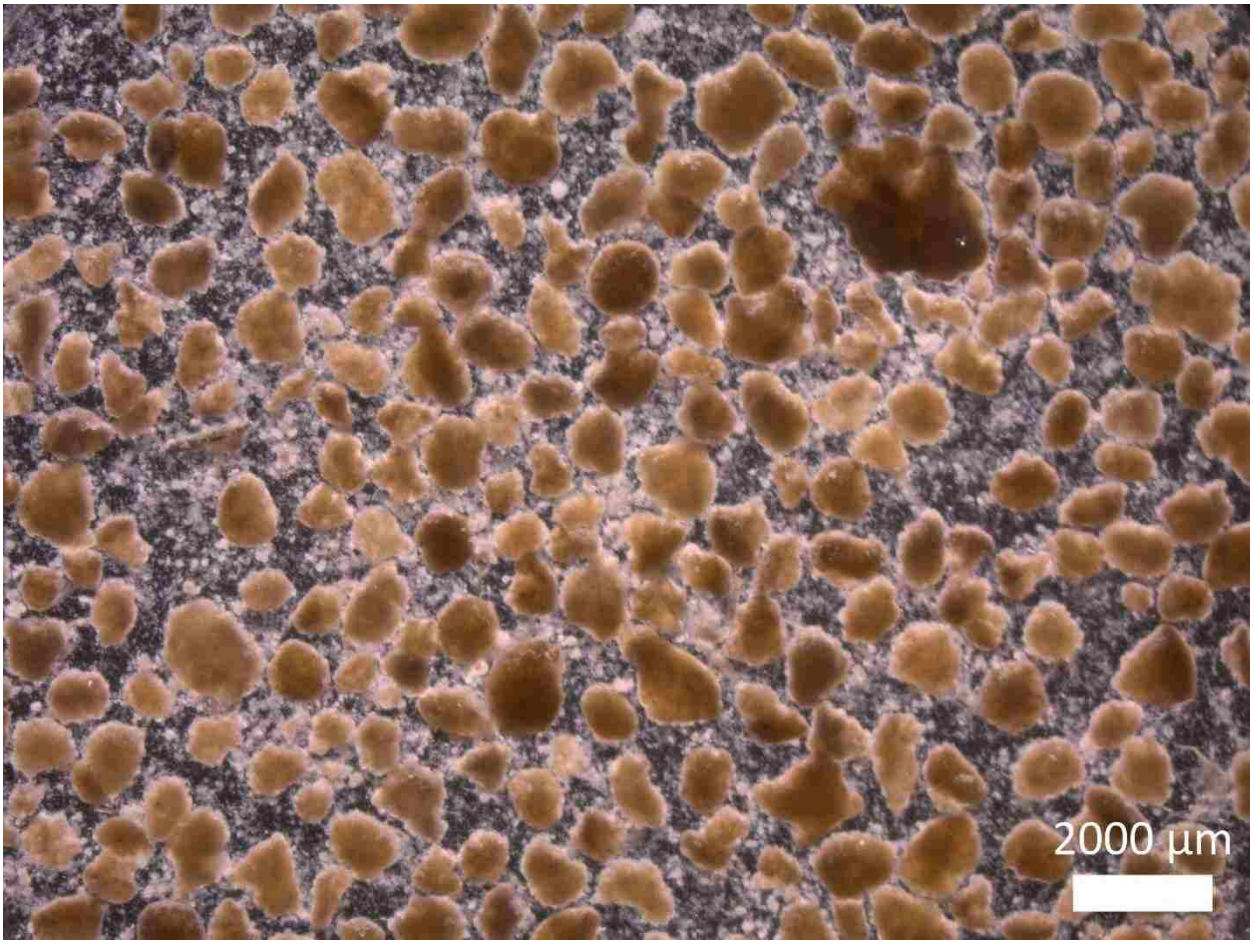

Figure C-2. March 22, 2018 Stereomicroscope Image with Scalebar

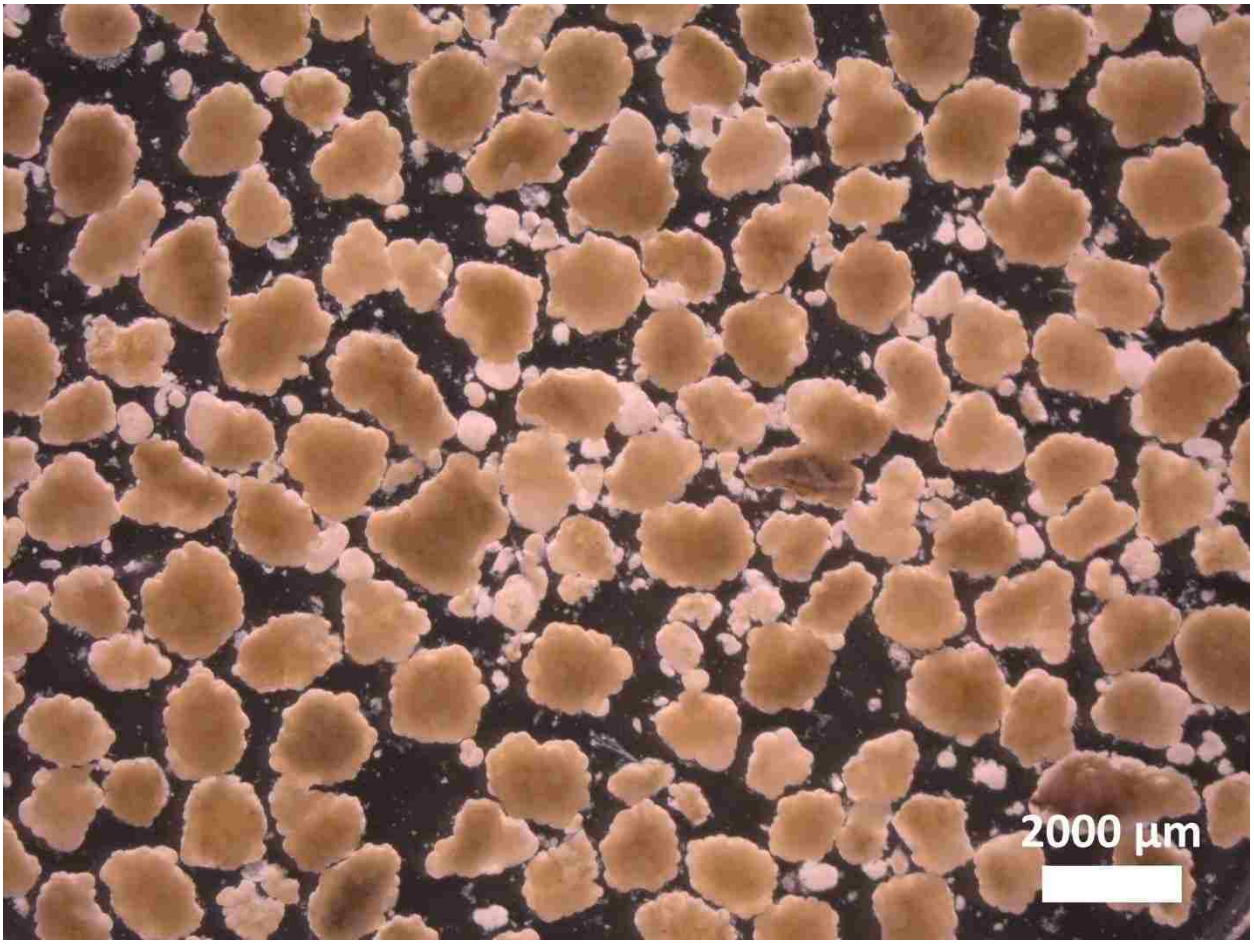

Figure C-3. April 26, 2018 Stereomicroscope Image with Scalebar

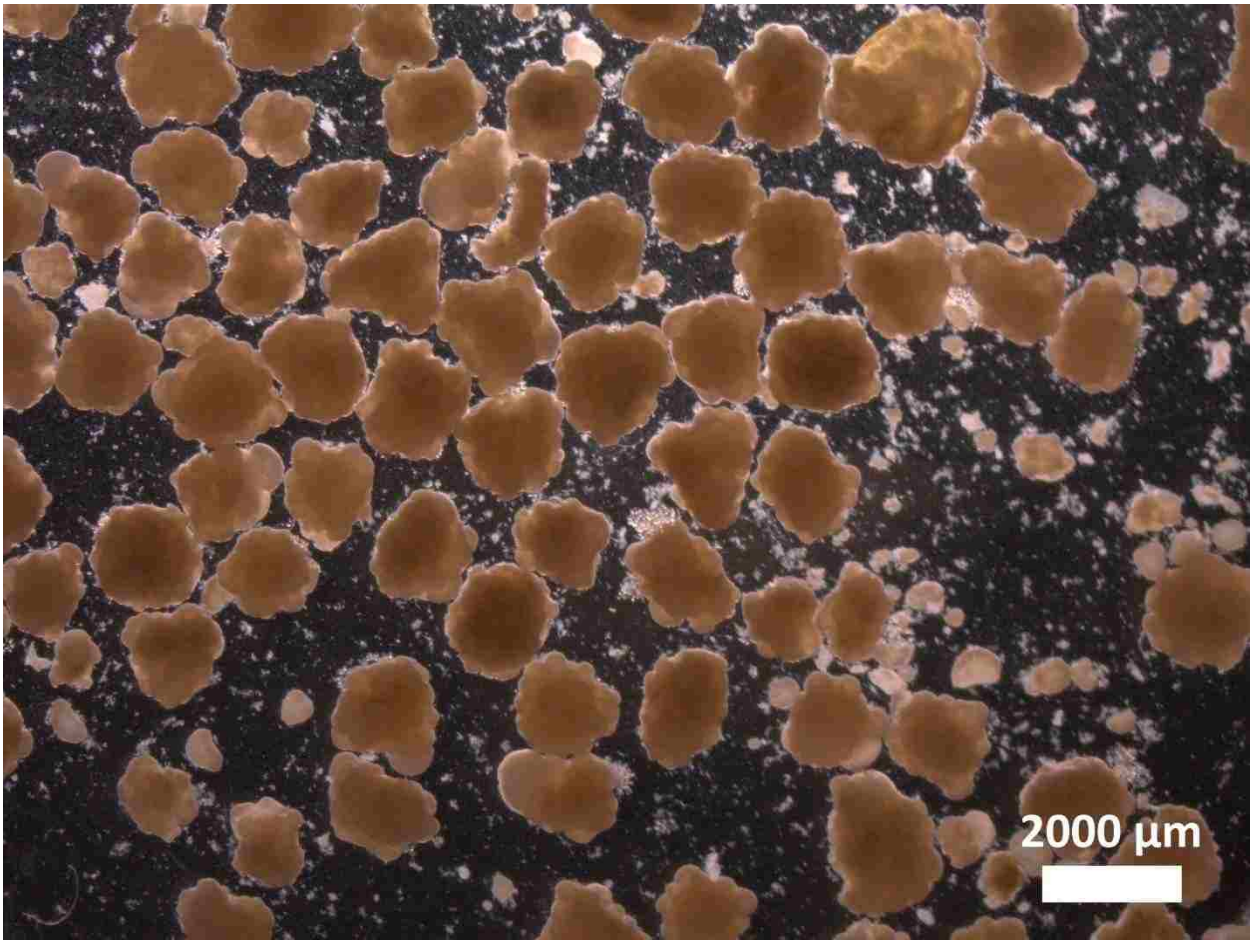

Figure C-4. May 24, 2018 Stereomicroscope Image with Scalebar

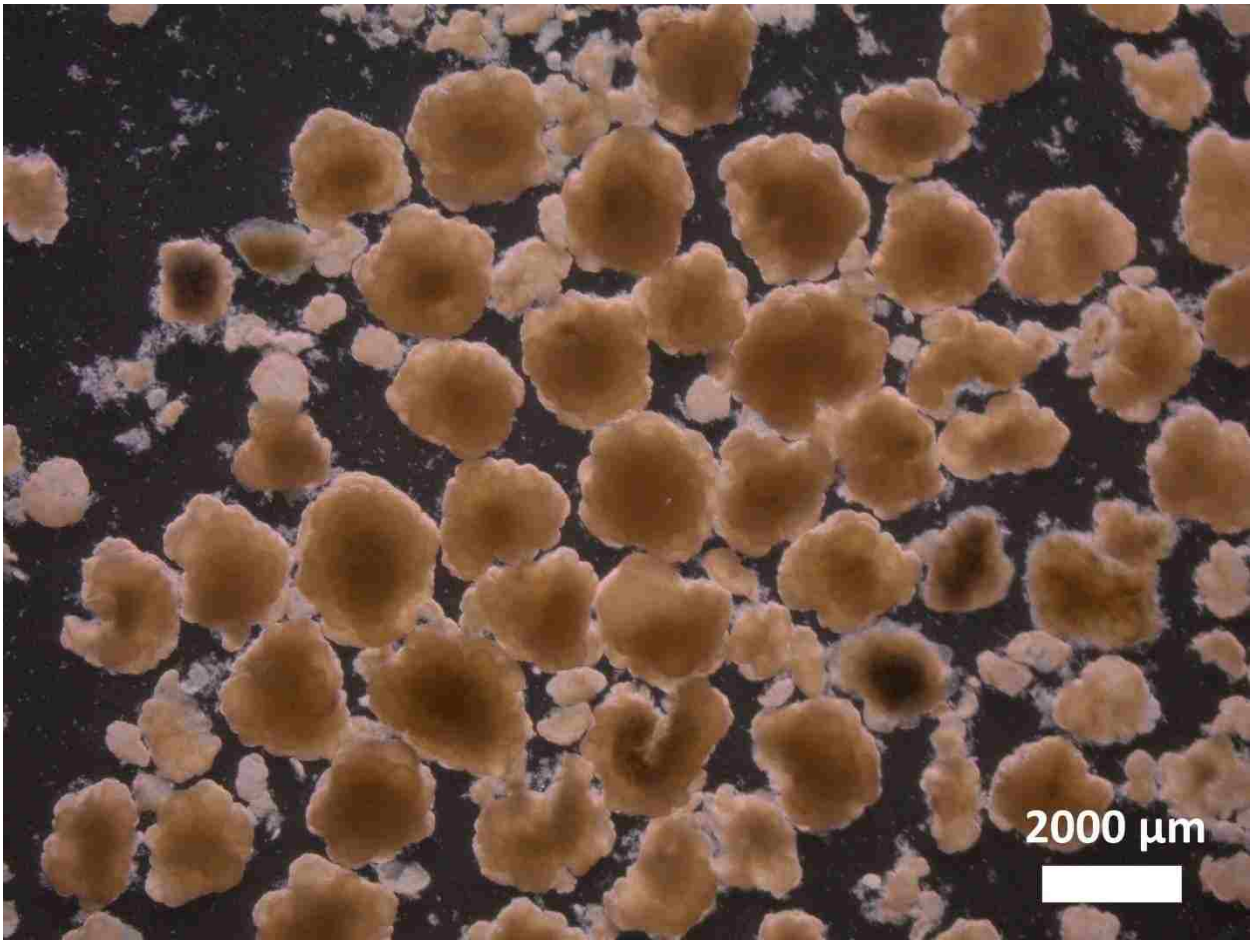

Figure C-5. June 25, 2018 Stereomicroscope Image with Scalebar

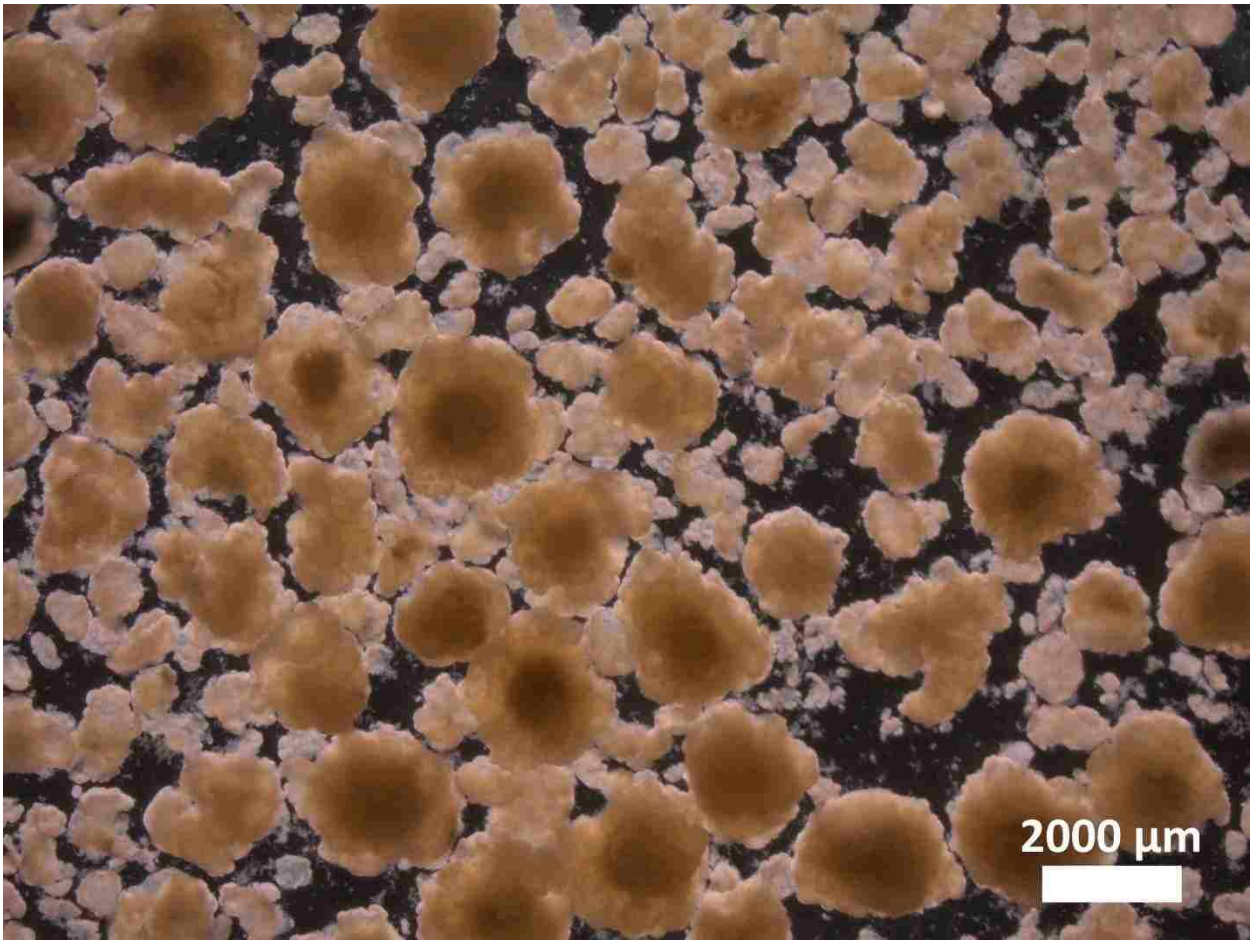

Figure C-6. July 23, 2018 Stereomicroscope Image with Scalebar

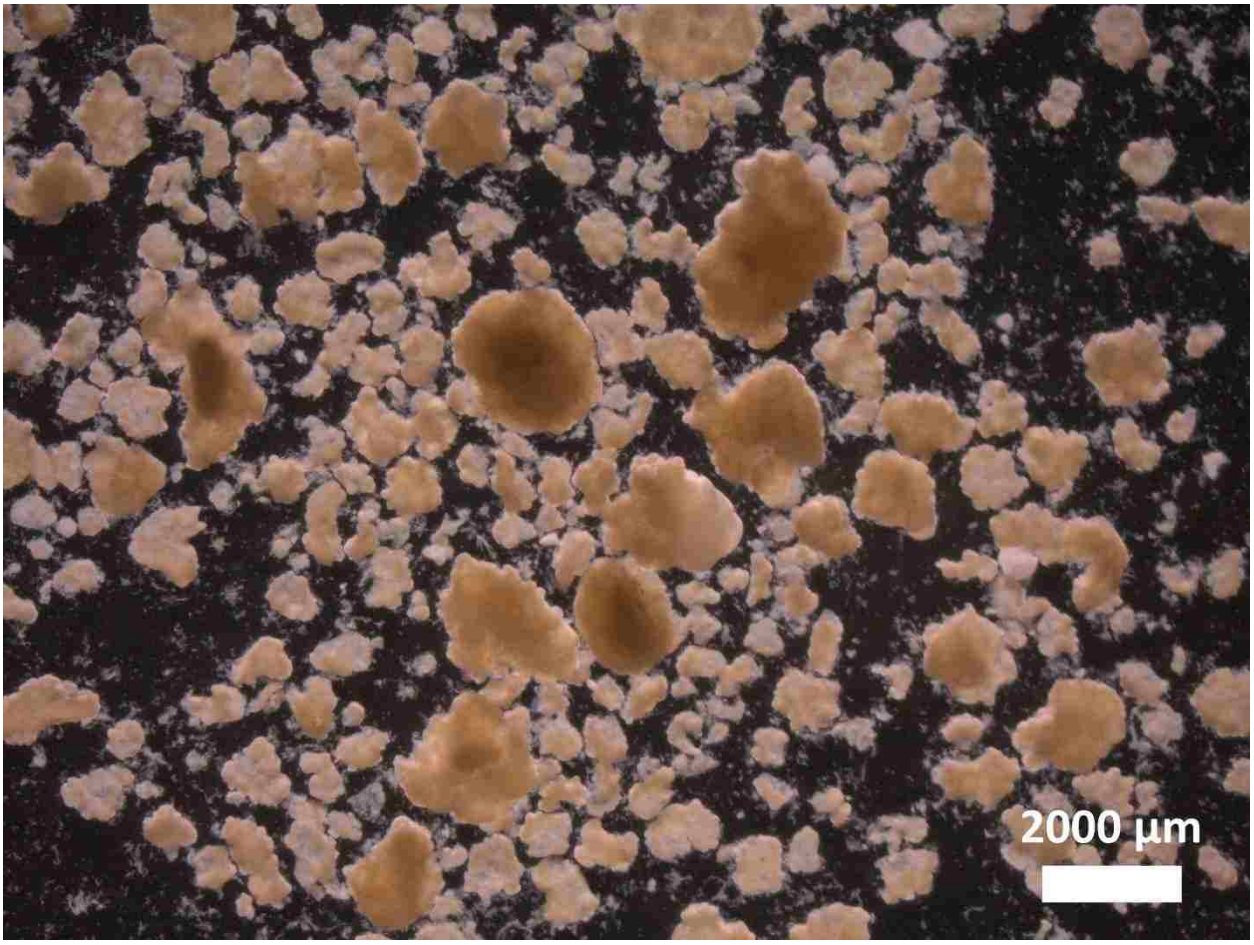

Figure C-7. August 23, 2018 Stereomicroscope Image with Scalebar

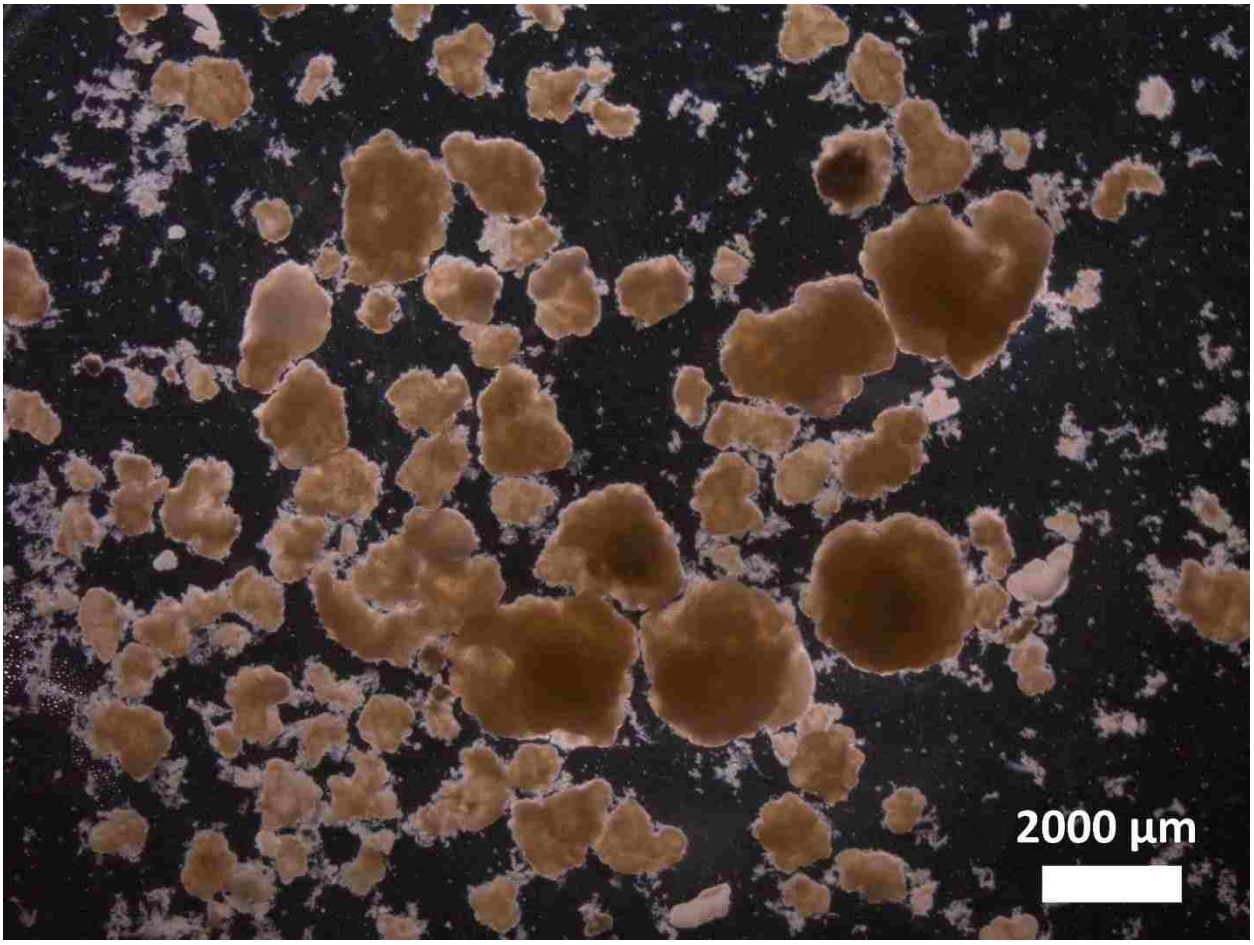

Figure C-8. September 24, 2018 Stereomicroscope Image with Scalebar

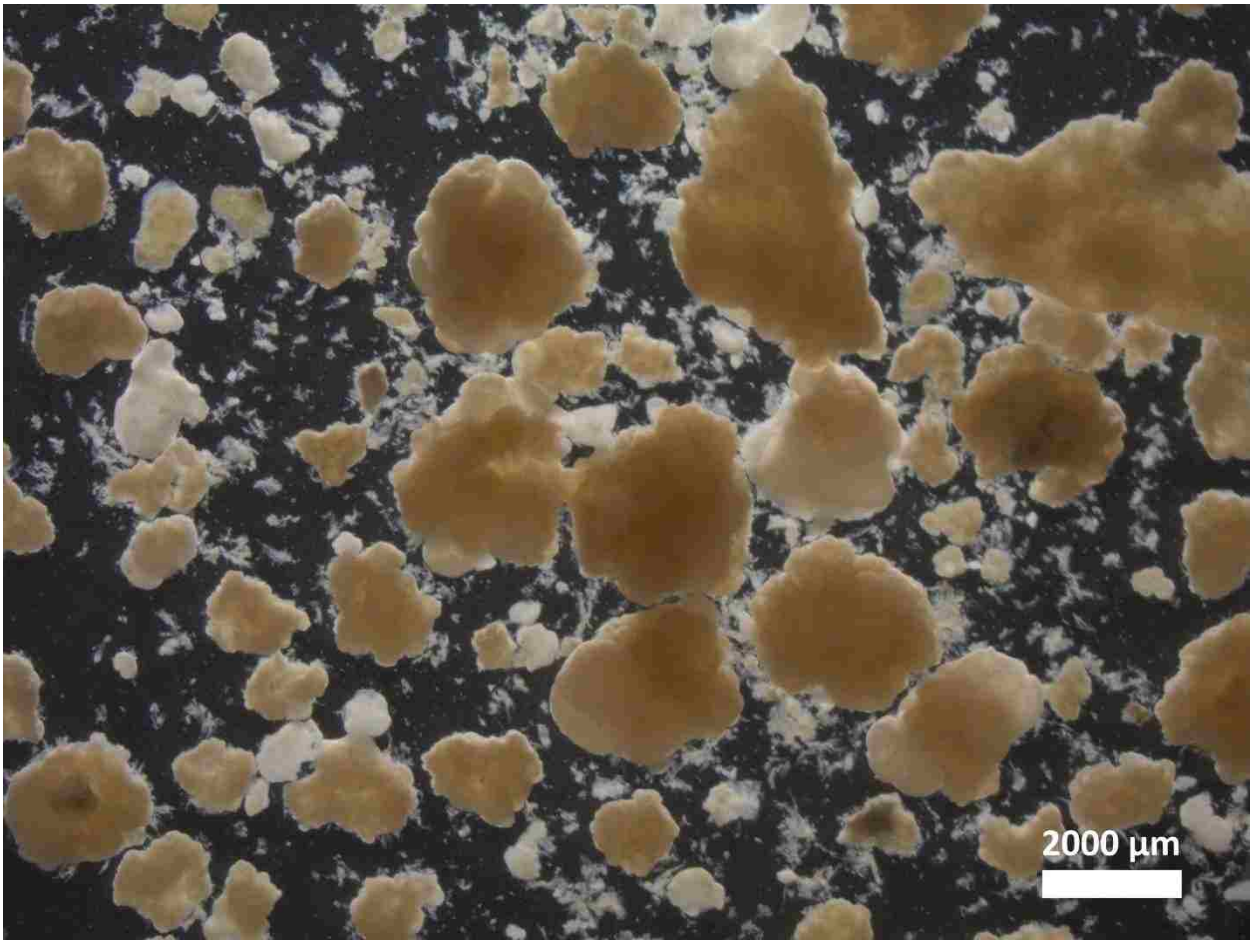

Figure C-9. October 25, 2018 Stereomicroscope Image with Scalebar

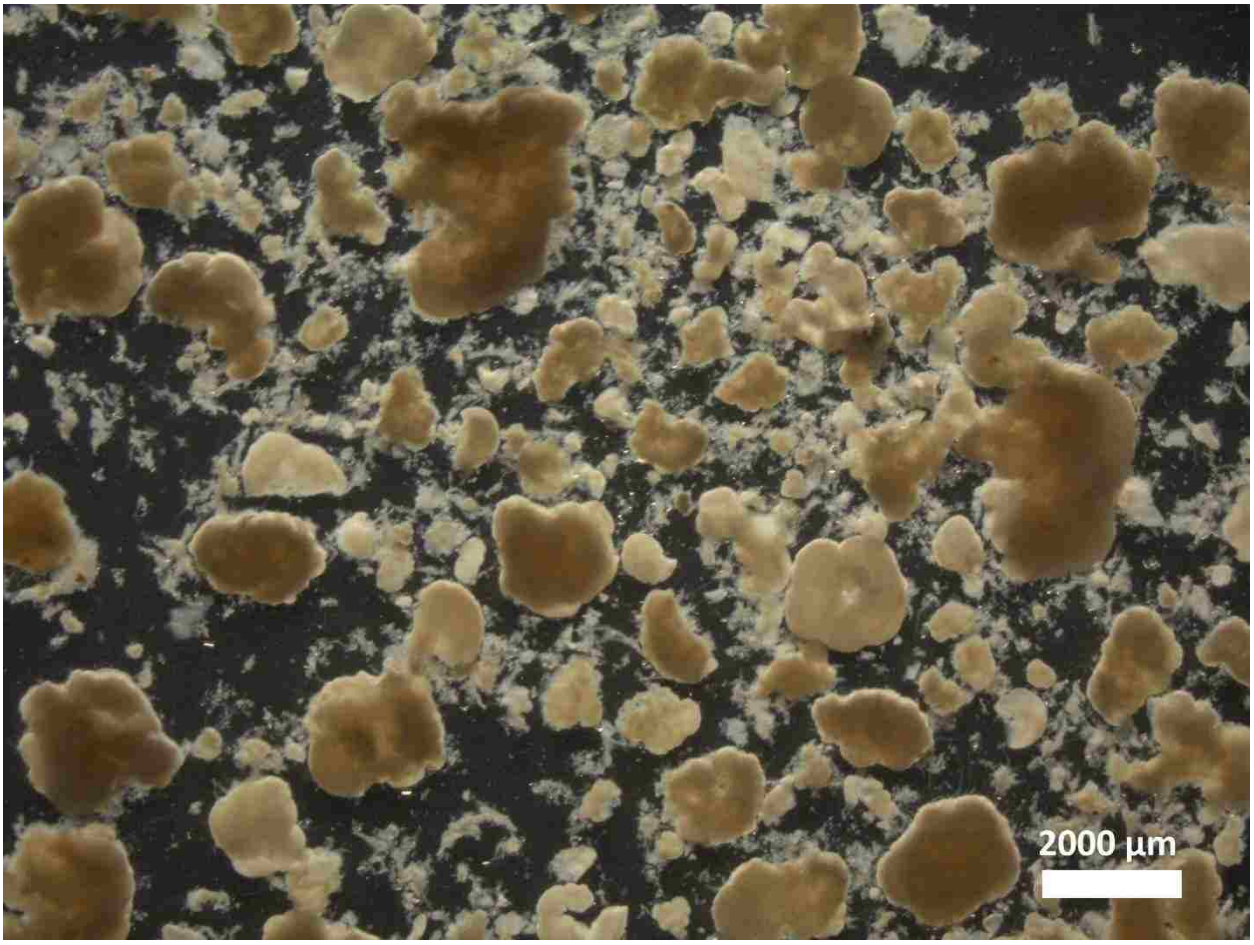

Figure C-10. November 15, 2018 Stereomicroscope Image with Scalebar

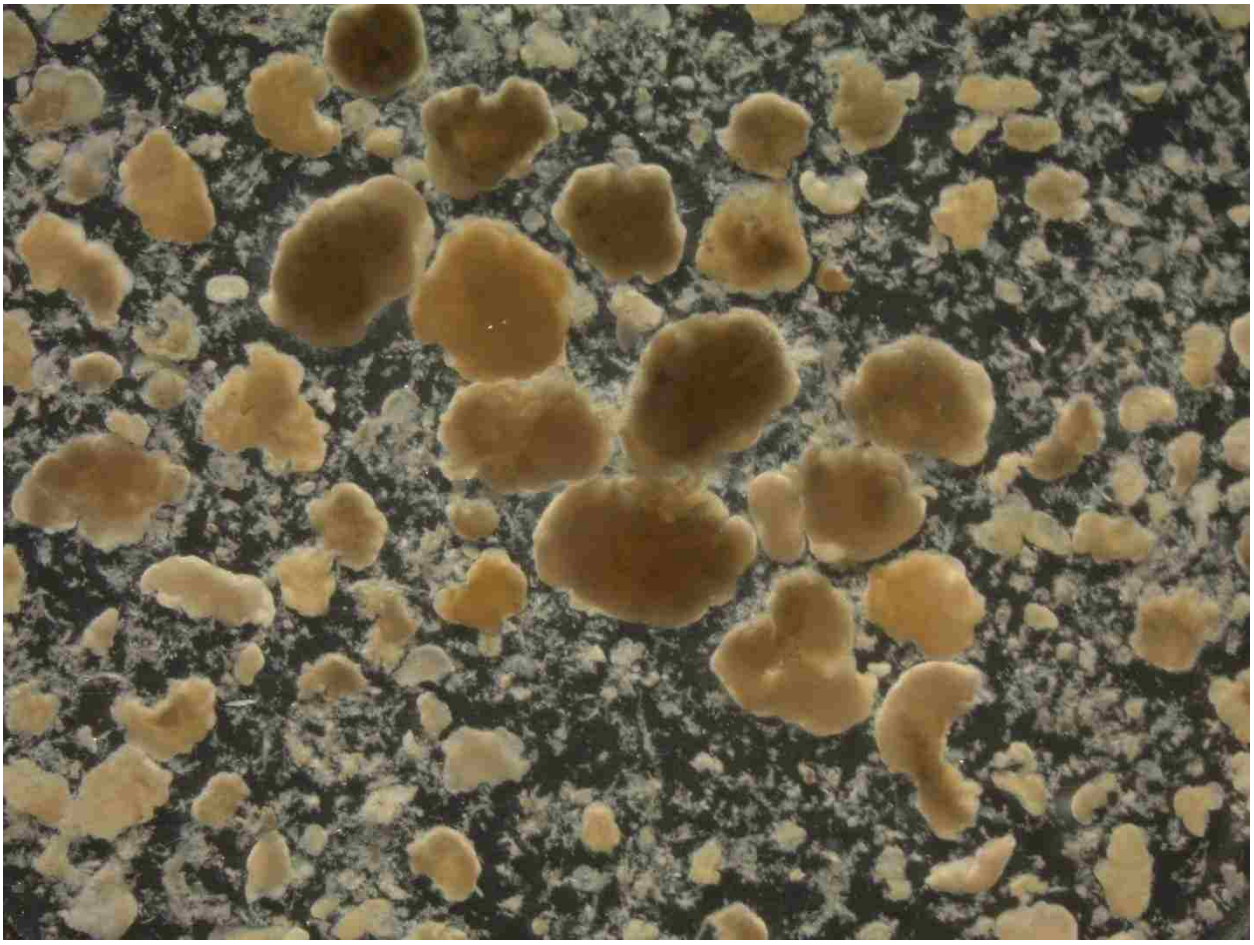

Figure C-11. November 28, 2018 Stereomicroscope Image with Scalebar

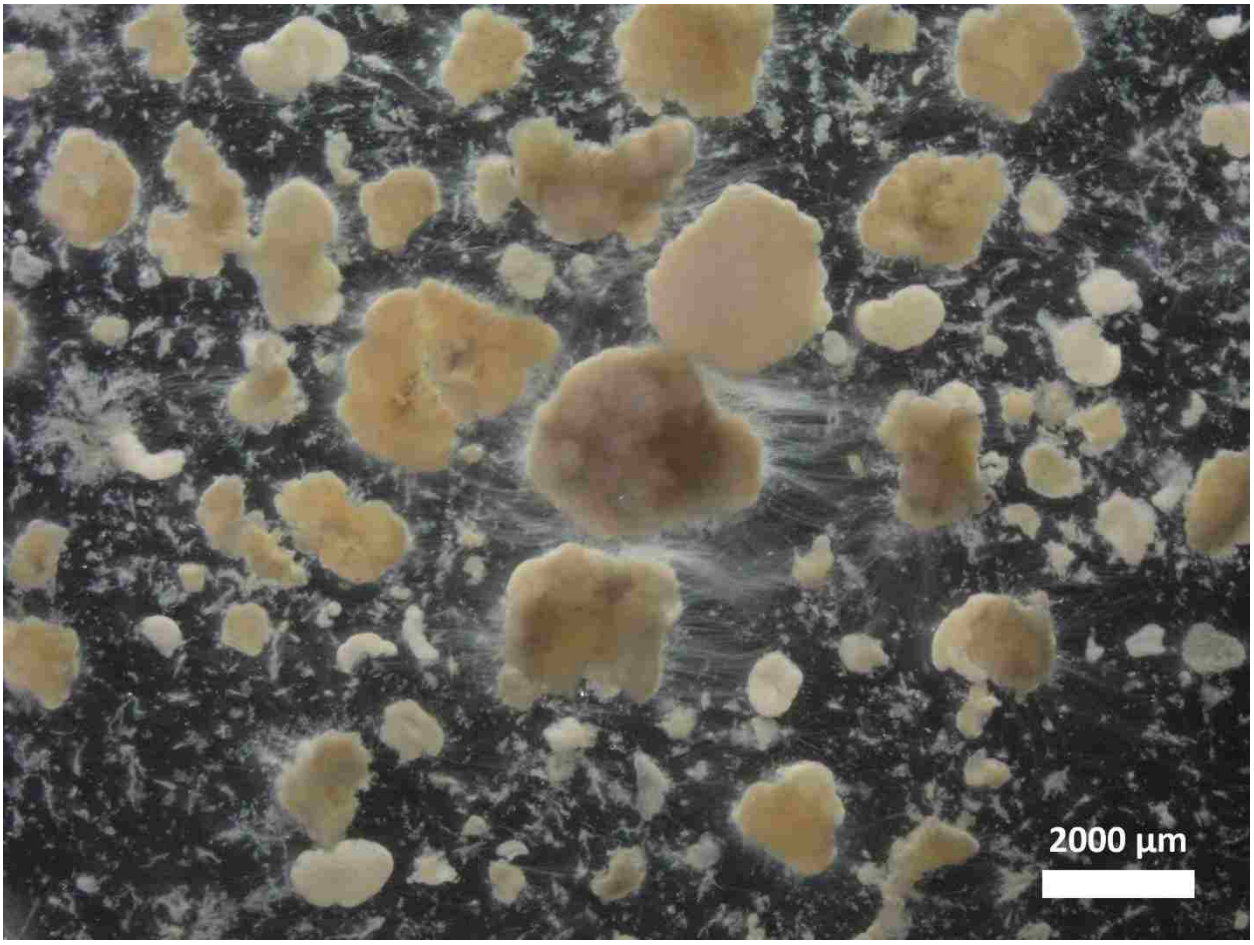

Figure C-12. December 18, 2018 Stereomicroscope Image with Scalebar

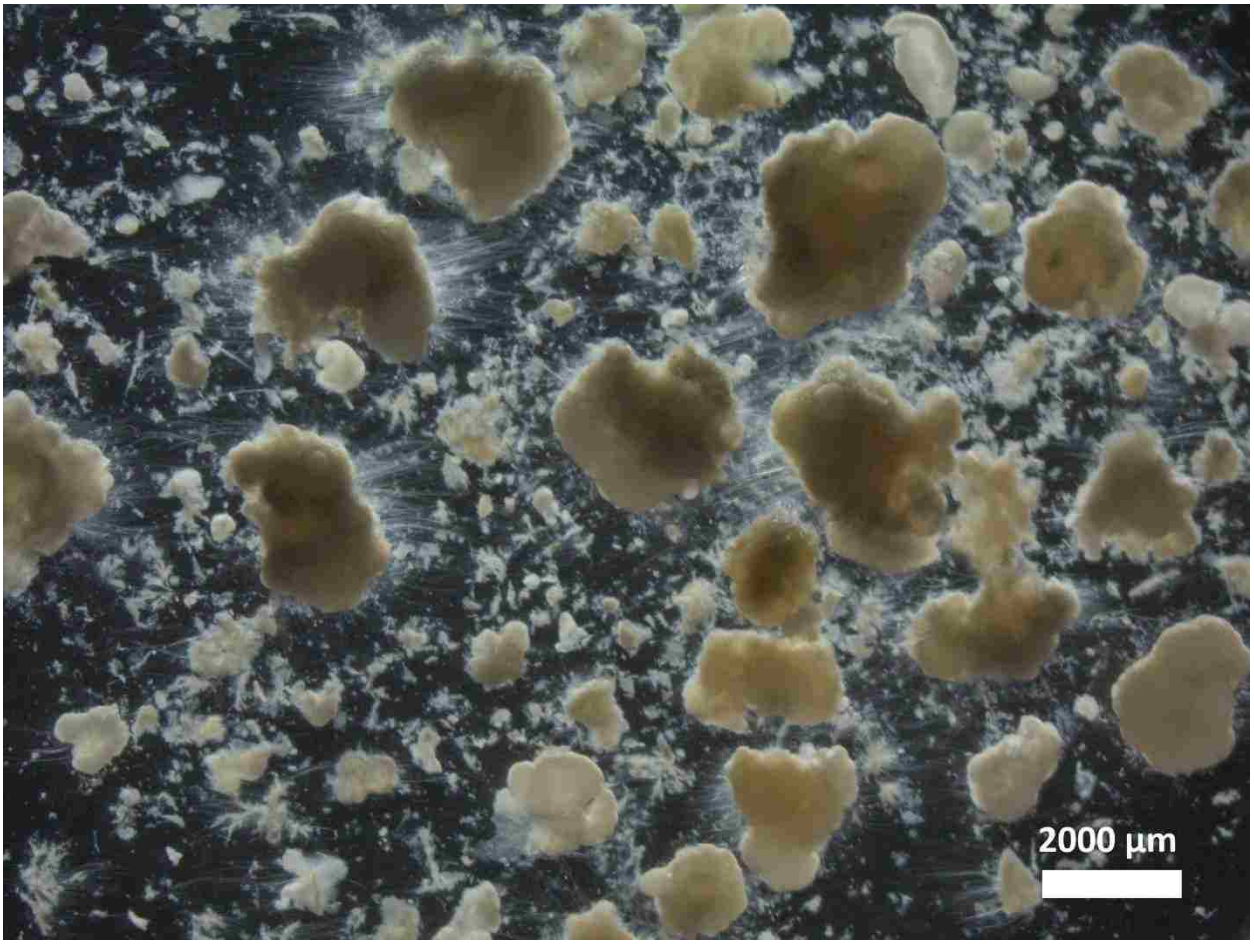

Figure C-13. January 4, 2019 Stereomicroscope Image with Scalebar

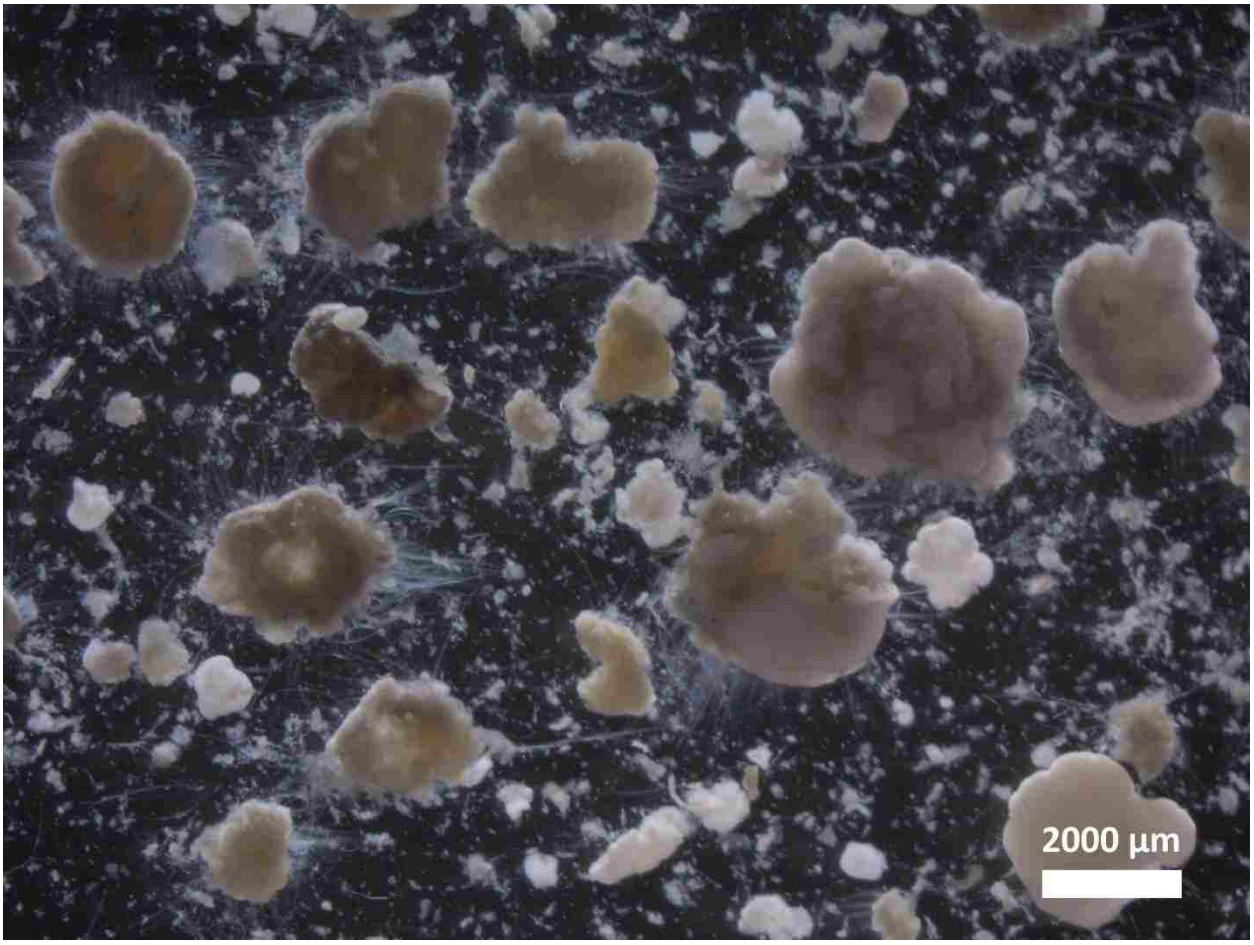

Figure C-14. January 25, 2019 Stereomicroscope Image with Scalebar

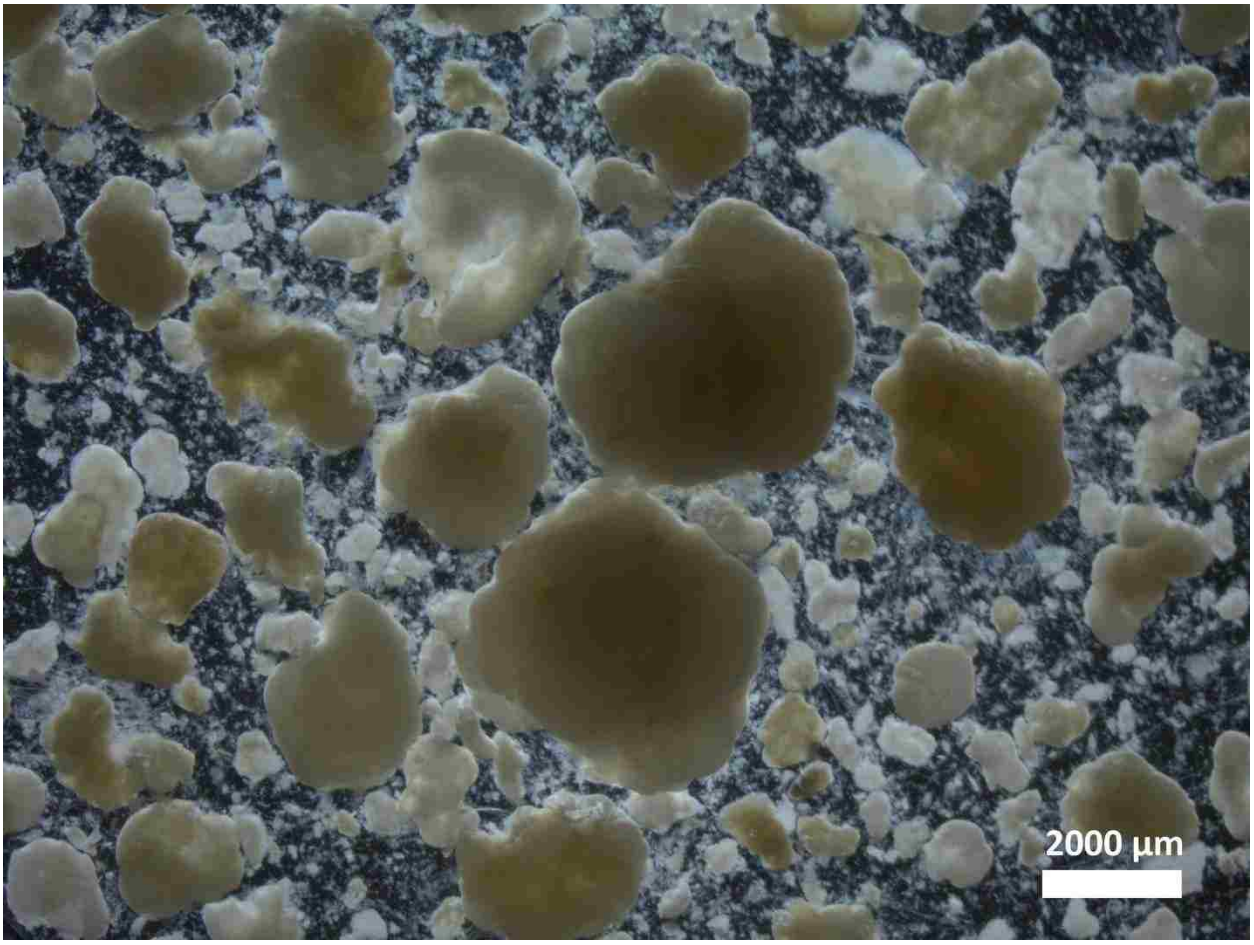

Figure C-15. February 28, 2019 Stereomicroscope Image with Scalebar

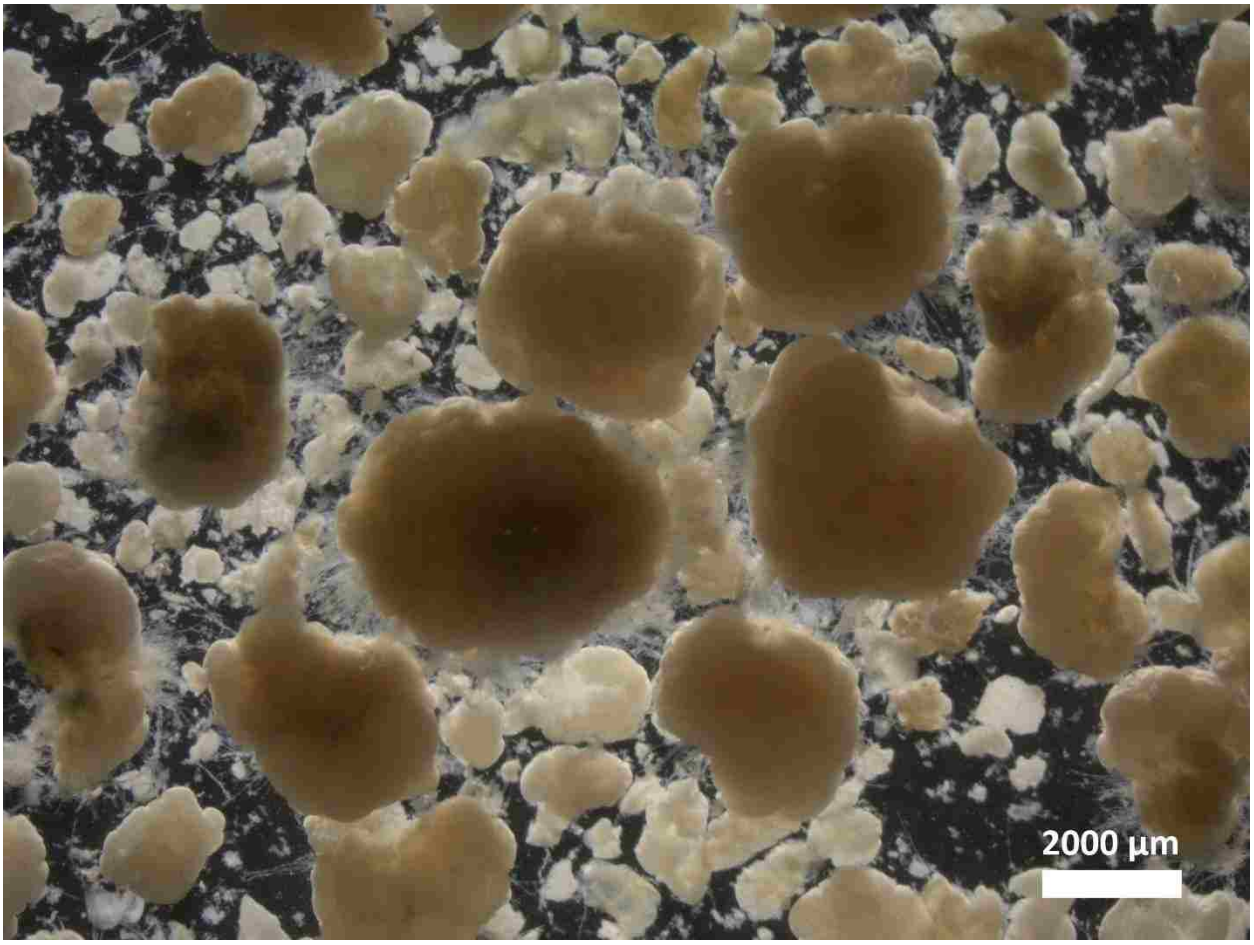

Figure C-16. March 25, 2019 Stereomicroscope Image with Scalebar

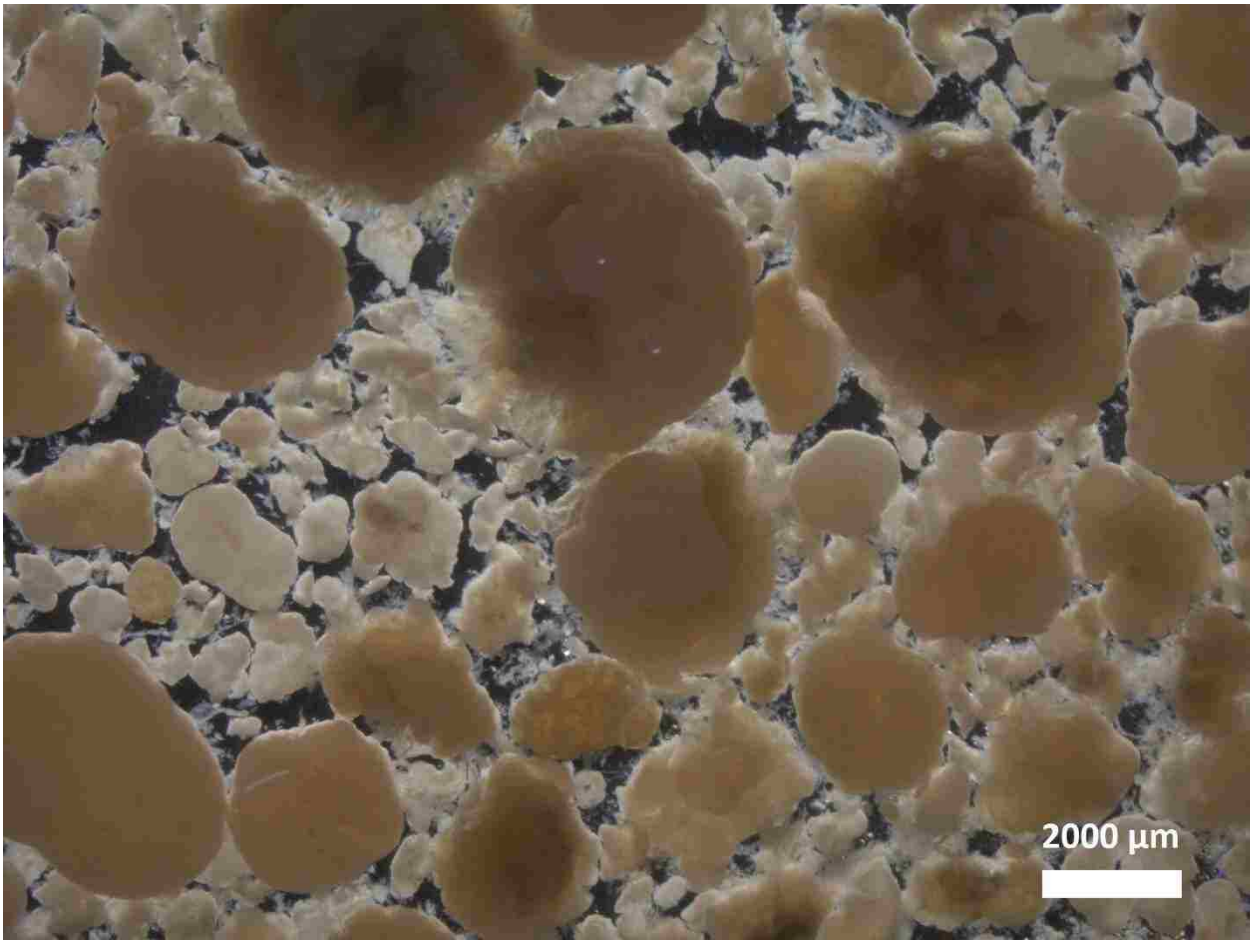

Figure C-17. April 25, 2019 Stereomicroscope Image with Scalebar

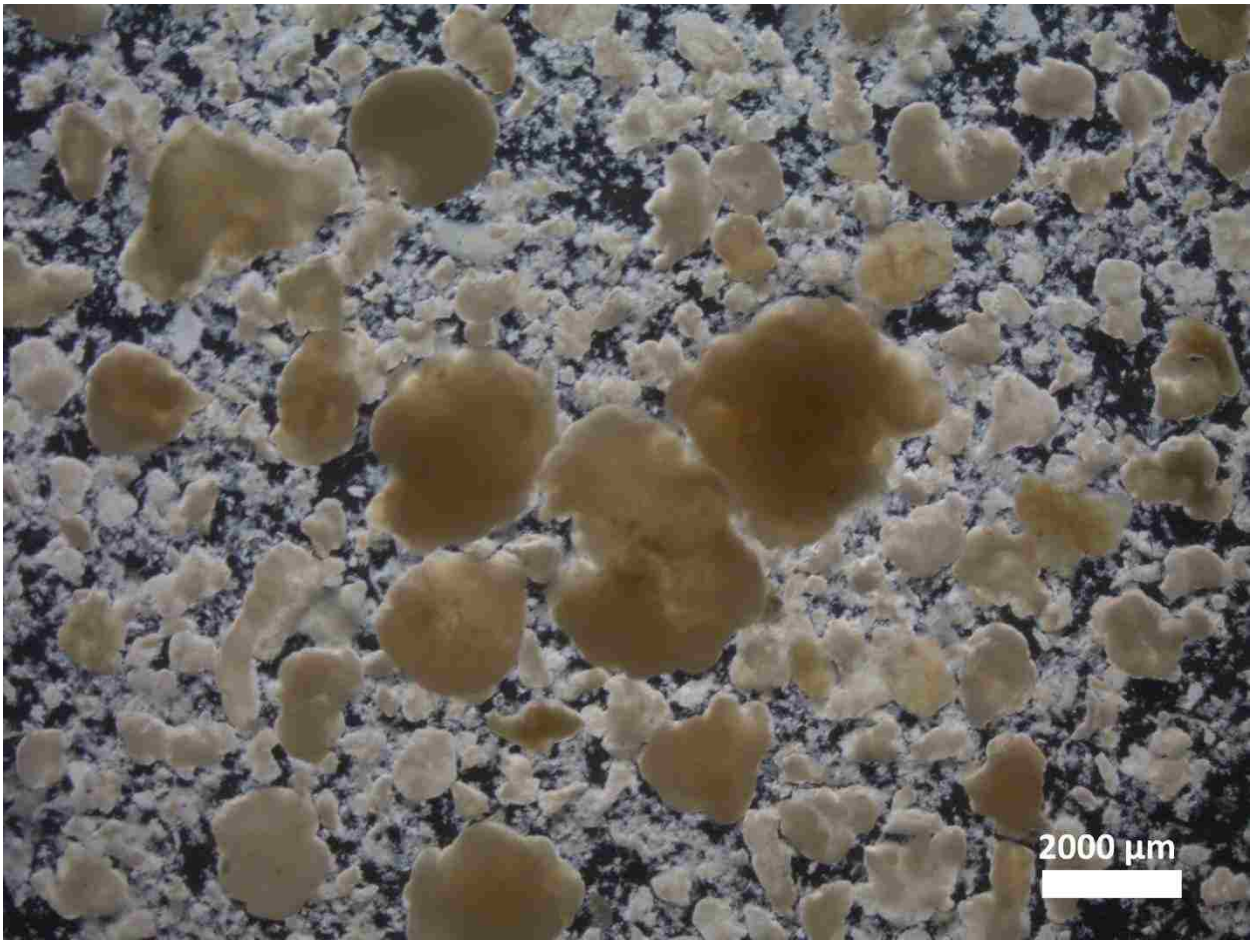

Figure C-18. May 10, 2019 Stereomicroscope Image with Scalebar